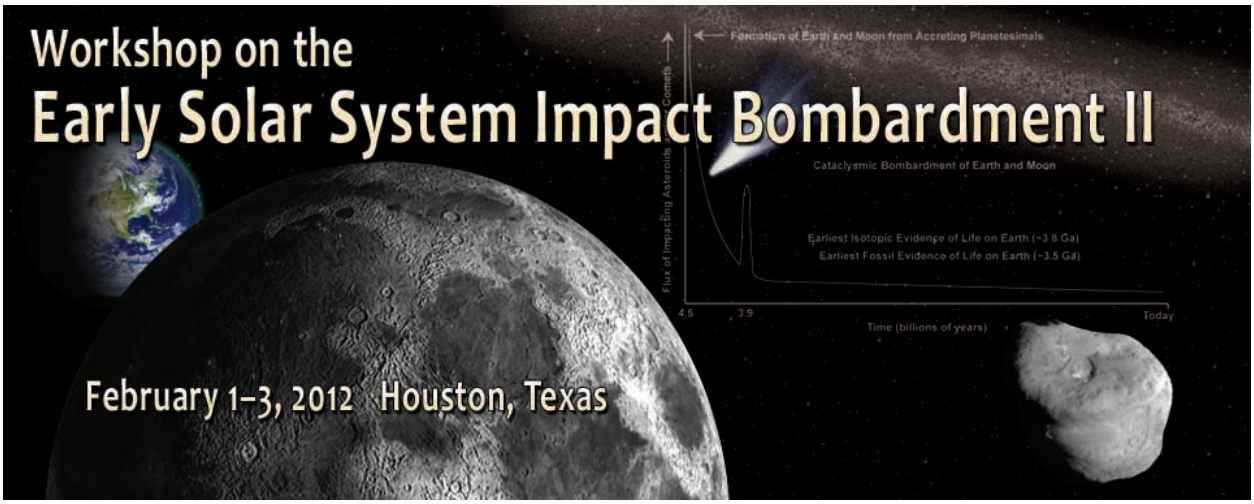

Program and Abstract Volume

LPI Contribution No. 1649

LUNAR AND PLANETARY INSTITUTE

USRA

Workshop on the

Early Solar System Impact Bombardment II

February 1–3, 2012 • Houston, Texas

Sponsors

National Aeronautics and Space Administration
Universities Space Research Association
Lunar and Planetary Institute
NASA Lunar Science Institute

Conveners

David A. Kring
Center for Lunar Science and Exploration
Lunar and Planetary Institute

William F. Bottke
Center for Lunar Origin and Evolution
Southwest Research institute

Scientific Organizing Committee

Robin Canup
Southwest Research Institute

Gareth Collins
Imperial College London

James Head
Brown University

Alessandro Morbidelli
Observatoire de la Cote d'Azur (France)

Marc Norman
Australian National University

Richard Walker
University of Maryland

Lunar and Planetary Institute 3600 Bay Area Boulevard Houston TX 77058-1113

LPI Contribution No. 1649

Compiled in 2012 by

Meeting and Publication Services
Lunar and Planetary Institute
USRA Houston
3600 Bay Area Boulevard, Houston TX 77058-1113

The Lunar and Planetary Institute is operated by the Universities Space Research Association under a cooperative agreement with the Science Mission Directorate of the National Aeronautics and Space Administration.

Abstracts in this volume may be cited as

Author A. B. (2012) Title of abstract. In *Workshop on the Early Solar System Bombardment II,* p. XX. LPI Contribution No. 1649, Lunar and Planetary Institute, Houston.

ISSN No. 0161-5297

Preface

This volume contains abstracts that have been accepted for presentation at the Workshop on the Early Solar System Bombardment II, February 1–3, 2012, Houston, Texas.

Administration and publications support for this meeting were provided by the staff of the Meeting and Publication Services Department at the Lunar and Planetary Institute.

Contents

Program

Wednesday, February 1, 2012
COSMOCHEMICAL ASSESSMENT OF THE LUNAR BASIN-FORMING EPOCH
8:30 a.m. Lecture Hall

Lunar Samples are Analyzed to Determine the Age of Impact Events and the Impactors that Produced Them

Chairs: **Richard Walker**
David Kring

8:30 a.m. Kring D. A. *
Welcome and Introduction

8:35 a.m. Wasserburg G. J. *
The Terminal Lunar Cataclysm and the Late Heavy Bombardment of the Inner Solar System

9:00 a.m. Kring D. A. *
New Insights to Early Bombardment Processes from Accretion Through the Basin-Forming Epoch **[#4015]**

9:20 a.m. Norman M. D. * Nemchin A. A.
Large Impacts at 4.2 Ga from Uranium-Lead Dating of Lunar Melt Breccias **[#4013]**

9:40 a.m. Zellner N. E. B. * Swindle T. Delano J. W.
Understanding the Significance of Lunar Sample Data for Interpreting Lunar Impact History **[#4011]**

10:00 a.m. *Coffee Break*

10:10 a.m. Neukum G. Basilevsky A. T. * Kneissl T. Michael G. G. Ivanov B. A.
On the History of Early Meteoritic Bombardment of the Moon: Did the Lunar Terminal Cataclysm Occur? **[#4022]**

10:30 a.m. Fritz J. P. * Fernandes V. A. S. M.
The Heavy Bombardment of the Moon **[#4044]**

10:50 a.m. Galenas M. G. Liu J. G. * Walker R. J.
$^{187}Os/^{188}Os$ and Highly Siderophile Element Characteristics of Apollo 16 and 17 Impact-Melt Breccias **[#4003]**

11:10 a.m. Joy K. H. * Zolensky M. E. Ross D. K. McKay D. S. Kring D. A.
Direct Detection of Projectile Relics on the Moon **[#4035]**

11:25 a.m. *Lunch*

Wednesday, February 1, 2012
GEOLOGICAL MEASURES OF EARLY LUNAR BOMBARDMENT
1:30 p.m. Lecture Hall

Cratered Surfaces are Used to Evaluate Impactor Sources and the Relative Timing of Basin-Forming Events

Chair: Gareth Collins

1:30 p.m. Fassett C. I. * Head J. W. Kadish S. J. Mazarico E. Neumann G. A. Smith D. E. Zuber M. T.
Stratigraphy, Sequence, and Crater Populations of Lunar Impact Basins from Lunar Orbiter Laser Altimeter (LOLA) Data: Implications for the Late Heavy Bombardment **[#4023]**

1:55 p.m. Kirchoff M. R. * Sherman K. M. Chapman C. R.
Preliminary Results on the Evolution of Small Crater Populations on the Moon **[#4020]**

2:15 p.m. Marchi S. * Bottke W. F. Kring D. A. Morbidelli A.
Two Populations of Early Lunar Impactors as Recorded in Its Ancient Crater Populations **[#4018]**

2:35 p.m. Morbidelli A. * Marchi S. Bottke W. F. Jr.
The Sawtimeline of the First Billon Year of Lunar Bombardment **[#4014]**

2:55 p.m. Hartmann W. K. *
Empirical Studies of Lunar Bombardment Around 3.6–4 Gy Ago **[#4025]**

3:15 p.m. *Coffee Break*

Wednesday, February 1, 2012
INVENTORY AND EVOLUTION OF IMPACT BASINS
3:25 p.m. Lecture Hall

Geophysical Methods and Modeling are Used to Further Evaluate Impact Basins

Chair: James Head

3:25 p.m. Frey H. V. * Meyer H. M. Romine G. C.
Improving the Inventory of Large Lunar Basins: Using LOLA Data to Test Previous Candidates and Search for New Ones **[#4005]**

3:45 p.m. Potter R. W. K. * Collins G. S. Kiefer W. S. McGovern P. J. Kring D. A.
Thermal Conditions During the Lunar Basin-Forming Epoch: Insights from the Numerical Modeling of Lunar Basin-Forming Impacts **[#4009]**

4:05 p.m. Kiefer W. S. * McGovern P. J. Potter R. W. K. Collins G. S. Kring D. A.
The Collapse of Super-Isostasy: The Thermal Evolution of Large Lunar Impact Basins and a Volcanic Intrusion Model for Lunar Mascon Gravity Anomalies **[#4026]**

4:25 p.m. Roberts J. H. * Barnouin O. S.
The Effect of the Caloris Impact on the Mantle Dynamics and Volcanism of Mercury **[#4037]**

Wednesday, February 1, 2012
POSTER SESSION: VARIOUS VIEWS OF EARLY SOLAR SYSTEM BOMBARDMENT
5:00 p.m. Great Room

Martellato E. Benkhoff J. Colangeli L. Foing B. Marchi S.
Numerical Modeling of the Caloris Basin **[#4030]**

Crow C. A. McKeegan K. D. Gilmour J. D. Crowther S. A. Taylor D. J.
Are Apollo Zircons Witness to a Lunar Cataclysm? **[#4024]**

Niihara T. Schaffer L. Kring D. A.
Petrology of the Impact Melt Clasts in 60016, Ancient Regolith Breccia **[#4016]**

Singer S. F.
Questions About Lunar Origin **[#4008]**

Cuk M. Stewart S. T.
Resonances and the Angular Momentum of the Earth-Moon System **[#4006]**

Thursday, February 2, 2012
ACCRETION AND IMPACT BOMBARDMENT OF THE EARTH
8:30 a.m. Lecture Hall

Developing Methods to Evaluate the Accretion and Bombardment of the Earth

Chairs: **Marc Norman**
David Kring

8:30 a.m. Salmon J. J. * Canup R. M.
How Much Earth-Like Material Could the Moon Accrete? **[#4012]**

8:50 a.m. Walker R. J. * Touboul M. Puchtel I. S.
Application of the ^{182}Hf-^{182}W Isotope System to Constraining the Timing of Late Accretion to the Earth and Moon **[#4004]**

9:10 a.m. Koeberl C. *
Search for a Geochemical Record of the Late Heavy Bombardment on Earth **[#4046]**

9:30 a.m. Wielicki M. M. * Harrison T. M. Schmitt A. K.
Geochemical Signatures and Magmatic Stability of Impact Produced Zircon **[#4041]**

9:50 a.m. Bell E. * Abbott S. Harrison M.
A Search for Evidence of Extraterrestrial Impacts in Jack Hills Zircons **[#4047]**

10:10 a.m. *Coffee Break*

10:20 a.m. Abramov O. * Kring D. A. Mojzsis S. J.
Modeling of Impact-Induced Age Resetting and Partial Pb-Loss in Zircon Grains **[#4042]**

10:40 a.m. Johnson B. C. * Melosh H. J.
New Estimates for the Number of Large Impacts Throughout Earth's History **[#4027]**

11:00 a.m. Bottke W. F. * Vokrouhlicky D. Minton D. Nesvorny D. Morbidelli A.
Brasser R. Simonson B.
The Great Archean Bombardment **[#4036]**

11:20 a.m. Goderis S. * Belza J. Claeys Ph.
The Impact Cratering Record for Clues on the Rate of Collisions and Provenance **[#4010]**

11:40 a.m. de Niem D. * Kührt E. Morbidelli A. Motschmann U.
Planetary Atmospheres During an Enhanced Bombardment **[#4021]**

12:00 p.m. *Lunch*

Thursday, February 2, 2012
THE COLLISIONAL RECORD ON MARS AND AMONG ASTEROIDS
1:30 p.m. Lecture Hall

Cosmochemical and Geological Data are Evaluated
to Constrain the Collisional Evolution of Mars and the Asteroid Belt

Chairs: **William Bottke**
Alessandro Morbidelli

1:30 p.m. Bogard D. D. *
LHB Evidence on Asteroids **[#4001]**

1:55 p.m. Hopkins M. D. * Mojzsis S. J.
Early Thermal Events in the HED Parent Body (4 Vesta) Recorded in Zircon U-Th-Pb Depth Profiles from Millbillillie Brecciated Eucrite **[#4029]**

2:15 p.m. Cohen B. A. *
The Vestal Cataclysm **[#4017]**

2:35 p.m. O'Brien D. P. * Marchi S. Schenk P. Mittlefehldt D. W. Jaumann R. Ammannito E. Buczkowski D. L. De Sanctis M. C. Filacchione G. Gaskell R. Hoffmann M. Joy S. Le Corre L. Li J. Y. Nathues A. Polanskey C. Preusker F. Rayman M. Raymond C. A. Reddy V. Roatsch T. Russell C. T. Turrini D. Vincent J. B. Dawn Science Team
The Impact History of Vesta: New Views from the Dawn Mission **[#4031]**

2:55 p.m. Corrigan C. M. * Cohen B. A. Hodges K. Lunning N. L.
3.9 Billion Years Ago and the Asteroid Belt **[#4034]**

3:15 p.m. *Coffee Break*

3:25 p.m. Schmedemann N. * Kneissl T. Michael G. Wagner R. Neukum G. Nathues A. Sierks H.
Crater Size-Frequency Distributions and Chronologies of Asteroids **[#4045]**

3:45 p.m. Minton D. A. * Bottke W. F. Frey H. V. Lillis R. J. Roberts J. H. Stewart S. T.
The Early Bombardment History of Mars Revealed in Ancient Megabasins **[#4040]**

4:05 p.m. Robbins S. J. * Hynek B. M.
Revising the Earliest Recorded Impact History of Mars and Implications for the Late Heavy Bombardment **[#4039]**

4:25 p.m. Righter K. *
Martian Mantle HSE Abundances Do Not Require Late Chondritic Addition **[#4033]**

4:45 p.m. Cuk M. *
LHB was Caused by Mars-Crossers, and It Was Not All that Heavy **[#4002]**

Friday, February 3, 2012
THE VIEW FROM THE OUTER SOLAR SYSTEM AND BEYOND
8:30 a.m. Lecture Hall

Does the Collisional Evolution of the Outer Solar System Differ from that of the Inner Solar System and, If So, What does that Imply?

Chair: **Alessandro Morbidelli**

8:30 a.m. Turrini D. * Coradini A. Federico C. Formisano M. Magni G.
The Formation of Jupiter and the Jovian Early Bombardment **[#4019]**

8:50 a.m. Richardson J. E. * Minton D. A. Thomas P. C.
Exploring the Bombardment History of the Outer Solar System via Saturnian Satellite Cratering Records **[#4028]**

9:10 a.m. Lisse C. M. * Chen C. H. Wyatt M. C. Morlok A. Thebault P. Sitko M. Watson D. M. Manoj P. Sheehan P. Currie T. M.
Spitzer Evidence for a Late Heavy Bombardment and the Formation of Urelites in η Corvi at ~1 Gyr **[#4038]**

9:30 a.m. *Coffee Break*

Friday, February 3, 2012
DISCUSSION OF MISSION CONCEPTS AND LANDING SITES
TO TEST WORKSHOP HYPOTHESES
9:50 a.m. Lecture Hall

The Community Discusses Mission Concepts and Landing Sites
(such as the Schrödinger, South Pole-Aitken, and Nectaris Basins) that Can Test Workshop Hypotheses

Moderators: **David Kring**
William Bottke

11:30 a.m. *Meeting Adjourns*

MODELING OF IMPACT-INDUCED AGE RESETTING AND PARTIAL PB-LOSS IN ZIRCON GRAINS.

O. Abramov[1], D. A. Kring[2], and S. J. Mojzsis[3], [1]USGS Astrogeology Research Program, 2255 N. Gemini Dr., Flagstaff, AZ 86001 [2]Lunar and Planetary Institute, 3600 Bay Area Blvd., Houston, TX, 77058, [3]Center for Lunar Origin and Evolution, NASA Lunar Science Institute, Department of Geological Sciences, University of Colorado, 2200 Colorado Ave., Boulder, CO 80309. E-mail: *oabramov@usgs.gov*

Introduction: Impact bombardment in the first billion years of the solar system fundamentally altered several key aspects of the terrestrial planets, and continues to be the subject of intense research interest within and beyond the planetary sciences. Effects of bombardments include: Changes in surface morphology, expressed as cratered terrains; chemical composition changes via delivery of materials, melt mixing and differentiation; changes to primordial atmosphere compositions and atmospheric densities, and thereby of paleoclimate; and perhaps the overall thermal structures of terrestrial planets. Also, heating due to impacts may have had important biological consequences.

One promising approach in understanding the bombardment history of the early solar system lies in the study of zircons, minerals that significantly predate the Late Heavy Bombardment (~3.9 Ga), some of which are almost 4.4 Ga. In particular, in addition to well-documented complete age-resetting of zircons in impact melts [e.g., 1,2], several studies have suggested partial resetting. These include: (i) Ultra-high spatial resolution ion microprobe depth-profiles of pre-3.9 Ga terrestrial zircons from the Jack Hills (Western Australia) that recorded ~3.95 Ga, 2 to 4 μm mantles over the old igneous zircon cores (up to 4.3 Ga). These minute mantles show Pb-loss (up to 90% discordance) over narrow domains that could be the result of impact-induced heating [3]. (ii) Zircons from the K/T distal ejecta, as well as from the Onaping Formation of Sudbury crater, appear to contain two components, based on $^{207}Pb/^{206}Pb$ ages: one with the age of target lithologies, and another with the time of impact, with the relative proportion of the latter increasing with the degree of impact shock [2,4].

This preliminary study explores conditions under which zircons may suffer complete or partial Pb loss, with the aim of making laboratory data easier to interpret, as well as making predictions for future studies.

Methods: We use well-constrained, laboratory-derived equations for diffusion of Pb in zircon, in both undamaged [5] and radiation-damaged crystals [6]. These equations require as inputs: (i) temperature and (ii) time spent at that temperature, and thus can be readily coupled to 1-, 2-, or 3-dimensional thermal models. We have previously developed a model of the response of zircons to impact bombardments on a global scale [7], and here we examine individual impact structures in an attempt to further understand the mechanism(s) behind age-resetting of zircons by impacts. Two numerical models are used in this study:

Crater cooling model: We use a previously-published simulation of the post-impact cooling of the ~180-km Sudbury crater (Ontario, Canada) [8] and model Pb-loss in zircons emplaced within the structure. The model includes cooling by hydrothermal activity, and was performed using modified version of the publicly available program HYDROTHERM, which simulates water and heat transport in a porous medium [9]. Rock properties appropriate for the Sudbury site are used. The initial temperature distribution of the Sudbury crater was previously calculated using the SALEB hydrocode [10]. The crater cooling simulation was coupled to equations of Pb-loss in zircon [5,6], which were solved numerically at each model time step.

Ejecta cooling model: Because the crater cooling model did not incorporate the deposition of hot ejecta outside the rim, an important process for larger (>100 km) impact craters, a separate 1-dimensional ejecta cooling model was constructed. The program used for this model is HEATING 7.3, a general-purpose, finite-difference heat transfer code. Thermal and physical parameters of the ejecta were based on those of granite, as specified in the HEATING materials library. The hot ejecta overburden was modeled on a 1000-node grid with a radiative upper boundary, overlying a 2000-node original surface with an initial temperature of 0 °C. Thickness and initial temperature of the ejecta are specified as inputs.

Results: *Crater cooling model:* In the case of undamaged zircons (Figure 1a), there is a rather strong dichotomy -- either 100% Pb-loss within zircon grain or none at all, with very few areas of partial Pb-loss. This result is remarkably independent of grain diameter. The areas of the crater that have 100% Pb-loss are central uplift (initial temperature of ~1,000 °C) the central melt sheet, as well as the small melt sheet in the annular trough (initial temperature of ~1700 °C). In addition, since the thermal decomposition temperature of zircon is 1673 °C [11], complete loss of grains emplaced within the melt is likely.

In addition, we modeled Pb-loss in shock-damaged zircons. Wittmann et al. [12] described granular textures within a variety of shocked zircon grains from several impact structures, which exhibit Raman characteristics that overall follow the trend of natural

radiation damage. As a first-order approximation of this, we used the diffusion equation for radiation-damaged zircons [6], which have a significantly faster rate of Pb-loss. The results, illustrated in Figure 1b, show a significantly larger rock volume within the crater that suffers complete Pb-loss, as well as a somewhat wider band of partial Pb-loss.

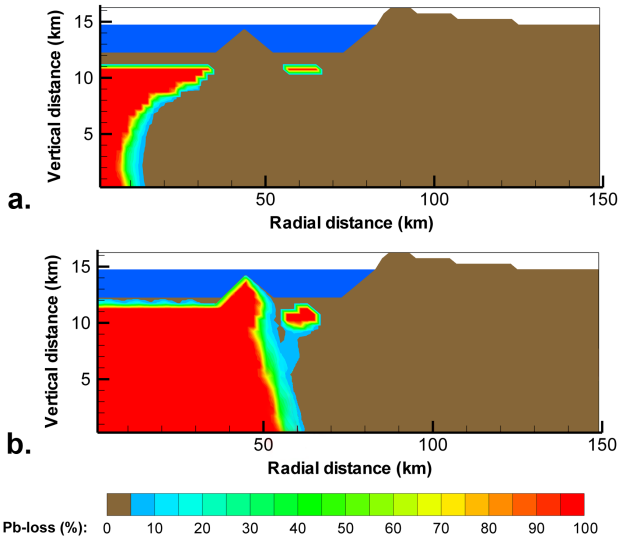

Figure 1. Percentage of Pb-loss in 50-µm zircon grains within a 180-km terrestrial impact crater. Pb-loss in the ejecta is not included in this model. a) Normal zircon grain. b) Shock-damaged zircon grain.

Ejecta cooling model: Much like the crater cooling model, the ejecta cooling model results indicate that there is a fairly narrow parameter space that yields partial Pb-loss. In the case of undamaged zircon grains (Figure 2a), only a temperature of 1200 °C results in partial Pb-loss in zircon grains within the ejecta. Other initial temperatures tested (300 °C, 600 °C, and 900 °C) result in no appreciable Pb-loss. In the case of shock-damaged zircons (Figure 2b), initial temperatures of 1200 °C and 900 °C resulted in complete Pb-loss throughout most of the ejecta blanket, 300 °C resulted in zero Pb-loss, and only 600 °C resulted in partial Pb-loss.

Concluding remarks: The models presented above suggest either complete Pb-loss or none at all within most impact structures. Since this appears at odds with evidence for partial Pb-loss presented above, it is likely that another mechanism needs to be invoked. For example, Krogh et al. [4] suggest that partial loss results from a post-impact thermal pulse during the grain's residence in the fireball cloud. Based on the equations used here, this does not appear likely, as Pb needs ~1 hour at ~1673 °C (thermal decomposition temperature of zircon) to diffuse 1 µm, in both damaged and undamaged grains. However, even with a fireball a few hundred km in diameter, ejecta traveling at half escape velocity would take only ~30 s to clear it. Other possibilities include rapid quenching of the breccias within the crater, for example, by post-impact flooding, and shock-heating, where the grain experiences very high temperatures for very short periods of time between the passages of compression and rarefaction waves.

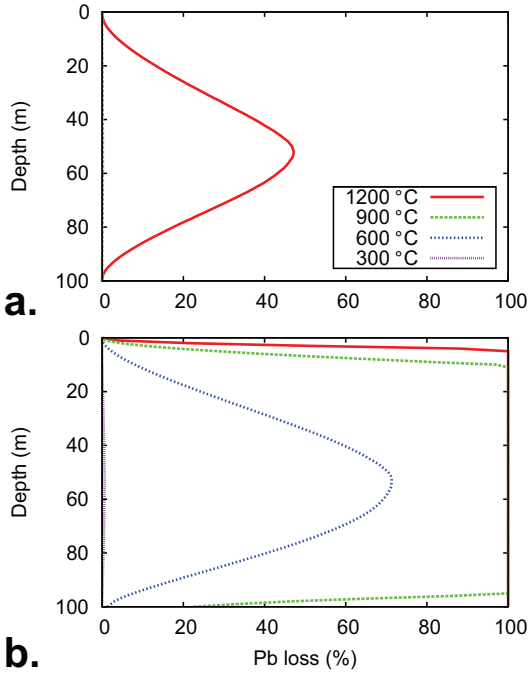

Figure 2. Percentage of Pb-loss in 50-µm zircon grains within a 100-m thick impact ejecta blanket of various temperatures. a) Normal zircon grain. b) Shock-damaged zircon grain.

References: [1] Kamo, S.L. et al. (1996) *Earth Planet. Sci. Lett*, *144*, 369-387. [2] Krogh, T.E., et al. (1996) In Earth Processes: reading the isotopic code, 343-353. [3] Trail, D. et al., *Geochim. Cosmochim. Acta*, *71*, 4044-4065. [4] Krogh T.E. et al. (1993) Earth Planet. Sci. Lett., 119, 425-429. [5] Cherniak D.J. and Watson E.B. (2001) *Chem. Geo*., 172, 5-24. [6] Cherniak D.J. et al. (1991) *Geochim. Cosmochim. Acta*, 55, 1663-1673. [7] Abramov, O. and Mojzsis, S.J. (2009) *Eos Trans. AGU*, 90(52), Fall Meet. Suppl., Abstract V13C-2040. [8] Abramov O. and Kring D. A. (2004) *JGR*, 109, doi:10.1029/2003JE002213. [9] Hayba, D. O. and Ingebritsen, S. E. (1994) U.S. Geol. Surv. Water Resour. Invest. Rep., 94-4045, 85 pp. [10] Ivanov, B. A. and Deutsch A. (1999), in Large Meteorite Impacts and Planetary Evolution II, 389-397. [11] Kaiser et al. (2008) *J. Eur. Cer. Soc*., *28*, 2199-2211. [12] Wittmann et al., *Meteor. Planet. Sci*., *41*, 433-454.

A Search for Evidence of Extraterrestrial Impacts in Jack Hills Zircons

Elizabeth Bell, Sunshine Abbott, and Mark Harrison
Department of Earth and Space Sciences, UCLA, Los Angeles, CA 90095

The Late Heavy Bombardment (LHB) is an intense flux of planetary debris into the inner solar system originally hypothesized to have occurred at ~3.9 Ga. The nature of the LHB is controversial and the known record of its existence is largely restricted to lunar samples. However, the interpretive basis from which $^{40}Ar/^{39}Ar$ age spectra have been used to infer lunar LHB activity is deeply flawed and alternate sources of evidence are needed before cleaer insights can be drawn. Although Earth would have experienced a ~20 times greater flux of impactors than the Moon – leading to significant crustal heating and even melting – the Hadean (pre-3.8 Ga) terrestrial rock record is virtually non-existent. Arguably the most complete record of the Hadean is found in detrital zircons from the Jack Hills, Western Australia, which semi-continuously span the period 4.38-3.8 Ga. Investigations of these grains have previously suggested the existence of a hydrosphere, continental crust, sedimentary cycling and plate boundary interactions on early Earth. We have undertaken several interrelated studies using Jack Hills zircons to address the question: do Hadean zircons preserve evidence of the LHB,? To address this, we have developed a Ti-U-Th-Pb depth profiling method to obtain continuous age vs. temperature (T^{xlln}) data from <4 Ga rims on >4 Ga zircons as an environmental monitor of the LHB-era. Results show anomalously high temperatures associated uniquely with LHB-era rim growth. In a companion study, geochemical characterization of <4 Ga Jack Hills zircon cores reveals a unique population at 3.84-3.91 Ga that is consistent with recrystallization during high temperature events, the likeliest source of which are LHB impacts. Thus our preliminary data may represent the first terrestrial evidence for impact-related heating during the LHB.

LHB EVIDENCE ON ASTEROIDS. DONALD BOGARD, LPI-USRA, HOUSTON, TX 77058
bogard@lpi.usra.edu; donbogard@comcast.net

The Moon. Shortly after return and analysis of the first lunar samples, it was recognized that the lunar surface had experienced significant heating about 4 Giga-years (Gyr) ago, which produced variable to total resetting of isotopic chronometers in highland rocks. This heating was attributed to a period of large-scale impact bombardment (LHB, Late Heavy Bombardment, or cataclysm) of the Moon, long after its formation [1]. Earlier, the origin of the impacting bodies was a mystery, but presently orbital interactions of the giant planets with the Kuiper and asteroid belts is thought to be the cause. The time period over which these large impacts occurred is still poorly known. Dating of rocks thought to have derived from the large Imbrium and Serenitatis basins indicate that these formed about 3.9 Gyr ago [2]. The youngest large basin, Oriental, is thought to have formed 3.7-3.8 Gyr ago, primarily based on crater densities, not radiometric dating. Earlier, the 16th youngest basin, Nectaris, was thought to have formed ~3.9 Gyr ago, but more recent studies suggest it may be considerably older [3]. Ages of the oldest impact basins are totally unknown, although reset or partially reset ages of >4 Gyr for highland rocks are relatively common. One difficulty in using radiometric ages to determine the time period of the lunar LHB is that the Moon was extensively gardened by large impactors and the rocks experienced multiple thermal events.

Evidence of the ending time of this LHB is given by a plot of crater densities against radiometric age for various lunar features, ranging from young craters, to mare, to older impact basins (Fig. 1). Several craters, ranging over 2-2200 Myr in age, and four younger mare surfaces (Apollo 12 & 15 and Luna 16 & 24) are approximately consistent with a constant flux over the past 3.5 Gyr. Some older mare (Apollo 11 and 17) and ejecta deposits at Apollo 14, 16, and other basins indicate an older impact flux which rises well above this constant flux curve, and which may have decreased over the period 4.1-3.6 Gyr ago. These data suggest that the end of the LHB on the Moon occurred ~3.5 Gyr ago.

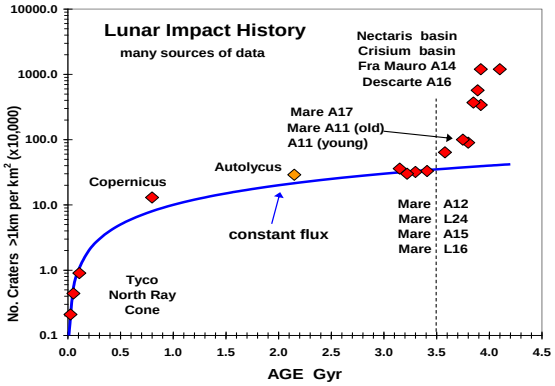

Asteroids. What about the LHB on other solar system bodies? Bogard [4] reviewed impact reset ages of meteorites and suggested that the LHB occurred on the parent bodies of HED meteorites, probably Vesta, H chondrites, and possibly IIE iron-silicate meteorites. K-Ar ages, measured by the ^{39}Ar-^{40}Ar technique, are particularly sensitive to impact resetting. No other meteorite types show obvious evidence of significant impact heating, and [4] attributed this observation to other meteorites having derived from smaller parent bodies. Hot ejecta deposits from large craters are required to reset radiometric chronometers, and such large impacts can occur only on large bodies like the Moon and Vesta, without destroying the body. Additional Ar-Ar ages of eucrites were presented by [5], and a recent review of Ar-Ar ages of meteorites and their impact history is given in [6]. Figure 2 presents a probability histogram of Ar-Ar ages from 43 different eucrites and eucritic clasts in howardites [6]. Each Ar-Ar age is represented by a Gaussian curve, where the spread of the curve is proportional to the age uncertainty; more precisely

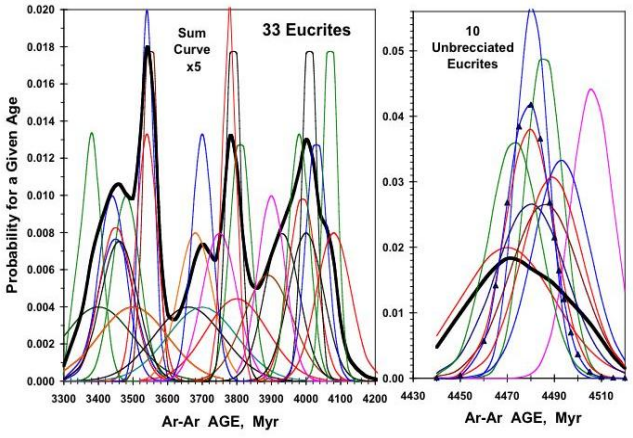

defined ages give taller and narrower curves. The 33 curves plotted to the left represent brecciated samples, which obviously experienced impact breakage, mixing, and heating. The 10 curves to the right represent unbrecciated samples, including both basaltic and cumulate eucrites [5], which do not exhibit obvious textural evidence of impact. The heavy black lines give an average of these data. Note that the age scale is approximately continuous between the two plots.

The brecciated samples suggest impact heating events at about 4.0, 3.7-3.8, and 3.4-3.5 Gyr. By analogy with impact reset ages of lunar rocks, these likely represent large impact events on Vesta at these times. Those inferred impacts over ~3.7-4.0 Gyr fall within the range of estimated ages of some lunar impact basins. The impact(s) at ~3.5 Gyr have similar age to the end of the lunar LHB as inferred from Fig. 1. Essentially no impact ages of brecciated eucrites give ages younger than 3.4 Gyr or older than 4.1 Gyr. Apparently the age range of ~3.4-4.1 Gyr defines the period of the LHB on the Vesta asteroid.

Ages of unbrecciated eucrites plotted to the right narrowly define a single impact-heating event at 4.48 Gyr. Other radiometric chronometers suggest disturbance for some of these same meteorites [5]. This 4.48 Gyr age is younger than the formation time of eucrites measured by U-Pb, and is unlikely to represent the time of metamorphism that partially homogenized Mg and Fe in eucritic pyroxenes. Neither can uncertainty in the ^{40}K decay parameters account for this 4.48 Gyr age being slightly younger than the times of formation or metamorphism [6]. This 4.48 Gyr age was attributed to an early impact-heating event on Vesta, one apparently unrelated to the LHB [5]. Impact heating at comparable times apparently occurred on some other meteorite parent bodies [6]. Assuming these unbrecciated eucrites derived from the same parent body as the brecciated eucrites, an obvious question is how these older samples escaped impact heating during the LHB. They may have been ejected in the 4.48 Gyr event as smaller vestoids, which escaped large LHB collisions. This implies one large Vesta crater is much older than the others. Alternatively, these older meteorites may have been deeply buried on Vesta

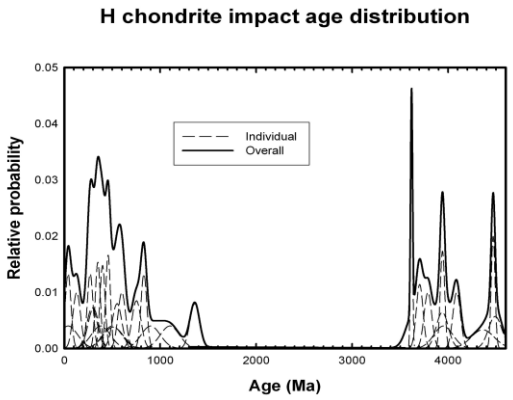

and only brought to the surface near the end of the LHB.

Some H chondrites also indicate LHB resetting of Ar-Ar ages in the same ~3.5-4.1 Gyr time period as eucrites, and minor evidence for LHB resetting exists in L and LL chondrites [4, 7]. Figure 3 (from Swindle & Kring, reference 7) gives Ar-Ar ages for H chondrites. In this figure, a few older ages may represent impact or parent body metamorphism. Many chondrite ages of <1.2 Gyr represent collisional impacts in the asteroid belt, and interestingly only chondrites seem to exhibit these young impact ages [6].

Conclusions. The LHB on the Moon also occurred on the parent body of HED meteorites, probably Vesta, and likely on the parent bodies of some chondrites. Other than possibly the IIE iron-silicate body, no other meteorite group gives obvious evidence for LHB age resetting. From meteorite data, the time of LHB resetting appears to have been confined to the period of 4.0-3.5 Gyr ago. This appears consistent with lunar data. Impactors producing large craters on Vesta would have been smaller than those producing the lunar basins, so Vesta and the Moon probably define different sizes of the LHB population.

[1] Tera, Papanastassiou, Wasserburg, *EPSL 22*, 1-21, 1974.; [2] Grange, Nemchin, Jourdan, 41st *LPSC* abstract #1275, 2010; [3] Norman, Duncan, Huard, GCA 74, 763-783, 2010; [4] Bogard, *Meteoritics 30*, 244-268, 1995; [5] Bogard &Garrison, *MAPS 38*, 669-710, 2003; [6] Bogard, *Chemie der Erde 71*, 207-226; [7] Swindle & Kring, LPI Early Solar System Bombardment Workshop, abstract #3004, 2008.

THE GREAT ARCHEAN BOMBARDMENT. W. F. Bottke[1], D. Vokrouhlický[1,2], D. Minton[1], D. Nesvorný[1], A. Morbidelli[1,3], R. Brasser[1,3], B. Simonson[4], *(1) Center for Lunar Origin and Evolution (CLOE), NASA Lunar Science Institute, Southwest Research Institute, 1050 Walnut St., Suite 300, Boulder, Colorado 80302, USA; bottke@boulder.swri.edu* , *(2) Institute of Astronomy, Charles University, V Holesovickach 2, CZ-18000, Prague 8, Czech Republic, (3) Observatoire de la Côte d'Azur, Boulevard de l'Observatoire, B.P. 4229, 06304 Nice Cedex 4, France, (4) Geology Dept., Oberlin College, Oberlin, OH 44074 USA* .

The Late Heavy Bombardment (LHB) is often defined as a solar system-wide barrage of comets and asteroids that produced many young lunar basins, with the last one Orientale formed at ~ 3.7 Ga. Curiously, Archean and early-Proterozoic terrains on Earth, which post-date this era, also show signs of numerous LHB-sized blasts in the form of impact spherule beds, globally-distributed ejecta layers created by Chicxulub-sized or larger cratering events: at least 10, 4, and 1 have been found between 3.47-3.23 Ga, 2.63-2.49 Ga, and 2.1-1.7 Ga, respectively. Here we explore their origin via simulations of late giant planet migration in the presence of a hypothesized extension of the primordial asteroid belt between 1.7-2.1 AU [1]. These ejected "E-belt" asteroids are advantageous; not only are they are ten times more likely to hit the Earth and Moon than main belt ones, but they also decay far more slowly, with some evolving onto high inclination orbits like the observed Hungaria asteroids. By scaling the initial E-belt population from the observed Hungarias, we find that the E- and primordial main belts together make ~ 12 lunar basins between 3.7-4.1 Ga, with the latter age occurring near the twelfth youngest lunar basin Nectaris. Older basins presumably come from other sources, such as planetesimals leftover from terrestrial planet formation processes. The key, however, is that expelled E-belt asteroids produce an extended LHB-era, with 15 basins made on Earth over the Archean as well as $\sim \mathbf{60}$ and $\sim \mathbf{4}$ Chicxulub-sized or larger craters on the Earth and Moon, respectively, between 1.7-3.7 Ga. These rates are sufficient to match both lunar and impact spherule bed constraints.

Model Runs. The best developed dynamical model of the LHB, referred to here as the Nice model [2], suggests that late giant planet migration drove resonances inward across the primordial main asteroid belt region. We use this framework to explore a possible missing source of late LHB-era impactors.

The main belt's inner boundary is currently set by the ν_6 resonance at 2.1 AU; objects entering this resonance have their eccentricities pumped up to planet-crossing values in < 1 My. Prior to the LHB, however, the giant planets and their resonances were in different locations [3], with the only remaining natural boundary being the Mars-crossing zone. Accordingly, it is plausible that the main belt once had an inner extension, or E-belt, that stretched as far as ~ 1.7 AU.

To track E-belt objects over 4.56 Ga, we integrated four sets of test bodies (see also [1]). In the *pre-LHB phase*, Venus-Neptune were placed on nearly-circular orbits consistent with Nice model initial conditions [4], while Mars was given 4 eccentricity values, with the maximum osculating value $e_{\rm MAX}$ reaching 0.025, 0.05, 0.12, and 0.17. Each E-belt population was composed of 1000 test bodies with $a = 1.7$-2.1 AU and e, i chosen from main-belt-like probability distributions [5], with the proviso that no test bodies were initially placed on Mars-crossing orbits. We integrated them for 0.6 Gy.

In the *LHB phase*, we assumed the Nice model occurred and placed all planets on their current orbits. This mimics the jump that Jupiter/Saturn had to have during the LHB [4]. We assumed Mars' eccentricity also reached its current value at this time by secular resonant coupling between the terrestrial/giant planets during planet migration. The remaining test bodies were tracked for 4 Gy, with the survivors cloned $10\times$ once 90% of the initial population was lost.

E-Belt Depletion. Overall, only 10-20% of the initial E-belt was lost over the first 0.6 Gy, and those that did escape had high collision probabilities and low impact velocities with the planets (e.g., for the Moon, median impact velocities before/after the LHB were 9 and 21 km/s, respectively). Interestingly, this velocity jump, when put through crater scaling laws, is enough to explain an increase in lunar basins sizes found near the transition between the Pre-Nectarian and Nectarian-eras [6]. This change may mark the starting time of the LHB.

Once the LHB begins, the E-belt decays to nearly 1/1000 its initial size, with the survivors driven into the Hungaria asteroid region at high i between 1.8-2.0 AU [7]. This region, bracketed by resonances, is dynamically "sticky"; objects finding a way in often take a long time to come back out. This allows the E-belt to produce a extremely long-lived tail of terrestrial planet impactors. *Thus, the E-belt makes Hungaria asteroids!*

Scaling from the observed Hungarias, we estimate that the E-belt's population just prior to the LHB was ~ 0.2-0.8 times that of the current main belt size distribution. The highest values of 0.6-0.8, correspond both to a nearly-circular Mars and a population density that matches that of the pre-LHB main belt, namely $4\times$ the current main belt population between 2.1-3.25 AU [3,4,8].

E-Belt Impactors. Numerical results show that E-belt asteroids are ten times more likely to hit the Earth and Moon than typical main belt asteroids. Thus, even a relatively small destabilized population can potentially make numerous impactors. Accordingly, we predict the

E-belt makes, on average, 9-10 lunar basins, with the combined contributions of E- and main belt making 12-13 lunar basins. This outcome suggests the start of the LHB is near the twelfth youngest basin Nectaris. As a check on this prediction, we compared crater counts on Nectaris terrains to our expected crater populations and found an excellent match.

Fig. 1 shows the Earth/Moon impact profile for our best-fit run. The top lunar curve was scaled to produce 9 LHB-era lunar basins, as calculated above. If correct, the lunar LHB lasted 400 My, with the end set by Orientale (3.72-3.75 Ga [6,10]). This puts the start of the LHB at 4.12-4.15 Ga. We consider this reasonable because several big things were happening at this time: (i) Nectaris basin may be 4.12 Ga [11,12], (ii) most ancient Apollo rocks affected by impacts have ages between 3.7-4.1 Ga [e.g., 12,13], (iii) H chondrites, eucrites, and ureilites have few Ar-Ar shock degassing ages between 4.1-4.4 Ga and many between $\sim$ 3.3-4.1 Ga [e.g., 13,14], (iv) Martian meteorite AL84001 has a well-defined Lu/Hf age of 4.1 Ga [15], and (v) the young shergottites have unusual Pb-Pb ages that suggest their source region was disturbed $\sim$ 4.1 Ga [16].

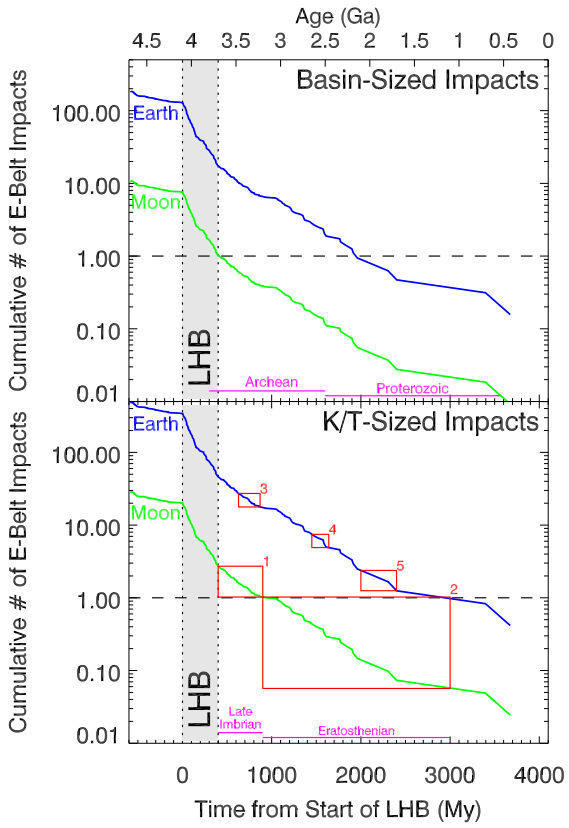

Figure 1. *The E-belt impactors that hit Earth/Moon and made basin-craters ($D > 300$ km) and K/T-sized craters ($D \sim 180$-300 km) over the last 4.6 Gy. During the Archean era, ~ 15 basins were produced on Earth. Boxes #1-#5 denote constraints described in text.*

To further test our model, we calculated the impact profile of K/T-sized craters formed on Earth/Moon after Orientale's formation. Models indicate comets and main belt asteroids are unlikely to make many K/T events at these times [2,5]. For the Late Imbrian era (**#1**; 3.7-3.2 Ga), there are 3 ± 2 such craters observed (i.e., Iridium, Humboldt, Tsiolkovskiy, with $D = 260$, 207, and 180 km, respectively), while for the Eratostenian era (**#2**; 3.2-1.0 Ga), there is 1 ± 1 observed (i.e., Hausen, with $D = 167$ km) [6]. Fig. 2 predicts 2 ± 1 and 1 ± 1 model K/T events should have taken place in these intervals, respectively, in agreement with observations.

On Earth, we predict that many tens of K/T-sized or larger events took place during the Archean-Proterozoic. These events are large enough that we can compare our model results to terrestrial spherule beds, a byproduct of such impacts that vaporize silicates and distribute melt droplets across the planet [17,18]. Observations indicate 10 ± 3 beds exist between 3.47-3.23 Ga (**#3**), 4 ± 2 beds exist between 2.63-2.49 Ga (**#4**), 2 ± 1 craters/beds exist between 2.1-1.6 Ga (**#5**), and 0 ± 1 crater/beds have yet been found between 1.6-0.6 Ga. Over the same time intervals, our model results are essentially identical: 9 ± 3, 3 ± 2, 1 ± 1, and 1 ± 1, respectively.

Implications. We predict that the terrestrial LHB produced $\sim$ 15 basins and $\sim$ 60 K/T-sized craters over the Archean and into the Proterozoic. Moreover, some of these impacts were likely Imbrium-sized [18]! The LHB tail likely produced the craters Vredefort (2.02 Ga) and Sudbury (1.85 Ga) [10]. Related impact profiles, scaled by collision probabilities and velocities, should also exist on Mercury, Mars, and possibly even Venus.

Impact cessation also produces eerie coincidences (e.g., the "Great Oxidation Event" [19] occurs once basin-sized impacts end at 2.5 Ga; the oceans enter into a Gy-long euxinic state [20] when all big impacts end at 1.85 Ga). Do connections exist? *The game is afoot!*

References. [1] Bottke *et al.* (2009) *LPSC* **41**, 1269. [2] Gomes *et al.* (2005) *Nature* **435**, 466. [3] Minton & Malhotra (2009) *Nature* **457**, 1109. [4] Morbidelli *et al.* (2010) *Astron. J* **140**, 1391. [5] Minton & Malhotra, (2010) *Icarus* **207**, 744. [6] Wilhelms (1987) *U.S. Geol. Surv. Prof. Pap. 1348*. [7] Warner *et al.* (2009) *Icarus* **204**, 172. [8] Bottke *et al.* (2010) *MAPS* **73**, 5152. [9] Bottke *et al.* (2007) *Icarus* **190**, 203. [10] Stöffler & Ryder (2001) *SSR* **96**, 9. [11] Warren (2005) *Treatise on Geochemistry* **1** 559. [12] Norman *et al.* (2010) *GCA* **74**, 763. [13] Bogard (1995) *MAPS* **30**, 244. [14] Swindle *et al.* (2009) *MAPS* **44**, 747. [15] Lapen *et al.* (2010) *Science* **328**, 347. [16] Bouvier *et al.* (2008) *EPSL* **266** 105. [17] Simonson and Glass (2004) *Ann. Rev. Earth. Planet* **32**, 329. [18] Lowe & Byerly *LPSC* **41**, 2563. [19] Kump (2008) *Nature* **451** 277. [20] Canfield (1998) *Nature* **396**, 450.

THE VESTAL CATACLYSM. B. A. Cohen, NASA Marshall Space Flight Center, Huntsville AL 35812 (Barbara.A.Cohen@nasa.gov).

Introduction: The currently operating Dawn mission shows asteroid 4 Vesta to be an extensively cratered body, with craters in a variety of morphologies and preservation states The crater size-frequency distribution for Vesta, modeled using the lunar chronology and scaled to impact frequencies modeled for Vesta, shows that both the north and south pole areas are ancient in age [1].

We have in our meteorite collection products from 4 Vesta in the form of the HED (howardite, eucrite, diogenite) meteorites. The HED parent body globally differentiated and fully crystallized by ~4.56 Ga; subsequently, the eucrites were brecciated and heated by large impacts into the parent body surface, reflected in their disturbance ages [2, 3].

Dawn images have also shown that Vesta is covered with a well-developed regolith that is spectrally similar to howardite meteorites [4, 5]. Howardites are polymict regolith breccias made up mostly of clasts of eucrites and diogenites, but which also contain clasts formed by impact into the regolith. Impact-melt clast ages from howardites extend our knowledge of the impact history of Vesta, expanding on eucrite disturbance ages and helping give absolute age context to the observed crater-counts on Vesta.

Howardite Impact-melt Clasts: We characterized texture, bulk composition, mineralogy, and ages of individual clasts within howardites EET 87513, QUE 94200, GRO 95574 and QUE 97001 in 100-µm thick, polished sections. Several clasts proved to be eucritic, but most were impact-melt clasts having a fine-grained, microporphyritic groundmass containing anhedral, relic mineral grains. The groundmass is usually too fine-grained to directly analyze the plagioclase or mafic portions. The relic clasts are dominated by plagioclase and pyroxene, with minor olivine, chromite, and other minerals. Pyroxene grains are typically homogeneous and unexsolved. Plagioclase has a wide range of compositions between typical eucrites and diogenites. Several clasts have symplectic textures with glassy areas. In these clasts, plagioclase can be significantly K-rich. The impact-melt clasts have bulk compositions ranging in between the eucrites and diogenites (Fig. 1), consistent with their interpretation as impact melt rocks made up of varying contributions of Vesta's two main lithologies.

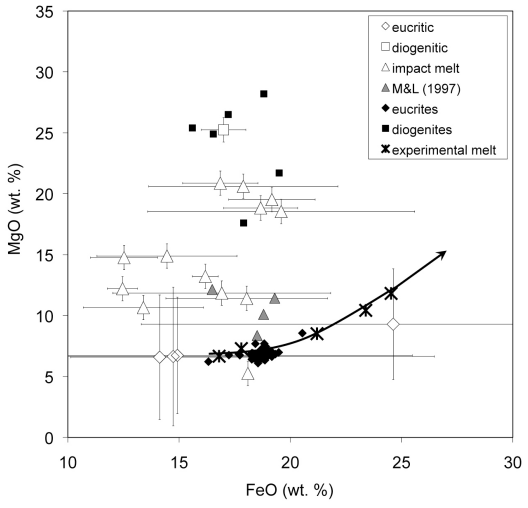

Fig. 1. The bulk composition of the impact-melt clasts is intermediate between eucrites and diogenites.

Samples were irradiated and step-heated using a CO_2 laser. Data were corrected for system blanks, decay time, and reactor-induced interferences. Resolution of cosmogenic and trapped argon components was attempted following [6, 7], but cosmogenic ^{36}Ar is not well-correlated with any specific component in these samples [3], so this correction was not pursued further. Most ages are reported from isochrons, which do not assume a trapped component; those with plateau ages assume a trapped contribution of zero and are therefore upper limits. Table 1 shows the new howardite ages, including the first impact-melt ages from HED meteorites. All of the new impact-melt ages fall between 4.0 and 3.5 Ga, and most are distinct from one another, meaning they sample different impact events on the surface of 4 Vesta.

Discussion: Our new impact-melt ages fall well within the age distribution of all HED impact-reset rocks, which features a short, intense spike at 4.48 Ga followed by a period of relative quiescence, then a ramping up of impact-reset ages between about 4.0 and

Table 1. Ages and types of samples in this study.

Sample	Type	Age (Ma)
A01	eucrite	3600 ± 300
A10	Impact melt	3330 ± 120
B5	eucrite	3200 ± 200
B11	breccia	3350 ± 60
B14	eucrite	2820 ± 190
B16	Impact melt	3560 ± 100
C14	eucrite	3540 ± 70
C15	Impact melt	3630 ± 130
C17	Impact melt	3960 ± 50
D01	Impact melt	3960 ± 30
D08	Impact melt	3720 ± 80
D11	Impact melt	3310 ± 130
D17	Impact melt	4000 ± 200
D19	Impact melt	3760 ± 150
D23	Impact melt	3600 ± 300

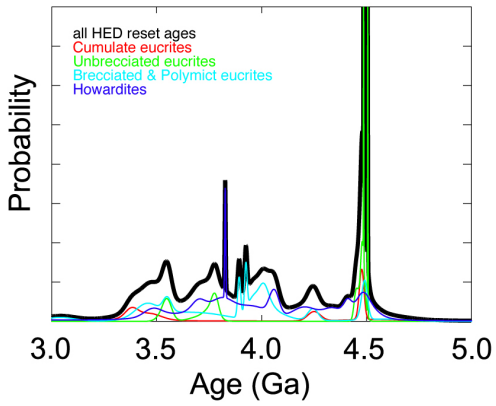

Fig. 2. Ideogram of Ar-Ar reset ages for HED meteorites, including 14 new ages.

3.5 Ga (Fig. 2). Bogard and Garrison [8] suggested that the early spike, largely contributed by unbrecciated eucrites, represents a single large impact into Vesta that caused widespread resetting and may have formed a secondary parent body, protecting the unbrecciated eucrites from further processing in the Vesta regolith.

Impact-reset ages in the HEDs are consistent with a quiescent period in the main belt, followed by increased activity in the period of the late heavy bombardment. However, this seems at odds with the observed crater distribution on Vesta, which shows a range of ages rather than a single resurfacing event. Rather, we suggest that the age distribution of HED meteorites only incompletely records the impact history of Vesta, because of the difficulty of resetting rock ages by collisions in the main belt.

Reset of argon-based ages is a diffusion-controlled process, where a combination of temperature and time is required to lose daughter Ar from the crystal lattice sites originally occupied by K cations. Eucrites (and howardites) contain K (and therefore Ar) primarily in pyroxene and plagioclase. Recent work on diffusion coefficients in these minerals [9, 10] permit a quick look at closure temperatures and diffusion rates in these minerals, which in turn constrains the conditions required to reset the age of these rocks.

Fig. 3 shows the time required to completely diffuse Ar (fully reset) through each mineral across different lengthscales. At elevated temperatures, plagioclase can diffuse Ar fairly rapidly, but pyroxene requires a very high temperature to fully reset, even on the single grain scale. At higher temperatures, complete melting occurs, which readily allows Ar diffusion and age reset. Temperatures in the range that enable significant diffusion over timescales of 1-100 years (fast cooling of a post-impact blanket) are relatively high, in the range of 1000°C.

Whether temperatures reach this high in the target rock is a strong function of the impact velocity. Typical impact velocities between objects in the main belt is about 5 km [11], which imparts far too little energy to raise the temperature of the target material above the closure temperature of typical eucrite minerals (300-400°C for plagioclase, 600-700°C for pyroxene). Of course, there is a velocity distribution, where some small fraction of impactors may achieve this high velocity, but these must be comparatively rare.

Our new impact-melt analyses deepen this story. In order to melt material on the surface of Vesta, an impact must have higher velocity still. The tail of the main belt velocity distribution doesn't stretch far enough to enable so much melt from so many different impact events spaced so closely in time. Therefore, we contend that these impact-melt clasts, and probably most of the impacts in this period, must be the result of highly velocitous impacts, possibly from an excited main belt (E-Belt) [12] or originating outside the main belt, as in the cometary flux of the Nice model [13]. Either way, howardite impact-melt clast ages record an unusual period of bombardment in the inner solar system beginning at around 4.0 Ga.

References: [1] Schenk, P.M., et al. (2011) *GSA Abstracts with Programs* **43**, 573. [2] Bogard, D.D. and D.H. Garrison (1993) *Meteoritics* **28**, 325-326. [3] Bogard, D.D. and D.H. Garrison (2003) *MAPS* **38**, 669-710. [4] Mittlefehldt, D.W., et al. (2011) *GSA Abstracts with Programs* **43**, 574. [5] McSween, H.Y., et al. (2011) *Geological Society of America Abstracts with Programs* **43**, 572. [6] Garrison, D., S. Hamlin, and D. Bogard (2000) *MAPS* **35**, 419-429. [7] Swindle, T.D., et al. (2009) *MAPS* **44**, 747-762. [8] Bogard, D.D. and D.H. Garrison (1999) *MAPS* **34**, 451-473. [9] Cassata, W.S., P.R. Renne, and D.L. Shuster (2009) *GCA* **73**, 6600–6612. [10] Cassata, W.S., P.R. Renne, and D.L. Shuster (2011) *EPSL* **304**, 407–416. [11] Farinella, P. and D.R. Davis (1992) *Icarus* **97**, 111-123. [12] Bottke, W.F., et al. (2010). *LPSC* **41**, 1533. [13] Gomes, R., et al. (2005) *Nature* **435**, 466-469.

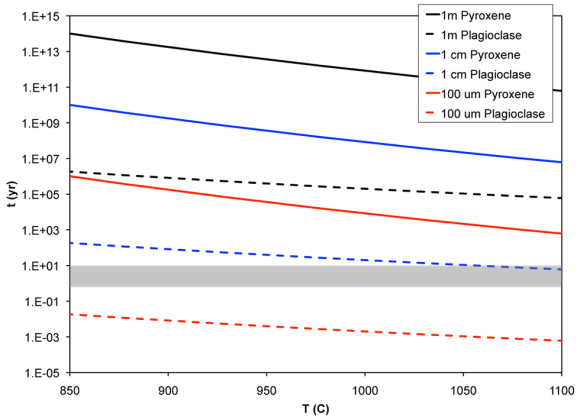

Fig. 3. Temperature-time curves for complete Ar diffusion over different length scales.

3.9 BILLION YEARS AGO AND THE ASTEROID BELT. C. M. Corrigan[1], B. A. Cohen[2], Kara Hodges[3], and Nicole Lunning[1], [1]Smithsonian Institution, NMNH, 10th St and Constitution Ave NW, Washington D.C., 20560, USA; corriganc@si.edu, [2]NASA Marshall Space Flight Center, Huntsville, AL, USA. barbara.a.cohen@nasa.gov. [3]Michigan Technological University, Department of Geological Science and Engineering, Houghton, MI, USA.

Introduction: Melted materials from the Moon and other meteorites show a peak in ages at 3.9 billion years [1,2,3,4]. For the Moon, this phemonenon has resulted in the highly debated topic of the lunar cataclysm [5,6], in an attempt to understand whether this 3.9 Ga peak is just the end of a steep decrease in impact cratering in which earlier-formed impact melts were destroyed by later events [6], or if the absence of materials older than 3.9 Ga indicated that a terminal cataclysm occurred at that time, resetting the lunar isotopic clock [3,4,5].

A series of papers [7-9] has postulated that the orbits of the gas giants evolved early in Solar System history until Jupiter and Saturn crossed the 2:1 mean motion resonance, increasing eccentricities of the planets. As a consequence, Uranus and Neptune moved outward rapidly, scattering icy planetesimals that would have existed beyond the orbits of the gas giants. At 878 Ma years after Solar System formation, planetesimals scattered throughout the inner Solar System, perhaps explaining the late heavy bombardment. Consistent with the scattering of material into the inner Solar System, [10,11] have postulated that the widespread ~3.5-4.0 Ga younger ages among asteroidal meteorites suggest a Solar System-wide disturbance.

Ordinary Chondrites: The concept of the late heavy bombardment and the possible bombardment of the entire inner solar system (and the lack of measurements made on ordinary chondrites to this end) is the driving force behind this study to examine ordinary chondrite impact breccias/melts within the Antarctic Meteorite collection. With 20,000 meteorites in the collection thus far (and approximately 90% of those being ordinary chondrites), the United States Antarctic collection provides a vast resource for searching out ordinary chondrite impact melt rocks, impact breccias, and clasts within these. While classification of the Antarctic meteorites has not long distinguished impact breccias, it is now being recorded, when obvious in the small chips sent to the Smithsonian for classification, and/or the larger meteorites sent for long-term storage. Binns [13] studied large ordinary chondrites at the Natural History Museum in London and found that ~20% of all ordinary chondrites were breccias and that brecciation is often revealed during the study of large masses of the meteorite.

To this end, we have begun a study of the ordinary chondrite impact breccias within the U.S. Antarctic collection. We have focused our research on meteorites that are over 500g in weight, in order to maximize the ability to find impact melt clasts far enough from the fusion crusted surface and weathering to provide reliable age dates using Ar-Ar techniques. This study follows that of [12] who recognized that many large Antarctic masses previously described as unbrecciated, are in fact, ordinary chondrite regolith breccias containing a varietly of clasts, some of which are regolith derived. In particular, [12] focused on MAC 87302 (and, it turned out, breccias paired with it), which is proving to contain numerous, large melt clasts, some of variable compositions relative to the classification of the host meteorite. Here we are focusing on L and LL chondrites, primarily, as there are fewer measurements made on impact melts within these meteorites than in H chondrites or HEDs [10, 14, 15], and the H chondrite parent body likely experienced a large break-up event, though we are not necessarily excluding H chondrites.

Figure 1 *- Plane polarized image of PCA 02071, melt clast circled. (FOV = 2 cm across)*

To date, in addition to further analyses of MAC 87302 pairing group, 12 ordinary chondrite impact breccias (Table 1) have been selected for this study. Impact melt clasts have been identified within these meteorites (Figure 1). These impact melt clasts have been analyzed with the FEI Nova NanoSEM Field Emission SEM and the JEOL JXA 8900R electron microprobe at the Smithsonian Institution. Backscattered electron mosaics and elemental maps (Figure 2) have been created for each impact melt clast large

enough to potentially provide a successful Ar-Ar date (Table 1). These meteorites are currently being prepared for shock analysis, to ensure that the melt clasts reached high enough temperatures to reset the Ar isotopic systematics.

Table 1. *Meteorite breccias identified thus far.*

Name	Type	Melt clasts IDed
MAC 87302 prs	L4 breccia	
MET 01002	L5 breccia	1
MET 01004	LL5 breccia	2
MET 01052	L5 breccia	1
MIL 99303	H5 breccia	1
MIL 07010	L inpact melt	-
PCA 02070	H5 breccia	1
PCA 02071	L5 breccia	2
PCA 02072	LL6 breccia	1
PRE 95400	H5 breccia	3
QUE 99012	H4 breccia	1

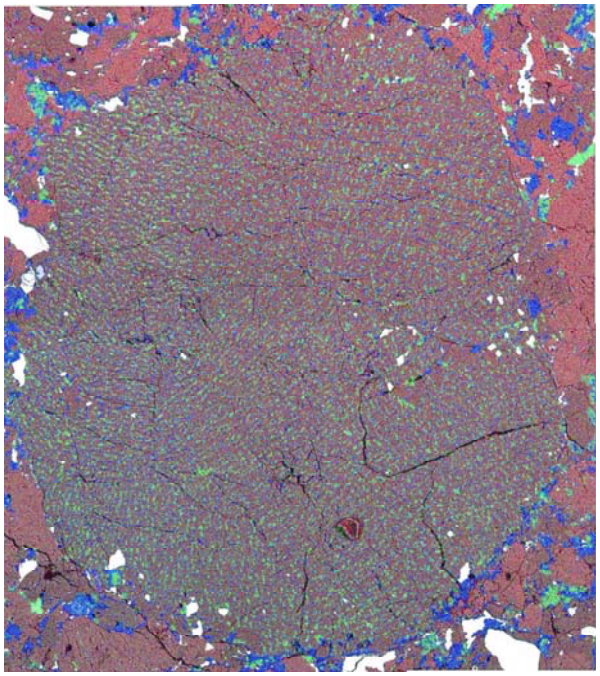

Figure 2 *– Elemental Map of Melt Clast in PRE 95400. Blue = Aluminum, Red = Magnesium, and Green = Calcium (FOV = 600 microns across)*

References: [1] Turner et al. (1973), *Proc. 4th LPSC*,1889-1914. [2] Tera et al. (1974), *EPSL* 12, 19-35. [3] Kring and Cohen (2001) *JGR* 107, doi: 10.1029/2001JE001529. [4] Cohen et al. (2005), *MAPS* 40, 755-777. [5] Ryder G. et al. (2002) *JGR* 107, 6-1. [6] Hartmann (2003) *MAPS* 38, 579-593. [7] Tsiganis et al. (2005) *Nature* 435, 459. [8] (2005) *Nature* 435, 462. [9] Morbidelli et al. (2005) *Nature* 435, 466. [10] Kring and Cohen (2002) *JGR* 107, 4.1-4.6. [11] Bogard and Garrison (2003) *MAPS* 38, 669-710. [12] Welzenbach L.C. et al., 2005, *LPSC XXXV*, #1425. [13] Binns R.A., 1967, *EPSL* 2, 23-28. [14] Swindle et al. (2008) *MAPS* 44, 762. [15] Wittmann (2010) *JGR* 115, doi: 10.1029/2009JE003433. [16] LaCroix and McCoy (2007) *LPSC XXXVIII* #1601.

Are Apollo Zircons Witness to a Lunar Cataclysm? C. A. Crow[1], K. D. McKeegan[1], J. D. Gilmour[2], S. A. Crowther[2], D. J. Taylor[1], [1]Earth and Space Sciences Department, University of California Los Angeles, Los Angeles, CA (ccrow@ucla.edu), [2]SEAES, University of Manchester, Manchester, UK

Introduction: Based on Pb isotope signatures, Tera et al. first suggested that the Moon experienced a period of heightened bombardment around 3.9 Ga [1]. It is generally agreed that there was a steep decline in impact frequency and impactor size after this time, but there remains controversy over whether the decline was preceded by a marked increase or if the impact rate at ~3.9 Ga is merely the tail end of a steadily decreasing flux since the Moon's formation. The hypothesis of a lunar cataclysm, a sharp spike in impacts, is based on two significant findings from Apollo samples. First is the lack of impact melts before ~4.0 Ga [2] and second is a peak in the distribution of Ar-Ar ages around 3.9 Ga [1]. The ages of the lunar impact basins have also been cited in support of a lunar cataclysm, with most having formed between 3.9 and 3.85 Ga except Orientale which formed later [3], but these ages themselves are controversial. Critics of the cataclysm hypothesis argue that large basin forming impacts would have destroyed earlier impact melts and reset Ar-Ar ages saturating the distribution with 3.9 Ga ages [4,5]. The timing and nature of a lunar cataclysm have importance beyond the Moon because it places constraints on dynamical models of the formation and evolution of the early solar system [6].

To investigate early lunar chronology and bombardment, samples are needed that are older than the proposed cataclysm at 3.9 Ga. Zircons are excellent for this study for multiple reasons. First, zircons are ideal for measuring U-Pb and Pb-Pb ages because they have very low initial Pb resulting in high precision measurements. Second, the distribution of crystallization ages of lunar zircons spans the period from ~3.9 Ga to ~4.4 Ga [7,8,9] satisfying the criterion that they be older than the proposed cataclysm. Third, zircons incorporate both U and Pu, so Xe degassing ages can be determined on the same crystals for which Pb-Pb crystallization ages are measured [10].

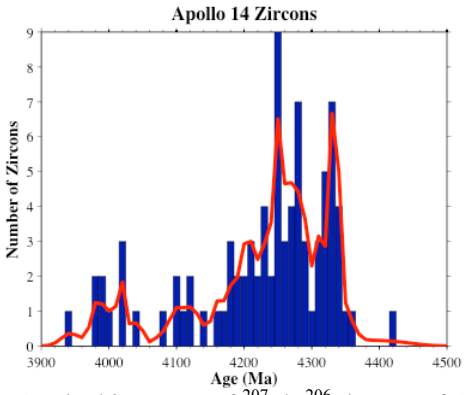

Figure 1: The histogram of ^{207}Pb-^{206}Pb ages of Apollo 14 zircons spans from ~3.95 to ~4.43 Ga, overplotted with the age density distribution. All zircons have crystallization ages that predate the proposed lunar cataclysm making them candidates for investigating early lunar bombardment history. Ages from [8,11].

Method: ^{235}U, ^{238}U and ^{244}Pu all produce significant fission Xe. Fission of ^{235}U is induced by thermal neutron bombardment whereas ^{238}U and ^{244}Pu may fission spontaneously. The relative abundances of these parents can be determined by comparing the abundances of the Xe isotopes in a sample. If the absolute abundance of U can be measured, and assuming the solar system's initial ^{244}Pu/^{238}U = 0.008 [12], the U-Xe and Pu-Xe degassing ages can be determined. The common method for measuring U-Xe ages involves irradiating the samples to determine the U absolute abundance. This method has been demonstrated on terrestrial Archean zircons from Jack Hills, Australia [13]. For the initial data reported here, we have not irradiated the samples due to concern that we would not be able to deconvolve the Xe isotope contributions of the irradiation in a reactor and potential exposure to secondary neutrons from cosmic rays that the samples experienced on the surface of the Moon. We are currently developing a method to measure absolute abundances of uranium in the zircons prior to Xe isotopic measurements.

Results: We measured Xe isotopic abundances of three large (~300 μm) individual zircons separated from Apollo 14 rocks 14321 and 14305 using the University of Manchester Refrigerator Enhanced Laser Analyser for Xenon (RELAX) [14, 15]. These rocks have cosmic ray exposure ages of 24 Ma [16, 17] and 27.6 Ma [18], respectively. Two samples produced sufficient xenon for precise xenon isotope ratios to be

determined, the other did not either due to low U/Pu concentrations or young degassing ages. The Pb-Pb crystallization ages of the two samples are 4.3 Ga (BZ2) and 4.2 Ga (BZ3). The results of the Xe analysis are shown in Figure 2. The corners of the ternary diagram represent the xenon isotopic compositions corresponding to fission of ^{244}Pu, ^{238}U and ^{235}U (neutron induced).

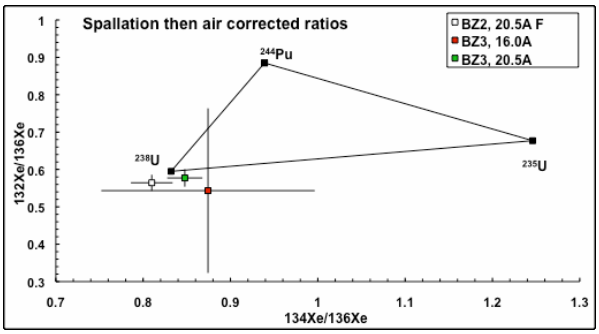

Figure 2: *Results of Xe isotopic analysis for 2 large lunar zircons with blank, spallation, and air corrections. Both BZ2 and BZ3 yielded high temperature releases consistent with spontaneous fission of 238U. Apparent 244Pu fission xenon in small amount of xenon released at low temperature from BZ3 is attributable to a small amount of associated atmospheric xenon*

All releases from the two samples are consistent with the ^{238}U end member on the ternary diagram suggesting that the there is little or no Xe contributed from ^{244}Pu fission and little or no contribution from fission of ^{235}U induced by cosmic ray secondary neutrons. The upper limit on the proportion of ^{244}Pu fission xenon corresponding to our data corresponds to a closure age to xenon loss of around 3.6-3.7 Gyr before the present (assuming a Pu/U ratio at zircon formation corresponding to an unfractionated reservoir produced from intial solar system material with Pu/U = 0.008).

The contrast between these data and data from terrestrial Hadean zircons is striking. Since we do not measure any plutogenic Xe, the zircons must have experienced complete Xe loss sometime after all the Pu had decayed, ~400 Myr after the formation of the Moon. Since we have not yet measured the U absolute abundance, we don't yet know the retention age of uranium-derived Xe. We are in the process of developing a technique to determine U-Xe ages in unirradiated lunar zircons and plan to extend this study to regolith samples from other Apollo landing sites.

References: [1] Tera F. et al. (1973) *LPS IV*, 723–725. [2] Ryder G. (1990) *Eos 71, 313*, 322–323. [3] Stöffler D. and Ryder G. (2001) *Space Sci. Rev., 96*, 9–54. [4] Hartmann W.K. (1975) *Icarus, 24,* 181– 187. [5] Grinspoon D.H. (1989) *Ph.D. thesis*, University of Arizona, Tucson, Section 2, 209 pp. [6] Morbidelli A. et al. (2001) *Meteoritics & Planet. Sci., 36*, 371-378. [7] Meyer C. et al. (1996) *Meteoritics & Planet. Sci., 31*, 370 – 387. [8] Taylor D. J. et al. (2009) *Earth & Planet. Sci. Letters, 279*, 157-164. [9] Nemchin A. A. (2008) *Geoch. Cosmochem. Acta, 72*, 668-689. [10] Turner G. et al. (2007) *Earth & Planet. Sci. Letters, 261*, 491-499. [11] Crow C. A. et al. (2011). *Metoritics & Planet. Sci., 46*, A52, Abstract. [12] Turner G. et al. (2005) AGU 86 Fall Meet. Suppl., Abstract V21F-05 [13] Turner G. et al. (2004) *Science, 306*, 89-91. [14] Gilmour J. D. et al. (1994) In: Matsuda, J. (Ed.) *Noble Gas Geochemistry and Cosmochemistry*. Terra Scientific Publishing. [15] Crowther S. A. et al. (2008) *Journal of Analytical Atomic Spectrometry*, 23, 938-947. [16] Burnett D. S. et al. (1972) LS III, 105-107, Abstract. [17] Lugmair G. W. and Marti K. (1972) Proc. 3rd Lunar Sci. Conf., 1891-1897. [18] Eugster O. et al (1984) Proc. 14th Lunar Planet. Sci. Conf. in J. Geophys. Res. 89, B498-B512.

LHB WAS CAUSED BY MARS-CROSSERS, AND IT WAS NOT ALL THAT HEAVY. Matija Ćuk[1, 2], [1] SETI Institute, Carl Sagan Center, 189 N Bernardo Ave, Mountain View, CA 94043, [2] Harvard University, Department of Earth and Planetary Sciences, 20 Oxford St, Cambridge, MA 02138.

Abstract: The Moon has suffered intense impact bombardment ending at 3.85 Gyr ago, and this bombardment probably affected all of the inner Solar System. Basin magnetization signatures and lunar crater size-distributions indicate that the last episode of bombardment at about 3.85 Gyr ago was less extensive than previously thought. We explore the contribution of the primordial Mars-crosser population to early lunar bombardment. We find that Mars-crosser population initially decays with a 80-Myr half-life, with the long tail of survivors clustering on temporarily non-Mars-crossing orbits between 1.8 and 2 AU. These survivors decay with half-life of about 600 Myr and are progenitors of the extant Hungaria asteroid group in the same region. We estimate the primordial Mars-crosser population contained about 0.01-0.02 Earth masses. Such initial population is consistent with no lunar basins forming after 3.8 Gya and the amount of mass in the Hungaria group. As they survive longer and in greater numbers than other primordial populations, Mars-crossers are the best candidate for forming the majority of lunar craters and basins, including most of the Nectarian system. However, this remnant population cannot produce Imbrium and Orientale basins, which formed too late and are too large to be part of a smooth bombardment. We propose that the Imbrian basins and craters formed in a discrete event, consistent with the basin magnetization signatures and crater size-distributions. This late "impactor shower" would be triggered by a collisional disruption of a Vesta-sized body from this primordial Mars-crossing population [1] that was still comparable to the present-day asteroid belt a 3.9 Gya. This tidal disruption lead to a short-lived spike in bombardment by non-chondritic impactors with a non-asteroidal size-frequency distribution, in agreement with available evidence. This body ("Wetherill's object") also uniquely matches the constraints for the parent body of mesosiderite meteorites. We propose that the present-day sources of mesosiderites are multi-km-sized asteroids residing in the Hungaria group, that have been implanted there soon after the original disruption of their parent 3.9 Gyr ago.

Further information: The preprint of the detailed paper (under review for Icarus) can be found at:
www.fas,harvard.edu/~cuk/papers/chronology.pdf

References: [1] Wetherill G. W. (1975) LPSC *Proceedings, 6,* 1539–1561.

RESONANCES AND THE ANGULAR MOMENTUM OF THE EARTH-MOON SYSTEM. Matija Ćuk[1, 2], Sarah T. Stewart[2], [1] SETI Institute, Carl Sagan Center, 189 N Bernardo Ave, Mountain View, CA 94043, [2] Harvard University, Department of Earth and Planetary Sciences, 20 Oxford St, Cambridge, MA 02138.

Lunar Formation Problems:

1. The Moon appears to be derived from Earth's mantle, but Earth was never spinning fast enough to lose material to orbit.

2.The Moon has significant orbital inclination, but should have none.

3. The impactor must have had very low v_{inf} to form the Moon

4. Earth's post-giant-impact obliquity was low, but it should have been random.

Our Solution:

We simulated lunar tidal evolution starting with a fast-spinning Earth, including the interaction between Earth's core and the
Moon. We find that multiple resonances of the Moon with both the Sun and Earth's core drained angular momentum from the system. Resonances also tilted Moon's orbit and lowered Earth's tilt. If post-giant-impact Earth was spinning very fast, the Moon could form from Earth's mantle in an impact-triggered fission.

Moon-Sun Resonances: The Moon appears to be made from Earth's mantle material [1], while the Giant Impact theory predicts that the Moon was derived from the impactor [2]. It has been suggested that an initially faster spinning Earth could explain this discrepancy [3], but the system would later need to lose excess angular momentum (AM).

Here we explore the possibility that the early Earth had faster spin and higher obliquity than predicted by AM conservation. We made a symplectic integrator based on work by Touma and Wisdom [4, 5, 6, 7] that includes rotating Earth (mantle and core), the Moon and the Sun, with both tidal and CMB dissipation. Tidal Q values for Earth and the Moon were set to ~100. Initial spin period of Earth was 2.5 hr and initial obliquity was 40°.

We find the Moon meeting "tiltover resonance" $[2\lambda_{Sun}+\Omega_{Moon}-3\Omega_{Sun}]$ at 5.9 Earth radii (R_E) , which excites lunar inclination to 2°.

At 6.8 R_E the Moon gets captured in the evection resonance $[2\lambda_{Sun}-2v_{Moon}]$. This capture is more robust than in [6], as faster Earth rotation (larger J_2) moves the resonance out. At 6.9 R_E tidal evolution is slower and solar perturbations stronger than at 4.5 R_E [6]. Eccentricity first rises and then levels out as the Sun drains AM from Earth. Eventually the lock is broken and the Moon's outward tidal evolution resumes.

Right after evection, the Moon passes through a mixed eccentricity-inclination resonance $[2\lambda_{Sun}-2v_{Moon}+W_{Moon}-W_{Sun}]$ ("eviction" in [6]) which increases lunar inclination to 2.5°.

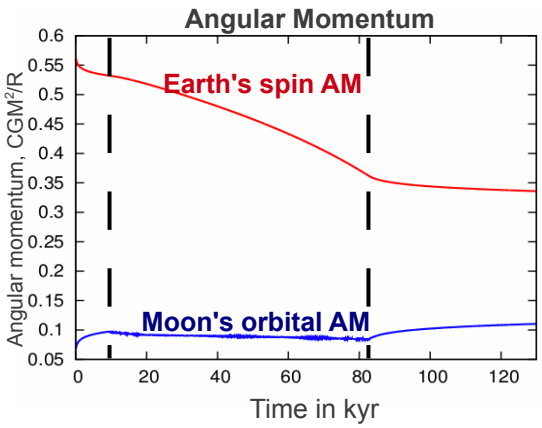

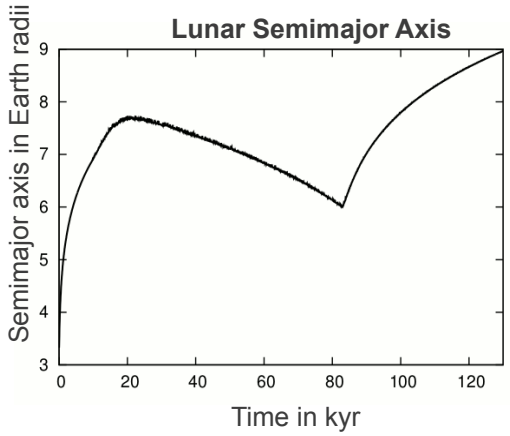

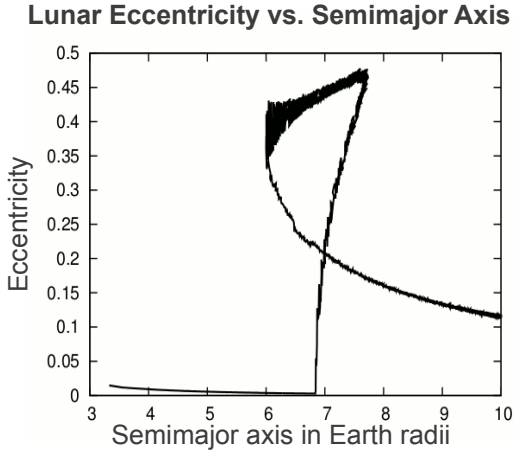

Earth's Core-Moon Resonances: Early Moon-Sun resonances always leave the Moon with inclination too low and Earth with obliquity and spin rate too high to match the present. However, additional resonances between the Moon's mean motion and the Free Core Nutation (FCN) of Earth are likely. Since early Earth's mantle was not solid, FCN must have swept a range of periods during mantle solidification (assumed to happen over ~10 Myr), trapping the Moon in an eccentric FCN resonance $[\lambda_{Moon}-\nu_{Moon}+W_{Core}-W_{Moon}]$. FCN resonance lowers Earth's obliquity and increases lunar free inclination and eccentricity. Simulating FCN resonance is very expensive, and only the initial capture is shown. We expect that the Moon will exit the resonance once it reaches the present angular momentum, but with e=0.45, which is lowered by tides and planetary resonances [8].

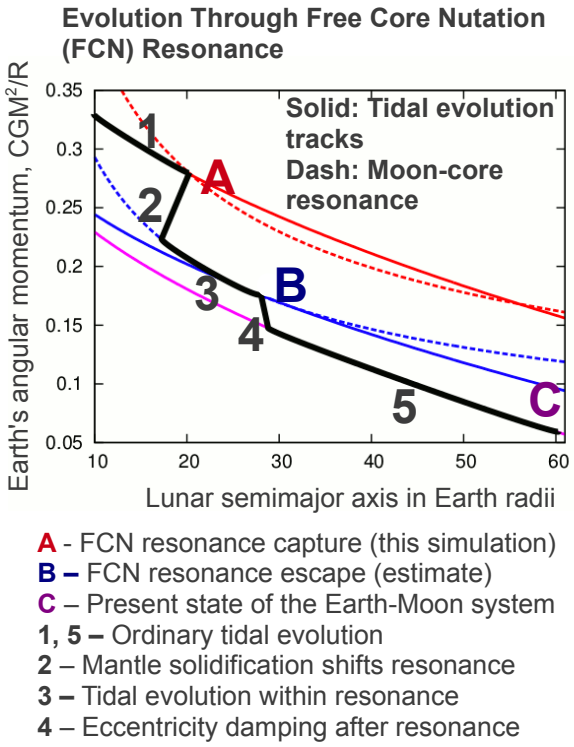

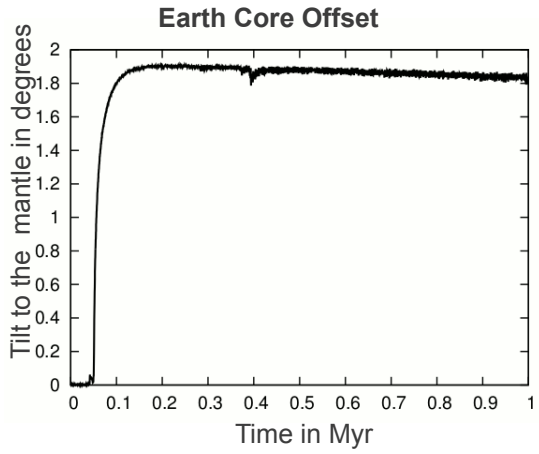

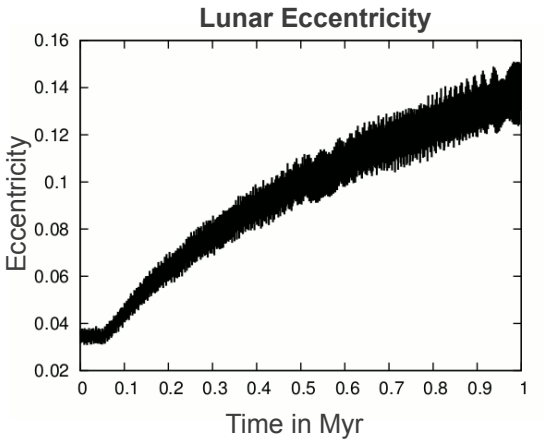

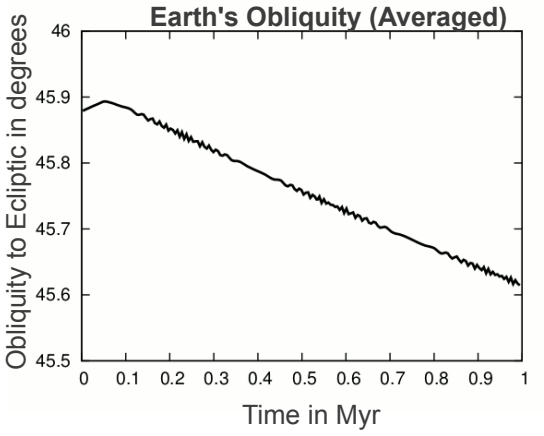

References: [1] Touboul, M., et al. (2007). *Nature* 450, 1206-1209. [2] Canup, R. M. (2004). *ARA&A* 42, 441-475. [3] Melosh, H. J. (2009). *MPS Sup.* 72, 5104. [4] Touma, J., Wisdom, J. (1994). *AJ* 108, 1943-1961. [5] Touma, J., Wisdom, J. (1994). *AJ* 107, 1189-1202. [6] Touma, J., Wisdom, J. (1998). *AJ* 115, 1653-1663. [7] Touma, J., Wisdom, J. (2001). *AJ* 122, 1030-1050. [8] Ćuk, M (2007). *Science* 318, 244-244.

Planetary Atmospheres during an Enhanced Bombardment

Detlef de Niem[1], Ekkehard Kührt[1], Alessandro Morbidelli[2], Uwe Motschmann[1,3], [1]DLR Institute of Planetary Research, Rutherford Str.2, D-12489 Berlin, Germany (detlef.deniem@dlr.de), [2]Observatoire de la Côte d'Azur, CNRS, BP 4229, 06304 Nice Cedex 4, France, and [3]Institute of Theoretical Physics, Technical University of Braunschweig, Mendelssohnstrasse 3, D-38106 Braunschweig, Germany

Hadean Earth lacks a clear record from a long-lasting or late heavy bombardment enduring more than ∼600 million years after its formation. Direct evidence comes from the Moon, more specifically from ages recorded in lunar samples returned by the Apollo astronauts [14]. The geological record of large lunar impact basins provides an estimate of the amount of material contemporaneously striking the Earth [9], suggesting a top-heavy size frequency distribution (SFD) of impactors [14, 6, 3]. Rare impacts of very large objects dominated erosion or accumulation of the atmospheres.

Because of the 'statistics of low numbers' consequences as arising in the Nice model [5], for example, have to be found with the help of Monte Carlo simulations rather than with differential equations such as [15]. As a byproduct this allows to compare formation ages of lunar basins arising in different scenarios. The nature of the impactors – asteroidal or cometary – is much debated [6, 5, 3] leading to rather different end-members in terms of planetary atmospheres following the bombardment era. Whereas impact velocities and probabilities are taken to correspond to dynamical simulations, SFDs are fit from models to observations of modern main belt asteroids (MBAs) [2] and Kuiper belt objects (KBOs). Size distributions are the product of a collisional evolution that has been more vigorous at times of a more massive population [3]. Highly simplified physical models for the survival and escape of atmophile gases [13, 12, 1, 4] are compared with results of hydrocode simulations [11, 10]. [11, 10] also provide small-size limits for the objects contributing to atmospheric erosion that are useful to define a reasonable interval of sizes in Monte Carlo runs however care is necessary when this is adapted to the conditions of a thin Martian atmosphere. Scaling properties of the quite different physical models with impactor and target planet/atmospheric parameters are analyzed before implementing them into the Monte Carlo code.

Interesting is to compare at least the Earth and Mars. We show consequences for Mars and the Earth under widely varying assumptions for the nature of impactors [8] and study the atmospheric response at the large-size end of the impactor SFD during a terrestrial LHB with an extented version of our previous multi-material method [7] adapted to spherical coordinates.

We find that accumulation dominates over erosion of atmospheres for the velocity distribution typical in the Nice model and moderate assumptions about volatile content of impactors. Net erosive behaviour is observed only for a bombardment by dry MBAs containing less than about 0.2% by mass CO+CO_2, in the case of the Earth whereas a significant contribution by KBOs will accumulate massive atmospheres equivalent to several bars unless these objects are dispersed or degassed on their way to the inner solar system. Consequences for Mars are similar despite the lower escape speed of this planet however the possibility of a significant atmospheric 'late veneer' depends on the ages of the large martian impact basins.

Acknowledgements: This research has been supported by the Helmholtz Association through the research alliance "Planetary Evolution and Life".

References

[1] T. J. Ahrens, *Annu. Rev. Earth Planet. Sci.* **21**, 525-555 (1993).

[2] W. F. Bottke, D. D. Durda, D. Nesvorny, R. Jedicke, A. Morbidelli, D. Vokrouhlicky, H. Levison, *Icarus* **175**, 111-140 (2005).

[3] W. F. Bottke, H. F. Levison, D. Nesvorny, L. Dones, *Icarus* **190**, 203-223 (2007).

[4] H. Genda, and Y. Abe, *Icarus* **164**, 149-162 (2003).

[5] R. Gomes, H. F. Levison, K. Tsiganis, A. Morbidelli, *Nature* **43**, 466-469 (2005).

[6] H. F. Levison, L. Dones, C. R. Chapman, S. A. Stern, M. J. Duncan, and K. Zahnle, *Icarus* **151**, 286-306 (2001).

[7] D. de Niem, E. Kührt, U. Motschmann, *Computer Phys. Comm.* **176**,170-190 (2007)

[8] D. de Niem, E. Kührt, A. Morbidelli, U. Motschmann *Icarus*, (submitted) (2011).

[9] G. Ryder, *J. of Geophys. Res.* **107, No E4**, 5022, 1-13 (2002).

[10] V.V. Shuvalov, *Meteoritics and Planetary Sci.* **44, No 8**, 1095-1105 (2009).

[11] V. V. Svetsov, *Solar System Research* **41, No 1**, 28-41 (2007).

[12] A. M. Vickery, and H. J. Melosh, *Geol. Soc. Am. Spec. Pap.* **247**, 289-300 (1990).

[13] J. C. G. Walker, *Icarus* **68**, 87-98 (1986).

[14] G. W. Wetherill, *Proc. Lunar Sci. Conf.* **6th**, 1539-1561 (1975).

[15] K. Zahnle, J. B. Pollack, and D. Grinspoon, *Icarus* **95**, 1-23 (1992).

STRATIGRAPHY, SEQUENCE, AND CRATER POPULATIONS OF LUNAR IMPACT BASINS FROM LUNAR ORBITER LASER ALTIMETER (LOLA) DATA: IMPLICATIONS FOR THE LATE HEAVY BOMBARDMENT. C.I. Fassett[1,2], J.W. Head[2], S.J. Kadish[2], E. Mazarico[3], G.A. Neumann[3], D.E. Smith[3,4], M.T. Zuber[4]. [1]Dept. of Astronomy, Mt. Holyoke College, South Hadley, MA 01075, [2]Dept. of Geological Sciences, Brown University, Providence, RI 02912, [3]Solar System Exploration Division, NASA/GSFC, Greenbelt, MD 20771, [4]Department of Earth, Atmospheric, and Planetary Sciences, Massachusetts Institute of Technology, Cambridge, MA 02139. (cfassett@mtholyoke.edu).

Introduction: New measurements of the topography of the Moon from the Lunar Orbiter Laser Altimeter (LOLA)[1] provide an excellent basemap for analyzing the large crater population ($D \geq 20$ km)of the lunar surface [2, 3]. We have recently used this data to calculate crater size-frequency distributions (CSFD) for 30 lunar impact basins, which have implications for their stratigraphy and sequence. These data provide an avenue for assessing the timing of the transitions between distinct crater populations characteristic of ancient and young lunar terrains, which has been linked to the late heavy bombardment (LHB). We also use LOLA data to re-examine relative stratigraphic relationships between key lunar basins.

Method: We derive the CSFD for each basin by mapping preserved basin-related materials (the region proximal to and within the basin rim that has not been resurfaced by volcanism or other processes). We use a buffered area correction and include craters which are superposed on the basin but which are centered outside the count region [e.g., 4] This technique slightly expands our effective count area, since large craters subtend more area than small ones. It also allows exclusion of resurfaced regions from the mapped count area without losing information about craters superposed on the edge of basin material.

For crater data, we start with the catalog of lunar craters ≥20 km in diameter from LOLA data [2,3]. We then re-examined each basin using the 64 ppd LOLA DTM and shaded relief to systematically search for additional craters beyond the global database. In total, a modest number of additional craters were found (12%); these are generally small (<40 km) and degraded. Crater measurement are made with CraterTools [5]; all areas and diameters are computed using equal area map projections.

Stratigraphy: Our measurements provide a test of the widely-used Wilhelms [6] sequence of lunar basins. There is strong qualitative agreement between this earlier sequence and our new measurements. However, there are substantial quantitative differences in the crater densities we observe, particularly for older basins. For example, the N(20) (# of craters ≥20 km normalized to an area of 10^6 km^2) we derive for the Nectaris basin is 135±14 compared to Wilhelms's 79±14. This difference has implications for the cratering history of the Moon and the crater frequency of the Pre-Nectarian/Nectarian boundary: Wilhelms's data [6] would imply the Moon had ~1900 impacts ≥20 km between Nectaris and Imbrium, whereas our data would suggest that ~4000 such craters formed.

Impactor Populations and the LHB: There has been a long debate in lunar science about whether heavily-cratered highlands records a distinct population of impactors from the lunar maria [7,8,9,10,11]. Measurements of the CSFDs of the highlands and mare imply that the highlands have a lower ratio of ~20-40 km craters to ~80-100 km craters than the mare [9; see also 2]. This difference is statistically significant at 96% confidence when applying the two-sample Kolmogorov-Smirnov (K-S) test to their CSFDs.

This observation does not guarantee that the difference in CSFDs is a result of a shift in the impactor populations. An alternative is geologic processes such as volcanism or repeated cratering preferentially removed small craters on ancient surfaces in a manner that resulted in the observed change [10]. Although possible, this hypothesis seems less likely given that a similar shift in CSFDs is observed on Mercury [9, 12] and Mars [9] to what is observed on the Moon. Given their distinct geologic histories, there is no reason that crater removal on each planet should be similar.

Strom et al. [9] propose that the shift in crater populations is related to the LHB. They note that the early population (Pop. 1) is similar to what would be expected from direct delivery of a collisionally-evolved population like the Main Asteroid Belt, and the younger population (Pop. 2) matches well with the Near-Earth Objects, which have a 'flatter' shape on an R-plot than Population 1 and are delivered via a more size-selective process [13].

Our measurements of basin CSFDs allows us to examine when the hypothesized transition between populations occurred. We examine this change by aggregating the statistics of basins from a given period, since counting statistics of individual basins alone are insufficient to assess population differences. We combine the crater counts and areas for the Imbrian basins (including Imbrium; aggregate N(20) of 22±3), the Nectarian basins (including Nectaris; aggregate

N(20) of 110±5), and Pre-Nectarian basins (excluding SPA to avoid it dominating the statistics; N(20)=188±7).

These aggregated data imply that both the Imbrian-aged basins and the Nectarian-aged basins are consistent with the flatter Population 2 (more mare-like) shapes (Fig. 1). The K-S test suggests that the Pre-Nectarian and Nectarian-aged basins are distinct from each other at the 94% confidence level.

These observations are surprising, since the transition from Population 1 to 2 has previously been linked to the transition from the LHB population to the modern population [9], and the basins formed during the Nectarian are commonly assumed to be part of the Late Heavy Bombardment. Moreover, because of the high crater flux during this time period, 65-75% of the craters that we measure on the Nectarian basins actually formed during the Nectarian period. If Population 1 dominated at that time, we would expect to see its signature in the Nectarian basin curve. Instead, the impactor size-frequency distribution by the mid-Nectarian is consistent with that of the lunar mare, despite the high flux during this period, rather than with the size-frequency distribution characteristic of the lunar highlands. These data would suggest that the transition observed in the lunar impact crater population occurred earlier than has been previously suggested. It is unknown whether the transition between the two impactor populations was gradual or abrupt, but Population 1 cannot have remained the predominant source of lunar impacts as late as Imbrium.

Relative Stratigraphy of Lunar Basins: *Crisium and Humboldtianum:* The relationship between Crisium and Humboldtianum is uncertain despite their close proximity and good preservation state. LOLA data (Fig. 2a) suggest that secondary craters and sculpture from Humboldtianum reach to, or across, the outer ring of Crisium. These stratigraphic relationships, which agree with crater statistics, support the interpretation that Humboldtianum is younger than Crisium.

Serenitatis and Nectaris: The relationship of Serenitatis to its surrounding basins is a long-standing problem in lunar science and is closely tied to the interpretation of samples from Apollo 17. In general early crater counting preferred an interpretation where Serenitatis was Pre-Nectarian [e.g., 14], a view that has been advocated anew based on analyses of the sculptured hills of the Taurus-Littrow region with Lunar Reconnaissance Orbiter Camera data [15]. LOLA topography provides support for the interpretation that Serenitatis is older than Nectaris as well: (1) crater counting, which finds a crater density in the Taurus Mountains at a factor of two times that of Crisium or Nectaris, with more than sufficient counting statistics, and (2) evidence in LOLA topography for sculpturing from Nectaris on the south-eastern rim of Serenitatis near the Apollo 17 landing site (Fig. 2b-c).

References: [1] Smith, D.E. et al. (2010), Space Sci. Rev., 150, 209-241. [2] Head, J.W. et al. (2010) *Science, 329*, 1504-1507. [3] Kadish, S.J. et al., *LPSC 42,* 1006. [4] Fassett, C.I., Head, J.W. (2008), *Icarus, 195*, 61-89. [5] Kneissl, T. et al. (2010), *PSS*, *59*, 1243–1254. [6] Wilhelms, D.E. (1987), *The Geologic History of the Moon*, USGS PP no. 1348. [7] Whitaker, E.A., Strom, R.G. (1976), *Abs. LPS*, 7, 933–934. [8] Wilhelms, D.E. et al. (1978), *Proc. Lunar Plan Sci. Conf.*, *9*, 3735–3762. [9] Strom, R.G. et al. (2005), *Science*, *309*, 1847–1850. [10] Hartmann, W.K. (1995), *Meteoritics*, *30*, 451–467. [11] Neukum, G. et al. (2001), *Space Sci. Rev.*, *96*, 55–86. [12] Fassett, C.I. et al. (2011), *GRL*, *38*, L10202. [13] Morbidelli, A., Vokrouhlický, D. (2003), *Icarus*, *163*, 120-134. [14] Hartmann, W.K., Wood, C.A. (1971), *Moon*, 3, 3–78. [15] Spudis, P.D. et al. (2011), *JGR,* in press, doi:10.1029/2011JE003903.

Fig. 1. R-plot showing the CSFDs for Pre-Nectarian, Nectarian, & Imbrian basins. Nectarian basins have a distribution consistent with the mare-like, Population 2. The Pre-Nectarian basins are more similar to Population 1. This suggests the transition from predominantly Pop. 1 to 2 happened by the mid-Nectarian, as the Nectarian basins primarily accumulated craters from Population 2.

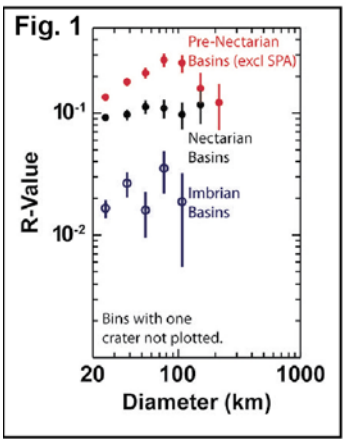

Fig. 2. (a) LOLA shaded-relief overlaid by topography, showing sculptured ejecta from Humboldtianum superposed on Crisium. (b) Context and (c) closeup views of the Serenitatis basin and Taurus mountains, showing potential sculpture from Nectaris superposed on Serenitatis.

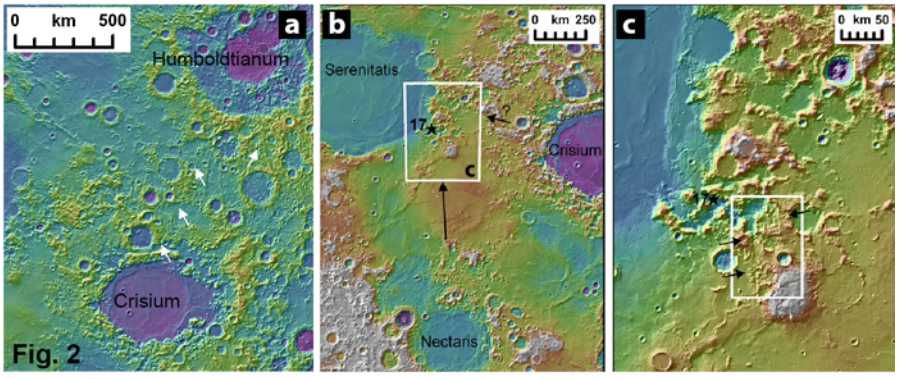

IMPROVING THE INVENTORY OF LARGE LUNAR BASINS: USING LOLA DATA TO TEST PREVIOUS CANDIDATES AND SEARCH FOR NEW ONES H.V. Frey, Geodynamics Branch, Goddard Space Flight Center, Greenbelt, MD 20771, Herbert.V.Frey@nasa.gov, H.M. Meyer, Geology & Environmental Geosciences, College of Charleston, Charleston, SC, and G.C. Romine, Physics & Astronomy, San Francisco State University, San Francisco, CA.

Summary: Topography and crustal thickness data from LOLA altimetry were used to test the validity of 98 candidate large lunar basins derived from photogeologic and earlier topographic and crustal thickness data, and to search for possible new candidates. We eliminate 23 previous candidates but find good evidence for 20 new candidates. The number of basins > 300 km diameter on the Moon is almost certainly a factor 2 (maybe 3?) larger than the number of named features having basin-like topography.

Introduction: Unified Lunar Control Net 2005 data [1] and model crustal thickness data [2] were previously used to search for possible previously unrecognized large lunar impact basins [3,4]. An inventory of 98 candidate topographic basins > 300 km in diameter was found [5]. This includes 33 named features (only those having basin-like topography) out of the 45 listed by Wilhelms [6], 38 additional Quasi-Circular Depressions (QCDs) found in the ULCN2005 topography, and 27 Circular Thin Areas (CTAs) found in model crustal thickness data [2]. Most named features and adddditional QCDs have strong CTA signatures, but there may be a class of CTAs that are not easily recognized in the old and low resolution ULCN2005 topography.

Lunar Orbiter Laser Altimeter (LOLA) data have recently become publically available. We used these data to (a) refine the center and ring diameters of known basins, (b) test the viability of the candidate basins previously found (as described above), and (c) search for additional candidate basins not revealed by the earlier lower resolution data. We used the LOLA topography directly but also a recent new model crustal thickness data that includes Kaguya gravity data [7]. We repeated a "Topographic Expression" (TE) and a "Crustal Thickness Expression" (CTE) scoring exercise originally done with the basins found in ULCN and earlier model crustal thickness data [5]. Each candidate was scored on a scale from 0 (no topographic basin or circular thin area signature) to 5 (strong circular low or strong circular thin area signature). These were combined into a total score used to rank the probability for each candidate basin. We used the same GRIDVIEW software to stretch, contour and profile the LOLA and new crustal thickness data as was done with the ULCN2005 and older model crustal thickness data.

Figure 1 compares ULCN2005 and LOLA topography for three named basins. LOLA data clearly shows better the circular basin and raised rim structure of obvious features like Orientale or Poincare. Orientale rates a 5 Topographic Expression (TE) score in both data sets. Poincare QCD structure, evident in the older data, is even more obvious in the higher resolution LOLA data. The TE scores for this basin are 3 and 4 for ULCN and LOLA topography, respectively. Australe was previously noted as not having basin-like structure in ULCN2005 topography [5]; the same is true in LOLA data. Australe could have had a TE score of -1 or -2 in ULCN data; from the LOLA data we give it a 0.

Figure 2 shows a similar comparison between older [2] and more recent [7] crustal thickness data for the Lorenz Basin. The CTE score goes up considerably in the new data.

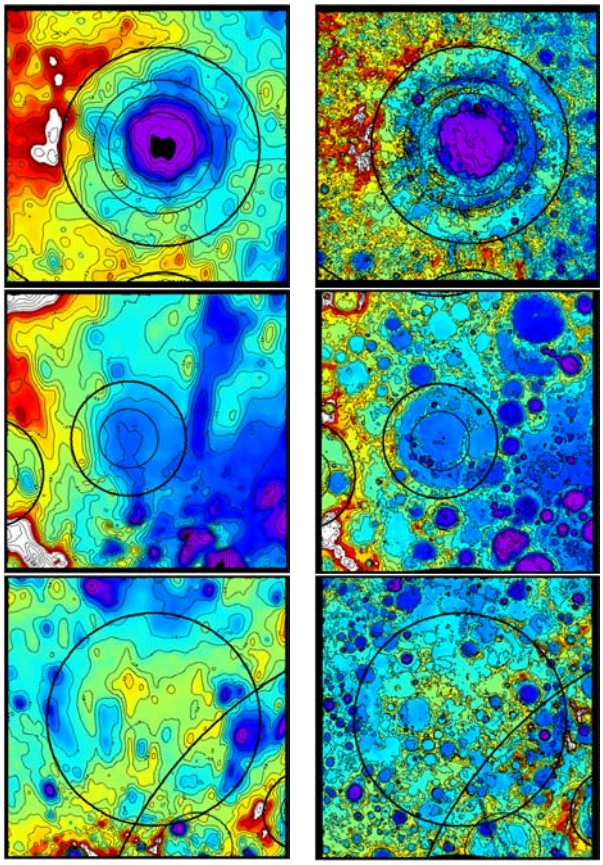

Figure 1a. ULCN2005 (left) and LOLA (right) topography for the area around the (top to bottom) Orientale (D=930 km), Poincare (D=331 km) and Australe (D=880 km) Basins, all named in Wilhlems' [6] list. Contour interval is 400 m for both. The much improved resolution of the LOLA data is obvious. Orientale and Poincare are obvious basins; Australe lacks basin-like structure.

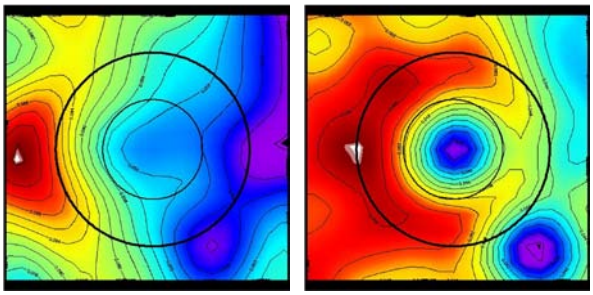

Figure 2. Older [2] (left) and more recent [7] (right) model crustal thickness data for the area around the Lorenz Basin. A weak Circular Thin Area (CTA) structure was suggested by the older data (CTE score = 1) but is very obvious in the newer model (CTE score $\geq$ 4).

Testing the previous candidates: For all previous candidates two or more of us re-evaluated the TE score (HF, GR, HM) and the CTE score (HF, HM). We are in good agreement for nearly all candidates, and especially on which candidates should be eliminated from the earlier inventory. **Named Basins:** The earlier study [5] found no topographic basin structure for 10 named basins [6]. The same 10 are again eliminated because LOLA data also shows no basin-like structure. In addition, Sikorsky-Rittenhouse is now dropped because LOLA data show that the diameter is actually < 300 km [8], the cutoff for our inventory. **Additional QCDs:** We eliminate 11 additional QCD candidates from the earlier study [5] mostly because the improved resolution of LOLA data show that both the apparent large circular structure and the depth of the proposed candidate basin can be explained by clusters of deep smaller craters [8] (see Figure 3). **Other CTAs:** We also removed 11 CTA candidates from the earlier inventory. In some cases the new model crustal thickness data [7] fails to show the CTA signature found in the earlier model data; sometimes that area actually has positive topographic relief [8]. In other cases clusters of small and deep craters likely explain the apparent CTA structure previously observed [9]. **Overall:** We deleted a total of 23 candidates from the earlier inventory [5] including all features with summary scores (TE + CTE) < 3. Thus 75 of the original 98 candidates survive. To this we add a number of new candidate large basins as described below.

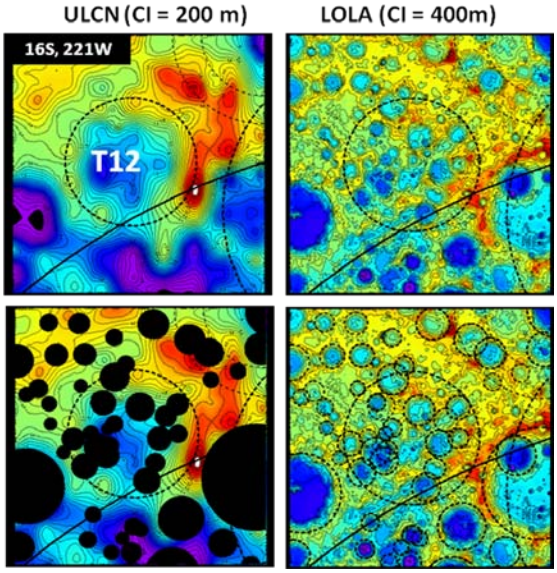

Figure 3. ULCN (left) and LOLA (right) topographic data for the area near QCD T12 [5]. The apparent large roughly circular low can be explained by the cluster of small and deep craters revealed in the LOLA data, as indicated in the bottom panels.

New Candidate Basins: A number of new candidate basins were revealed by LOLA data [9, 10]. Though generally subtle, often overprinted by other more prominent basins, and small, at least one is of Imbrium size (Figure 4) and has both QCD and CTA structure. The newer crustal thickness data also suggests several new candidate basins [9], some of which do not have obvious QCD structure (Figure 5).

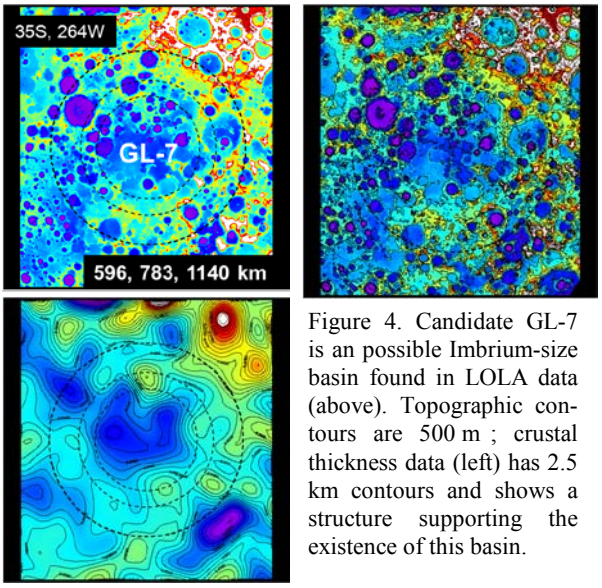

Figure 4. Candidate GL-7 is an possible Imbrium-size basin found in LOLA data (above). Topographic contours are 500 m ; crustal thickness data (left) has 2.5 km contours and shows a structure supporting the existence of this basin.

Figure 5 (below). Candidate CTA basin HM-15 [9] is ~ 304 km in diameter. The CTA signature in the new model crustal thickness data [7] is obvious, but the topographic signature is not convincingly basin-like.

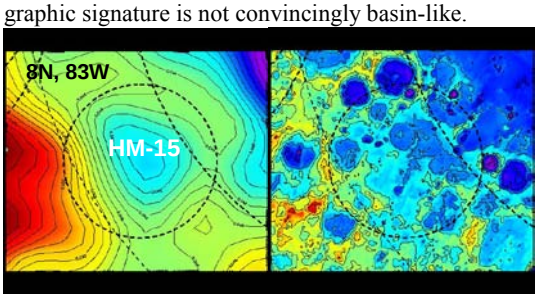

Summary: LOLA based topographic and crustal thickness data suggest 23/98 candidate basins found using older data should be dropped. But these same data suggest there could be 20 new candidates that should be added to the inventory: these include 12 new QCDs and 8 new CTAs, all with summary scores > 3 . There are 83 candidates with summary scores > 4 and 63 with summary scores > 5. The likely inventory is at least a factor 2 (maybe a factor 3) greater than the number of named basins having basin-like structure.

References. [1] Archinal, B.A. et al. (2006) USGS Open File Report 2006-1367. [2] Wieczorek, M.A. et al. (2006) New views of the Moon: Reviews in Mineralogy and Geochemistry, vol. 60, 221-364, 2006. [3] Frey, H.V. (2008) LPSC 39, abstract #1344. Frey, H.V. (2008) Workshop on Early Solar System Impact Bombardment, Houston, TX. [4] Frey, H.V. (2009) LPSC 40, abstract #1687. [5] Frey, H.V. (2010) Chapter 2, GSA Special Publication *Recent Advances and Current Research Issues in Lunar Stratigraphy*. [6] Wilhelms, D.E, (1987) The Geologic History of the Moon, USGS Professional Paper 1348. [7] Wieczorek, M.A., private communication. [8] Romine, G. and H. Frey (2011) LPSC 42, abstract #1188. [9] Meyer, H. and H. Frey (unpublished data). [10] Frey, H. and G. Romine (2011) LPSC 42 abstract #1190.

THE HEAVY BOMBARDMENT OF THE MOON. J. P. Fritz and V. A. S. M. Fernandes, Museum für Naturkunde, Leibnitz Institut an der Humboldt Universität zu Berlin, Invalidenstr. 43, 10115 Berlin. joerg.fritz@mfn-berlin.de; veraafernandes@yahoo.com.

Introduction: The ancient lunar crust bears testimony of an early (>3.7 Ga) period that is characterized by frequent hypervelocity impacts of 10´s to 100´s km sized projectiles that detonated ~40 basin sized (>300 km diameter) impact structures into the lunar crust [e.g., 1]. By implication, a larger number of such massive impact events affected the early Earth [2], but the traces of these events are erased by crustal recycling of our geological active planet. An important debate in lunar and planetary science relates to the period of time during which these lunar basins formed. The finding that ~3.9 Ga old impact reset rocks were collected on all 6 Apollo landing sites gave rise to the concept of a strong "Late Heavy Bombardment (LHB)" or "terminal lunar cataclysm" where most or all of the basins formed during a <200 Ma time interval centered around 3.9 Ga [3-6]. The LHB hypothesis gained popularity with dynamical models presenting celestial mechanisms for a "late" reconfiguration of the Solar System architecture that could provide abundant projectiles for such a "late" event [7, 8].

However, the interpretation that the Apollo and Luna samples and lunar meteorites bear evidence for a "terminal lunar cataclysm" is repeatedly criticized [i.e. 9- 11]. Currently the dominance of ~3.9 Ga ages in Apollo and Luna mission samples is thought to be due to either 1) the resetting of the different radiogenic chronometers (e.g. Rb/Sr, Ar/Ar) around 3.9 Ga by a large number of impacts at that time [i.e. 12], or 2) because all Apollo missions mainly sampled Imbrium ejecta [9,10].

In order to contribute to the aims of the lunar community for acquiring a more comprehensive view of the impact history of the Earth-Moon system, we briefly 1) revisit the first 800 Ma of lunar history, 2) review radiometric ages (including correction for K-decay and monitor ages as appropriate; [13-15]), 3) review petrography of Apollo and Luna samples and 4) discuss four different approaches for constraining the time interval during which the lunar basins formed.

1) Relating impact melt rocks to specific basins by geological arguments – The Nectaris case -

The age of the Nectaris basin (and it difference in age to Imbrium basin) is considered key for testing the putative LHB [16]. Proposed ages for Nectaris formation range between 4.2 Ga [17] and 3.85 Ga [18]. The assignment of a 3.9 Ga [19] and 3.85 Ga[18] age for Nectaris are based on formation age (minimum age given by the youngest clast within the breccia) of rock sized breccias collected on the rim of the North Ray Crater (NRC). Later, Norman et al. [20] reported KREEP-rich impact melt clasts of 3.85 Ga within some of the NRC breccias. They concluded that this breccias bear no information for the age of Nectaris, because the KREEP signature should be indicative of Imbrium derived ejecta.

A 4.2 Ga age was proposed for Nectaris to account for the variety of lithologies related to the Descartes formation [17]. In addition, different publications report rocks with impact reset ages up to 4.3 Ga for samples collected by Apollo 16 astronauts [21, 22], (Fig. 1). Thus, the Moon surface was impacted before 4.0 Ga ago. Moreover, a variety of impact craters, including basins Tranquilitatis, Nectaris, Serentiatis and Imbrium, delivered material to the Apollo 16 landing site. Thus, relating individual samples collected from the lunar surface with a specific impact basin will always be ambiguous. Therefore, additional information is required to constrain the heavy bombardment of the Moon.

The lunar curst: Understanding the formation, thickening and cooling of the lunar crust is essential to constrain the:

1) formation time when impacts could leave lasting marks, i.e., it provides a maximum age for lunar basins.

2) thickening time after which the crust was too thick for the delivery of meteoritic PGE´s to the mantle by even the largest impact events, i.e., the 0.02 % of lunar mass equivalent of meteoritical material required to explain the chondritic PGE signature in lunar basalts [23] had to be delivered before that time .

3) cooling time of the lunar crust which increases viscosity and by this the support for retaining the topographic relief of impact structures for the past ~4 billion years [i.e. 9. 24].

2) Time estimates based on geological independent processes:

In order to estimate the time lapse between formation of different basins Baldwin [9, 24] argued that the ages of lunar basins can be deduced by comparing the topographic relief of the impact structures (categorized from young to old correspond to class 1 to 10, respectively). The older crater structures (>161 km diameter) that formed in a less viscous (warmer) lunar crust would display a higher degree of topographic smoothing compared to younger crater structures that formed on a cooler and thus a more supportive lunar crust. At about 3.7 Ga ago, the viscosity of the lunar crust had increased to high values allowing it to support the prominent topographic relief of Imbrium and Orientale for billions of years. Baldwin [9, 24] argued that the prominent morphological differences of Orientale (class 2) and Nectaris (class 7) require that the latter basin to be older by a few 100´s Ma.

3) Impact exhumation scenario: Basin-sized impacts into a warm and less viscous lunar crust [9, 24] would be consistent with an impact exhumation scenario for some lunar rocks by considering: 1) crystallization in deep and warm crustal areas with an open system behaviour for some isotopic systems, followed by impact-exhumation by large impacts, and then cooling on or near the lunar surface. This impact exhumation scenario can explain the difference be-

tween the Sm-Nd crystallization age and the K-Ar age for FAN rock 60025 with crystallization at 4.44 Ga and resetting of the K-Ar system at ~4.2 Ga [25-27]. It could also explain the 4.36 Ga Pb-Pb age, and 4.32 Ga ^{146}Sm-^{142}Nd ages reported recently for 60025 [28] within the petrological context of the standard lunar magma ocean (LMO) model. The standard LMO model [29, and refs. therein] interprets FAN rocks as flotation cumulates that formed during crystallization of the LMO. Hence, the FAN rock 60025 must have formed earlier than the 4.36 Ga Pb-Pb ages since the LMO crystallization is constrained to have been completed before 4.42 Ga ago, as given by the isotopic age of the KREEP reservoir [29]. The impact excavation model could explain the isotopic age of FAN rocks being younger than the reservoir age of the KREEP source. 60025 could have formed early (>4.42 Ga) during the LMO crystallization at deep crustal levels where temperatures remained for an extended period above the closing temperatures of the different isotopic systems. The 4.2 Ga Ar-age of FAN rock 60025 [21,22, 25-27] would then date the time of a basin sized impact.

4) Impact age frequencies for meteorites from the Moon and the asteroid belt can provide another test for an extreme intense bombardment during a putative LHB. Statistical age distribution for impact reset H and L chondrites and HED [30] and lunar [11] meteorites provide no evidence for a brief (<200 Ma) and extremely high impact rate centered around 3.9 Ga. Instead, the ages distribution shows a similar number of impact ages between 4.2 and ~3.0 Ga.

Conclusion: The currently available lunar impact record dates back to [at least] 4.3 Ga ago. The lithologic variety of impact reset rocks older than 4.0 Ga show that not all basins formed around 3.9 Ga ago. Despite that some of the large lunar basins (Imbrium and Orientale) formed "late", it has to be seriously considered that a large number of lunar basins formed are older than 4.0Ga (see also [59], i.e., could reasonably be part of the tail end of planetary accretion [60].

Acknowledgement: JPF and VASMF thank ISSI for supporting an international Team of discussion on the lunar bombardment. Financial support of JF by the Helmholtz Alliance "Planetary Evolution and Life", and VASMF thanks financial support from the DFG-ICDP FE-130074.

References: [1] Wilhelms (1987) U.S.G.S. Prof. Paper 1348. [2] Maher & Stevenson (1988) Nature 331, 612-614. [3] Tera et. al. (1974) EPSL 22, 1-21. [4] Turner et al. (1973) PLPSC IV, 1889-1914 [5] Ryder (1990) EOS 71, 322-323. [6] Cohen et al.(2005) MaPS 40, 755-777. [7] Gomes et al. (2005) Nature, 435, 466. [8] Morbidelli et al. (2007) AJ, 134, 1790. [9] Baldwin (1974) Icarus 23, 157-166. [10] Haskin et al. (1998) MaPS 33, 959-975. [11] Chapman et al. (2007) Icarus 189, 233-245. [12] Stöffler & Ryder (2001) Space Sci. Rev. 96, 9-54, 2001. [13] Steiger & Jäger (1977) EPSL 36, 359–362. [14] Jourdan & Rene (2007) GCA 71, 387–402. [15] Schwarz & Trieloff (2007) Chem.Geol. 242 218–231. [16] Norman (2009) Elements 1, 23-28. [17] Schäffer et al. (1976) PLPSC VII, 2067-2092. [18] Stöffler et al. (1985) PLPSC XV 90, C449-C506. [19] James (1981) LPSC XII, 503-505. [20] Norman et al. (2010) GCA 74, 763-783. [21] Fernandes et al. (2008) Early S.S. Impact Bombard., #3028. [22] Fernandes & Fritz (2011) LPSC XLII, #1189. [23] Day et al. (2007) Science 315, 217-219. [24] Baldwin (2006) Icarus 184, 308-318. [25] Carlson & Lugmair (1988) EPSL 90, 119-130. [26] Schäffer & Husain (1973) PLPSC IV, 1847-1863. [27] Schäffer & Husain (1974) PLPSC V, 1541-1555. [28] Borg et al. (2011) Nature 477, 70–72. [29] Shearer et al. (2006) Rev. Mineral. Geochem. 60, 365-518. [30] Bogard (2011) Chem. der Erde 71, 207-226. [31] Fernandes et al. (in revision GCA). [32] Kirsten et al. (1973) PLPSC IV, 1757-1784. [33] Kirsten & Horn (1974) PLPSC V, 1451-1475. [34] Cadogan & Turner, 81976) PLPSC VII, 2267-2285. [36] Schäffer & Schäffer (1977) PLPSC VIII, 2253-2300. [37] Maurer et al. (1978) GCA 42, 1687-1720. [38] Staudacher et al. (1978) PLPSC IX 1098-1100. [39] McGee et al. (1978) PLPSC IX, 743-772. [40] Dalrymple & Ryder (1996) JGR 101, 26,069-26,084. [41] Culler et al. (2000) Science 287, 1785-1788. [42] Levine et al. (2005) GRL 32, L15201, doi:10.1029/2005GL022874. [43] Barra et al. (2006) GCA 70, 6016–6031. [44] Norman et al. (2006) GCA 70, 6032–6049. [45] Zellner et al. (2006) LPSC XXXVII, #1745. [46] Norman et al. (2007) XXXVIII, # 1991. [47] Hudgins et al. (2008) 72, 5781–5798. [48] Fernandes et al. (2000) MaPS 35, 1355-1364. [49] Fernandes et al. (2004) XXXV #1514. [50] Fernandes et al. (2008) Goldschmidt Conf. #A264. [51] Fernandes et al. (2009) MaPS 44, 805-821. [55] Gnos et al. (2004) Science 305, 657-660. [56] Burgess et al. (2007) XXXVIII # 1603. [57] Haloda et al. (2009) GCA 73, 3450-3470. [58] Sokol et al. (2009) GCA 72, 4845-4873. [59] Frey (2011) GSA Spec. Paper 477, 53-75. [60} Morbidelli et al. (this volume).

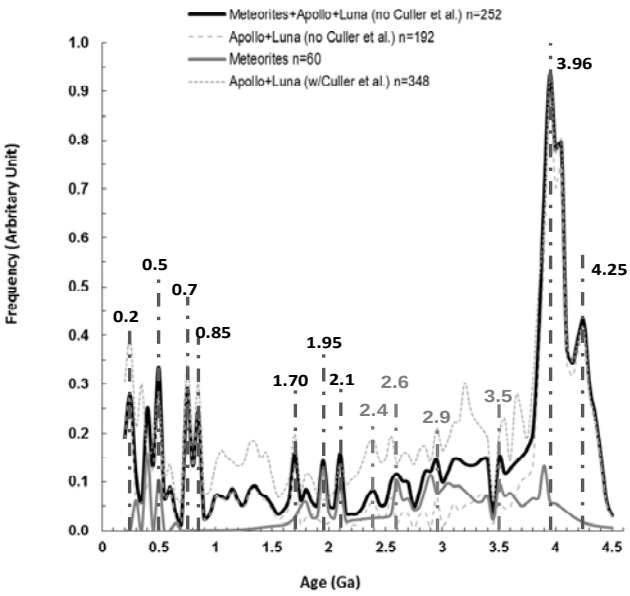

Figure 1: Gaussian probability curve calculated using published ^{40}Ar/^{39}Ar impact ages obtained for samples from Apollo 12, 14, 16 and 17 and Luna 16 and 24 missions [26, 27, 31-47] and lunar meteorites [7, 48-58]. To calculate this curve, the sample age and error were combined in bins of 0.05 Ga (50 Ma) which is representative of the average error in ^{40}Ar/^{39}Ar age determination. Where necessary, the age was corrected for monitor age and decay-constant. The thick black line is the cumulative impact ages for Apollo, Luna and meteorites and does not include the [41] due to uncertainty in the glass origin, i.e., volcanic or impact. However, for comparison, the same line with the [41] data is plotted and shown using the thin dotted line.

$^{187}Os/^{188}Os$ and Highly Siderophile Element Characteristics of Apollo 16 and 17 Impact-melt Breccias. M. G. Galenas, J. G. Liu and R. J. Walker. Department of Geology, University of Maryland, College Park, MD 20742 (gobyliu@umd.edu).

Introduction: Although only small proportions of impactor materials are normally incorporated into impact-generated melts, likely impactor materials, such as chondrites and iron meteorites, are typically enriched in highly siderophile elements [1, 2] (HSE: here including Re, Os, Ir, Ru, Pt, and Pd) compared to planetary crusts, such as the lunar crust [3]. The relative abundances of the HSE in impact melt breccias that are highly leveraged towards the impactor composition, can therefore, be used to fingerprint the nature of impactors responsible for basin-forming events on the Moon [e.g., 4, 5]. Comparisons to various meteoritic materials are commonly made by determining the relative abundances of HSE using $^{187}Os/^{188}Os$ (a proxy for long-term Re/Os) and slopes of linear trends generated from plots of Ir versus other HSE. The goal of this study is to present results for Apollo 16 and 17 impact melt breccias and use the data to constrain the chemical nature of impactors that contributed to basin forming events near these landing sites.

Samples: Lunar impact melt breccias from Apollo17 (73235, 72435, and 76035), and 16 (67095) landing sites are the target of this study. Sample 73235 is an aphanitic melt breccia collected from the regolith at Station 3 at the base of South Massif of the Apollo 17 landing site. In contrast, sample 72435 is a poikilitic rock that was chipped from a large melt-rock boulder at Station 2. Sample 76035 is also a poikilitic breccia that was collected near a boulder at Station 6. Sample 67095 is a basaltic impact melt rock that was collected from the rim of the North Ray Crater at the Apollo 16 landing site. This sample contains substantial metal globules, and metal and troilite crystals, which are rich in HSE. Sizable (50-250µm) metal and troilite grains were separated for study using a laser ablation ICP-MS technique and will be digested individually for analyses of Os isotopes and HSE abundances.

Analytical Methods: Analytical procedures followed those reported in Puchtel et al. [5]. Each breccia specimen (1-2 g) was gently broken up with an alumina mortar and pestle and separated into approximately ten ~30-300 mg sub-samples. Any granulitic (for Apollo 17 rocks) or exterior material was removed using a dry-cut saw blade. Each sub-sample was then spiked and digested using 3ml of concentrated HNO_3 and 2ml of concentrated HCl in sealed Pyrex Carius tubes at 270°C for at least 72 hours. Osmium was separated from the rest of the HSE by solvent extraction and analyzed using by negative thermal ionization mass spectrometry. The rest of the HSE were separated and purified by anion exchange chromatography and analyzed using a *Nu-Plasma* MC-ICP-MS. Average blanks (pg) were: Re 1.9, Os, 0.9, Ir 0.5, Ru 7.2, Pt 7.0, and Pd 14. The blanks constituted generally less than 0.5 % for Os and Ir, 2.0 % for Ru, Pt and Pd, but as much as 10 % for Re.

Results: The average $^{187}Os/^{188}Os$ of nine sub-samples of aphanite 73235 is 0.1309±10 ($2\sigma_{mean}$), which is slightly higher than that of 11 sub-samples of aphanites 73215 and 73255 examined previously (0.1295±4 [5]). In contrast, this ratio, is somewhat lower than averages for various poikilitic samples examined here and previously: 0.1322±5 for 72435 (n=9), 0.1329±3 for 76035 (n=4), and 0.1324±7 for 72395 and 76215 (n=22) [5]). In contrast to Apollo 17 impact melt rocks, 10 sub-samples of Apollo 16 sample 67095 yield a substantially higher $^{187}Os/^{188}Os$ of 0.1349±7, which is comparable to that of a poikilitic Apollo 16 breccia 60315 reported by [6].

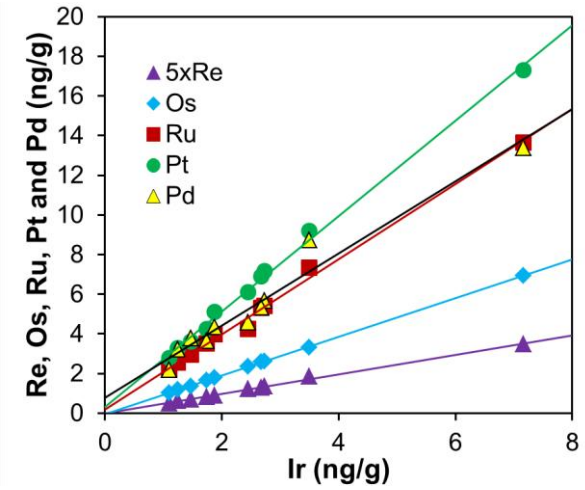

Fig. 1. Plot of Ir vs. Re, Os, Ru, Pt, and Pd for sub-samples of Apollo 16 basaltic melt breccia 67095.

The sub-samples of Apollo 17 breccias show a relatively large range of Ir contents (e.g., 1.0 to 3.9 ng/g for 73235, 1.5 to 12.3 ng/g for 72435, and 5.6 to 13.9 ng/g for 76035). Subsamples of Apollo 16 impact melt rock 67095 show a similar range with Ir contents ranging from 1.1 to 7.2 ng/g. Iridium is generally well correlated with other HSE in sub-samples (e.g., 67095; **Fig. 1**). Regressions of HSE vs. Ir were conducted using ISOPLOT [7]. Ru-Ir and Pd-Ir regressions show some scatter not visibly associated with sample petrol-

ogy. The y-intercepts for the Apollo 16 and 17 breccias are statistically indistinguishable from zero consistent with target material being relatively free of HSE. Thus, the slopes of regression lines between Ir and HSE most likely represent the relative abundances present in the dominant HSE-rich impactors [e.g., 4, 5]. The two Apollo 17 poikilitic samples show similar raised Ru/Ir and Pd/Ir in comparison with major chondrite groups as previously measured poikilitic rocks [5, 6] (**Fig. 2**), while the aphanitic sample 73235 has slightly lower but still suprachondritic Ru/Ir ratios. Pd/Ir ratios overlap with the majority of chondrites, due to the relatively large uncertainties. The Apollo 16 basaltic melt breccia 67095 has suprachondritic Ru/Ir and Pd/Ir ratios that are comparable to the three Apollo 17 samples, as well as those of the Apollo 16 poikilitic breccia 60315 reported by [6].

Discussion: Our new HSE results, combined with results from [5], show that the Apollo 17 poikilitic breccias from three geographically separate stations appear to have a single dominant impactor signature. Of greatest note is that the new aphanitic sample 73235 differs from the previous results on the Apollo 17 aphanitic breccias 73215 and 73255 [5]. Those samples exhibited relative HSE abundances and $^{187}Os/^{188}Os$ within the range of ordinary chondrites. The new aphanite has only slightly lower Ru/Ir and $^{187}Os/^{188}Os$ than the poikilitic Apollo 17 samples (**Fig. 2**). By and large, the results for sample 72325 suggest that some aphanitic impact melt breccias have a similar signature to that of the poikilitc rocks. This, in turn, suggests that these two types of Apollo 17 breccia samples may have been generated by the same impact, most likely the Serenitatis impactor.

Compared to the poikilitic Apollo 17 breccias, the higher $^{187}Os/^{188}Os$ ratios of the Apollo 16 basaltic melt breccias 67095 and poikilitic melt breccia 60315 [6], appear to indicate a different type of impactor with a higher Re/Os, for at least some Apollo 16 melt breccias. Alternately, the different isotopic composition may reflect some unidentified fractionation process that affected the relative abundances of the HSE during formation of the melt breccias.

Assuming that the Earth received similar meteoritic material as the Moon during their histories of late accretion, the high Ru/Ir and Pd/Ir ratios, as well as $^{187}Os/^{188}Os$ (the value in Fig. 2 may be underestimated [8]), of the primitive (upper) mantle can potentially be accounted for by calling on impactors with HSE characteristics that are similar to, but not represented in the chondritic suite sampled by Earth today.

References: [1] Horan M.F. et al. (2003) *Chem. Geol.* 196, 5-20. [2] Fischer-Godde M. et al. (2010) *GCA* 74, 356-379. [3] Day J.M.D. et al. (2010) *EPSL* 289, 595-605. [4] Norman M.D. et al. (2002) *EPSL* 202, 217-228. [5] Puchtel I.S. et al. (2008) *GCA* 72, 3022-3042. [6] Fischer-Godde M. et al. (2010) *LPSC XXXXI.* 2262. [7] Ludwig K.R. (2003) *Berkeley Geochron.* Center Spec. Pub No. 4. [8] Walker R.J. *Chemie der Erde* 69, 101-125. [9] Meisel T. et al. (2001) *GCA* 65, 1311-1323. [10] Becker H. et al. (2006) *GCA* 70, 4528-4550.

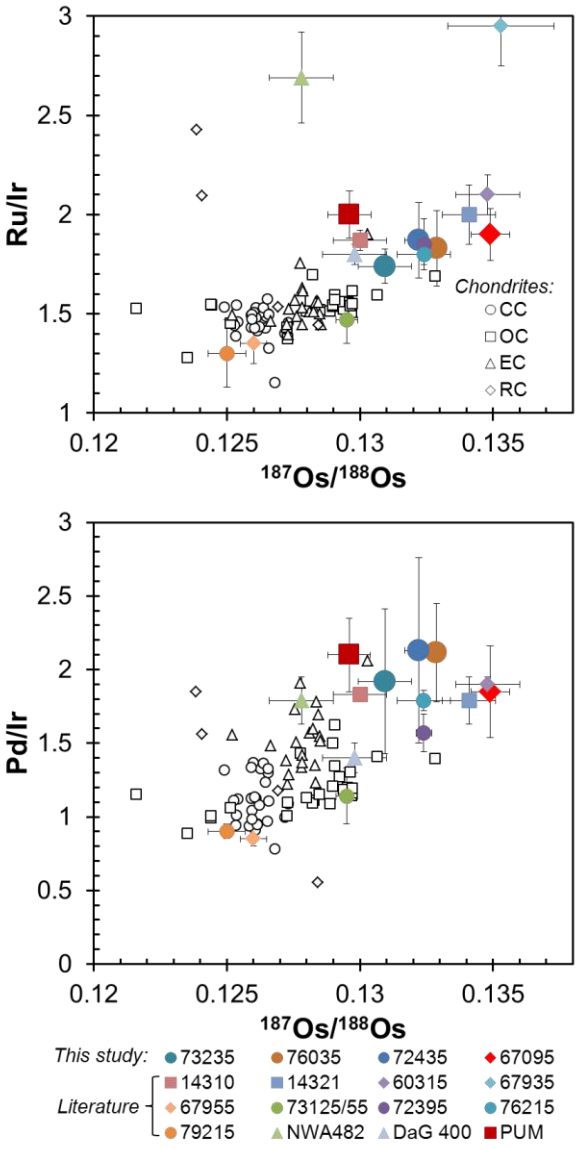

Fig. 2. $^{187}Os/^{188}Os$ vs. Ru/Ir (upper panel) and Pd/Ir (lower panel) for lunar impact melt breccias from this study (Apollo 16 and 17) and literature [5,6] in comparison with chondrites [1, 2] and the estimate of the primitive upper mantle (PUM) [9, 10].

THE IMPACT CRATERING RECORD FOR CLUES ON THE RATE OF COLLISIONS AND PROVENANCE. S. Goderis[1], J. Belza[1] and Ph. Claeys[1], [1]Earth System Science, Dept. of Geology, Vrije Universiteit Brussel, Pleinlaan 2, B-1050 Brussels, Belgium (Steven.Goderis@vub.ac.be).

Introduction: During crater formation on a planetary body a small amount of meteoritic material (vapor and/or melt) is incorporated into the impacted lithologies. This extraterrestrial contamination induces a measurable geochemical signal in these molten and/or shocked rocks that differs from the crustal signature. This signal can first confirm the impact origin of the structure and in ideal cases determine the precise nature of the projectile or in other words, the type of impacted meteorite. Precise characterization of the projectile can eventually link the impacted fragment to an asteroid family and help determine its provenance. At least three major geochemical methods are capable of detecting very small amounts of extraterrestrial material present in impact-related lithologies that, in most cases, do not exceed 1 wt% of bulk meteoritic material. Next to atypical isotope ratios (e.g., $^{187}Os/^{188}Os$, $^{53}Cr/^{52}Cr$, and $^{54}Cr/^{52}Cr$), elevated concentrations of specific siderophile elements (e.g., Cr, Co, Ni, and the platinum group elements [PGE: Ru, Rh, Pd, Os, Ir, Pt]) and associated inter-element ratios (e.g., Rh/Ir, Pt/Pd, etc.) can be applied to study the extraterrestrial contributions incorporated into terrestrial rocks. As PGE concentrations in chondrites are generally two to four orders of magnitude higher than common crustal or mantle abundances, these are ideally suited for the detection and characterization of minute amounts of PGE-enriched meteoritic material admixed in impactites. However, this approach does not work for PGE-poor meteorites, including specific types of differentiated achondrites. Comprehensive comparative reviews have recently been published, evaluating their advantages and limitations [1, 2].

Terrestrial impactor population: To understand the origin of projectiles falling on Earth, we have started to characterize the projectiles responsible for the formation of large craters (>1 km) over the last 3 billion years. So far, the record is rather incomplete. Of the terrestrial craters larger than 1 km, most of the projectiles have only been characterized down to the level of chondrites or iron meteorites without further details [3]. This is insufficient to link them to asteroid families or disruption events, or to identify possible changes in the frequency or type of impacted meteorites through time. Seven of the Phanerozoic structures (>1 km) for which the projectiles have been characterized down to the level of specific class types are ordinary chondrites (OC). Only one, the 200-km in diameter Chicxulub crater stands out as a carbonaceous chondrite. Recent work on other impact structures such as 6 km Sääksjärvi, 23 km Rochechouart, 5 km Gardnos, and 19 km Dellen reveals another recurrent type of projectile: non-magmatic iron (NMI) meteorites [4-6]. Based on the existing record, the OC and NMI seem to be the two most common types of impactors falling on Earth since the beginning of the Phanerozoic. They are both composed of olivine, pyroxene and some metal in different proportions [7]. The sources of these bodies could both be represented by a fraction of the S-type asteroids. This class of asteroids has widely varying spectra and is well represented among the NEO and in the Inner Main Belt population between 1.9 and 2.8 AU, a zone that is affected by some of the strongest resonances [8]. Further back in time, we can speculate on the possibility of a somewhat different distribution in projectile types. While for several yet to be correlated late Archean (2.63-2.49 Ga) spherule layers in the Hamersley Basin (Australia) and Griqualand West Basin (South Africa) ordinary chondritic projectiles have been proposed [9], for three early Archean spherule beds in Barberton, South Africa, a carbonaceous chondritic impactor is confirmed using Cr isotope ratios [10].

Lunar impactor population: A number of authors have tried to determine the composition of the projectile components in the lunar samples collected during the Apollo missions in the 1970s (see [11] for a summary). Recently, the impactor components in the Apollo 17 aphanitic melt breccias and in the lunar meteorite NWA482 show the closest affinities to chondritic meteorites [11]. However, the impactor components in Apollo 17 poikilitic melt breccias and impact melt clasts from Apollo 14 breccia 14321 clearly differ from those in bulk chondrites in $^{187}Os/^{188}Os$, Ru/Ir, Pt/Ir, and Os/Ir ratios. The authors explain these characteristics as the result of differentiated iron-rich impactor bodies. This explanation is not fully satisfactory, clearly further studies are needed to refine our understanding of the origin of the lunar impactors.

Rate of collision and provenance: Discussing collisions on the Earth-Moon system, several other crucial questions surface. It is currently difficult to judge if the rate of impact remained constant since the Late Heavy Bombardment, or if it varied, with possible higher collision rates during specific periods, as apparently indicated by recent data. The constancy of the source of these projectile is another key question, has the projectile provenance changed through geological time? Several possible clusters of impact events can be recognized. For example an asteroid shower is consid-

ered most likely to explain the elevated interplanetary dust particles flux and high concentration of impact craters present some ~35 million years ago in the late Eocene [12-14]. Another example occurred some 470 million years ago [15]. It is characterized by abundant (micro)meteorites (L-chondrites) preserved in Ordovician limestone layers of southern Sweden. Although the record is poor, several craters seem to concentrate in this same time window. In the Phanerozoic and late Archean, impact debris also seems to cluster in two time windows of 2.65 to 2.5 billion years ago and 3.47 to 3.24 billion years ago [16]. Finally, the most dramatic collisional event is certainly the Late Heavy Bombardment, between 4 and 3.8 billion years ago that devastated the Earth-Moon system and most likely the whole inner solar system [17]. It is linked to a major shift in the orbits of the giant gas planets [18]. The other elevated terrestrial impact rates probably derived from collisions of various magnitudes taking place in the asteroid belt. The Ordovician event is linked to a major disruption of the L chondrite parent body [19]. Also for the Chicxulub impact in Yucatán, 65 million years ago, that sealed the fate of the dinosaurs and triggered the late major mass extinction on Earth, the disruption of a parent body in the main asteroid belt has been proposed [20]. So can we compare peaks in the impact record considering their differences in magnitude, and how? What does the compositional difference of the impactors imply, especially when contradicting the domination of asteroid populations by C-type asteroids?

Conclusion: Although our present knowledge on projectile population distribution and on the existence of periods with abnormal bombardment rates (e.g., the Late Heavy Bombardment, Early Ordovician, late Eocene) is incomplete, terrestrial and lunar projectile identification studies have unraveled a few simple trends that need to be confirmed and interpreted. Systematic application of one or more of the methodologies described above in all available impact material samples might give further hints about the nature of and the processes that take place in the asteroid belt.

References: [1] Koeberl C. (2007) *Treatise of Geochemistry, Vol. 1, Elsevier, online edition,* pp. 1.28.1 - 1.28.52. [2] Tagle R. and Hecht L. (2006) *Meteoritics & Planet. Sci., 41,* 1721-1735. [3] Tagle R. et al. (2007) *Meteoritics & Planet. Sci., 42,* 1841-1854. [4] Tagle R. et al. (2009) *Geochim. Cosmochim. Ac, 73,* 4891-4906. [5] Goderis S. et al. (2009) *Chem. Geol., 258,* 145-156. [6] Tagle R. et al. (2008) *LPS XXXIX,* Abstract #1787. [7] Mittlefehldt D. W. et al. (1998) *Planetary Materials. Min. Soc. of Am.,* pp. 4-1 to 4-195. [8] Gaffey M.J. et al. (1993) *Meteoritics & Planet. Sci., 28,* 161-187. [9] Simonson B. M. et al. (2009) *Precambrian Res., 175*, 51-76. [10] Kyte F.T. et al. (2003). *Geology, 31,* 283-286. [11] Puchtel I.S. et al. (2008) *Geochim. Cosmochim. Ac, 72,* 3022-3042. [12] Farley K. A. et al. (1998) *Science, 280,* 1250. [13] Tagle R. and Claeys Ph. (2004) *Science, 305,* 492-492. [14] Kyte et al. (2011) *Earth Planet. Sc. Lett., 302,* 279-286. [15] Heck et al. (2004) *Nature, 430,* 323-325. [16] Simonson B. M. and Glass B. P. (2004) *Annu. Rev. Earth Planet. Sci.*, 32, 329–361. [17] Ryder et al. (2000) *Origin of the Earth and Moon,* pp. 475-492. [18] Gomes et al. (2005) *Nature, 435,* 466-469. [19] Korochantseva et al. (2007) *Meteoritics & Planet. Sci., 42,* 113-130. [20] Bottke et al. (2007) *Nature, 449,* 48-53.

EMPIRICAL STUDIES OF LUNAR BOMBARDMENT AROUND 3.6-4 GY AGO. W. K. Hartmann, Planetary Science Institute, 1700 E Ft Lowell Rd, Ste 106, Tucson, AZ 85719-2395, USA, hartmann@psi.edu

Neither lunar nor asteroidal meteorite data, published to date (1-3), shows the sharp, narrow spike in impact-related materials, that Ryder (4) presented from Apollo impact-melts as proof of a sharp (150-My long) cataclysm at 3.9 Gy ago (and that was incorporated into an early version of the Nice model). What appears to be common to most lunar data sets is the difficulty of finding samples older than about 4.0 Gy – an observation which was cited along with Imbrium impact effects in the original 1970s papers that proposed the cataclysm (5). Figure 1 demonstrates these points.

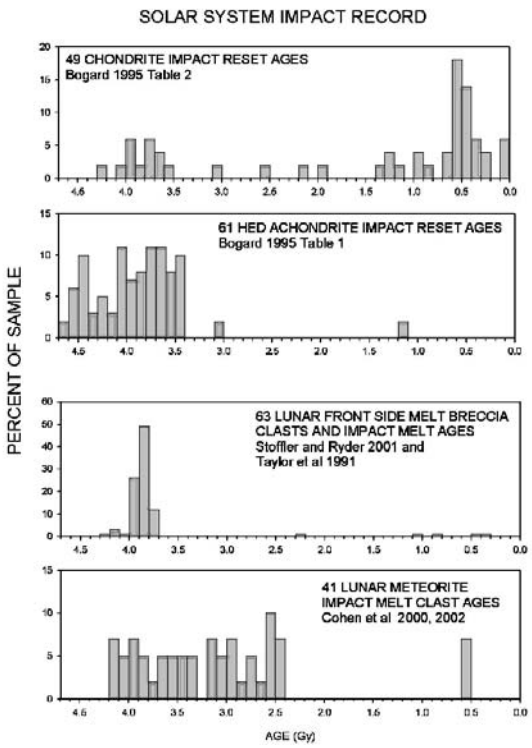

Figure 1. Age distributions for various impact-related samples. Asteroids (top two graphs) show a broad peak of impact ages from roughly 4.3 to 3.5 Gy, with chondrite samples dominated by a recent catastrophic breakup event at ~0.5 Gy. Lunar front-side Apollo impact melt rocks show a peak at about 3.8-3.9 Gy (the time of the Imbrium impact), but non-KREEP lunar meteorite impact-related clasts do not show show that peak. All lunar impact-related samples show a dearth of material pre-dating ~4.0-4.1 Gy ago.

Cratering data do show a decline in cratering rate from about 3.8 Gy to 3.5 or 3.0 Gy ago, from values at least a couple of orders of magnitude higher than today, as noted even in pre-Apollo data, when the phrase "intense early bombardment" or "EIB," was coined (6). An example of the effect of such a curve is shown in Fig. 2.

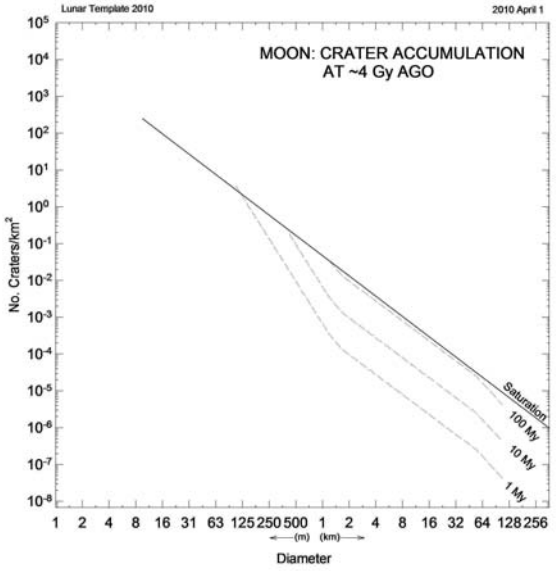

Figure 2. This crater size-distribution diagram uses an estimated cratering rate at about 4 Gy, extrapolated from observed cratering rates at 3.4-3.8 Gy ago. It shows that such a rate, crater densities would simultaneously approach saturation at crater diameters 2 km-60 km in geologically short intervals of order 100 My. The approach to saturation produces a catastrophic gardening and mega-regolith within ~100 My intervals, around 4 Gy. This means that samples on or near the surface, around 4 Gy ago, would be pulverized to regolith-like properties within 100 My, even without a Wasserburg/Ryder-type or Nice-type cataclysmic bombardment at that time. This effect may help explain the paucity of impact melt samples from before that time (cf. reference 3).

Modern interpretation of lunar samples, relative to cataclysm and basin formation, needs to involve more study of the relation between cratering rates, regolith evolution, and sample survival.

A new attempt is made here to measure the impact flux in the 200-300 My period between Imbrium impact and the tail-off of Imbrium mare emplacement. Note that the possibility has not been ruled out that the Orientale impactor was a satellite of the earth-crossing Imbrium impactor; if it

missed the moon during the Imbrium impact event, it could have hit a few years later. It is thus not a firm parameter for claiming a very short period or sharp rate of decline for independent basin-forming impacts (though it has been so used).

The distinctive feature of the 3.8-4.1 Gy period of lunar history (in addition to the Imbrium impact) may be not a 150-My wide cataclysmic spike in cratering, but rather that the cratering rate across the whole size spectrum, before and/or during that time, was so high that rocks *placed on lunar surface* before then had much reduced chance of surviving intact to be collected or ejected to Earth today. Thus, the 4.0 Gy period is notable for marking the beginning of the easily-acquired sample record. This effect is shown in Fig. 3. In that view, the Nice-type scattering event may have been more smeared out in time, and may have been ending about 3.8 Gy ago. This is more consistent with the asteroidal record (3), and is also consistent with suggestions in 1987-90 that an "early intense flux" of scattered, black, outer solar system asteroids account for the number of black, probably-captured satellites, such as Phobos and Phoebe (7, 8), and also with new work on the Nice model, presented by Bottke in 2011 (9).

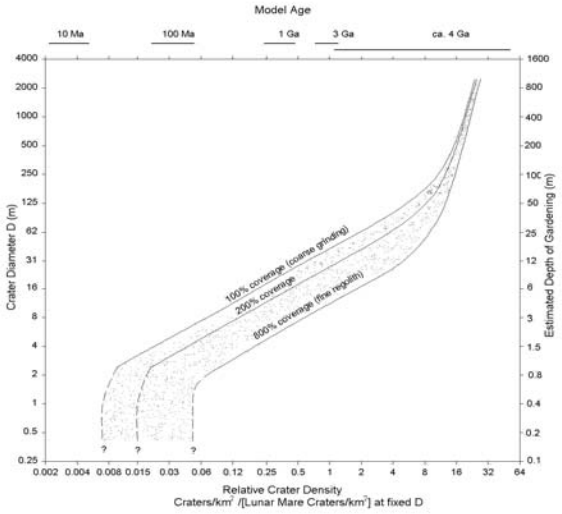

Figure 3. This diagram shows the explosive growth of mega-regolith as crater densities (abscissa, bottom) approach saturation values (about 32 × lunar mare crater densities, as observed in lunar highlands). At such crater densities (or higher), 100% of the area has high probability of having experienced formation of a multi-kilometer crater. (Curves for 200% and 800% represent high probability of multiple impacts of given crater size at a given site.) Right-hand ordinate scale indicates depths of expected regolith pulverization. These effects suggest why pre-4.0 Gy materials are found more often as clasts in impact melt breccias than as intact rocks.

References: (1) Cohen B. A., Swindle T. D. and Kring D.A. (2000) Science 290, 1754-1756. (2) Cohen B. A., Swindle, T. D. and Kring D. A. (2005) Meteorit. Planet. Sci. 40, 755-777. (3) Hartmann W. K. (2003) Meteorit. Planet. Sci. 38, 579-593. (4) Ryder G. (1990) EOS 71, 313. (5) Tera F., Papanastassiou D. A., and Wasserburg G. J. (1974) Earth Planet. Sci. Lett. 22, 1-21. (6) Hartmann W. K. (1966) Icarus 5, 406-418. (7) Hartmann W. K. (1987) Icarus 71, 57-68. (8) Hartmann W. K. (1990) Icarus 87, 236. (9) Bottke W. F. (2011) DPS abstract #1884.

EARLY THERMAL EVENTS IN THE HED PARENT BODY (4 VESTA) RECORDED IN ZIRCON U-TH-PB DEPTH PROFILES FROM MILLBILLILLIE BRECCIATED EUCRITE Michelle D. Hopkins[1,2,#] and Stephen J. Mojzsis[1,2,3], [1]University of Colorado, Geological Sciences, 2200 Colorado Ave., UCB 399, Boulder, CO, 80309 USA; [2]NASA Lunar Science Institute, Center for Lunar Origin and Evolution (CLOE); [3]Laboratoire de Géologie de Lyon, Université Claude Bernard Lyon 1, Villeurbanne, France. [#](michelle.hopkins@colorado.edu)

Introduction: Investigation of early thermal events recorded in objects beyond the Earth-Moon system is essential to our understanding of the impact bombardment history and dynamical evolution of the inner solar system. Geochemical analyses of minerals from asteroidal meteorites are a window to these early thermal processes, and are an accessible resource to be compared to what is documented for lunar bombardment history. Eucrites, the E class of the HED achondrite meteorites (howardite—eucrite-diogenite), are the crystallization products of melts from a large asteroid, likely 4 Vesta [1]. These meteorites are documented to contain accessory mineral phases that robustly preserve parent-daughter ratios in long-lived radiogenic (e.g. zircon, apatite, baddeleyite).

We report the results of our investigations of the early thermal evolution of 4 Vesta by comparative ultra-high resolution U-Th-Pb zircon depth profiles from the brecciated eucrite Millbillillie. Preserved $^{235-238}U/^{207-206}Pb$ ratios in different mineral domains (cores, mantles) within individual zircons may be used to identify the timing and intensity of thermal events that affected the asteroids. Domains within zircons can reveal distinct events that can be correlated to previously reported radiometric ages for the eucrites, as well as lunar and ancient terrestrial rocks and minerals that overlap in time with the bombardment epoch. This is a new means to expand on the chronology of impacts to the Moon, Earth and other inner solar system bodies.

Methods: Crushed and sieved ~15g aliquots of powdered material were separated using reagent grade methylene iodide to extract the largest zircons. Four grains (mb1_gr1 ~40µm ∅; mb7_gr1 ~20µm ∅; mb14_gr1 ~10µm ∅; mb17_gr1 ~10µm ∅) were imaged by back-scattered electrons, and the internal distributions of U-Th-Pb in each zircon measured on the UCLA Cameca ims1270 ion microprobe in depth-profile mode [2,3].

Results: Grain mb1_gr1 was analyzed along a ~7 µm depth profile (200 analysis cycles). Data show that mb1_gr1 preserves a concordant $^{207}Pb/^{206}Pb$ core age of 4561±13 Ma (2σ; mswd=0.72; n=7) and a 3 µm-wide overgrowth at 4524±9 Ma (2σ; mswd=2.52; n=19) (Fig.1a). Grain mb7_gr1 (Fig.1b) was depth profiled for ~5 µm and shows one domain $^{207}Pb/^{206}Pb$ age of 4537±10 Ma (2σ; mswd=3.0; n=19) over 135 analysis cycles. A ~3 µm (75 cycles) depth profile of grain mb14_gr1 yields one domain $^{207}Pb/^{206}Pb$ age of 4516±100 Ma (2σ; mswd=0.67; n=13) and ~3 µm profile (50 cycles) of grain mb17_gr1 shows a solitary domain $^{207}Pb/^{206}Pb$ age of 4489±76 Ma (2σ; mswd=0.21; n=10) (data not shown here).

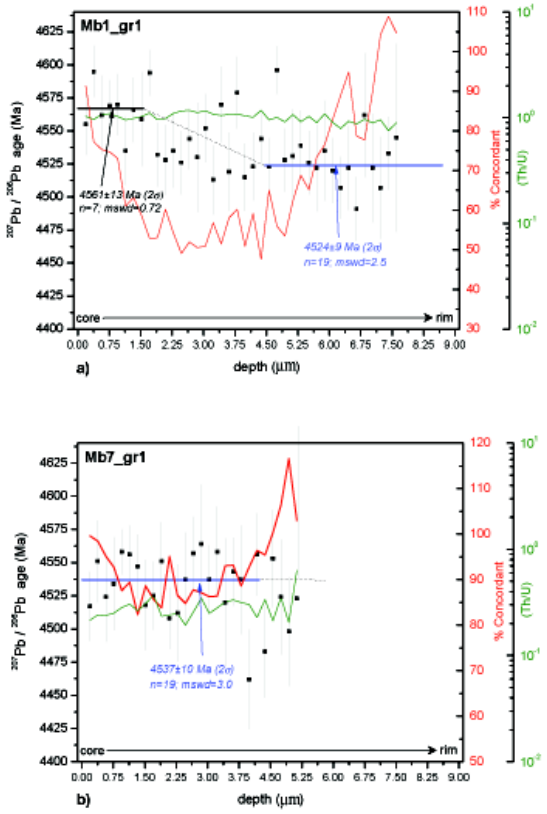

Figure 1- Individual $^{207}Pb/^{206}Pb$ ages for the depth profiles are represented by black squares (1σ errors), where each square represents a block of 5 cycles. U-Pb concordance % is shown in red. Th/U ratios are shown by in green.

Discussion: Grain mb1_gr1 displays a core $^{207}Pb/^{206}Pb$ age (4561±13 Ma) that correlates with other reported crystallization ages for eucrites [4] and ^{40}Ar-^{39}Ar ages of unbrecciated eucrites [5]. The overgrowth region of grain mb1_gr1 is 4524±9 Ma. Since the decay of ^{26}Al was effectively complete 5 Myr after t_0 [6], we propose that the event recorded here – 40 Myr after crystallization of Vesta's crust – was caused by massive thermal resetting. This age is statistically indistinguishable from the younger mantle in zircon mb7_gr1 (4537±10 Ma). Th/U ratio for the mb1_gr1 core yields values (0.8-1) consistent with exchange

equilibrium of bulk Millbillillie Th/U (0.75-0.89) [7,8] and is indicative of igneous origin (Fig.1a). Younger mantle age from mb7_gr1 preserve lower Th/U ratios (0.1-0.5) consistent with the Th/U (0.3-0.5) of various fragmented pieces of Millbillillie eucrite [8] and points to a meta-igneous origin for this component (Fig.1b). The core of grain mb1_gr1 is concordant (92%) and decreases to ~55% from mixing of Pb-Pb ages between an old core and younger rim, then returns to 105% as younger rim age is breached (Fig.1a). U/Pb concordance % for grain mb7_gr1 stays mostly concordant throughout depth profile (Fig. 1b).

Due to the small size (~10 μm) of grains mb14_gr1 and mb17_gr1, and the analytical challenge of depth profiling such small grains, data are of lower quality. Results from mb14_gr1 show a $^{207}Pb/^{206}Pb$ age of 4516±100 Ma (2σ); mb17_gr1 yields a $^{207}Pb/^{206}Pb$ age of 4489±76 (2σ). Both statistically overlap with the crystallization and overgrowth ages reported in mb1_gr1 and mb7_gr1. Th/U ratios values are broadly consistent with an igneous origin, however larger internal errors became a problem. U/Pb concordance % is also highly variable throughout each depth profile.

Implications for bombardment history: Crystallization ages of eucrites are constrained at ~4.56 Ga by U-Pb and $^{207}Pb/^{206}Pb$ ages from zircons [4,9,10], whole rock ^{40}Ar-^{39}Ar ages of unbrecciated eucrites [5] and Hf-W data [11]. It is intriguing to compare subsequent thermal events recorded in eucrites to timing of bombardments to the Moon (and Earth). Apollo samples probably show a cataclysmic "spike" in impacts from ~3.8-4.1 Ga [12]. Dynamical models [13] contend that the impact spike would not be limited to the Earth-Moon and should be present in asteroids. Several brecciated eucrites and igneous clasts in howardites show impact ages within the range of 3.4–4.5 Ga [5]. A follow-up study [14] on impact-melt clasts in howardites show a bimodal age distribution with 2 clasts at ~4.3 Ga and remaining clasts spread between 3.9 and 3.4 Ga. Zhou *et al.* [15] reported crystallization ages from 2 eucrite zircons (Cachari-4546±9.9Ma) and (Béréba-4556±22Ma) and later thermal event $^{207}Pb/^{206}Pb$ age of 4195±13Ma from an apatite grain found in Béréba. They suggest the apatite age represents the beginning of the LHB on the asteroids. Our results do not show "events" coinciding with the LHB. This may be due to the small size of Vesta (~530 km diameter) and locally low impact velocities (~5 km/s). An energetically large impact is required to produce sufficient melt to either completely recrystallize or form new zircon.

Ancient thermal events that pre-date the LHB are recorded in eucrites. Bogard and Garrison [5] observed a cluster of ^{40}Ar-^{39}Ar ages at ~4.48 Ga for unbrecciated and cumulate eucrites; it was suggested they were reset by a big impact event that produced the largest crater observed on 4Vesta. Cohen [14] reported 2 impact-melt clasts in howardites with impact ages of ~4.3 Ga. Our eucritic zircon data (Fig. 1a & 1b) document a thermal event at ~4530 Ma. This age (~40 Myr after initial solar system formation) statistically falls within range of proposed Hf-W model ages of the Giant Impact (GI) formation of the Moon 30-110 Myr after t_0 [16-18]. Such "Moon-forming impact ages" in eucrites could mean that the gravitational conditions which precipitated the GI by orbital crossing by a Mars-sized impactor to the Proto-Earth were not restricted to the area around 1 AU. Planetesimal models show that gravitational interactions between planetesimals combine to produce a few tens of Moon-to-Mars-size planetary embryos in roughly 0.1–1 Myr; that these embryos collide to form the planets in 10–100 Myr [19] means that it is plausible that the asteroid belt experienced bombardment events throughout this formative time.

References:

[1] Keil K. (2002) *Asteriods III,* 573–584. [2] Mojzsis S.J. and Harrison T.M. (2002) *Earth Planet. Sci. Lett., 202,* 563-576. [3] Trail D. *et al.* (2007) *Geochim. Cosmochim., 71,* 4044-4065. [4] Bukovanska M. *et al.* (1997) *Jour. of GEOsciences, 42,* 20. [5] Bogard D.D and Garrison D.H. (2003) *Meteorit. Planet. Sci., 38,* 669-710. [6] Srinivasan G. *et al.* (1999) *Science, 284,* 1384-1350. [7] Shukolyukov and Begemann (1996) *Meteorit. Planet. Sci., 31,* 60-72. [8] Miura Y. *et al.* (1998) *Geochim. Cosmochim., 62,* 2369-2387. [9] Tera F. *et al.* (1997) *Geochim. Cosmochim., 61,* 1713–1731. [10] Misawa K. *et al.* (2005) *Geochim. Cosmchim., 69,* 5847–5861. [11] Kleine T. (2004) *Geochim. Cosmchim., 13,* 2935-2946. [12] Hartman W. *et al.* (2000) in Origin of the Earth and Moon (eds Canup, R. & Righter, K.) 493–-512 (Univ. Arizona Press, Tucson). [13] Gomes R. *et al.* (2005) *Nature, 435,* 466-469. [14] Cohen B. (2007) *MetSoc LXX,* 5212. [15] Zhou Q. *et al.* (2011) *LPS XLII,* 2575. [16] Yin Q. *et al.* (2002) *Nature, 418,* 949-952. [17] Kleine T. *et al.* (2005) *Science, 310,* 1671-1674. [18] Halliday A. (2008) *Phil. Trans.R. Soc. A, 366,* 4163-4181. [19] Chambers J. (2004) *Earth Planet. Sci. Lett., 223,* 241-252.

Acknowledgements: We thank NASA Lunar Science Institute, Center for Lunar Origin and Evolution (CLOE) for support of this work. On-going discussions and debates with Bill Bottke, Hal Levison, Oleg Abramov, Barb Cohen and Dave Kring are gratefully acknowledged.

NEW ESTIMATES FOR THE NUMBER OF LARGE IMPACTS THROUGHOUT EARTH'S HISTORY.
B. C. Johnson[1] and H. J. Melsoh[2], [1]Pudue University Department of Physics (Johns477@purdue.edu), [2]Purdue University Department of Earth and Atmospheric Sciences.

Introduction: The Earth's impactor Size Frequency Distribution (SFD) is a measure of the number and size of extraterrestrial objects that have struck the Earth. Traditionally we recreate the Earths SFD using the cratering record of the Moon because large craters on Earth are quickly erased by active erosion. Here we present a new method to estimate the size of an impacting body based on the thickness of that global ejecta layer it creates. Using this method and measurements of ejecta layers that are preserved in the geologic record, we create the first impactor SFD for the Earth using only Earth based observations. At impactor sizes larger than ~40km the SFD we obtain is consistent with that implied by cratering on the Moon. This result suggests that the known ejecta layers provide a nearly complete record of very large impacts on Earth in the past 3.5 Gyr. In addition to an impactor SFD, we also present the first estimates of impact velocities based only on ejecta layer data.

Large objects impacting the Earth at typical velocities, greater than ~16km/s, vaporize a significant amount of silicate material. This material is originally shocked to extreme temperatures and pressures; it then expands with velocities comparable to the impact velocity in a large vapor plume or fireball. As this vapor plume cools, spherules or molten droplets condense from the vapor. [1][2][3] The high velocities in the vapor plume lead to global dispersion and deposition of these spherules. For large impacts, with an impactor size larger than ~10km diameter, spherules fall in a layer that completely covers the Earth.[4] The global nature of these layers makes their preservation much more likely than their associated craters, which are destroyed or obscured on short time scales due to tectonic processes and surface weathering.[5] The first spherule layer recognized as impact origin is the 65Myr old Cretaceous–Paleogene (or K-Pg) boundary layer, Alvarez discovered this layer more than ten years before the associated Chicxulub impact structure was recognized.[6][7] Since the discovery of the K-Pg boundary layer, other scientists have found at least 10 similar layers.[5]

There have been several attempts to model the process of spherule formation in the hope that the models may be used to determine the properties of an impacting body from spherule layer data. These simplified models show that spherule size has a strong dependence on the size of an impactor and a weak dependence on the impact velocity.[1][2][8][9] A more detailed model that includes the temperature dependence of surface energy shows the impact velocity, not the size of an impactor, is the main factor that determines the resultant spherule size. [3] This new finding invalidates impactor size estimates based on spherule sizes. Additionally, if impactor size is known, this new model coupled with estimates of spherule sizes can be used to estimate the impact velocity.

Results: In this work, we show that even though we cannot use spherule size to determine the size of an impactor, we can use the thickness of a spherule layer for the same purpose. We have derived the following expression, which gives us the impactor diameter in km as a function of only the reduced spherule layer thickness in cm.

$$D_{imp} = 17\left(\frac{t_r}{\xi}\right)^{\frac{1}{3}} \quad (1)$$

The reduced thickness $t_r = 2tf_{sp}$, where t is the layer thickness in cm and f_{sp} is the volume fraction of spherules in the layer. Additionally ξ is a factor that has a range from $\xi = 0.5 - 2$. We can test the accuracy of equation 1 by comparing the resulting impactor size to the size as determined by other methods. The K-Pg boundary layer has been found at several sites globally and has a thickness of ~3mm and is ~50% spherules by volume.[4] Using the entire range of ξ we find $D_{imp} = 9.0 - 14\ km$. This is consistent with 10 ± 4 km size of the Chicxulub impactor as determined by Ir fluence and similar estimates obtained from the size of the Chicxulub impact structure.[6][10]

We have compiled data on spherule layer thickness and spherule diameter for all of the known spherule layers in table 1. Assuming that all of the layers are indeed globally uniform vapor condensate spherule layers, and using equation 1 we are able to estimate the size of the impactor responsible for creating the layers based only on the layers thickness. In addition to impactor size we have also calculated impact velocity using the average spherule size and the model put forward by Johnson and Melosh [3]. We include these estimates of impactor size and impact velocity in Table 1. The average estimated impact velocity from all the know spherule layers is $\sim 21.8 \pm 2.3\ km/s$ which is comfortably close to the expected average of ~20.9 km/s.[11]

As previously stated, we traditionally recreate the Earths impactor SFD using the cratering record of the Moon. Now that we have estimates of the size of the impactors responsible for the known spherule layers, we can create an impactor SFD using only Earth based observations. Figure 1 shows both the SFD based on the Moon's cratering record and the SFD based on

spherule layer data and the corresponding impactor diameters repoted in Table 1.

Conclusion: Although the history of large impacts on Earth seems novel by itself, the record that spherule layers provide may also allow us to look into the solar system's past. All of the largest impacts with an impactor diameter >30km occurred more than 1.85 Gyr ago. This indicates that the impactor flux was much higher in the past than it is now. Some solar system models that include a so-called E-belt or extended asteroid belt predict a steady decrease of post Late Heavy Bombardment impactor flux with time.[12][13] Our data seems to be consistent with these predictions and may help validate these models, although more thin layers created by impactors with a diameter less than 40 km may need to be found in order to make this claim more robust.

References: [1] de Neim D. (2002) *Geol. Soc. Am. Spec. Pap.* **356**, 631-644. [2] Raĭzer, Y.P. (1960) *Sov. Phys. JETP* **37 (10)**, 1229-1235. [3] Johnson B.C. and Melosh H.J. (2011) *Icarus* (In Review). [4] Smit J. (1999) *Annu. Rev. Earth Planet. Sci.* **27**, 75-113. [5] Simonson B.M. and Glass B.P. (2004) *Annu. Rev. Earth Planet. Sci.* **32**, 329-361. [6] Alvarez L.W. et al. (1980) *Science* **208**, 1095–1108. [7] Hildebrand et al. (1991) *Geology* **19**, 867–871. [8] Melosh H.J. and Vickery A.M. (1991) *Nature* **350**, 494-497. [9] O'Keefe J.D. and Ahrens T.J. (1982) *Geol. Soc. Am. Spec. Pap.* **190**, 103-120. [10] Collins G.S. et al. (2002) *Icarus* **157**, 24-33. [11] Ivannov B.A. and Hartman W.K. (2007) *Treatise on Geophysics, Volume 10: Planets and Moons*. Elsevier. Retrieved from www.knovel.com 202-242. [12] Botke et al. (2011) 42nd LPSC, 2591. [13] Minton D.A. and Malhotra R.A. (2009) *Nature* **457**, 1109-1111.

Table 1:

Name	Age (Gyr)	Impactor Diameter (km)	Impact Velocity (km/s)
S1	3.47	29-53	18.8-21.2
S2	3.26	37-58	17.7-25.6
S3	3.24	41-70	20.6-22.8
S4	3.24	33-53	18.2-22.2
Jeerinah *	2.63	6.3-17	21.9-25.1
Monteville *	2.60-2.65	29-46	20.4-21.4
Carawine *	2.63	49-90	19.9-21.1
Reivilo º	~2.56	17-27	22.4-23.9
Puraburdoo º	2.57	17-27	22.1-23.4
Wittenoom	2.54	6.3-21	21.7-26.1
Brockmann	2.48	31-49	20.1-21.7
Grænsesø	1.85-2.13	46-73	19.1-21.3
K-Pg	0.065	9.0-14	20.4-21.5
Cpx	0.035	4.6-7.3	22.0-27.0

* Possibly from the same impactor
º Possibly from the same impactor

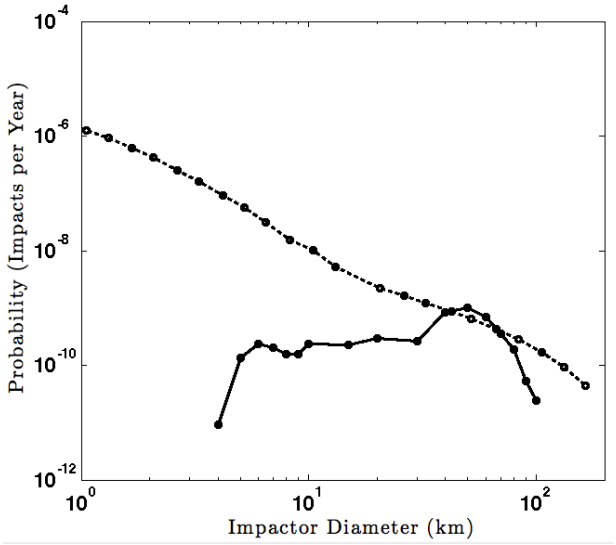

Figure 1:
The impactor size frequency distribution is plotted as the probability in number of impacts per year versus impactor diameter. The solid curve represents the SFD based on the spherule layer data and equation 1**.** The dashed curve represents the Earth's impactor SFD as inferred from the Moon's cratering record. [11] This impactor size frequency distribution is made in the conventional method using data from table 1 and logarithmic bins with Dr/Dl=sqrt(2) where Dl is the minimum diameter and Dr is the maximum diameter of the bin.[11] To allow a single impactor so span a range of sizes, we define the fractional contribution of any impactor to a bin below as
f = (size range in bin)/(total size range of impator). The total number of impactors in a bin divided by the time since the record began gives the probability of impacts per year. We estimate this time to be ~3.5 Gyr or the age of S1. We also assume that layers indicated as possibly being from the same impactor, are indeed created by the same impactor and that the impactor ranges in size from the smallest to largest reported diameter. For instance we assume that the three spherule beds Jeerinah, Carawine, and Montevile were created by a single impactor which may be anywhere from 6.3 – 90 km in diameter.

DIRECT DETECTION OF PROJECTILE RELICS ON THE MOON. K. H. Joy[1,2], M. E. Zolensky[2,3], D. K. Ross[3,4], D. S. McKay[2,3], D. A. Kring[1,2]. [1]CLSE, LPI/USRA, 3600 Bay Area Blvd., Houston, Texas 77058, USA (joy@lpi.usra.edu). [2]NASA Lunar Science Institute. [3]ARES, NASA Johnson Space Center, Houston, TX 77058, USA. [4]ESCG-Jacobs Technology, 2224 Bay Area Blvd. Houston TX 77058, USA.

Introduction: A key lunar science goal is to understand the sources of projectiles that formed the large (>300 km) lunar basins. Resolving the sources of these basin-forming impactors will help to provide constraints for models of Solar System dynamics, understand the delivery of volatiles to the early Earth-Moon system, and to explain the causes of possible spikes in the ancient impact record [1]. Comparing these records to post-basin forming impactor populations will illustrate how source regions and delivery mechanisms of projectiles evolve with time.

Chemical signatures of material accreting to the Moon have been detected in the past, generally in the form of highly-siderophile elements (HSE) in impact melt rocks and bulk soils. A more direct method of identifying the projectiles is to locate relics that survived collision with the lunar surface.

Regolith breccia time-capsules: Regolith breccias, which are consolidated samples of the lunar regolith (soil), were closed to further impact processing at the time they were assembled into rocks [2]. They are, therefore, time capsules of impact bombardment at different times through lunar history.

Here, we present a study of regolith breccias collected by the Apollo 16 (A16) mission from the Cayley Plains Formation. We used a revised calibration (after [3]) of the ratio of trapped $^{40}Ar/^{36}Ar$ ('parentless' ^{40}Ar derived from radioactive decay of ^{40}K, ratioed to solar wind derived ^{36}Ar) to semi-quantitatively calculate the timing of the assembly of the Apollo 16 regolith breccias (see Joy et al. [4] for more details, where the Apollo 16 $^{40}Ar/^{36}Ar_{Tr}$ values were taken from McKay et al. [2]). Our revised calibration [4] indicates that the Apollo 16 ancient regolith breccia population was assembled between 3.8 and 3.4 Ga, consistent with regoliths developed and closed after the Imbrium basin-forming event (~3.85 Ga), during the time of declining basin-forming impacts.

We compare ancient regolith breccia archive to younger regolith breccias and soils from A16 and other Apollo landing sites. The A16 young regolith breccia population was closed between the time of Imbrium (3.85 Ga) and ~2.3 Ga [4]. A16 Soil-like regolith breccias include samples that were closed by 1.7 Ga until more recent times [4].

Methods: We have used optical microscope and FEG-SEM techniques to identify non-lunar compositionally 'exotic' rock and mineral fragments within thin sections of these sample. Samples are then analysed using the NASA JSC Cameca SX100 electron microprobe (EMP) to derive mineral (1 μm beam) and bulk fragment (10-20 μm beam) compositions.

Ancient breccia projectile relics: In ancient (~3.8-3.4 Ga) regolith breccias 60016, 60019, 61135, 66035 and 66075 we have identified a suite of ultra-magnesian mafic fragments (UMMFs). These fragments contribute 0.02 to 0.25 % to the surface area of the fine fraction (<2 mm) regolith component in each thin section.

The UMMFS have different igneous textures: (1) Microcrystalline (porphyritic olivine and pyroxene POP: Fig. 1b) and (2) barred olivine (BO) fragments (Fig. 1c) are formed of forsteritic olivine grains (Fo_{95-98}), sometimes enclosing near end-member enstatitic pyroxene ($En_{90-96}Fs_2Wo_{2-8}$). MnO concentrations in the forsteritic olivine are variable, with FeO/MnO ratios of 40-70 in some grains and up to 122-190 in others The clasts sometimes also contain small (<5 μm) irregular interstitial phases, including an Al, Ca, Na, P and K component. (3) Cryptocrystalline fragments (Fig. 1a) are fine grained clasts consisting of intergrowths between forsteritic olivines and enstatitic pyroxenes (<3 μm; too fine grained to be compositionally determined by EMPA). They are frequently porous, with small (<5 μm) pores often aligned throughout a fragment to give a mottled texture (Fig. 1a). They also include microcrsyts (<1 μm) of a felsic and Ti-rich phase. They have a bulk a composition intermediate to forsterite and enstatite. (4) Radial olivine fragments are also compositionally intermediate to forsterite and enstatite.

The olivines and pyroxenes in the UMMFs are more magnesian than any lunar indigenous mafic minerals previously analysed (Mg-Suite lithologies typically have olivine with Fo_{80-93}, whilst some are magnesian dunites that extend those compositions to Fo_{95} [5]). The mafic phases are also compositionally distinct from experimentally produced and theoretically calculated minerals from the early mantle cumulates of the lunar magma ocean [6,7]. The bulk composition of all of the UMMFS are highly magnesian (bulk Mg# 93-99) compared with known lunar rocktypes.The bulk composition and olivine compositions of the UMMFS are as magnesian (Fig. 2a) as chondrules [8] and chondrule olivines from carbonaceous chondrite groups. This compositional evidence suggests that the UMMF are non-lunar, and possibly originate from a primitive chondritic meteoritic source.

Post-basin forming projectile population:

Fragments in A16 young regolith breccias. Examples of post-basin forming projectiles include an (~200 × 320 μm) ultramafic magnesian olivine (Fo_{96-97}) fragment within the splash coat of 60275 (2.3 Ga) that is similar to the composition of UMMFs found in the ancient Apollo 16 regolith breccias: it likely represents silicate (chondrule) material from primitive carbonaceous chondrite projectile. In sample 60255 (1.7 Ga) we have identified at least three different projectile relics. One is a small (<50 μm) ultramafic magnesian fragment, with a bulk composition (Mg# 99, FeO/MnO ratio of 35) similar to Type-1 chondrules in carbonaceous chondrites. Another small fragment (<20 μm) represents reworked fragments of a Type-1 carbonaceous chondrite assemblage (magnesian pyroxene and olivine fragments surrounded by a groundmass of melted sulphide-rich material). A third fragment is a larger (~250 × 120 μm) olivine-phyric basalt (Fig. 1e) that has a porphyritic texture with phenocrysts of olivine (Fo_{86-90}), with non-lunar compositions (FeO/MnO 44-60), in an interstitial mesostasis, formed of radiating laths of plagioclase (An_{65-72}) and a mafic Si-rich phase (pyroxene?) and small grains of Cr-rich spinel. The fragment also has troilite (FeS) enclosing grains of taenitic (high-Ni) metal, indicating that it originates from a reduced parent body. The fragment is potentially an impact or magmatic melt from an asteroidal source.

Fragments in soils and regolith breccias of unknown age. Other examples of projectiles delivered to the Moon after the basin-forming epoch include a CM carbonaceous-chondrite fragment found in soil 12037 (Bench Crater meteorite [9]: Fig. 1g), an enstatite-chondrite in soil 15601 (Hadley Rille meteorite [10]: Fig. 1d), a potential mesosiderite fragment in soil 10084 [11] and iron meteorite (bronzite-bearing) fragment in soil 10085 [12].

Two additional meteorite fragments found in lunar samples have uncertain delivery times, but probably were delivered after the formation of the Imbrium basin at 3.85 Ga. An Ir-rich micrometeorite fragment was found in Apollo 16 drive-tube 60014 [13]. A chondrule fragment (Fig. 1f) is present in feldspathic lunar meteorite regolith breccia Pecora Escarpment (PCA 02007) [14].

Summary: In ancient (~3.8-3.4 Ga) regolith breccias 60016, 60019, 61135, 66075 and 66035 we have identified a suite of ultra-mafic magnesian fragments that are consistent with material delivered to the Moon by primitive chondritic projectiles during the last stages of the basin-forming epoch. In young regolith breccias 60255 and 60275 we have also located primitive chondritic debris. In 60275 we have also located an asteroidal crystalline impact/magmatic melt clast.

Our investigation demonstrates that detailed analytical studies can be employed to search the lunar regolith for meteoritic material; helping to address several key scientific objectives for the exploration of the Moon [1].

References: [1] NRC (2007) The Scientific Context for the Exploration of the Moon. ISBN: 0-309-10920-5 [2] McKay D. S. et al. (1985) *JGR, 91,* D277–303 [3] Eugster O. et al. (2001) *Meteoritics and Planetary Science* 36, 1097-1115. [4] Joy K. H. et al. (2011) *Geochimica et Cosmochimica Acta.* 75, 7208-7225. [5] Papike J. J. et al. (1998) Planetary Materials. *Reviews in Mineralogy 36.* [6] Elardo S. M. et al. (2011) *Geochimica et Cosmochimica Acta* 75, 3024–3045 [7] Longhi J. (2010) *Geochimica et Cosmochimica Acta* 74, 784-798. [8] McSween (1977) *Geochimica et Cosmochimica Acta* 41, 1843-1860. [9] Zolensky M.E.(1996) *Meteoritics and Planetary Science* 32, 15-18 [10] Rubin A.E. (1997) *Meteoritics and Planetary Science* 32, 135-141. [11] Wood J. A. et al. (1970) SAO Special Report #307 [12] Quaide and Bunch (1970) *LSC I* , 711-729. [13] Jolliff et al. (1993) LPSC XXIV, 729-730. [14] Day et al. (2006) *Geochimica et Cosmochimica Acta* 70, 5957 - 5989.

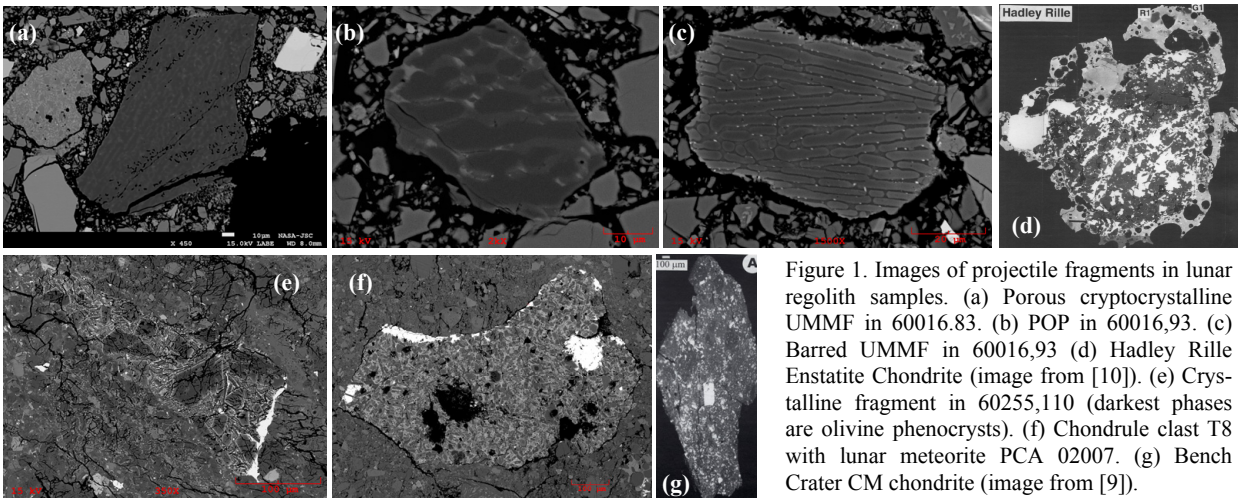

Figure 1. Images of projectile fragments in lunar regolith samples. (a) Porous cryptocrystalline UMMF in 60016.83. (b) POP in 60016,93. (c) Barred UMMF in 60016,93 (d) Hadley Rille Enstatite Chondrite (image from [10]). (e) Crystalline fragment in 60255,110 (darkest phases are olivine phenocrysts). (f) Chondrule clast T8 with lunar meteorite PCA 02007. (g) Bench Crater CM chondrite (image from [9]).

THE COLLAPSE OF SUPER-ISOSTASY: THE THERMAL EVOLUTION OF LARGE LUNAR IMPACT BASINS AND A VOLCANIC INTRUSION MODEL FOR LUNAR MASCON GRAVITY ANOMALIES

Walter S. Kiefer[1], Patrick J. McGovern[1], Ross W.K. Potter[2], Gareth S. Collins[2], and David A. Kring[1], [1]Lunar and Planetary Institute, 3600 Bay Area Blvd., Houston TX 77058, kiefer@lpi.usra.edu , [2]Impacts and Astromaterials Research Centre, Dept. Earth Science and Engineering, Imperial College, London SW 7 2AZ, UK.

Introduction

Gravity observations of the Moon have long been known to have large positive free-air gravity anomalies over impact basins such as Imbrium, Crisium, and Orientale [1-4]. It is not generally expected to find large gravity highs over topographically low basins, and these results require the presence of high density material somewhere in the crustal column beneath the impact basin. Two primary alternative models have been developed, involving either flexurally supported extrusions of dense mare basalts [5] or super-isostatic uplift of the crust-mantle interface [6]. Although extrusive basalt flows are present at many but not all mascon basins, the available constraints on basalt flow thicknesses [7-9] are such that surface basalts by themselves can not account for the observed gravity anomalies. Thus, the consensus has been that some degree of super-isostatic mantle uplift beneath large impact basins is necessary [10-13].

If super-isostatic uplift of the mantle is present, it imposes a load on the lithosphere that will drive visco-elastic flow, which acts in the direction of relaxing the uplift towards an isostatic state. The rate at which basins relax depends strongly on the temperature and viscosity of the crust and mantle. A number of visco-elastic [14-16] or flexural [17] evolution models for lunar basin structure have been presented in recent years. However, these models have not considered the strong influence of impact heating of the lithosphere by the basin-forming impact. We show here that this heating allows very rapid relaxation of the basin structure and precludes the long-term preservation of super-isostatic mantle uplift.

As an alternative model of mascon gravity anomalies, we propose the existence of a thick layer of intrusive volcanic material filling the pervasively fractured pore space in the crust below the impact zone [18]. Such volcanism can occur long after the basin-forming impact, allowing time for the lithosphere to cool and thicken after the impact. This model is both an important modification to our understanding of large impact basin formation and a significant enhancement to the inferred volume of lunar volcanism.

Post-impact Thermal Structure

The impact energy associated with the formation of a large lunar impact basin will significantly heat the lunar mantle beneath the impact zone. Several research groups have explored this using the iSALE and CTH impact hydrocodes [19-22]. For an impact appropriate for large lunar basins (impact diameter ~60 km, impact velocity 15-18 km/sec), the mantle beneath the impact is partially molten to a depth of several hundred km and to a distance of about half the basin radius out from the basin center. This partially molten material has no long term strength, which has important implications for the post-impact evolution of basin structure. Because the impact heating decays with distance from the impact, the heating at the rim of the basin is small.

Long-term Thermal Evolution

The focus of this study is understanding how this impact heating affects the lithospheric structure of the Moon and thus the visco-elastic evolution and compensation state of impact basin structures such as mascons and basin rims. The initial thermal state in our models is based on the output of hydrocode simulations of the formation of an Orientale-size impact basin [20,21]. We assume that convection in the partially molten zone will rapidly cool the melt to the solidus and thus begin our modeling with the maximum temperature set to the pressure-dependent solidus temperature. Because of the approximate circular symmetry of many large lunar impact basins, we model the thermal evolution in spherical axisymmetric geometry. We use the spherical axisymmetric version of the well known convection code CONMAN, which has been previously used to study mantle plume volcanism on Mars [23, 24]. The basic conceptual approach of the thermal model is similar to other recent studies [25, 26]. Our models include radioactive heating at a magnitude appropriate for early lunar history [27, 28].

The time evolution of the elastic lithosphere thickness is calculated using a standard strength envelope approach [24]. The upper crust, lower crust, and mantle are represented by dry anorthite, dry diabase (as a proxy for norite), and dry olivine respectively. Brittle portions of the strength envelope are modeled using Byerlee's law. The initial lithosphere thickness at the center of the basin is at most a few kilometers and is controlled by the impact heating, independent of the pre-impact thermal state. As the lithosphere cools, its

thickness increases to more than 20 km at the basin center 100 million years after the impact (Figure 1).

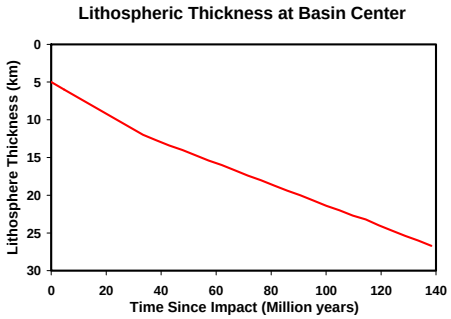

Figure 1. Elastic lithosphere thickening at basin center due to post-impact cooling of the lithosphere.

Visco-elastic Flow and the Collapse of Super-isostasy

We calculate the visco-elastic flow associated with super-isostatic uplift of the crust-mantle interface in an Orientale-size basin using the finite element code TEKTON [29]. In Figure 2, a degree of compensation of 1.0 corresponds to Airy isostasy and a degree of compensation of 1.5 corresponds to a large amount of initial super-isostatic uplift. The hydrocode post-impact thermal field corresponds to an effective near-surface thermal gradient of 20-25 K/km or more. For those thermal gradients, Figure 2 shows that any initial superisostatic uplift is largely relaxed in 100,000 to 10 million years. Thus, the large amount of super-isostatic uplift required by standard mascon models does not survive for geologically long times after the impact. On the other hand, impact heating does not alter the pre-existing thermal gradient at the basin rim. This is ~10-15 K/km at the time of the Orientale impact. Figure 2 shows that for such gradients, the relaxation time is very long, consistent with the long term preservation of the basin rim topography.

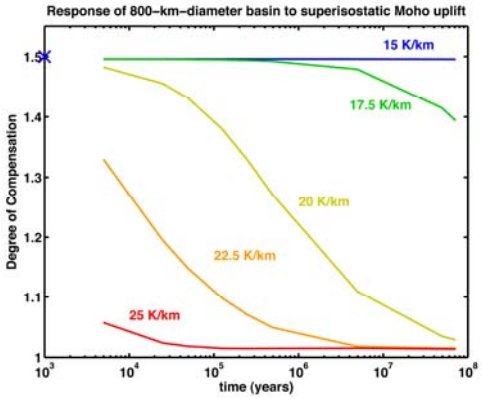

Figure 2: Visco-elastic relaxation time of an Orientale-size basin as a function of initial thermal gradient.

Volcanic Intrusion Mascon Model

Collectively, Figures 1 and 2 imply that any flexurally supported structure that contributes to the mascon gravity must be created at least 50-100 million years after the basin impact in order to allow the lithosphere to cool and thicken enough to provide at least partial flexural support for the load. At Orientale, the peak rate of volcanic filling was about 200 million years after the impact [9]. The crust below the impact zone must be pervasively fractured, forming a major reservoir for magma ponding within the crust. Calculations using the DISKGRAV modeling software [30] show that for plausible choices of basalt density, crustal porosity, and the rate of pore closure with depth, the volcanic intrusion model can explain the Orientale gravity anomaly [18]. Filling the pore space may be necessary to permit buoyant eruption of magma at the surface. Variations in the relative contributions of intrusive magmatism and surface lava flows may explain the different types of mascon documented by the Kaguya mission [13].

References [1] Muller and Sjogren, Science 161, 680-684, 1968. [2] Konopliv et al., Icarus 150, 1-18, 2001. [3] Mazarico et al., JGR 115, 2009JE003472, 2010. [4] Matsumoto et al., JGR 115, 2009JE003499, 2010. [5] Conel and Holstrom, Science 162, 1403-1405, 1968. [6] Wise and Yates, JGR 75, 261-268, 1970. [7] Williams and Zuber, Icarus 131, 107-122, 1998. [8] Thomson et al., GRL 36, 2009GL037600, 2009. [9] Whitten et al., JGR 116, 2010JE003736, 2010. [10] Neumann et al., JGR 101, 16,841-16,863, 1996. [11] Wieczorek and Phillips, Icarus 139, 246-259, 1999. [12] Hikida and Wieczorek, Icarus 192, 150-166, 2007. [13] Namiki et al., Science 323, 900-905, 2009. [14] Mohit and Phillips, JGR 111, 2005JE002654, 2006. [15] Balcerski et al., LPSC 42, abstract 2432, 2011. [16] Kamata et al., LPSC 42, abstract 1648, 2011. [17] Andrews-Hanna and Stewart, LPSC 42, abstract 2194, 2011. [18] Kiefer et al., AGU Fall Meeting abstract P33G-02, 2011. [19] Ivanov et al., GSA Special Paper 465, pp. 29-49, 2010. [20] Potter et al., LPSC 42, abstract 1452, 2011. [21] Potter et al., Icarus, in review, 2011. [22] Stewart, LPSC 42, abstract 1633, 2011. [23] Li and Kiefer, GRL 34, 2007GL030544, 2007. [24] Kiefer and Li, GRL 36, 2009GL039827, 2009. [25] Ghods and Arkani-Hamed, JGR 112, 2006JE002709, 2007. [26] Watters et al., JGR 114, 2007JE002964, 2009. [27] Korotev, JGR 103, 1691-1701, 1998. [28] Taylor et al., Geochim. Cosmochim. Acta 70, 5904-5918, 2006. [29] Melosh and Raefsky, JGR 88, 515-526, 1983. [30] Kiefer, Earth Planet. Sci. Lett. 222, 349-361, 2004.

PRELIMINARY RESULTS ON THE EVOLUTION OF SMALL CRATER POPULATIONS ON THE MOON. M. R. Kirchoff, K. M. Sherman[1], C. R. Chapman. Southwest Research Inst. 1050 Walnut St., Suite 300, Boulder, CO 80302. [1]Also at University of Colorado, Boulder, CO. Email: kirchoff@boulder.swri.edu.

Introduction: The Moon is the only solar system body for which we have both crater size-frequency distributions (SFDs) *and* ages of known terrains. These are keystones for understanding the crater production function through time. While there has been previous work developing the lunar production function [e.g., 1, 2, 3], these efforts are decades old. New imaging from Lunar Reconnaissance Orbiter Camera (LROC) and results from dynamical calculations of plausible impactor populations [e.g., 4, 5] encourage a reevaluation, especially at small diameters (D<20 km). For this purpose, we are compiling superposed crater SFDs for several craters with D=80-100 km, and Hausen crater and Birkhoff basin. These provide new data for the small crater distribution (down to D~700 m) over a wide range of locations and lunar history [cf. 6].

Crater Measurement Methods: Within each larger crater, superposed craters are measured manually on the LROC Wide Angle Camera (WAC) mosaic (pixel scale =100 m/pixel) using the 3-point crater tool in JMARS for the Moon (http://jmars.asu.edu/). Points are selected by the investigator along the crater rim. JMARS fits a circle to the points, and outputs center latitude and longitude and crater D. Degradation class is assigned to each crater, ranging from 1 (fresh) to 4 (most degraded). A crater may also be identified as an "obvious secondary" ("OS") by being part of an obvious cluster or chain. Note that our term "All Classes" refers to all degradation classes, excluding "OS"s.

Preliminary Results and Discussion: Fig. 1 shows the "All Classes" SFD for superposed craters within the larger craters in Relative (R) plot format [7]. The larger craters have been divided into groups by their relative age (cumulative density N(D=0.95 km) per 10^2 km^2; Table 1). Here we define these groups as: "old" for >20,000, "intermediate" for 10,000-20,000, and "young" for <10,000. They are plotted separately (Fig. 1a-c) as an attempt to increase comprehensibility. Lines are drawn by eye to illustrate average trends of the data; they are not quantitative fits.

We observe two trends for superposed crater SFDs for the oldest, larger craters (excluding Birkhoff basin; Fig. 1a). For D~0.7-2 km, R-values decrease with increasing D indicating a steeper slope (negative index of power-law SFD). A steep slope is generally characteristic of secondary craters [e.g., 8]; therefore we suggest that these data represent a secondary population for this D range. The second trend is as D increases beyond 2 km, R-values also increase indicating a shallower slope. This slope might be consistent with a primary crater population already observed and named "Population 1" by Strom et al. [9] for *larger* craters. Strom et al. [9] were also able to correlate "Population 1" SFD with the Main Belt Asteroids (MBA) SFD, implying this may represent the production population of *large* primary craters on the Moon. However, we CANNOT necessarily extend "Population 1", and its suggested representation of the primary production population, to the small craters we are observing. First, the frequent similarity between "All Classes" SFDs and degraded class (3 & 4) SFDs, and dissimilarity between "All Classes" SFDs and fresher class SFDS (1

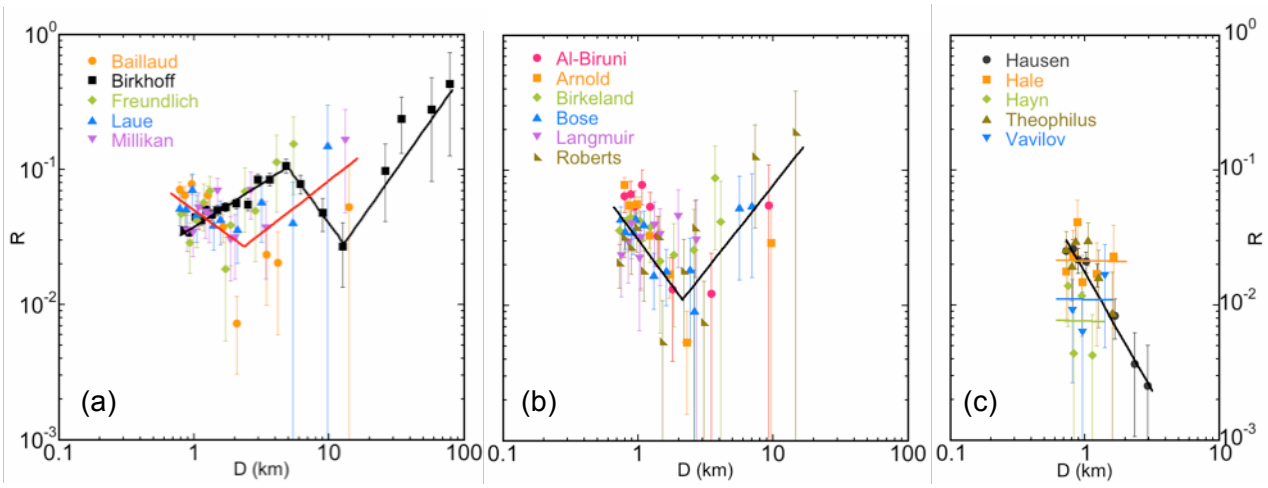

Figure 1. SFDs in R plot format of superposed craters within the larger craters in these relative age subgroups (a) "old", (b) "intermediate", and (c) "young". (See also text and Table 1.) Data is shown for "All Classes". Lines drawn by eye to illustrate general trends discussed in text. (a) red line shows trend for all except Birkhoff, black line is trend for Birkhoff. (c) black line is trend for Hausen and Theophilus, while other lines are for associated data in the same color.

& 2) (e.g., Fig. 2), imply small craters are in degradation equilibrium. Degradation at different rates for different diameters alters the intial production SFD to a new equilibrium population that is not representative of crater production. Second, even though the slope is shallower, we cannot be certain there are no secondary craters, and that we are observing only the primary population. Finally, because the MBA has not been observed down to the size range for producing these small craters, we have no direct comparison to resolve if our data represents a production population.

We observe differences from the other larger craters for superposed craters SFD in Birkhoff basin, which is the largest (D=325 km) and likely oldest (Table 1) examined (Fig 1a). The most prominent is a shift of the secondary population to larger D. A steeper slope occurs at D~4.5-15 km, likely because these are larger basin secondaries from the Moon's basin-forming epoch. For D<4.5 km and D>15 km, a shallow slope consistent with the other SFDs is observed. The shallow slope for D<4.5 becomes apparent only because of minimal contribution from the secondaries, either due to an inherent lack or earlier removal by degradation processes of smaller secondaries.

Fig. 1b shows the data for superposed craters within the "intermediate" aged larger craters (Table 1). These SFDs have more variation in R-values, but the trends are overall similar to the ones observed for the older, larger craters. This hints that characteristics of the crater populations we are observing did not considerably change through formation of the older, larger craters. Future work will define what this time frame is in absolute ages using the Model Production Function (MPF) developed by Marchi et al. [10].

Fig. 1c shows the SFDs of superposed craters within the youngest, larger craters (Table 1). These have big error bars due to poor statistics related to presence of few superposed craters. We suggest a tentative trend of steeper slopes for D=0.7-3 km. This is primarily suggested by Hausen and Theophilus SFDs, but SFDs for the others are not inconsistent. This may imply that we are seeing a secondary population, which would agree with results from the older, larger craters. The issue for larger, younger craters, however, is no obvious source craters to produce secondaries. These craters are typically the youngest in their immediate region. This suggests further investigation into some aspects of secondary cratering, concerning whether they travel farther than currently predicted, or production of self (or auto)-secondaries [e.g., 11].

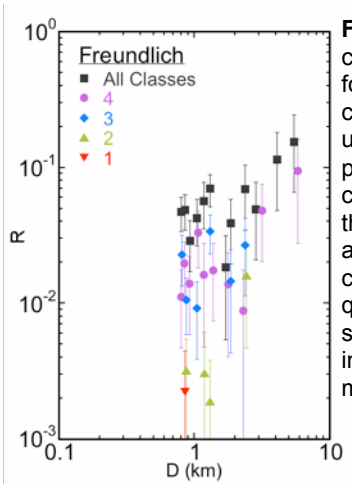

Figure 2. Degradation classes SFDs in R plot format of superposed craters within Freundlich. This plot exemplifies the similarity in classes 3 & 4 SFDs to the "All Classes" SFD, and the lower density of classes 1 & 2 SFDs frequently observed for superposed crater SFDs in our "old" and "intermediate" larger craters.

SFDs for craters on the floors of Hale, Hayn, and Vavilov could also be consistent with a flat slope. Previously, Strom et al. [9], studying younger lunar surfaces, have called this flat slope "Population 2" and correlated it with the Near Earth Object (NEO) SFD, thus demonstrating it is likely a production population. Currently, our data are just too poor to propose that we are seeing "Population 2" at smaller diameters. We are currently compiling superposed crater SFDs for ~25 more larger craters of various ages across the Moon to augment these interpretations.

References: [1] Hartmann, W.K., et al. (1981) in *Basaltic Volcanism on the Terrestrial Planets*. 1049-1127. [2] Wilhelms, D.E. (1985). *LPSC XVI*, p. 904-905 (Abst.). [3] Basilevsky, A.T., et al. (1980) *EMP*. **23**, 355-371. [4] Gomes, R., et al. (2005) *Nature* **435**, 466-469. [5] Bottke, W.F., Jr., et al. (2005) *Icarus* **175**, 111-140. [6] Baldwin, R.B. (1985) *Icarus* **61**, 63-91. [7] Crater Analysis Techniques Working Group (1979) *Icarus* **37**, 467-474. [8] McEwen, A.S. and E.B. Bierhaus (2006) *AREPS* **34**, 535-567. [9] Strom, R.G., et al. (2005) *Science* **309**, 1847-1850. [10] Marchi, S., et al. (2009) *AJ*. **137**, 4936-4948. [11] Plescia, J.B. and M.S. Robinson (2011). *42nd LPSC*. Abst. #1839.

Table 1. Relative Ages of the Larger Craters.

Crater	Relative Age*
Birkhoff	29100±700
Freundlich	26300±3800
Millikan	25800±3100
Baillaud	25600±2300
Laue	25000±3900
Al-Biruni	19800±3300
Birkeland	18800±4200
Bose	16500±2500
Arnold	16000±1900
Langmuir	15500±3900
Roberts	13600±2500
Hausen	7600±900
Hale	7400±2800
Theophilus	7100±2000
Vavilov	3600±2100
Hayn	1800±1000

*N(D=0.95 km) per 10^6 km^2; $\sqrt{n}$ errors, where n = number of craters measured

SEARCH FOR A GEOCHEMICAL RECORD OF THE LATE HEAVY BOMBARDMENT ON EARTH.
Christian Koeberl[1,2], [1]Department of Lithospheric Research, University of Vienna, Althanstrasse 14, A-1090 Vienna, Austria; [2]Natural History Museum, Burgring 7, A-1010 Vienna, Austria; e-mail: christian.koeberl@univie.ac.at.

Introduction: If a late heavy bombardment during the time period of about 3.8 to 4 billion years ago occurred on the Moon, the Earth must have been subjected to an impact flux somewhat more intense as that recorded on the Moon. The consequences for the Earth must have been devastating, although the exact consequences – such as a total remelting of the crust – are still unclear. So far, no unequivocal record of a late heavy bombardment on the early Earth has been found. The earliest rocks on Earth date back to slightly after the end of the heavy bombardment, although there are relict zircons that have ages of up to 4.4 Ga (in which no impact-characteristic shock features have yet been found). In terms of evidence for impact on Earth, the first solid evidence exists in the form of various spherule layers found in South Africa and Australia with ages between about 3.4 and 2.5 Ga; these layers represent several (the exact number is still unknown) large-scale impact events. The oldest documented (and preserved) impact craters on Earth have ages of 2.02 and 1.86 billion years. Thus, the impact record for more than half of the geological history of the Earth is incomplete and not well preserved, and we mostly have only indirect evidence regarding the impact record and its effects during the first 2.5 billion years of Earth history.

Early Impact Evidence: As there are no rock preserved on Earth that exceed an age of 4 billion years, and the rock record covering the pre-3.5 billion year range is extremely sparse, it is very difficult to search for terrestrial evidence of a late heavy bombardment, which is indicated in lunar rocks for the period 3.8 to 4 Ga. Detrital minerals, especially zircons, with ages beyond 4 billion years exist, but none have been shown any clear evidence of shock features. Part of the problem might be the extreme heat associated with early impacts that could have erased any shock features. Besides the search for shock features in minerals and rocks, another important line of evidence for impact processes comes from geochemical indications of the presence of an extraterrestrial component. Only elements that have high abundances in meteorites, but low abundances in terrestrial crustal rocks are useful for such studies – for example, the siderophile platinum-group elements (PGEs: Ru, Rh, Pd, Os, Ir, and Pt) and other siderophile elements (e.g., Co, Ni). Elevated abundances of siderophile elements in impact melt rocks or breccias (and impact ejecta), compared to target rock abundances, can be indicative of the presence of either a chondritic or an iron meteoritic component. There are, however, cases in which the PGE interelement abundances might be fractionated.

These problems can, in part, be overcome by the use of isotopic tracers for extraterrestrial components. Most prominent among those are the Os and Cr isotopic methods. The Os isotopic method, which is based on the decay of Re-187 to Os-187, is very sensitive and can detect sub-percent levels of extraterrestrial components in impact breccias and melt rocks, but it is not possible to determine the meteorite type.

In contrast, the Cr isotopic method relies on the fact that all terrestrial rocks have a uniform Cr isotopic composition, whereas different meteorite types have different isotopic anomalies. The Cr isotopic method is, thus, selective not only regarding the Cr source (terrestrial vs. extraterrestrial), but also regarding the meteorite type..

Tungsten Isotopes: Another isotope recently suggested as a tracer for a meteoritic component in terrestrial material is ^{182}W, which has been produced by the decay of now extinct ^{182}Hf ($T_{1/2}$=8.9 Ma). Each group of meteorites and the terrestrial crust have distinct W isotopic compositions. There have been suggestions that W isotope analyses supposedly indicate a evidence of the late heavy bombardment on Earth by a W isotope anomaly in early Archean (3.8 Ga) metasedimentary rocks [1]. However, W isotope analyses in a variety of impactites and ejecta from confirmed impact deposits, which had unequivocally been identified by other geochemical proxies, the isotopic composition of W was identical with analytical error to that of the Earth's continental crust, and no ^{182}W anomalies are present, even in the samples containing a significant (percent level) meteoritic component [2]. Any W isotope anomalies rather have a terrestrial origin. Therefore, W isotopes cannot provide proper evidence of a meteoritic component or confirm a LHB on Earth, and still other methods for such a search must be employed.

References: [1] Schoenberg R. et al. (2002) *Nature* 418, 403–405. [2] Moynier F. et al. (2009) *Earth Planet Sci. Lett.* 286, 35–40

NEW INSIGHTS OF EARLY BOMBARDMENT PROCESSES FROM ACCRETION THROUGH THE BASIN-FORMING EPOCH. David A. Kring [1,2], Timothy D. Swindle[3,2], and Richard J. Walker[4,2], [1]Center for Lunar Science and Exploration, Lunar and Planetary Institute, Universities Space Research Association, 3600 Bay Area Blvd., Houston, TX 77058, kring@lpi.usra.edu, [2]NASA Lunar Science Institute, [3]Lunar and Planetary Laboratory, University of Arizona, Tucson, AZ 85721, [4]University of Maryland, College Park, MD 20742.

The Accretional Epoch: We begin with the discovery of a fragment of rock that survived a collision among planetesimals that occurred during the accretion of Earth and prior to the formation of the Moon. The MIL 05029 meteorite is an impact melt breccia that was produced in a collision ~4.54 Ga that created a 25-60 km diameter crater and shattered the interior of the 100-200 km diameter L-chondrite parent body [1]. In a similar study, we had previously shown that the Portales Valley meteorite was produced beneath the floor of a >20 km diameter crater on the 150-200 km diameter H-chondrite parent body [2] in an event that occurred >4.46 Ga [3]. Other collisions during the accretional epoch have been detected on the E-chondrite (~4.53 Ga), IAB (>4.47 and perhaps >4.52 Ga), HED (~4.48 Ga), and L-chondrite (4.46 and 4.43) parent bodies ([4] and references therein). Collectively, these data indicate sizeable impact events were occurring among planetesimals as the accretional phase wound down and the largest planetary collisions (e.g., the Moon-forming giant impact) were occurring.

The Magnitude and Duration of the Lunar Cataclysm: After the Moon accreted, there may have been a significant decline in the impact flux between ~4.4 and ~4.1 Ga because there are very few impact ages within that interval. In contrast, there are large numbers of ~4.0-3.8 Ga impact ages in samples collected around the Apollo landing sites [5,6]. That data imply a severe period of bombardment that has been called the lunar cataclysm. Additional analyses of impact melts that were extracted from lunar meteorites (and, hence, come from other locations on the Moon) are consistent with that interpretation [7,8].

The canonical lunar cataclysm is defined by ~15 basin-forming impacts that occurred during the Nectarian Period and Early Imbrian Epoch. Nearly 30 additional basins were produced during the pre-Nectarian on the Moon, but they were not sampled during Apollo. It is not yet clear if they were produced during the the same cataclysmic surge of cratering events and they are, thus, targets of future lunar missions [e.g., 9].

Sources of Impactors: Siderophile signatures of impactors are entrained in lunar impact melts and suggest the impactors were dominated by asteroids rather than comets ([10] and references therein). Recent analyses of Apollo 17 specimens [11,12] indicate a pre-Serenitatis impactor (>3.89 Ga) had affinities with ordinary chondrites, the Serenitatis impactor (~3.89 Ga) was a chondritic asteroid (but unlike any meteorites in our current collection from the asteroid belt), and that a post-Serenitatis (~3.75 Ga) impactor had affinities to enstatite chondrites or, marginally, ordinary chondrites. Interestingly, these data imply there were more ordinary chondrite planetesimals than those currently represented by the LL, L, and H groups of meteorites.

A completely independent assessment of the impactors can be derived from the size distribution of the lunar basins and smaller craters in the ancient cratered highlands of the Moon [13]. That analysis suggests asteroids dominated the flux and that the asteroid belt was sampled in a size-independent fashion. That latter observation implies resonances swept through the asteroid belt and that Jupiter's orbit shifted.

That same method was recently used to probe the crater size distribution further ([14] and Marchi et al., this workshop). That study discovered a shift in the size distribution of craters that implies a shift in the impact velocities of impacting asteroids. At some point between the formation of the South Pole-Aitken and Nectaris basins, impact velocities may have roughly doubled. This is consistent with a shift in the orbits of Jupiter and other outer solar system planets that has previously been implied [e.g., 15, 13] for the production of the Nectarian and Early Imbrian basins. It also implies, however, that some of the pre-Nectarian basins, including the South Pole-Aitken Basin, were produced independently through other collisional mechanisms.

A third independent assessment of the source of impactors can be derived from the lunar regolith. A recent study of Apollo 16 samples discovered the first mineralogic and lithologic remnants of projectiles during the latter phase of the basin-forming epoch ([16] and Joy et al., this workshop]. Those results are also consistent with an asteroidal source for the impactors. Indeed, the relics are dominated by fragments of chondrules similar to those in chondritic meteorites.

The Inner Solar System Cataclysm: The Moon has provided an incredibly useful measure of the collisional events that shaped early solar system evolution. Additional evidence has also been gleaned from asteroids, some of which confirms interpretations of lunar data and some of which provides other insights.

A recent analysis of impact melt breccias from the H-chondrite parent body indicate significant collisional activity 4.0-3.5 Ga [17], followed by a sharp decline in the flux of impacting debris. Impact ages in that same 4.0-3.5 Ga interval have been seen in a large number of samples from the HED parent body and in a smaller number of samples from the L and LL chondrite parent bodies [e.g., 18,19,4]. In addition, a major collision involving the IIE parent body occurred ~3.7-3.6 Ga [e.g., 4]. The large number of impact events among asteroids 4.0-3.5 Ga implies the lunar cataclysm is really an inner solar system cataclysm [10].

In almost all cases, the samples being measured come from simple craters and the ejecta around simple craters. Thus, most of the impact events represented by the chondritic samples are smaller than those that produced the lunar basins. (A collision among planetesimals with the same energy needed to produce a lunar basin would completely disrupt the planetesimals.) Thus, collisional age spectra dominated by simple cratering events on chondritic bodies may be similar, but not identical, to the age spectra of basin-size events on the Moon. This is likely one reason chondritic ages range from 4.0-3.5 Ga, while the basin-forming epoch on the Moon ended 3.8-3.7 Ga. It also seems likely that the dynamical situation (asteroids are closer to the source of the impators than the Moon) may produce subtle differences in the age spectra among asteroids and the Moon.

Flux of Asteroids to the Moon: If the lunar cataclysm occurred within 20 to 200 Myr, then the annualized mass flux to the Moon was ~3.5×10^{13} to ~3.5×10^{14} g/yr for a Nectarian and Early Imbrian event [20]. If the pre-Nectarian basins were also involved, then the annualized mass flux was 2.3×10^{14} to 2.3×10^{15} g/yr. Asteroids contain significant quantities of H_2O and other biogenic elements [21]. Recent data [11,12,16] imply chondritic projectiles, some with affinities to enstatite, ordinary, and carbonaceous chondrites. That implies ~6×10^{19} to ~1×10^{21} g of H_2O were delivered to the Moon during the Nectarian and Early Imbrium, and an additional ~3×10^{20} to ~7×10^{21} g of H_2O during the pre-Nectarian, although some of that mass would have been lost from the Moon as high-velocity ejecta. The mass flux to the Earth was at least 13 times greater. While substantial, the canonical cataclysm could not have delivered the entire inventory of Earth's water. A large fraction of Earth's water was delivered during the earlier accretional phase.

Preparing for Future Missions: To further test the lunar cataclysm hypothesis and determine the duration of the basin-forming epoch, we need to recover new impact samples from the lunar surface that have a well-understood geologic context and have properties suitable for complementary analyses of their ages and siderophile content. A series of landing site studies are underway and a leading candidate that has emerged is Schrödinger Basin [22]. This is the second youngest basin on the Moon. It also resides within the oldest and largest basin on the Moon, South Pole-Aitken Basin. Thus, samples within Schrödinger Basin may provide the ages of both basins and effectively bracket the duration of the entire basin-forming epoch.

If the age of samples of the South Pole-Aitken Basin indicate it is part of the lunar cataclysm, then that implies there were ~3 times more basin-forming impacts than in the canonical model. On the other hand, if the age of South Pole-Aitken Basin is much older (consistent with [14]), then pre-Nectarian basins with successively younger relative ages need to be sampled to determine when the cataclysm began. Candidate targets include the Nubium Basin (middle pre-Nectarian), Smythii Basin (slightly younger), and the Apollo Basin (the last of the pre-Nectarian Basins and also within the South Pole-Aitken Basin). The timing of the latter third of the basin-forming epoch and the nature of the projectiles involved will require better documented samples of impact melt or impact-metamorphosed samples from Nectaris, Serenitatis, Crisium, Schrödinger, and Orientale.

References: [1] Weirich J. R. et al. (2011) *Meteoritics & Planet. Sci., 45,* 1868–1888. [2] Kring D. A. et al. (1999) *Meteoritics & Planet. Sci., 34,* 663–669. [3] Bogard D. D. and Garrison D. H. (2009) *GCA, 73*, 6965–6983. [4] Bogard D. D. (2011) *Chemie der Erde, 71*, 207–226. [5] Turner G. et al. (1973) *Proc. Lunar Sci. Conf., 4th*, 1889–1914. [6] Tera F. et al. (1974) *EPSL, 22*, 1–21. [7] Cohen B. A. et al. (2000) *Science, 290*, 1754–1756. [8] Cohen B. A. et al. (2005) *Meteoritics & Planet. Sci., 40,* 755–777. [9] National Research Council (2007) *The Scientific Context for Exploration of the Moon*. [10] Kring D. A. and Cohen B. A. (2002) *JGR, 107*, doi: 10.1029/2001JE001529. [11] Puchtel I. S. et al. (2008) *GCA, 72*, 3022–3042. [12] Galenas M. G. et al. (2011) *LPS XXXXII,* Abstract #1413. [13] Strom R. G. et al. (2005) *Science, 309*, 1847–1850. [14] Marchi S. et al. (2011) *LPS XXXXII,* Abstract #1192. [15] Gomes R. et al. (2005) *Nature, 435*, 466. [16]] Joy K. (2011) *LPS XXXXII,* Abstract #2103. [17] Swindle T. D. (2009) *Meteoritics & Planet. Sci., 44,* 747–762. [18] Bogard D. D. (1995) *Meteoritics, 30,* 244–268. [19] Swindle T. D. and Kring D. A. (2008) *Early Solar System Bombardment Workshop*, Abstract #3004. [20] Kring D. A. (2008) *NLSI Lunar Science Conference*, Abstract #2140. [21] Kring D. A. et al. (1996) *EPSL, 140*, 201–212. [22] O'Sullivan K. M. et al. (2011) *GSA Special Paper, 477*, 117–128.

Spitzer Evidence for a Late Heavy Bombardment and the Formation of Urelites in η Corvi at ~1 Gyr. **C.M. Lisse[1], C. H. Chen[2], M. C. Wyatt[3], A. Morlok[4], P. Thebault[5], M. Sitko[6], D.M. Watson[7], P. Manoj[7], P. Sheehan[7], T.M. Currie[8]** [1]JHU-APL, 11100 Johns Hopkins Road, Laurel, MD 20723 carey.lisse@jhuapl.edu [2]STScI [3]IoA, Univ of Cambridge, Madingley Road, Cambridge CB3 0HA, UK [4]PSSRI, The Open University, Milton Keynes, MK7 6AA [5]Observatoire de Paris, F-92195 Meudon Principal Cedex, France [6] Space Science Institute, 475Walnut St., Suite205, Boulder, CO80301 sitko@spacescience.org [7]Department of Physics and Astronomy, University of Rochester, Rochester, NY 14627 [8]Department of Astronomy, Cornell University, 108 Space Sciences Bldg., Ithaca, NY 14853 [8]Code 667, NASA-GSFC, Greenbelt, MD 20771

Introduction. We have analyzed the Spitzer IRS 5 – 35 um spectrum of the warm, ~360K circumstellar dust around the nearby MS star η Corvi (F2V, 1.4 ± 0.3 Gyr), a known IRAS excess object with a very high 24um excess luminosity for its age (Fig. 1). The Spitzer spectrum (Fig. 2) shows clear evidence for warm, water- and carbon-rich dust at ~ 3 AU from the central star, uncoupled and in a separate reservoir from the system's extended sub-mm dust ring at 150 ± 20 AU [2,3] (Figs. 1 & 3).

Spectral features similar in kind and amplitude to those found for ultra-primitive material in ISO HD100546 spectra were found (water ice & gas, olivines & pyroxenes, amorphous carbon and metal sulfides), in addition to emissions due to impact produced silica and high temperature/pressure carbonaceous phases [4]. A large amount, at least 3 x 10^{19} kg, of 0.1 – 1000 μm warm dust is present, in a roughly collisional equilibrium distribution with dn/da ~ $a^{-3.5}$. This is the equivalent of a 140 km radius asteroid of 2.5 g cm^{-3} density or a "comet" of 260 km radius and 0.40 g cm^{-3} density. If we allow for particles larger than 1 cm, the mass present increases by (largest particle size/1000 μm)$^{0.5}$, and the equivalent parent body radius increases by the 0.167th power.

Findings From Our Analysis [4] :

- The η Corvi system emits > 1000 times as much 24 um flux as other co-eval (~1 Gyr) dusty disk systems. It is within a factor of 2 of the age of the solar system during the LHB.

- The η Corvi system contains an extended belt of cold Kuiper Belt dust (Mass ~ 2 x 10^{23} kg = 3 M_{Moon}) at ~150 AU from the primary.

- The η Corvi system contains a reservoir of warm (~360K) dust massing ~10^{-4} the mass of the Kuiper Belt dust) at ~3 AU from the primary, in the system's Terrestrial Habitability Zone (THZ), spatially separated by more than 50 AU from the cold dust.

- The warm dust is ***very*** primitive, & definitely not from an asteroidal parent body. It is very water ice & carbon rich, and its spectrum matches best the emission seen from the cold, extended dust disk found around HD100546, an ~10 Myr old Herbig A0V.

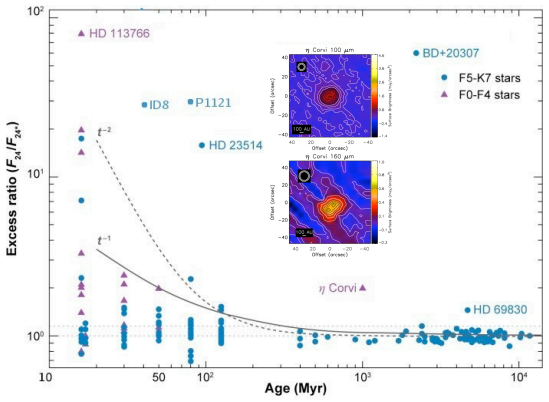

Figure 1 - Dusty disk IR excess luminosity vs time. η Corvi is the 3rd brightest of [1]'s 59 IRAS-excess systems, and the only one which is a "mature" MS system of ~1.4 Gyr age, or about 1/3 of its total MS lifetime. The 1/t and 1/t^2 trend lines fit most of the sources in the current sample except outliers like η Corvi, which clearly has a high $L_{IR}/L_* = 3 \times 10^{-4}$ for its age, suggesting something unusual has occurred in this system. *Inset*: 100 um (top) and 160 um (bottom) Herchel PACS FIR images of the extended bright η Corvi Kuper Belt, after [2]. Contours are shown at 0, 10, 30, 50, 60, 70, 80, 90 and 99% of the peak in the map. Circles in the upper left corner of each panel mark the nominal beam sizes.

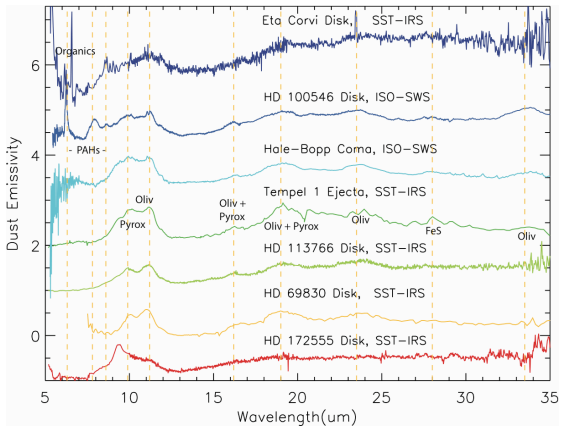

Figure 2 – Comparison of the mid-IR spectra of η Corvi with the spectra of dust from: a young, organic rich Herbig A0 star building a giant planet (HD100546) [5]; two comets (Hale-Bopp and Tempel 1) [5]; a young F5 star building a terrestrial planet (HD113766) [6]; the silica-rich debris created by a hypervelocity impact in the HD172555 system [7]; and a mature main sequence star with a densezodiacal cloud (HD69830) [8]. The similarity between the ~1 Gyr old η Corvi dust and the ~10Myr old HD100546 spectra is readily apparent.

- The warm dust mass is 10^4 – 10^7 larger than that of a solar system comet (10^{12} – 10^{15} kg), but is very simi-

lar to the mass of a large Centaur or medium sized Kuiper Belt object (10^{19} – 10^{21} kg).

- The warm THZ dust contains ~40% amorphous silica, not found in primitive solar system materials like comets and meteorites in such high abndance, arguing for an impact delivery of the material.

- The particle size distribution of the dust is dn/da ~$a^{-3.5}$, with a deficit for particles ≤ 1 μm in size, as expected for dust created from collisional grinding of impact fragments over > 10^3 yrs.

- The *Spitzer* warm dust excess spectrum closely matches spectra reported for the Ureilite meteorites of the Sudan Almahata Sitta fall in 2008, suggesting, since the source of the η Corvi warm dust is its excited Kuiper Belt, that the Ureilite parent body was formed in our solar system by an impact between a KBO and an S-type asteroid.

- The amount of water tied up in the observed circumstellar material, ~10^{18} kg, is > 0.1% of the water in the Earth's oceans, & the amount of carbon present is also considerable, ~10^{18} kg. The total amount of warm dust mass is similar to the 10^{19} – 10^{20} kg estimated to have been delivered to the Earth-Moon system during the solar system's LHB.

Conclusions. The best model for what is going on in the η Corvi (F2V) system is that some process (*e.g.,* planetary migration) is dynamically exciting the Kuiper Belt, causing frequent collisions amongst KBOs and producing the observed copious Kuiper Belt dust. As part of this process, one or more of the excited KBOs was scattered onto an orbit that sent it into the inner system, where it collided with a planetary-class body at ~3 AU, releasing a large amount of thermally unprocessed, primitive ice and carbon-rich dust.

The parent body for the observed warm dust was thus a Kuiper-Belt or Centaur-like body, which captured a large amount of early primitive stellar nebula material and kept it in deep freeze for ~1 Gyr, and was then prompted by dynamical stirring of its parent Kuiper Belt into colliding with a rocky body at ~3 AU at moderate velocities (5-10 km sec^{-1}). The impact velocity was slow enough to preserve most of the original refractory silicates but also fast enough to refreeze ~1/3 of it as silica material, while also delivering large amounts of water (~1% of the mass of Earth's Oceans) and carbon rich material to the planetary body.

While this system is likely a good analogue for the LHB processes that occurred in the early Solar System at 0.6 – 0.8 Gyr after the formation of the CAIs, many things are still not clear: the number of bodies impacting the inner system; the timing and duration of the impacts; the nature of the rocky impactee; or the role the system's planets play in causing the impacts. **η Corvi is thus worthy of further detailed study in order to understand the nature of our LHB**, and to perform a search for a rocky planetary body at ~3 AU (the impactee), and for a giant planet at ~115 AU (the KB dynamical stirrer at ~ the 3:2 resonance of the KB dust at 150 AU).

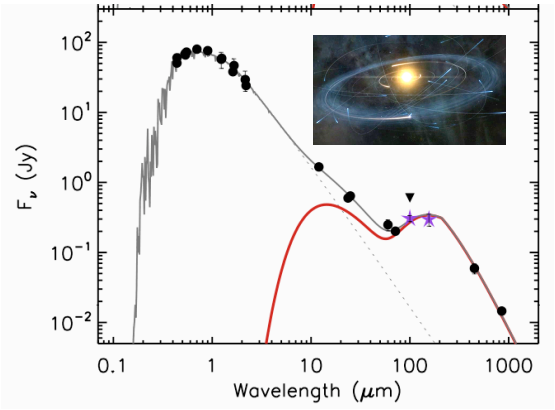

Figure 3. SED for η Corvi showing the 0.4 – 2.2 μm BVR/2MASS system photometry dominated by stellar photospheric emission, the stellar/circumstellar dust MIR flux measurements of IRAS and Spitzer, & the cold FIR excess measured by Herschel and JCMT/SCUBA [2]. Solid grey line: combined fit to the η Corvi SED using a 2-blackbody model (red) with warm (350K) & cold (35K) dust reservoirs + emission from a Kurucz F2V photosphere (dashed line) [4].

References: [1] Chen, C. H., *et al.* 2006, *ApJS* **166**, 351; [2] Matthews, B.C., *et al.* 2010. *Astron. & Astrophys.* **518**, L135 [3] Wyatt, M.C. *et al.* 2005. *Astrophys. J.* **620**, 492; **[4]** Lisse, C.M., *et al.*, 2011. *ApJ* (in press; published on-line as 2011arXiv1110.4172L**); [5]** Lisse, C.M. *et al.*, 2007, *Icarus* **187**, 69; [**6**] Lisse, C.M. *et al.*, 2008, *ApJ* **673**, 1106 [7] Lisse, C.M. *et al.*, 2009, *ApJ* **701**, 2019; [**8**] Lisse, C.M., *et al.* 2007, *ApJ* **658**, 584

Acknowledgements: C.M. Lisse gratefully acknowledges support for performing the modeling described herein from JPL contract 1274485, the APL Janney Fellowship program, and NSF Grant AST-0908815**.**

TWO POPULATIONS OF EARLY LUNAR IMPACTORS AS RECORDED IN ITS ANCIENT CRATER POPULATIONS. S. Marchi[1,2], W.F. Bottke[1], D.A. Kring[3], A. Morbidelli[2], [1]Center for Lunar Origin and Evolution, Boulder, CO (marchi@boulder.swri.edu), [2]Observatoire de la Cote d'Azur, Nice, France, [3] Center for Lunar Science & Exploration, Houston, TX.

Introduction: The earliest bombardment history of the Moon potentially provides powerful constraints for solar system evolution models.

The density of craters on lunar terrains of different ages have been used to study the temporal evolution of the lunar impactor flux. According to these studies [1,2,3], the bombardment of the early Moon experienced a rapid but smooth decay as the leftovers of planetary accretion were gradually eliminated. This declining bombardment phase ended about ~3.7 Ga ago.

This view contradicts the analyses of Apollo lunar samples [4,5] and lunar meteorites [6], which collectively show a clustering of impact-reset Ar-Ar ages and extensive crustal U-Pb mobilization at 3.8-3.9 Ga. These data suggest the Moon was affected by a spike of impacts that would have lasted for a few tens to hundreds of My. This is often referred to as the lunar cataclysm (LC).

If a cataclysm really occurred, it could have left traces in the crater size-frequency distribution (SFD) resulting from impactors leftover from planetary accretion and from impactors responsible for the cataclysm. In order to investigate the above issues, we undertook new lunar crater counts on old lunar terrains.

Terrain choice and crater counts: Crater identification and counts have been performed on digital terrain model (DTM) produced by the Lunar Orbiter Laser Altimeter (LOLA) [7] on board the Lunar Reconnaissance Orbiter. The resolution of the DTM was 64-pixel-per-degree. We analyzed three major regions.

The first region corresponds to a wide portion of the Pre-Nectarian terrains on the northern farside (PNT hereinafter). The second region includes Pre-Nectarian terrains on the floor of the largest impact basin on the Moon, South Pole-Aitken basin (SPAT hereinafter). Both regions are among the oldest ones on the Moon. The third region is made of a part of Nectaris basin floor, its rim regions, and a portion of its ejecta blanket (NBT hereinafter). Nectaris is a benchmark basin used to define time periods on the Moon [8]. It is also the oldest, closest basin to the Apollo 16 landing site in the lunar highlands and has an estimated radiometric age of 3.9 to 4.1 Ga [9,10].

The first challenge is to define geological units that can be used for cratering studies. For instance, most of the Pre-Nectarian terrains are covered by several ejecta blankets from different basins, therefore they may not correspond to an unique age. Nevertheless, empirical estimate of the relevant basins' ejecta thickness [11] suggest they were not able to efficiently obliterate D>15 km craters. We also examined multiple areas within the PNT, SPAT, and NBT terrains to determine if endogenous processes, largely connected to the obliteration of pre-existing craters by the emplacement of lava flows, influenced our results. No effects were found as long as we avoided obvious mare regions on the basin floors. This analysis also showed that the (crypto)mare present in the central part of the SPA basin floor did not significantly affect the D>15 km crater population relative to the peripheral parts of said floor. Finally, by comparing several PNT regions, we determined that large secondary craters did not significantly influence our crater counts in any one of them. The resulting crater SFDs are shown in Figure 1 A, B.

Discussion: Several points of interest stand out from Fig. 1. First, PNT has a higher surface crater density than SPAT for 15<D<60 km. On the other hand, PNT and SPAT are indistinguishable in the range 60<D<150 km. NBT crater density is lower than both SPAT and PNT, as expected given its presumed relatively younger age.

These observations provide us with several curiosities. For example, it is difficult to explain why PNT and SPAT differ for 15<D<60 km yet are within error bars for 60<D<150 km. Our immediate concern was that the overlap was due to crater saturation effects [12]. Using a crater formation code that could model how crater saturation would affect these terrains [13], we determined PNT and SPAT are not saturated.

If the crater SFDs are not saturated, they must reflect the impactors that formed them. The conclusions above imply that the observed crater SFDs reflect their respective impactor SFDs. Therefore, in the light of the higher crater density of PNT, it must be the oldest among the three terrains considered here. Interestingly, all the crater SFDs in a log-log plot are well reproduced by two-sloped distributions up to D=150 km (Fig. 1 C). The cumulative slopes (in log-log plot) derived by best fitting are -1.25±0.03 and -2.6±0.1 for small and large D, respectively. The substantial increase in the slope for small craters with respect to large ones produces a characteristic elbow whose corresponding crater size (D_{elbow}) varies from one distribution to another. Using Monte Carlo simulations we determined that the resulting D_{elbow} is ~47, ~61, ~67 km for PNT, SPAT and NBT, respectively.

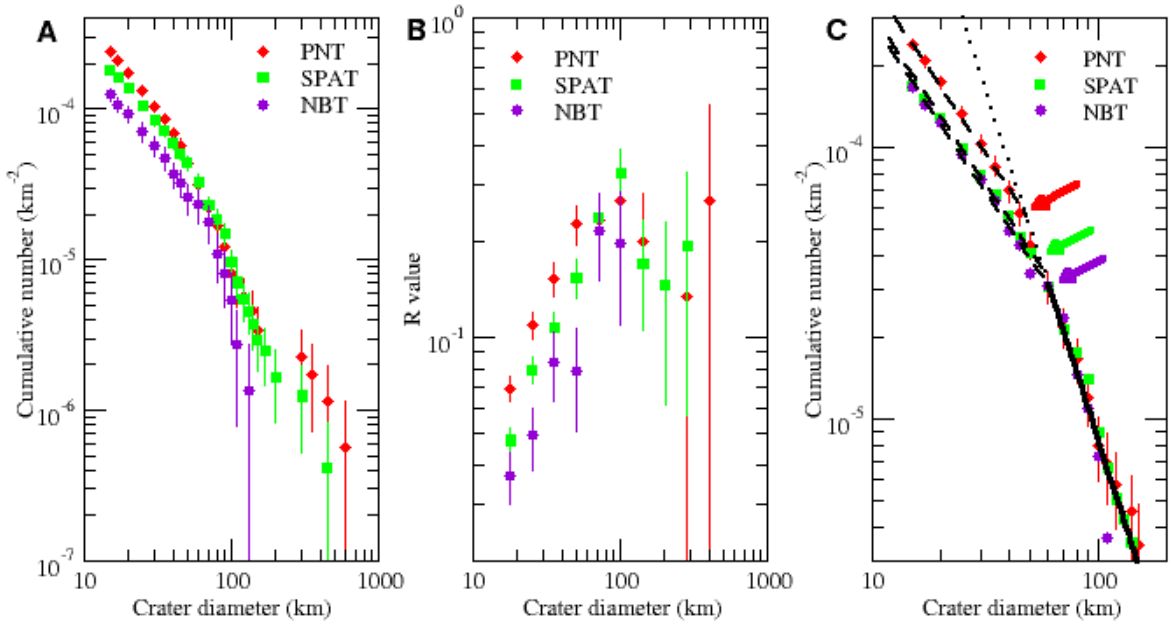

Figure 1: ***A-B:*** *Observed crater SFDs on PNT, SPAT and NBT expressed in cumulative and R-values, respectively.* ***C:*** *Rescaled crater SFDs.* The solid and dashed curves indicate the two-sloped branches of the distributions, and the arrows indicate the approximate positions of the intersection points (see text).

This finding suggests the elbow position shifted to larger sizes from older terrains (PNT) to younger ones (NBT).

Conclusions: We believe the simplest way to explain the observed similarity of the shapes of the crater SFDs is if the impactor SFD stayed constant but the impact velocity increased on the youngest terrains. Higher velocities would boost the sizes of the craters on NBT terrains, thereby collectively shifting its crater SFD to larger values. To test our hypothesis we attempted to reproduce via Monte Carlo simulations the PNT, SPAT and NBT crater SFDs assuming that they recorded, in sequence, two impact populations having distinct velocities, each producing craters with distinct values of D_{elbow}. The combination of these two impacting populations that best fits the observations is achieved by assuming that i) NBT was hit uniquely by an impactor population producing D_{elbow}~60 km, that we call ``late population'' and ii) PNT and SPAT record, in addition to this late population, an ``early population'' producing D_{elbow}~45 km.

Overall the early population accounts for 48% and 32% of the craters D≥15 km observed on PNT and SPAT, respectively. The crater SFDs obtained by this combination of impacting populations pass through the error bars of all the data on all terrains.

In the light of these findings, we conclude that the observed shift in the elbow is most likely due to a variation in the mean impact velocity. According to the Pi-group crater scaling law [14], the crater size scales as $v^{0.44}$, where v is the impact velocity. Therefore, we estimate that the elbow shift from the early to the late population corresponds to a variation of the impact velocity of a factor of ~2 $(=(60/45)^{1/0.44})$. Such an increase in the impact velocity implies a major change to the impactor population. As such, it has major implications for the early history of the solar system. This dramatic velocity increase is consistent with the existence of a lunar cataclysm and potentially with a late reconfiguration of giant planet orbits, which strongly modifies the source of lunar impactors.

References: [1] Neukum and Ivanov, *Hazard due to comets and asteroids*, 1994. [2] Hartman et al., *Basaltic Volcanism on Terrestrial Planets*, Pergamon Press, 1981. [3] Marchi et al., *AJ* 137, 2009. [4] Turner et al., *Proc. Fourth Lunar Sci. Conf.*, 1973. [5] Tera et al., *EPSL* 22, 1974. [6] Cohen et al., *Science* 290, 2000. [7] Smith et al., *JGR* 2010. [8] Wilhelms, *US Geol. Surv. Prof. Pap.* 1348, 1987. [9] Stoffler & Ryder, *Space Sci. Rev.* 96, 2001. [10] Norman et al., *Geochim. Cosmochim. Acta* 74, 2010.[11] Kring, *JGR* 100, 1995. [12] Gault, *Radio Sci.* 5, 1970. [13] Bottke & Chapman, *37th Ann. Lunar and Planet. Sci. Conf.*, 2006. [14] Schmidt & Housen, *Int. Jour. Imp. Eng.* 5, 1987.

Numerical modeling of the Caloris basin. E. Martellato[1], J. Benkhoff[1], L. Colangeli[1], B. Foing[1] and S. Marchi[2, 3], [1]European Space Agency - ESTEC, Keplerlaan 1, 2201 AZ Noordwijk, The Netherlands (corresponding author: emartell@rssd.esa.int), [2]Dept Cassiopee, Université de Nice - Sophia Antipolis, Observatoire de la Côte d'Azur, CNRS, France, [3]NASA Lunar Science Institute Center for Lunar Origin and Evolution, Boulder, CO, USA.

Introduction: Mercury has remained the most enigmatic among the terrestrial planets for more than three decades (e.g., [1]), as all our knowledge has relied on the few data acquired by the NASA Mariner 10 mission. The recent Discovery mission MESSENGER acquired a so new amount of data during its three flybys with the planet and more than half a year of data acquisition from orbit that raises a new perspective into this planet.

Background on Caloris: The Caloris basin (Fig. 1), one of the most important feature of the planet, is the largest well preserved impact basin of Mercury, being its estimated diameter of about 1550 km ([2]). MESSENGER color data, observed embayment relations and the discovery of rimless depressions interpreted to be volcanic vents around Caloris, support a volcanic origin for the interior smooth plains material (e.g., [3]; [4]). According to [5], the Caloris infilling is placed after the Late Heavy Bombardment Event.

Unlike any lunar basin, Caloris also exhibits an extensive system of extensional troughs that are younger than the wrinkle ridges and display orientations that range from radial at the center to dominantly circumferential at the edge of the basin ([2]).

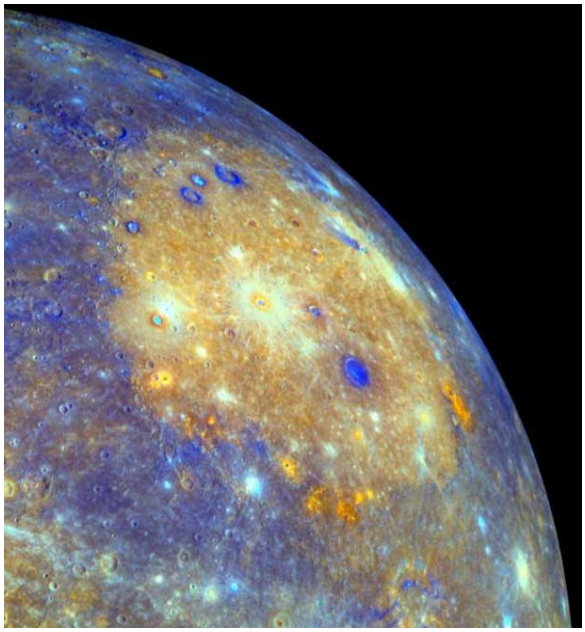

Fig. 1. An oblique color–component of the basin interior obtained from MESSENGER multispectral WAC. *Courtesy of NASA, MESSENGER database*.

The impact event itself holds an important role in the entire tectonic of the planet, as Caloris is believed not only to have affected large areas its surrounding, but also to have caused a great amount of fracturing and surface disruption at its antipode. A possible explanation is that these hilly and lineated terrains are originated by seismic waves focusing at the antipodal regions with respect to the impact (e.g., [1]).

Numerical Modeling: In this work, we will present the preliminary results regarding the numerical modeling of the Caloris basin. We used iSALE multimaterial, multi-rheology shock code ([6], [7], [8], [9], [10], [11]) to simulate the impact event that gave origin to such a basin. The aim of this first study is to investigate the dependence of the basin general outcome from the internal thermal state of the planet, whose evolution has been re-evaluated in light of the new findings of the new data provided by MESSENGER [12].

Mercury is modeled as a half-space as thick as the value of its radius, i.e. 2440 km. The internal structure is set accordingly to [13], [14], and precisely, made up by an upper crust of 40 km, on top on a 600 km mantle, in turn laying above 1800 km core. The different strata are represented by basalt (ρ = 2.86 g/cc), dunite (ρ = 3.31 g/cc) and iron (ρ = 7.84 g/cc), respectively for the crust, the mantle and the core. The thermodynamic behavior of each material is described by tables generated using the Analytic Equation of State (ANEOS).

The projectile is assumed to be a basaltic object, striking the surface at 30 km/s (typical velocity on Mercury's orbit accounting for the 45° impact angle) [15].

Acknowledge: We gratefully acknowledge the developers of iSALE, including Gareth Collins, Kai Wünnemann, Boris Ivanov, Jay Melosh and Dirk Elbeshausen.

References: [1] Strom R.G. and Sprague A.L. (2003) Exploring Mercury: the iron planet, *Springer–Praxis*. [2] Murchie S.L. et al. (2008) *Science, 321, 73–76*. [3] Head J.W. et al. (2008) *Science, 321, 69–72*. [4] Watters T.R. and Nimmo F. (2010) in: Planetary Tectonics, *Cambridge Univ. Press*. [5] Massironi M. et al. (2009) *GRL, 36, L21204,1–6*. [6] Amsden A.A. et al. (1980). Los Alamos National Lab., Rep. LA–8095. [7] Collins G.S. et al. (2004) *Meteoritics & Planet. Sci., 39, 217–231*. [8] Ivanov B.A. et al. (1997)

Int. JIE, 20, 411–430. [9] Melosh H.J. et al. (1992) *JGR, 97, 14,735–14,759*. [10] Wünnemann, K. and Ivanov B.A. (2003) *SSR, 51, 831–845*. [11] Wünnemann K. et al. (2006) *Icarus, 180, 514–527*. [12] Marchi et al. *PSS, In press*. [13] Hauck S.A. et al. (2004) *EPSC, 222, 713–728*. [13] Redmond H.L. and King S.D. (2007) *PEPI, 164, 221–231*. [15] Marchi S. et al. (2005) *A&A, 431, 1123–1127*.

THE EARLY BOMBARDMENT HISTORY OF MARS REVEALED IN ANCIENT MEGABASINS. D. A. Minton[1], W. F. Bottke[2], H. V. Frey[3], R. J. Lillis[4], J. H. Roberts[5], S. T. Stewart[6] [1]Purdue University, Dept. of Earth & Atm. Sci., 550 Stadium Mall Dr., West Lafayette, IN 47907, daminton@purdue.edu, [2]Southwest Research Institute and NASA Lunar Science Institute, 1050 Walnut St. Ste. 300, Boulder, CO 80302, [3]Geodynamics Branch, Goddard Flight Center, Greenbelt, MD 20771, [4]University of California, Berkeley, Space Sci. Lab, 7 Gauss Way, Berkeley, CA 94720 [5]JHU/APL Space Department, 11100 Johns Hopkins Rd., Laurel, MD 20723 [6]Harvard University, Dept. of Earth and Planetary Sci., 20 Oxford Street, Cambridge, Massachusetts 02138

Introduction: Information regarding the early bombardment of Mars is encoded in its largest basins. Using the record of Mars basins (craters with D_{crat}>300 km) that overprint megabasins (basins with D_{crat}>1000 km), including suspected basins in the form of "Quasi-Circular Depressions" (QCDs) that appear in maps of martian crustal thickness variations [1,2], we show that there are two distinct populations of megabasins on Mars:

1) Ancient basins exist that show evidence of remanant crustal magnetism, subdued crustal thickness expression, and high N(300) Crater Retention Age (CRA).

2) The youngest four basins, Utopia, Hellas, Argyre, and Isidis, show no evidence of crustal magnetism and have large crustal thickness contrast with the surrounding terrain and low N(300) CRA.

Furthermore, we show, using a Monte Carlo basin formation code, that the N(300) CRA of these ancient megabasins is indicative of a population in cratering equilibrium, or saturation.

Megabasins and the Late Heavy Bombardment: Based on the lunar rock record, it has been suggested that the Late Heavy Bombardment (LHB) was a spike in the impact rate onto the terrestrial planets at ~4.1-3.9 Gy ago [3-6]. The similarity of the size-frequency distributions between ancient terrains on the Moon, Mars, and Mercury suggests that the LHB impactors originated in the Main Asteroid Belt and were liberated via a size-independent mechanism, such as resonance sweeping [7,8]. This line of evidence suggests that all ancient terrains are part of a common impactor population, and suggests that LHB-era cratering reached equilibrium, or saturation [9]. In contrast, it has been suggested [10,11] that on the Moon, the heavily-cratered terrains may contain a mix of populations with different SFDs, however this contention has been debated [12,13].

Crustal Thickness and Magnetic Anomolies: Using a crustal thickness model for Mars [2], many large circular depressions that may represent ancient buried basins have been discovered [1]. Using the set of D>300 km basins that overprint the D_{crat}>1000 km megabasins, we calculate the N(300) CRA of several megabasins (Figure 1).

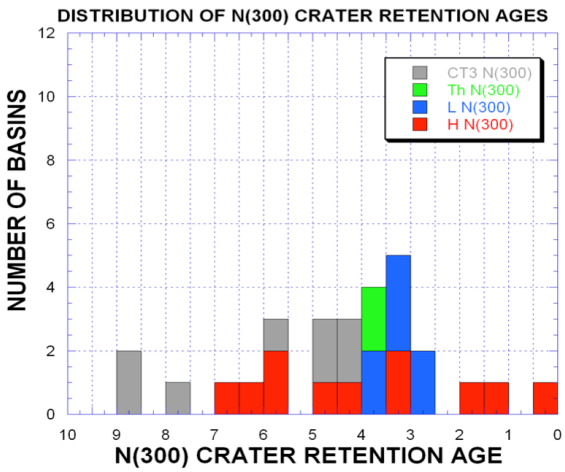

Figure 1 Histograms of N(300) CRA for megabasins on Mars. Red are highland basins, blue are lowland basins, green are basins in the Tharsis region, and grey are new candidate basins derived from the MarsCrust3 crustal thickness model(2).

The four youngest megabasins on Mars (Utopia, Hellas, Isidis, and Argyre) have relatively low N(300) CRA values (<3). These basins are unlikely to be in cratering equilibrium for D_{crat}>300 km craters, and so their N(300) CRA values are related to their ages. These four basins show much more pronounced crustal thickness contrast than the ancient basins. Crustal thickness constrast is measured by taking the ratio between the average crustal thickness, D, at the center of the basin with that outside the rim (Figure 2). In Figure 2 the basin center crustal thickness is defined as the average of D within 0.4 R, where R is crater radius, and the crustal thickness outside the basin rim is defined as the average of D between 1.2 and 1.4 R. The four youngest basins are also distinguished from the ancient megabasins by the weak or non-existent crustal magnetisim associated with them.

The low topographic relief and magnetization of the most ancient megabasins may be a result of formation when Mars had a warmer thermal gradient and a global magnetic field. Models of basin formation into the cooling crust of Mars may help constrain the amount of time that passed between the formation of Utopia basin and the set of ancient megabasins. It is

plausible that the timing of both the loss of the martian magnetic field and a change in the rheologic state of the upper mantle that allowed the high crustal thickness contrast of a large basin to persist were concurrent. If this were the case, then the four youngest basins may be a part of a continuous impact flux, and Utopia simply marks the boundary when both the Mars dynamo ended and the upper mantle heat flow become low enough that basins retained substantial inner-/outer crustal thickness contrast. Alternatively, the four young non-magnetized, high contrast basins may represent a population that impacted Mars well after the earlier magnetized basins.

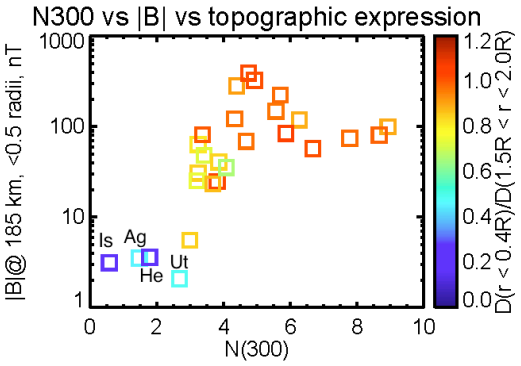

Figure 2 Basin magnetization vs. N(300) CRA age and for megabasins on Mars (D>1000 km). Colors are coded for crustal thickness ratio (inside basin/outside basin). The youngest four basins (Isidis, Argyre, Hellas, and Utopia) show both greater crustal thickness contrast and weaker magnetization than the other basins.

Megabasin Equilibrium Cratering: Using a Monte Carlo basin formation code [14] we show that the population of ancient megabasins shown in Figure 2 that generally have high magnetization, high N(300) CRA, and subdued topography may be in crater equilibrium or saturation. Figure 3 shows the results of our Monte Carlo crater code, plotted has histograms of N(300) CRA values, similar in style to Figure 1. In our code, we track the number of D_{crat}>300 km basins that overprint D_{crat}>1000 km megabasins. The code craters a surface at some rate that is set by the user in arbitrary time interval units. Figure 3 shows the histograms of N(300) CRA for megabasins on the same surface, one set of histograms display 1 time interval after the start of the model and second displays 3 time intervals after the start of the model. The results show that once the surface is in equilibrium total number of megabasins increases, but the peak in the N(300) CRA values remains constant.

The value of the peak of the N(300) CRA histogram depends strongly on the slope of the basin cumulative SFD, where slope refers to the power law index q for a cumulative SFD of the form $N \propto D^q$, as well as the process by which young craters destroy old ones. In equilibrium, the N(300) CRA of individual basins can be modeled as being taken from a normal distribution with a mean that depends on the slope of the basin SFD. The results of our Monte Carlo code also indicate that some change occurred in the most ancient population of impactors recorded on Mars. Two possibilities are that the source region of large impactors was different for these very ancient basins, or that the impactor velocity changed.

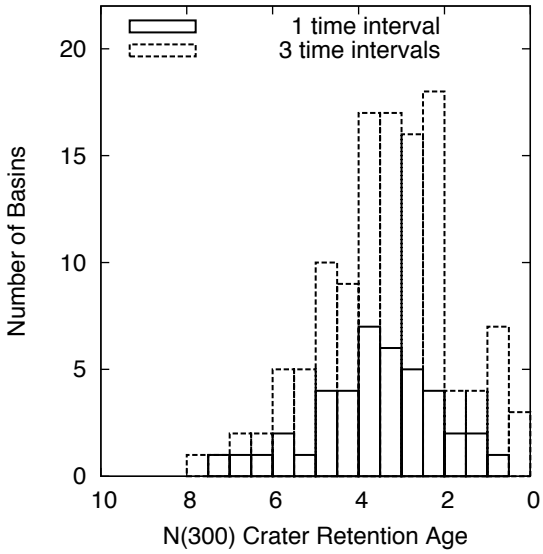

Figure 3 Histograms of N(300) CRA values from a Monte Carlo cratered terrain evolution code. The modeled surface had the same surface area of Mars and the bombardment rate was constant. The solid histogram is the result after one arbitrary time interval, and the dashed line is the result after three time intervals.

References:

[1] Edgar LA, Frey HV. Geophys. Res. Lett. 2008 Jan.;35(2):02201. [2] Neumann G et al. 37th COSPAR Scientific Assembly. 13-20 July 2008. 2008 [3] Tera F et al. Abstracts of the LPSC. 1973 Mar. 1;4:723. [4]Tera F. et al. EPSL. 1974 Apr. 1;22:1. [5] Ryder G. JGR. 2002 Apr. 1;107:5022. [6] Bottke WF et al. 41st LPSC. 2010 Mar. 1;41:1269. [7] Strom RG et al. Science. 2005 Sep. 1;309:1847–1850. [8] Gomes R et al. Nature. 2005 May 1;435:466–469. [9] Richardson JE. Icarus. 2009 Dec. 1;204:697–715. [10] Ćuk M et al. Icarus. 2010 Jun. 1;207:590–594. [11] Fassett CI et al. 42nd LPSC. 2011 Mar.;42:1539. [12] Malhotra R, Strom RG. Icarus. 2011 Nov.;216(1):359–362. [13] Ćuk M et al. Icarus. 2011 Nov.;216(1):363–365. [14] Richardson JE et al. Icarus. 2005 Dec. 1;179:325–349.

POLAR WANDER ON GANYMEDE: A POSSIBLE SOLUTION TO THE APEX-ANTAPEX CRATERING CONUNDRUM. P. S. Mohit[1,2], B. T. Greenhagen[1,3], and W. B. McKinnon[1], Department of Earth and Planetary Sciences and McDonnell Center for the Space Sciences, Washington University, Saint Louis, MO 63130 (mckinnon@wustl.edu), [2]now at Strategic Policy Branch, Environment Canada, Gatineau, QC, K1A 0H3, [3]now at Jet Propulsion Laboratory, Pasadena, CA 91109.

Introduction: The observed leading-trailing hemisphere asymmetry in crater density on Ganymede is far weaker than that predicted by cratering models. We explore polar wander of a floating ice shell as a possible explanation. Due to the latitude dependence of absorbed solar radiation, the surface temperature at the poles is much less than that at the equator. We calculate the resulting ice thickness variations, assuming a conductive, elastic floating ice shell in equilibrium with interior radiogenic heat production. We find pole-equator thickness differences of up to 15 km at 4 Ga and 85 km at the present time. Through their effect on the principal moments of inertia, these thickness variations may cause the shell to become unstable with respect to the rotation axis. We find that the degree-2 thickness variations are sufficient to destabilize the shell for any reasonable value of the relevant parameters. We investigate the possibility of ductile flow in the shell reducing the thickness variations. We find strong thickness variations can be maintained until the onset of convection, which should have occurred when the shell was 30–55 km thick (~1-to-2.5 Ga for monotonically declining radiogenic heat flow).

The Conundrum: Dynamical simulations show that impact cratering occurs preferentially on the leading hemisphere of a synchronously orbiting satellite. Thus, the apex (the center of the leading hemisphere) should show a significantly higher crater density than the antapex (the center of the trailing hemisphere). For Ganymede in particular, cratering models predict an apex-antapex disparity on Ganymede of ~15–40 times. However, the observed crater density at the apex of Ganymede is only ~4 times that at the antapex [e.g., 1,2]. Several mechanisms have been proposed to explain this phenomenon: (1) the surface may be saturated or nearly saturated with craters; (2) a large fraction of the craters may have been made by planetocentric debris or some other unknown source, rather than heliocentric comets; and (3) the ice shell may have rotated nonsynchronously during geologic time [1–3].

In this work, we explore a form of nonsynchronous rotation: polar wander due to thickness variations in the ice shell. This idea has previously been studied for Europa by Ojakangas and Stevenson [4,5], but only potential reorientation due to the impact basin distribution has been considered for Ganymede [6]. Both of the above groups concluded that polar wander by these mechanisms was indeed possible.

A necessary condition for reorientation (of the sort considered here) to occur is that the ice shell be decoupled from the interior of the satellite by an ocean. Galileo magnetometer results suggest the presence of a liquid ocean on Ganymede at the present time [7,8], and it is likely to have existed for much or all of solar system history [8,9]. Polar wander may occur when large variations in ice shell thickness cause the shell to become unstable with respect to its principal moment of inertia (MOI) directions, resulting in inertial interchange polar wander in which the poles exchange positions with apex and antapex. Following the method of [4,5], we estimate thickness variations of Ganymede's cooling ice shell throughout its history and their effect on Ganymede's ice shell MOI. We then investigate the potential for ductile flow in the shell to counteract this by reducing the thickness variations.

Results: Using a model of a conductive, cooling viscoelastic ice shell, we can establish conditions necessary for the reorientation of Ganymede's ice shell. We neglect tidal heating to first order, because for Ganymede tidal heating is far smaller than radiogenic heating today (and throughout most of the past in dynamical models of the Laplace resonance [10]). The thickness variations produced in Ganymede's ice shell by the pole-equator temperature contrast (15–85 km, Fig. 1) should be sufficient to destabilize the shell any point during the its history. As the shell thickens, however, the time scale of viscous flow in shell decreases, eventually resulting in the relaxation of thickness variations when surface heat flows drop below ~6–11 mW m^{-2}.

As the ice shell thickens, it also becomes less stable against solid state convection. Models of grain size evolution in an ice shell suggest that the minimum thickness at which convection is possible (for a Ganymede equatorial surface temperature) would be in the range 30–55 km [11] — corresponding to a heat flux of ~7–15 mW m^{-2}. Convection would bring warm ice from the base of the shell region to the cold lid, producing an adiabatic temperature gradient. This would 1) facilitate relaxation of thickness variations, and 2) reduce the pole-equator temperature contrast responsible for creating the thickness variations. As a result,

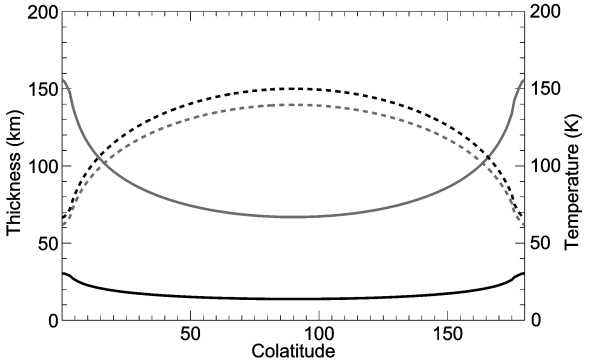

Fig. 1. Temperature (dashed) and ice shell thickness (solid) on Ganymede 4 Gyr ago (black) and today (grey). Local conductive radiogenic steady-state is assumed, but the thickness is only realistic when heat flows are high and ice thicknesses low, which prevents convection and limits viscous relaxation at the base of the shell.

polar wander would be unlikely to occur once the shell had thickened sufficiently to allow convection, which would be expected to occur between 1–2.5 Ga, for a monotonically declining, radiogenic steady state heat flow.

By the same token, the dynamics of polar wander are beyond the scope here — but are nevertheless crucial to the question of whether the shell will reorient. In a viscoelastic ice shell, the torque produced by the unstable MOI configuration must overcome the internal dissipation of the shell (both viscous and frictional) in order for polar wander to occur. The process is very sensitive to the viscosity variation with depth in the shell and is therefore difficult to accurately model. The work of [5] has shown that polar wander is dynamically difficult to achieve on Europa in the absence of 1) a significant low-conductivity regolith, which would greatly reduce the viscosity of ice near the surface, or 2) surface fractures, possibly lubricated by melt water, which extend to a depth where the ice behaves viscously on polar wander time scales. These requirements should also hold here, although the greater thickness variations of Ganymede's ice shell should facilitate the process.

In sum, we argue that polar wander is likely to have occurred early in Ganymede's history, when the satellite's ice shell was thin This would also have been concurrent with the heavy bombardment of what are now recognized as Ganymede's ancient cratered terrains (plausibly due to a heavy cometary flux during a Nice-model-like Solar System rearrangement). Ganymede's shell would need to be thinner than ~55 km; realistically, it would probably need to be substantially thinner in order to overcome the resistance of the shell. An episode of strong tidal heating, such as that proposed by [10], might also have produced the necessary conditions (including thinning and weakening the lithosphere); however, the ice thickness distribution would differ in detail from that discussed here.

A single episode of inertial interchange polar wander (90° of rotation) would not by itself fully erase any apex-antapex crater density differences on Ganymede, but if repeated (or if a continuous process) would be able to do so. If such reorientation(s) did occur, the current modest apex-antapex disparity in crater density on Ganymede must have developed since the last episode of polar wander. Logically, similar arguments might be applied to other icy satellites that possess internal oceans and which in principle had thin ice shells very early in their histories (e.g., Callisto). For other satellites, the lack of a pronounced apex-antapex cratering asymmetry may be due to one of the other causes given above. Is there any real doubt that Rhea, for example, is not saturated with craters (essentially) everywhere?

References: [1] Zahnle K. et al. (2001) *Icarus, 153,* 111–129. [2] Schenk P. M. et al. (2004) in *Jupiter–TPSAM,* Bagenal F. et al. (eds.), CUP, 427–456. [3] Dones L. et al. (2009) in *Saturn from Cassini-Huygens,* Dougherty M. K. et al. (eds.), Springer, 613–635. [4] Ojakangas G. W. and Stevenson D. J. (1989) *Icarus, 81,* 220–241. [5] Ojakangas G. W. and Stevenson D. J. (1989) *Icarus, 81,* 242–270. [6] Murchie S. L. and Head J. W. (1986) *Geophys. Res. Lett., 13,* 345–348. [7] Kivelson M. G. et al. (2002) *Icarus, 157,* 507–522. [8] Schubert G. et al. (2004) in *Jupiter–TPSAM,* Bagenal F. et al. (eds.), CUP, 281–306. [9] Spohn T. and Schubert G. (2003) *Icarus, 161,* 456–467. [10] Showman A. P. et al. (1997) *Icarus, 129,* 793–801. [11] Barr A. C. and McKinnon W. B. (2007) *J. Geophys. Res., 112,* E02012

THE SAWTOOTH-LIKE TIMELINE OF THE FIRST BILLION YEAR OF LUNAR BOMBARDMENT.

A. Morbidelli[1], S. Marchi[2,1] and W.F. Bottke[2], [1]Observatoire de la Cote d'Azur (B.P. 4229, 06304 Nice Cedex 4, Nice, France; morby@oca.eu) , [2]Southwest Research Institute (1050 Walnut St.,Boulder, CO 80302).

Introduction: Two radically different views of the Moon's bombardment history can be found in the literature: one describing a smooth exponential decline of the bombardment rate from 4.5 to 3.6 Ga ago [1] and the other arguing for a prominent impact spike about 3.9 Ga ago [2]. Both scenarios claim to be consistent with crater counts on lunar terrains of "known" radiometric ages. In reality, however, only the youngest units, starting with the Imbrium basin ~3.8-3.9 Ga ago, have well established radiometric ages, whereas the ages of older basins, like Nectaris and Serenitatis, are subjects of debate [3]. The view arguing for a smooth exponential decline assumes that the age of Nectaris is ~4.1 Ga, while the view arguing for an impact spike assumes that its age is ~3.9 Ga. This younger age implies a steeper decline of the bombardment rate in the 3.9-3.7 Ga period which, when extrapolated back to 4.5 Ga, requires am unrealistic number of starting projectiles: hence the need for an impact spike.

In this abstract, we revisit the problem from a combination of theoretical considerations (by looking at plausible source of projectiles and their dynamical evolutions) and calibrations on constraints. Our results support a view which is somewhat intermediate between the two endmember views described above. In fact, we argue for the need of an impact spike, but as early as ~4.1 Ga ago and not as prominent as in [2].

The Nice model and the E-belt: The Nice model [4,5] showed that an impact spike on the terrestrial planets is possible and plausible, due to a sudden change in the orbital configuration of the giant planets. Such a change is needed in order to explain the current structure of the outer Solar System, but the time when it occurred is not known a priori (see [6] for a review). The most recent and interesting development of the Nice model is the E-belt concept [7], which stems from the realization that the current inner boundary of the asteroid belt (~2.1 AU) is set by the nu6 secular resonance whose existence is specifically related to the current orbits of Jupiter and Saturn. Before the giant planets changed their orbital configuration, Jupiter and Saturn were closer to one another and were on more circular orbits; this meant the nu6 resonance was not present. Hence the asteroid belt could extend closer to Mars (i.e. down to 1.7-1.8 AU). This putative E-belt population between 1.7-2.1 AU is now nearly gone, with the survivors making up the Hungaria asteroids.

The original population in this region is calibrated in two independent ways, leading to very similar population estimates. The Size Frequency Distribution (SFD) of the E-belt objects is assumed to be the same as in the current main asteroid belt. With these settings, when the E- and main belts were destabilized by giant planet migration, about 12 basins formed on the Moon [7] over a period of ~400 Ma,. Knowing that the last basin on the Moon (Orientale) formed ~3.7 Ga ago, this implies that the ~12th from the last basin (i.e. Nectaris) formed about ~4.1 Ga ago, in agreement with [1]. Moreover, the number of craters per unit area formed since the destabilization of the E-belt is consistent with crater counts on Nectaris. And finally, the decay rate of the bombardment rate since the destabilization of the E-belt is in very good agreement with the bombardment decline in [1] (see Fig. 1). In summary, the Nice model agrees and supports the view of [1] for times up to ~4.1 Ga ago.

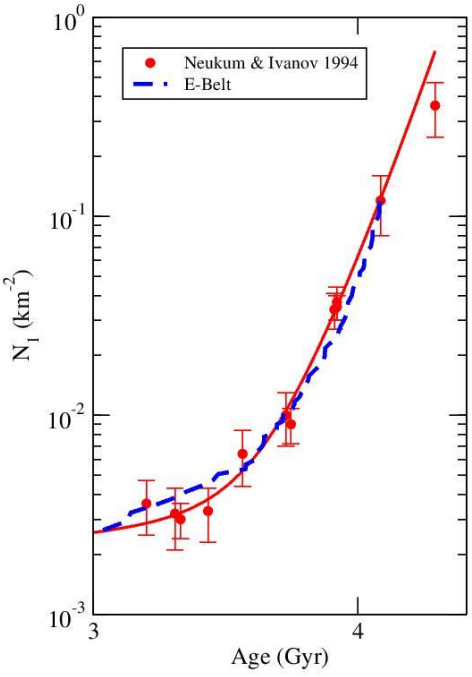

Red curve: the total number of craters larger than 1km per km^2 as a function of unit's age, according to [1]. Dash-blue: the same, for the E-belt model [7]. Notice the almost perfect match between 3.4 and 4.1 Ga.

The need for a bombardment spike: The bombardment rate in [1] before 4.1 Ga is estimated by a simple backward extrapolation of the bombardment

rate inferred in the 3.4-4.1 Ga period. It is possible, however, that this extrapolation is not justified: (i) no source of projectiles has ever been shown to be able to decay over ~1 Gy with the rate implied in [1]; (ii) if the extrapolation were correct, the total mass accreted by the Moon since its formation would have been ~5 times larger than that inferred from the Highly Siderophile Element (HSE) content of the Lunar mantle ($1.7x10^{19}$kg, [8]).

In agreement with our improved understanding of the early Solar System evolution, we postulate that the Moon experienced two distinct bombardments: (a) a post-accretion bombardment, due to the planetesimals leftover from the terrestrial planet formation process and (b) a late bombardment, triggered at ~4.1 Ga by the displacement of the giant planets orbits and the destabilization of the E-belt. Here we assume for simplicity that the decay rate of the post-accretion bombardment was the same as that of the late bombardment (a better estimate of the decay rate of the early bombardment is in progress, from recent simulations of terrestrial planet formation [9]). Thus, we are left with only a single free parameter, which is the total intensity of the post-accretion bombardment. The latter is calibrated by total amout of material accreted by the Moon since its formation, as constrained by the Lunar HSE abundance, though here we assume that most of the early projectile mass reaches and is mixed into the lunar mantle through a presumably thin conductive lid.

Conclusions: The resulting timeline of lunar bombardment is reported in Fig. 2, both in differential and cumulative forms. The differential view suggests that, rather than a impact spike, the timeline of the Moon bombardment has a sawtooth profile. The cumulative view shows that the bombardment since 4.1 Ga ago, including the late bombardment caused by the destabilization of the E-belt, accounts for about 1/3 of the total bombardment suffered by the Moon since its existence. This is in agreement with the total number of basins on the Moon (~40), of which only ~12 are Nectarian and post-Nectarian (i.e. younger than ~4.1 Ga). We note that this could be an underestimate because some ancient basins have probably been erased.

Large portions of the lunar highlands have a crater density that is about twice of that of Nectaris [10]. According to the cumulative bombardment shown in Fig. 2, this would imply that these portions of highlands started to retain craters about 4.35 Ga ago, consistent with recent estimate of the timescale for the thickening of the lunar lithosphere [11]. This age also matches the closure age of the crust, as derived from the model ages for KREEP (P. Spudis, pers. comm.) This suggests that the lunar lithosphere could retain the imprint of basins earlier than the imprint of small craters.

The sawtooth-like bombardment timeline has profound implications for Earth's habitability. In the view of [1], the Earth was increasingly hostile to life going back in time, as the bombardment raised exponentially. In the view of [2] the prominent impact spike 3.9 Ga ago might have sterilized the Earth. In the sawtooth view, the bombardment rate was perhaps never exceptionally high, though big impactors did occur over an extended period. Life might have formed early in the Earth history and survived from that time.

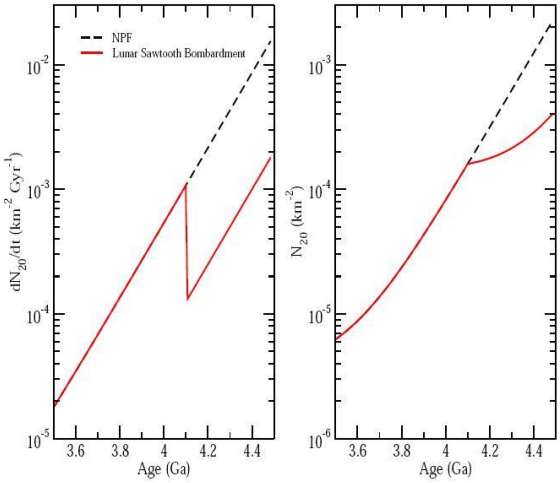

The timeline of the Moon bombardment. Black dashed (labeled NPF): the view in [1]. Red curve: our results combining a post-accretion bombardment and the late E-belt bombardment. The left panel shows the bombardment rate as a function of time; the right panel shows the cumulative bombardment suffered by a terrain as a function of its age. The unit on the vertical axes is the number of craters larger than 20km per km^2.

References: [1] Neukum G. and Ivanov B. (1994) *LPSC, 25*, 991. [2] Ryder G. (1990) *LPSC 746*, 42. [3] Norman M.D. et al. (2010) *GCA 74*, 763. [4] Gomes R. et al. (2005) *Nature*, *435*, 466. [5] Morbidelli A. et al. (2007), AJ, *134*, 1790. [6] Morbidelli A. (2010) *C.R. Physique 11*, 651-659. [7] Bottke W.F. et al. (2011) *LPSC, 42*, 2591. [8] Day J.M.D. et al. (2010*) Earth Planet. Sci. Lett. 289*, 595. [9] Walsh K. et al. (2011) *Nature*, *475*, 206 [10] Strom R.G. (1977) *Physiscs of the Earth and Planetary Interiors*, *15*, 156. [11] Meyer J. et al. (2010) *Icarus*, *208*, 1

Acknowledgments: A.M. and S.M. are grateful to the Helmoltz Allainace "Planetary Evolution and Life" for funding this work. W.B. and S.M. thank the funding provided by NASA's Lunar Science Institute.

ON THE HISTORY OF EARLY METEORITIC BOMBARDMENT OF THE MOON: DID THE LUNAR TERMINAL CATACLYSM OCCUR? Gerhard Neukum[1] Alexander Basilevsky[1,2], Thomas Kneissl[1], Greg Michael[1], Boris Ivanov[1,3] 1- Free University of Berlin, Berlin, Germany; 2 - Vernadsky Institute, Moscow, Russia; 3 – Institute of Dynamics of Geospheres, Moscow.

Introduction: Here we consider the issue of the terminal lunar cataclysm (also called Late Heavy Bombardment) which is a potential feature of the so-called early intense bombardment. The concept of the latter in relation to the Moon was first suggested even before the Apollo-Luna sample returns (Hartmann, 1965, 1966). The isotopic measurements of absolute ages of samples of lunar rocks brought by the Apollo/Luna missions seemed to confirm this concept (e.g., Papanastassiou and Wasserburg, 1972; Hartmann, 1972; Turner et al., 1973; Turner, 1977). Some of the works considered the early intense bombardment as the final stages of the planetary accretion with the half-life of the bombardment rate decrease being $\leq 10^8$ years (e.g., Hartmann, 1972; Neukum et al., 1975), while others considered it the result of large collisions in the asteroid belt (e.g., Turner et al., 1973).

The hypothesis of a "lunar terminal cataclysm" is one possible scenario of the early intense bombardment. It suggests that approximately 3.9 Ga ago there was a strong peak in meteorite bombardment of the Moon when most of the craters observed in the lunar highlands and thus most of the lunar highland impact breccias were formed (Tera et al., 1973, 1974). It is based on the observation that the ages of highland samples from all lunar missions determined by a variety of isotopic techniques group around 3.9–4.0 Ga. This is considered as evidence for widespread shock metamorphism and element redistribution resulting from large-scale impacts on the Moon during that relatively narrow time interval. Since its first publication, the hypothesis has been widely debated with arguments for and against (e.g., Hartmann, 1975; Grinspoon, 1989; Cohen et al., 2000; Stoffler, Ryder, 2001; Hartmann, 2003; Chapman et al., 2007; Hartmann et al., 2007). In this paper we reconsider whether the lunar terminal cataclysm did occur. For this purpose we first analyze the published results of K-Ar dating of lunar highland rocks (mostly breccias, impact melt and no-melt breccias).

Summary of Ar-Ar dating of lunar highland rocks: Here we consider the results of K-Ar dating of samples of lunar highland rocks, which are mostly made by application of the Ar-Ar technique. The K-Ar clock is easily reset by thermal events so the K-Ar dating is most sensitive to shock metamorphism and impact melting resulting from meteoritic bombardment. The major source of information for the samples considered and their ages is *The Lunar Sample Compendium* compiled by Charles Meyer at the JSC NASA (http://curator.jsc.nasa.gov/ lunar/compendium.cfm) with additions from recent publications. Below are plots of Ar-Ar ages of highland rocks brought by the Apollo 14, 15, 16 and 17 missions. The Apollo 14 and 15 missions brought samples from the sites located within the ejecta blankets of the Imbrium basin and thus dating when this basin formed (peaks at ~3.9 Ga). The Apollo 16 and 17 missions brought samples from sites where, together with distant ejecta from the Imbrium basin, ejecta from the nearby Nectaris and Serenitatis basins are expected.

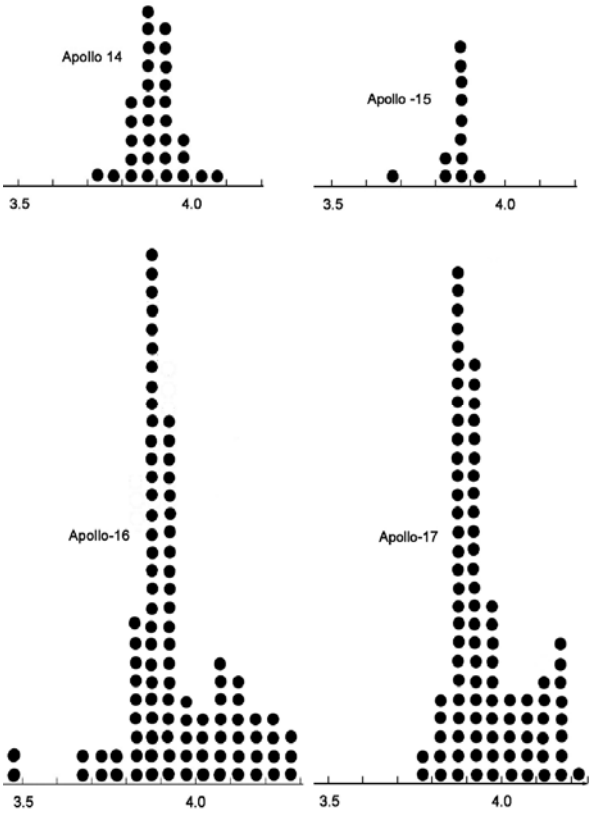

The above histograms for the Apollo 14 and 15 rocks show a prominent peak at ~3.9 Ga (which we interpret as the Imbrium signature) while histograms for the Apollo 16 and 17 rocks show not only the prominent peak at ~3.9 Ga, but secondary peaks at ~4.1 and 4.2 Ga.

This, in our opinion, suggests that the Nectaris and Serenitatis basins formed 100-200 My before Imbrium (~3.9 Ga), which is in contradiction with the hypothesis of a lunar cataclysm.

Summary of Ar-Ar dating of lunar meteorites: In an attempt to minimize the influence of Imbrium basin ejecta we summarized data on Ar-Ar ages of lunar meteorites, which are believed to be delivered to Earth from randomly distributed sites on the lunar globe. The sources of this information are *The Lunar Meteorite Compendium* compiled by Kevin Righter, also at the NASA Johnson Space Center, Houston, http://curator.jsc.nasa.gov/antmet/lmc/index.cfm, and the *Compendium of Lunar Meteorites*, run by Randy Korotev, Washington University in St. Louis, http://curator.jsc.nasa.gov/antmet/lmc/index.cfm. Data on the ages of lunar meteorites from recent publications are also

included. Based on these sources we have compiled results of Ar-Ar dating of 91 clasts from 20 lunar meteorites. A summary of Ar-Ar ages of highland rocks from lunar meteorites is shown in the form of a histogram at the end of this abstract.

It is seen in this histogram that the Ar-Ar ages of lunar meteorites, contrary to the Apollo highland rocks, show no prominent peak at 3.9 Ga. Instead there is a rather uniform frequency distribution of age values within the 2.4 to 4.25 Ga age interval, while within the 1.5 to 2.4 Ga age interval the frequency is also close to uniform, but there it is obviously lower. This character of distribution of ages of highland rocks and of lunar meteorites was noticed and discussed by Hartmann (2003), Hartmann et al. (2007) and Chapman et al. (2007). Folowing these authors we believe that this age distribution questions the hypothesis of a lunar cataclysm.

Summary of the cratering record of pre-mare impact structures: Using crater size-frequency data in combination with superpositional relationships it is possible to set up a complete relative stratigraphy for all established lunar pre-mare basins with diameters larger than 300 km. For this purpose we used mainly three different datasets: (a) crater size-frequency data as published by Wilhelms (1987) and Neukum (1977, 1983), (b) stratigraphic relationships as determined by Wilhelms (1987) (this contains superpositional relations and so-called "age groups"), and (c) newly determined crater-size frequency data for the South Pole-Aitken basin. The resulting relative stratigraphy indicates that 13 basins are younger than Nectaris and 32 basins are older. Assuming a formation age of 4.1Ga for Nectaris, this is in contradiction with a LHB spike in the lunar cratering rate and the according hypothesis of a lunar cataclysm.

Megaregolith evolution modelling: We have constructed a model to consider the production of impact melt on the Moon, together with its redistribution, burial and mixing at the lunar surface by impact 'gardening'. We expect to obtain an insight into the relative frequency of melts of different ages at the near-surface — the source of both the lunar samples and meteorites — for various hypothesised scenarios of the impact rate history. A terminal lunar cataclysm, if it occurred, should have left a global signature in the melts present at the surface, which would be identifiable in a sufficiently large sampling from random sites, as given by the lunar meteorites. The model will allow us to constrain the impact rate history to those scenarios consistent with the present sampling.

Conclusions: It follows from the above considerations that the hypothesis of a terminal lunar cataclysm is not consistent with the lunar meteorite record, and likely did not occur. The peak at ~3.9 Ga seen in the Apollo samples is interpreted as the signature of the Imbrium basin. A final solution to this problem needs new sample return missions from the Moon. Samples dating the largest and probably the most ancient South pole-Aitken basin would be especially helpful.

References:

[1] Chapman et al. (2007) Icarus, 189, 233-245. [2] Hartmann (1965) Icarus. 4, 207-213. [3] Hartmann (1966) Icarus. 5, 406-418. [4] Hartmann (1972) Astrophys. Space Sci. 12, 48-64. [5] Hartmann (2003) Meteorit. Planet. Sci. 38, 4, 579-593. [6] Hartmann et al. (2007) Icarus, 186, 11-23. [7] Neukum et al. (1975) Proc Lunar Sci Conf 6:2597-2620. [8] Papanastassiou & Wasserburg (1972) Earth Planet Sci Lett 16, 289-298. [9] Tera et al. (1973) LPSC – 4 abstracts, 723. [10] Tera et al. (1974) Earth Planet Sci Lett 22:1-21. [11] Turner et al. (1973) Proc. Lunar Sci. Conf. 4th. V. 2, 1889-1914. [12] Turner (1977) Phys Chem Earth 10:145-195. [13] Wilhelms, D.E. (1987) The Geologic History of the Moon. U.S. Geol. Surv. Prof. Paper 1348, 302 pp. [14] Neukum (1977) Phil. Trans. R. Soc. Lond. A 285, 267-272 [15] Neukum, G, (1983) Habilitation, Univ. Munich

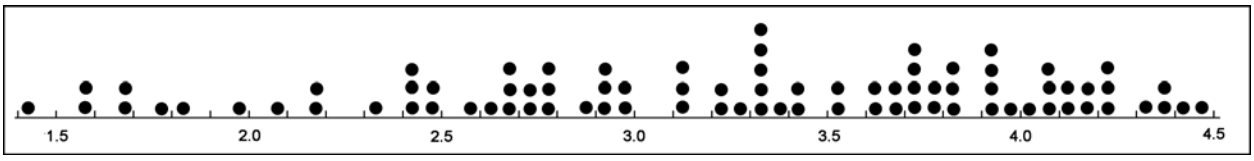

PETROLOGY OF THE IMPACT MELT CLASTS IN 60016, ANCIENT REGOLITH BRECCIA. Takafumi Niihara[1, 2], Lillian Schaffer[3], David A. Kring[1, 2]. [1]Center for Lunar Science and Exploration, Lunar and Planetary Institute, Houston, TX. 77058 (niihara@lpi.usra.edu), [2]NASA Lunar Science Institute. [3]Dept. of Earth and Atmospheric Sciences, University of Houston.

Introduction: Early impact bombardment dramatically affected the evolution of the Moon's surface. It has been hypothesized that the basin-forming epoch occurred in a cataclysmic spike of impactors [1–3] that are dominantly from the asteroid belt [4, 5]. Data remain scarce, however, and the hypothesis requires additional tests. In particular, it is still necessary to compare the impact age distributions among different populations of impact melt. We are, thus, examining fragments of melt that survive in cm-size clasts within the 60016 ancient regolith breccia. This rock was classified as a B2-type ancient regolith breccia. It was assembled from regolith produced from the Cayley Formation [e.g., 6].

Samples and Analytical Procedure: We have been allocated six impact melt clasts that are 1-2 cm in size (Clasts 1-6). Here we report petrological analyses of three of six clasts: Clast 1 (,319), Clast 2 (,320), and Clast 6 (,321). We conducted optical microscopic observations, back-scattered electron (BSE) image observations, and elemental mapping using a Field Emission –Scanning Electron Microscope (JEOL JSM-7600F), and major elements analyses using an Electron Probe Micro Analyzer (EPMA; CAMECA SX-100) at JSC. EPMA analyses of silicates were performed with an accelerating voltage of 15 kV, electron beam current of 20 nA, and a focused beam. Defocused beam (20 μm diameter) analyses (DBA) of representative areas for each clast were performed by EPMA to estimate bulk compositions.

Results: *Clast 1, a clast-rich poikilitic melt,* contains ~45 % of relict mineral fragments of plagioclase ($An_{97\text{-}95}$ $Or_{0.6\text{-}0}$; 39 %), olivine ($Fo_{79\text{-}69}$; 5 %), and pyroxene ($En_{77\text{-}58}Wo_{2.5\text{-}5.2}$; 1 %). Plagioclase relicts have a slightly Na-rich overgrowth along their rims and show euhedral to anhedral morphologies. The Na-rich rims contain small Fe-Ni droplets (less than 1 μm in diameter). Melt products locate at the interstices of relict fragments. Interstitial materials consists pyroxene ($En_{82\text{-}46}Wo_{42\text{-}3}$), plagioclase ($An_{97\text{-}95}$ $Or_{0.6\text{-}0}$), Fe-Ni metal, sulfides, oxide and glass. Pyroxene encloses fine-grained euhedral to subhedral plagioclase and rounded relict olivine.

Clast 2, a clast-poor poikilitic melt, contains ~15 % of relict olivine ($Fo_{82\text{-}73}$; 12 %), plagioclase ($An_{97\text{-}93}$ $Or_{0.4\text{-}0}$; 2 %), and pyroxene ($En_{84\text{-}78}Wo_{3.9\text{-}2.8}$; 1 %). Plagioclase relicts have a slightly Na-rich rim and have euhedral to anhedral crystal morphologies. The Na-rich rims contain small Fe-Ni droplets (less than 1 μm in diameter). Olivine and pyroxene are irregular in shape. This clast has a poikiloblastic texture of up to 2 mm pyroxene ($En_{83\text{-}49}Wo_{41\text{-}3}$) that encloses fine-grained euhedral plagioclase ($An_{96\text{-}84}$ $Or_{1.3\text{-}0.1}$) and is embedded in an olivine- and feldspar-bearing mesostasis.

Clast 6, a clast-poor porpyiritic melt, contains ~15 % of relict olivine ($Fo_{86\text{-}80}$; 9 %) and plagioclase ($An_{98\text{-}90}$ $Or_{1.0\text{-}0}$; 6 %). Plagioclase relicts are rimmed and have euhedral to anhedral shapes. The groundmass of this clast is filled by large amounts of fine-grained dendritic pyroxene, plagioclase ($An_{97\text{-}90}$ $Or_{0.6\text{-}0.1}$), and interstitial glass.

Bulk compositions (DBA): Clast 1 has high Al_2O_3 (26.6 wt. %) and low FeO+MgO (9.78 wt. %) values, similar to those of Group2 melts [e.g. 7]. Clast 2 and 6 have high K_2O (~0.50 wt. %) and FeO+MgO (~19.6 wt. %) values, and low Al_2O_3 (~19.1 wt. %) similar to Group 1 melts [e.g. 7].

Discussion and summary: Clast 1 has a different bulk composition than the other two samples (Fig.1). The high concentration of Al and low concentrations of Fe and Mg in the clast 1 probably reflects the large amount of relict plagioclase. The compositions of relict olivine and plagioclase in Clasts 1 and 2 are similar, but those in Clast 6 are significantly different. Relict olivine in Clast 6 is more forsteritic than that in the other clasts (Fig. 2). In addition, the compositional range in plagioclase in Clast 1 is wide; Clast 6 contains more sodic plagioclase grains (Fig. 3). Although bulk chemical compositions for Clast 2 and 6 are similar, differences in compositions of relict minerals imply that these clasts originate from at least two different impact melts. Thus, the three clasts represent three different types of impact melts.

Acknowledgements: Samples are allocated from Astromaterials Acquisition and Curation Office at JSC. We are grateful to D. K. Ross, and A. H. Peslier for support on FE-SEM and EPMA analyses.

References: [1] Turner G. et al. (1973) Proc. LPSC 4, 1889–1914. [2]Tera et al. (1974) EPSL 22, 1–21. [3] Cohen et al, (2000) Science 290, 1754–1756. [4] Kring D. A. and Cohen B. A. (2002) JGR 107, E2, 5009. [5] Strom et al. (2005) Science 309, 1847–1850. [6] Joy K. H. et al. (2011) GCA. Doi: 10.1016/j.gca.2011.09.018 (in press). [7] Korotev (1994) GCA 58, 3931–3969.

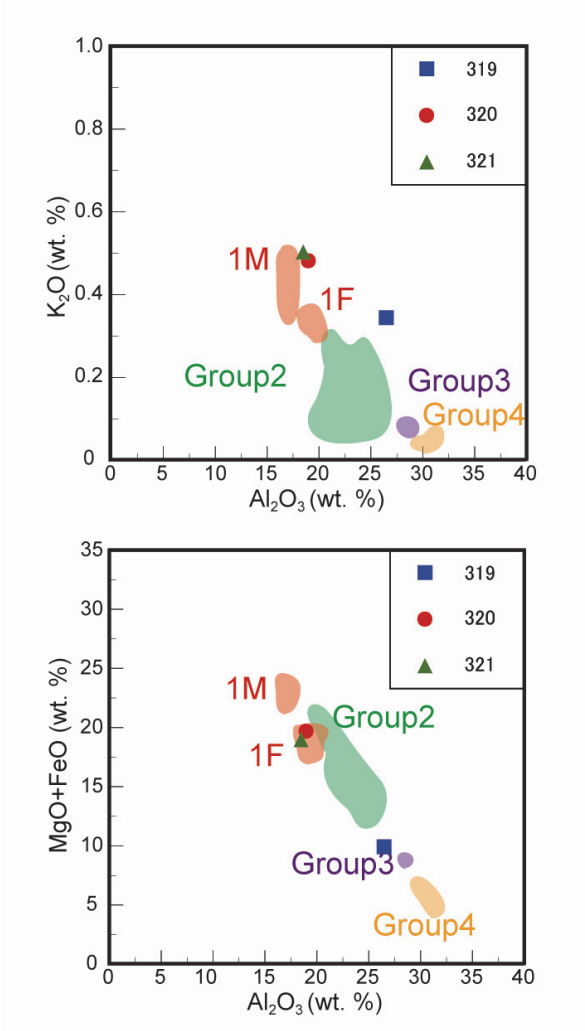

Fig.1. Al_2O_3 vs. K_2O and MgO+FeO plots for bulk (DBA) compositions of Clasts 1, 2 and 6. Reference values for impact melt groups were obtained from [7] and reference therein. These impact melts groups were classified on the basis of Sm and Sc concentrations [7].

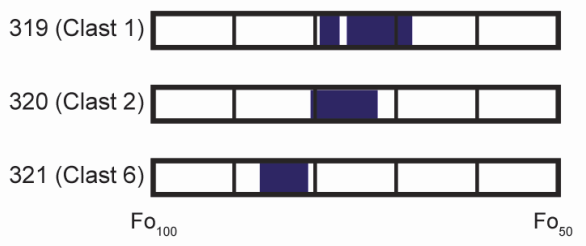

Fig.2. Composition of relict olivines in Clasts 1,2 and 6. Clast 6 has more folsteritic composition than other clasts.

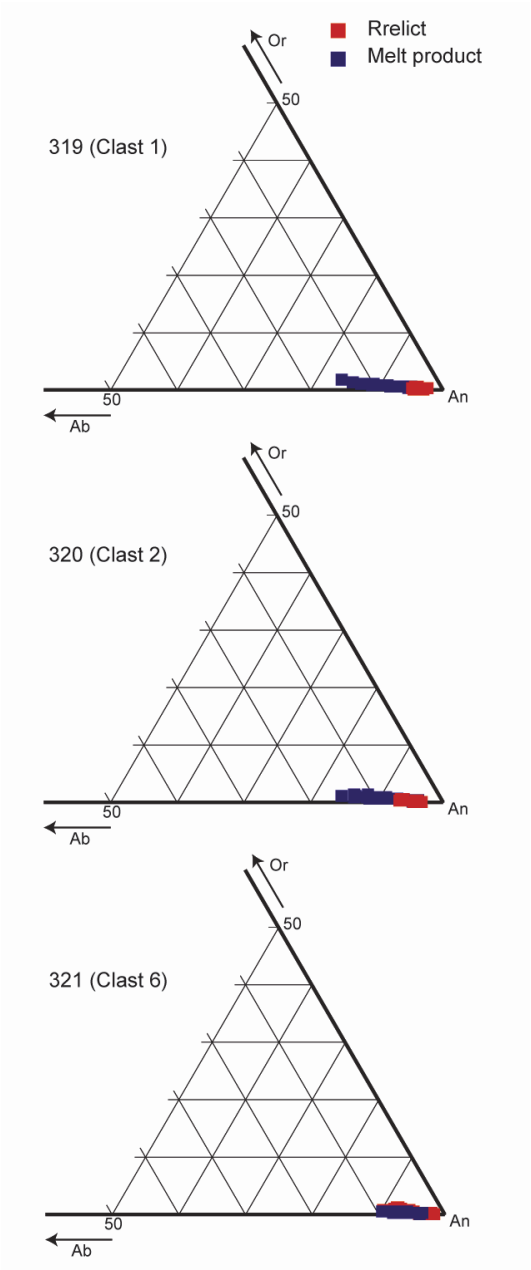

Fig.3. Composition plagioclase in Clasts 1,2 and 6. Red square: Relict plagioclase. Blue square: Melt products.

LARGE IMPACTS AT 4.2 GA FROM URANIUM-LEAD DATING OF LUNAR MELT BRECCIAS. M. D. Norman[1,2] and A. A. Nemchin[3], [1]Research School of Earth Sciences, Australian National University, Canberra ACT 0200 Australia (marc.norman@anu.edu.au), [3]Department of Applied Geology, Curtin University of Technology, Perth WA 6845 Australia (a.nemchin@curtin.edu.au).

Introduction: Crystallization ages of lunar impact melt rocks provide the primary evidence for a spike in the impact flux at ~3.9 Ga. Here we report U-Pb isotopic ages of accessory phases (apatite, zirconalite) in lunar melt breccia 67955 that confirm a crystallization age of ~4.2 Ga and reveal a younger overprint possibly related to entrainment of the breccia by one or more younger basins such as Imbrium.

Petrography: 67955 is a crystalline anorthositic norite breccia collected at North Ray crater. Its poikilitic texture suggested a plutonic igneous origin in early petrologic studies [1,2], but the abundance of FeNi metal, the Fe-Ni-Co compositions of the metal, and the high and chondritic relative abundances of siderophile trace elements in the metal indicates an origin as an impact melt rock rather than as an endogenous magmatic cumulate. The sample has been partially recrystallized, brecciated, and injected with glass veins, but areas with well-preserved, near-primary crystalline textures remain (Fig. 1) and were sampled for this study. Our isotopic and trace element studies of 67955 yielded a ^{147}Sm-^{143}Nd mineral isochron age of 4.20 ± 0.07 Ga, which was interpreted as the time of a major impact event on the Moon, and a geochemical signature of KREEP or Mg-suite plagioclase in the trace element compositions [3]. Major element compositions of the silicate phases fall within the Mg-suite field on a plot of An (plagioclase) vs. En (opx) [3].

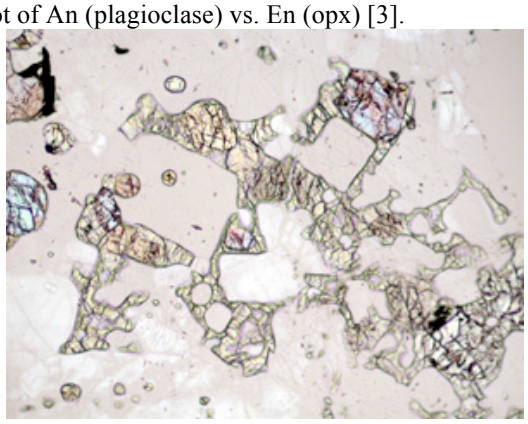

Fig. 1. Photomicrograph of 67955,78 illustrating the slightly annealed igneous texture of the clast analyzed for this study.

During petrographic examination we discovered small grains of a Ca-phosphate mineral (referred to here as apatite) and a Zr-Ti-Ca oxide phase tentatively identified as zirconalite. Ashwal [2] mentioned apatite but zirconalite has not been reported previously in this sample. Electron microprobe analyses of the zirconalite indicate 35-39% ZrO_2, 35-36% TiO_2, 7-10% CaO, 3-5% FeO, and percent level abundances of Y and Nb.

Trace elements in 67955 zirconalite and apatite: Laser ablation ICPMS analyses show that apatite in 67955 contains ~700-2000x CI of LREE with a slight negative slope to the chondrite-normalised pattern and a deep Eu anomaly (Fig. 2). Uranium and thorium concentrations in these apatites were 2.5-6.1 ppm and 10-30 ppm, respectively, while Sr contents were relatively low (140-150 ppm). The single zirconalite analysed by LA-ICPMS contained high contents of normally incompatible lithophile elements, with REE abundances ranging from ~1100 x CI for La to ~13,000 to 15,000 x CI for the middle HREE (e.g. Gd-Er), a deep negative Eu anomaly, and ~1.8 wt% yttrium. Uranium and thorium concentrations in this grain were ~1500 ppm and 4700 ppm, respectively. This grain also contained high concentrations of high-field strength elements such as Nb (7800 ppm), Ta (420 ppm), and Hf (3800 ppm) but low concentrations of Sr and Ba (~10 ppm).

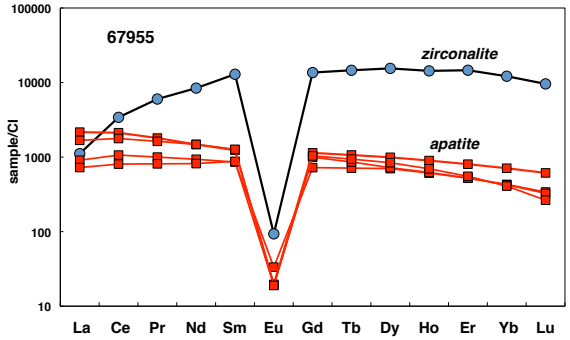

Fig. 2. Chondrite-normalised REE patterns of apatite and zirconalite in 67955.

U-Pb isotopic compositions: U-Th-Pb isotopic compositions and concentrations were measured on individual grains of apatite and zirconalite by SHRIMP ion microprobe at Curtin University. Apatite analyses were calibrated relative to BRA-1 (2058 Ma, 67 ppm U). No U-Pb reference standard is available for zirconalite so only the ^{207}Pb/^{206}Pb model ages calibrated against BRA-1 are reported here.

Apatite: Concordia relationships for the apatite produced an intercept age of 4.13 ± 0.05 Ga (Fig. 3). U contents of these grains ranged from 2-72 ppm. ^{207}Pb/^{206}Pb model ages based on the LA-ICPMS analy-

ses of the 67955 apatites are consistent with an age of 4.1-4.2 Ga. Four grains of apatite from the Duluth gabbro FC1 analysed by SHRIMP returned a concordia age of 1150 ± 59 Ma (MSWD = 2.9) compared to the accepted zircon age of 1099 Ma [4].

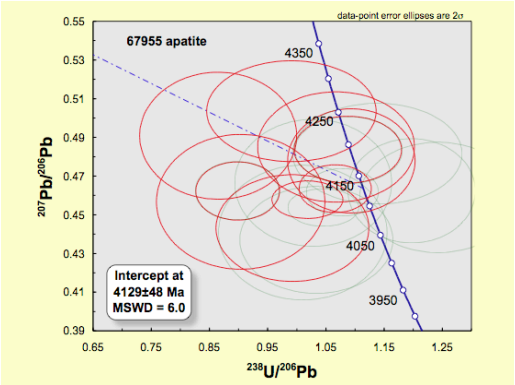

Fig. 3. Concordia diagram for 67955 apatite.

Zirconalite: Zirconalite grains show a wide range of U and Th contents, from 340-14800 ppm and 670-40700 ppm, respectively (Fig. 4). There appear to be two compositional groups, one with lower U (340-1800 ppm) and Th (670-3600 ppm) contents, and a second group with higher concentrations (U 4000-14800 ppm; Th 5400-40700 ppm). The lower concentration group shows a good correlation between U and Th contents whereas U and Th are not as well correlated in the higher concentration group (Fig. 4).

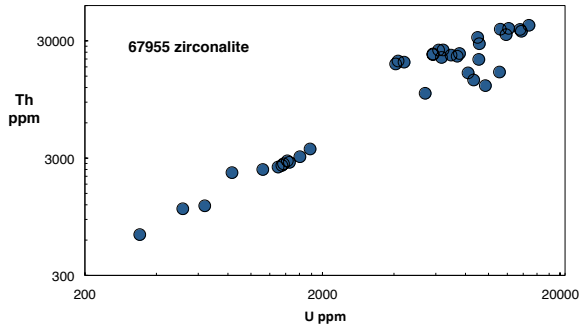

Fig. 4. U-Th concentrations in zirconalite from 67955.

There is also a correlation between U-Th concentrations and $^{206}Pb/^{207}Pb$ ages of the 67955 zirconalites, with the lower concentration group tending to have older ages and the higher concentration group having systematically younger ages (Fig. 5). The cluster of grains with <2000 ppm U shown in Fig. 5 has a mean age of 4.22 ± 0.02 Ga. The youngest age returned by the high concentration group is 3.93 Ga whereas most of these grains have $^{206}Pb/^{207}Pb$ ages that cluster around 4000 Ma (Fig. 5). Detailed mineralogical studies of the zirconalite may be required to determine whether the age-composition relationship (Fig. 5) represents recrystallization of the zirconalite or growth of new grains during a younger event.

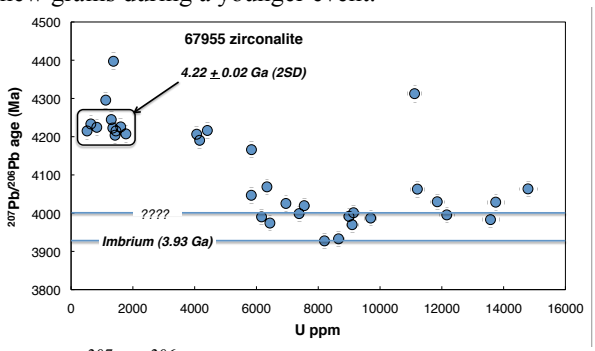

Fig. 5. $^{207}Pb/^{206}Pb$ model ages vs. U content for zirconalite in 67955. Imbrium age from [7].

Discussion: A variety of isotopic systems in lunar sample 67955 record clear evidence for a significant impact event on the Moon at 4.2 Ga. The coarse grain size, clast-poor and equant texture, and homogeneous mineral compositions distinguish this sample from other familiar lunar melt breccias. These characteristics imply slower cooling compared to many lunar impact melt rocks, comparable to some plutonic igneous cumulates [1,2]. This implies either a very large, possibly basin-forming event, or emplacement of the 67955 melt in a different geological environment, perhaps a central melt sheet rather than rim ejecta. When considered with other evidence from lunar zircons [5] and granulitic breccias [6] for significant impacts around this same time, it appears that the 'strong version' of the cataclysm hypothesis in which all basins formed at ~3.8-4.0 Ga is untenable. Either the geological evidence for older basins has been erased by younger impacts or the oldest basins still preserved on the Moon are ≥4.2 Ga. The KREEPy mineralogical and geochemical signatures contained within 67955 imply that the impact which created this rock likely occurred within the Procellarum-KREEP terrane. This provides additional evidence that the KREEP reservoir was well developed prior to 4.2 Ga, and supports an Imbrium provenance for the host Descartes breccias sampled at the Apollo 16 site. The younger limit of the zirconalite dates is consistent with the inferred age of Imbrium [7], but the significance of the clustering of $^{206}Pb/^{207}Pb$ ages around ~4.0 Ga is currently unclear.

References: [1] Hollister L. S. (1973) *PLSC 4*, 633-641. [2] Ashwal L. D. (1975) *PLSC 6*, 221-230. [3] Norman M. D. et al. (2007) *LPS 38*, Abstract #1991. [4] Paces J. B. and Miller J. D. (1993) *JGR 98*, 13997-14013. [5] Grange M. L. et al. (2011) *GCA 75*, 2213-2232. [6] Hudgins J. A. et al. (2008) *GCA 72*, 5781-5798. [7] Nemchin A. A. et al. (2009) *MAPS 44*, 1717-1734.

THE IMPACT HISTORY OF VESTA: NEW VIEWS FROM THE DAWN MISSION. D. P. O'Brien[1], S. Marchi[2], P. Schenk[3], D. W. Mittlefehldt[4], R. Jaumann[5], E. Ammannito[6], D. L. Buczkowski[7], M. C. De Sanctis[6], G. Filacchione[6], R. Gaskell[1], M. Hoffmann[8], S. Joy[9], L. LeCorre[8], J.-Y. Li[10], A. Nathues[8], C. Polanskey[11], F. Preusker[5], M. Rayman[11], C. A. Raymond[11], V. Reddy[8], T. Roatsch[5], C. T. Russell[9], D. Turrini[6], J.-B. Vincent[8] and the Dawn Science Team, [1]Planetary Science Institute, 1700 E. Ft. Lowell, Suite 106, Tucson, AZ 85719 (obrien@psi.edu), [2]NASA Lunar Science Institute, Southwest Research Institute, Boulder, CO, [3]Lunar and Planetary Institute, Houston, TX, [4]NASA Johnson Space Center, Houston, TX, [5]DLR, Institute of Planetary Research, Berlin, Germany, [6]Istituto Nazionale di Astrofisica, Rome, Italy, [7]Johns Hopkins University Applied Physics Lab, Laurel, MD, [8]Max-Planck-Institut für Sonnensystemforschung, Katlenburg-Lindau, Germany, [9]Institute of Geophysics and Planetary Physics, University of California, Los Angeles, CA, [10]University of Maryland, College Park, MD, [11]Jet Propulsion Laboratory, California Institute of Technology, Pasadena, CA.

Introduction: The Dawn mission has completed its Survey and High-Altitude Mapping Orbit (HAMO) phases at Vesta, resulting in 60-70 meter per pixel imaging, high-resolution image-derived topography, and visual and infrared spectral data covering up to ~50 degrees north latitude (the north pole was in shadow during these mission phases). These data have provided unprecedented views of the south polar impact structure first detected in HST imaging [1], now named Rheasilvia, and in addition hint at the existence of a population of ancient basins. Smaller craters are seen at all stages from fresh to highly-eroded, with some exposing atypically bright or dark material. The morphology of some craters has been strongly influenced by regional slope. Detailed studies of crater morphology are underway. We have begun making crater counts to constrain the relative ages of different regions of the surface, and are working towards developing an absolute cratering chronology for Vesta's surface.

South Pole Basin Rheasilvia: Rheasilvia is a broad depression approximately 500 km in diameter. It has a pronounced central peak roughly 100 km across that rises 20-25 km above the relatively flat basin floor (Fig. 1). The basin floor is deformed by a dense network of linear and curvilinear scarps and ridges, which form radial to spiral patterns that often intersect one another. The outer margin of the Rheasilvia basin is not regular, but ranges from a low ridge in some areas to a prominent scarp over 15 km high in other areas. Possible landslide features extend to the basin floor from both the margin and the central peak.

The area surrounding Rheasilvia varies in appearance, from heavily cratered areas which may have received little or no ejecta blanketing, to relatively smooth areas with possible flow features that may represent ejecta from the crater. A pronounced set of troughs circling the equatorial region may be related to the formation of Rheasilvia.

Ancient Basins: Numerous other depressions can be identified in the topography data that may be the remains of large impact basins. All appear to be more eroded than Rheasilvia, suggesting an older age, although detailed crater counts will be necessary to constrain the sequence of their formation. The largest of these is approximately 350-400 km in diameter, and appears to lie partially beneath Rheasilvia (Fig. 1). This basin does not appear to have a central peak, although the region where the central peak would occur corresponds to the rim of Rheasilvia, and thus it may have been destroyed or obscured. None of the other potential basins have central peaks, although most of these basins are heavily eroded.

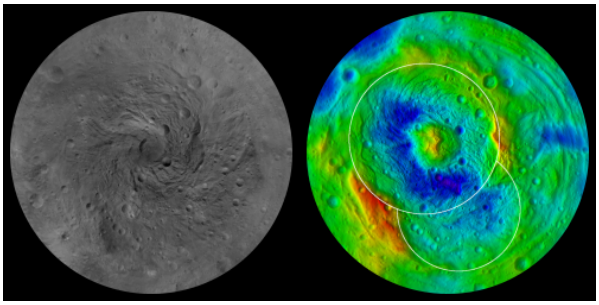

Figure 1: *Image mosaic (left) and topography (right) of the south polar region from -90 degree latitude to the equator. Blue represents low regions and red is high; the approximate margins of Rheasilvia and the second south polar basin are shown.*

The number of large basins may provide an important constraint on the impact history of Vesta and the dynamical history of the main belt. Furthermore, basin-forming impacts can potentially reset Ar-Ar ages of rocks on the surface of Vesta, and subsequent large impacts can then eject these rocks to space. These large basins are likely an important part of the story for understanding the Ar-Ar ages recorded in the howardite, eucrite and diogenite (HED) meteorites [2].

Crater Features and Morphology: Excluding the large basins, nearly all craters appear to have a simple bowl-shaped morphology, although there are several that could be central peak craters. Many craters show gravitational collapse and slumping from

their walls. This may affect the determination of the original transient crater size, which is important for estimating absolute ages of the surface. Topographic profiles of craters are currently being measured, which will establish crater morphology variation on Vesta and determine the critical sizes for transitions between different cratering regimes.

Some craters on Vesta expose atypically bright or dark material, the origin of which is the subject of detailed study. Topography can play a significant role in crater formation and modification processes on Vesta. For example, there are numerous cases of craters formed on slopes where pronounced collapse occurred on upslope sides of the craters with no collapse on downslope sides. In extreme cases, the material from upslope sides may have overrun the downslope rims and flowed out of the craters. Smooth flat regions are seen in the interiors of some craters, which could be due to ponded regolith or impact melt.

Developing a Cratering Chronology for Vesta: Radiometric dating of HED meteorites shows that Vesta dates back to the beginning of the Solar System [eg. 3], and its cratered surface potentially provides a record of impacts dating back to that early era. Understanding Vesta's impact record requires a crater chronology curve that relates crater density to surface age (which may be the formation age of the local crust or the time since the last major resurfacing event). One approach to the chronology is to use a lunar chronology curve [eg. 4] scaled to Vesta's current impact rate. Another approach, which we are currently developing, is to base the chronology on models of the primordial depletion and subsequent dynamical evolution of the main belt under the influence of giant planet migration and chaotic diffusion processes [eg. 5-7]. Possible chronology curves are shown in Fig. 2.

The theoretical curve shown in Fig. 2 is preliminary, although for all reasonable ranges of parameters, it lies significantly below the scaled lunar curve prior to 3 Gyr ago. In that range, a given crater density would imply a much older age using the theoretical curve than would be obtained using the scaled lunar curve, which has profound implications for the identification and dating of ancient surfaces on Vesta.

Analysis of Vesta's cratering record may be able to discriminate between these two curves. In particular, the number of ancient basins may provide a constraint on the total number of large impacts that Vesta has experienced over its history. The fact that Vesta's basaltic crust has not been eroded away by collisions also places an upper limit on the early

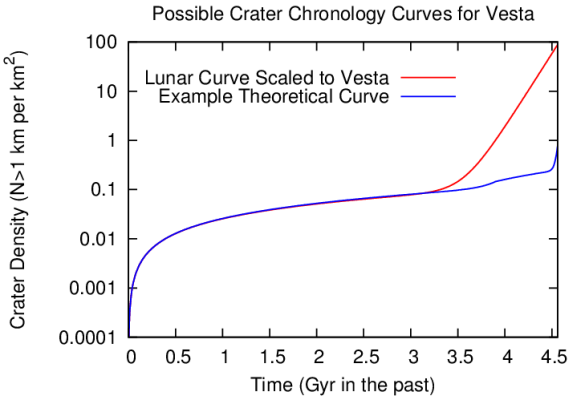

Figure 2: *Comparison of possible crater chronology curves for Vesta: A lunar chronology curve scaled to Vesta's current impact rate, and a theoretical curve based on models of main-belt dynamical evolution.*

impact rate [8]. Extending the scaled lunar curve back to 4.5 Gyr would imply the formation of hundreds of 100 km scale basins, which may be inconsistent with both of these constraints. The theoretical curve predicts a lower overall cratering intensity, but we must test that such a curve is consistent with the number of large basins and the crater density of the oldest surfaces on Vesta.

In addition to the cratering record, we have meteorites from Vesta, the HEDs, that record the ages of major impact events in their Ar-Ar ages. The Ar-Ar ages of eucrites suggest several such events occurred between 3.4 and 4.1 Gyr ago, and that an especially large impact event occurred 4.48 Gyr ago [2]. A primary goal as the Dawn mission proceeds is to tie Vesta's cratering record and the HED meteorite record together in the context of the dynamical and collisional evolution of the asteroid belt, as well as the impact histories of other cratered bodies in the inner Solar System.

Acknowledgements: D. P. O'Brien is supported by grant NNX10AR21G from NASA's Dawn at Vesta Participating Scientist Program. The Dawn mission to Vesta and Ceres is managed by JPL, for NASA's Science Mission Directorate, Washington, D.C. UCLA is responsible for overall Dawn mission science.

References: [1] P.C. Thomas *et al.* (1997) *Science,* **277**, 1492–1495. [2] D.D. Bogard (2011) *Chemie der Erde* **71,** 207-226. [3] L.E. Nyquist *et al.* (2009) *Geochim. Cosmochim. Acta* **73,** 5115-5136. [4] G. Neukum *et al.* (2001) *Space Sci. Rev.* **96**, 55-86. [5] D.P. O'Brien e*t al.* (2007) *Icarus* **191**, 434-452. [6] A. Morbidelli *et al.* (2010) *AJ* **140**, 1391-1401. [7] D.A. Minton and R. Malhotra (2010) *Icarus* **207**, 744-757. [8] D.R. Davis *et al.* (1985) *Icarus* **63**, 30-53.

THERMAL CONDITIONS DURING THE LUNAR BASIN-FORMING EPOCH: INSIGHTS FROM THE NUMERICAL MODELING OF LUNAR BASIN-FORMING IMPACTS R. W. K. Potter[1], G. S. Collins[1], W. S. Kiefer[2, 3], P. J. McGovern[2, 3], D. A. Kring[2, 3], [1]Impacts and Astromaterials Research Centre, Dept. Earth Science and Engineering, Imperial College London, London, SW7 2AZ, UK, ross.potter04@imperial.ac.uk; [2]Lunar and Planetary Institute, 3600 Bay Area Boulevard, Houston, TX, USA, 77058, [3]NASA Lunar Science Institute

Introduction: Over 50 multi-ring basins have been identified on the Moon [1], with the youngest, Orientale Basin, forming ~3.8 Ga. Lunar basins therefore formed within ~700 My of the Moon's existence; the majority are thought to have formed during the basin-forming epoch - the Lunar Cataclysm [2] - a spike in the impact bombardment rate ~4.1-3.9 Ga. The thermal state of the Moon during this basin-forming epoch is unclear, though the Moon is assumed to have been hotter than its present state [3].

Gravity-derived lunar basin structure [4,5] suggests two crustal features are common to lunar basins: (1) a (relatively) thin crustal layer beneath the basin center flanked by (2) a (relatively) thickened annulus (ring) of crustal material. These features are present in all but the oldest pre-Nectarian basins [5]. This implies thermal conditions (and subsequent post-impact processes) early on in the basin-forming epoch were different to those towards the end of the basin-forming epoch.

This work numerically models lunar basin-forming impacts using thermal profiles estimating conditions for a young, warm Moon during the basin-forming epoch. The results of the basin-scale simulations are compared to gravity-derived lunar basin crustal profiles and used to estimate basin features, such as transient crater diameter, for a suite of lunar basins. The simulation results and estimations are then used to suggest whether the investigated thermal profiles are suitable analogs for lunar thermal conditions during the basin-forming epoch.

Methods: Lunar basin numerical modeling was carried out using the two dimensional iSALE hydrocode [6,7] previously used to model large-scale terrestrial impacts such as Chicxulub [8].

The impact target was modeled as an infinite half-space divided into a crustal and mantle layer. A Tillotson equation of state derived for gabbroic anorthosite [9] and an ANEOS-derived equation of state for dunite [10] were used to model the crust and mantle response, respectively, to thermodynamic changes and compressibility. Material strength and thermal parameters for each layer were derived from fits to experimental gabbro and dunite rock strength data [11-14]. Impactor diameter was varied between 40 and 120 km; a constant resolution of 20 cells per projectile radius (CPPR) was used, resulting in cell sizes of 1-3 km. Impact velocity was varied between 10 and 15 km/s.

Thermal profiles (TP) estimating lunar conditions for an early, warm Moon, based on [15] were investigated. TP1 had a near-surface temperature gradient of 34 K/km, with a deep mantle temperature of ~1770 K; TP2 had a near-surface temperature gradient of 10 K/km with a deep mantle temperature of ~1670 K. Temperatures were bound by the solidus; they never exceeded the ambient melt temperature. An additional thermal profile, TP3, modified from [16], estimating a 0.5 Gy old Moon, was also used (Figure 1). Based on the thermal profiles, self-consistent pressure, density and strength fields were computed. The gravity field was set to a constant value of 1.62 m/s^2.

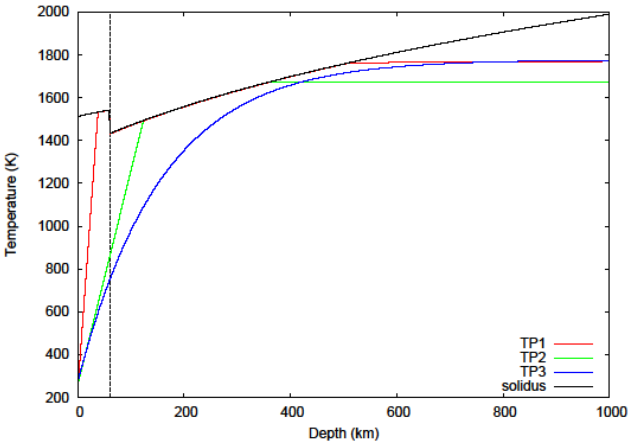

Figure 1. The three temperature profiles investigated. TP1 has near-surface gradient of 34 K/km and a deep mantle temperature of ~1770 K. TP2 has a near-surface thermal gradient of 10 K/km with a ~1660 K deep mantle temperature. The temperature profiles are bound by the solidus so temperatures never exceed the ambient melt temperature. TP3 is modified from [16] and estimates a 0.5 Gy old Moon.

Results: Due to the high internal temperatures, a far greater volume of melt was produced in the simulations compared to scaling law estimates for comparable lunar impacts [17,18]. In the simulations a significant volume of crustal material was removed forming a thinner post-impact crustal layer than that suggested by gravity-derived crustal profiles [4,5]; some simulations completely removed crustal material from the basin center. Coupled with the greater melt volume, the discrepancy between the simulations and the gravity-derived profiles could be resolved by differentiation of the voluminous melt pools formed in the simulations

into new crustal layers, as suggested by [19] for the South Pole-Aitken Basin-forming impact.

Simulations using TP2 and TP3 were however qualitatively consistent with the location and thickness of the thickened crustal annulus of gravity-derived crustal profiles [4] for a suite of lunar basins covering age groups I1 (Imbrium) to P11 (Smythii). To produce the same crustal annulus radius, greater impact energy was required for impacts using TP3 as it was cooler and stronger than TP2. Impacts into TP1 did not produce qualitatively similar basins to gravity-derived crustal profiles; hot crustal material flowed in towards the basin center smoothing out any topography and crustal thickening created during the initial stages of impact. TP1 therefore appears to be too warm to explain inferred basin structures for this suite of basins.

Assuming differentiation can account for the differences between the simulations and the gravity-derived crustal structure around basin centers, the basins formed in TP2 and TP3 were used to predict features for the suite of lunar basins, including transient crater and apparent basin rim size (Figure 2). By comparison to scaling law estimates and observed basin structure, TP2 appeared to be slightly too warm and weak to produce basins with features similar to those observed, while TP3 appeared to be slightly too cool and strong to produce basins with features similar to those observed.

Discussion: Thermal conditions during the latter stages of the lunar basin-forming epoch can be roughly constrained by mare volcanism; this is thought to have begun ~4 Ga [20] prior to the end of the basin-forming epoch. The mare basalt is a product of ultramafic magmas and is thought to have been sourced from depths between 150 and 400 km [21] suggesting some partial melting within the upper mantle. The upper mantle temperature in TP2 matches the mantle solidus between depths of 150-350 km, while upper mantle temperatures in TP3 approach the mantle solidus between depths of 300-500 km. Therefore a thermal profile with a similar near-surface thermal gradient to TP2 and TP3 (10 K/km) and a deep mantle temperature in between those of TP2 and TP3 could possibly produce basins with features similar to those observed and inferred and provide a reasonable estimate for thermal conditions during the latter stages of the basin-forming epoch.

Acknowledgements: We are grateful to Boris Ivanov, Jay Melosh, Kai Wünnemann and Dirk Elbeshausen for their work in the development of iSALE. RWKP and GSC were funded by NERC.

References: [1] Potter, R. W. K. et al (2011) *LPSC XLII*, #1452 [2] Tera, F. et al (1974) *EPSL*, 22, 1-21 [3] Shearer, C. K. et al (2006) *Rev. Min. Geochem.*, 60, 365-518 [4] Wieczorek, M A. & Phillips, R. J. (1999) *Icarus*, 139, 246-259 [5] Hikida, H. & Wieczorek, M. A. (2007) *Icarus*, 192, 150-166 [6] Amsden, A. A. et al (1980) *Los Alamos National Laboratory Report LA-8095* [7] Collins, G. S. et al. (2004) *MAPS*, 39, 217-231 [8] Collins, G. S. et al (2008) *EPSL*, 270, 221-230 [9] O'Keefe, J. D. & Ahrens, T. J. (1982) *GSA Spec. Pap. 190* [10] Benz, W. et al (1989) *Icarus*, 81, 113-131 [11] Azmon, E. (1967) *NSL 67-224* [12] Stesky, R. M. et al (1974) *Tectonophys.*, 23, 177-203 [13] Shimada, M. et al (1983) *Tectonophys.*, 96, 159-192 [14] Ismail, I. A. H. & Murrell, S. A. F. (1990) *Tectonophys.*, 175, 237-248 [15] Potter, R. W. K. et al (2011) Submitted to *Icarus* [16] Spohn, T. et al (2001) *Icarus*, 149, 54-65 [17] Cintala, M. J. & Grieve, R. A. F. (1998) *MAPS*, 33, 889-912 [18] Wünnemann, K. et al (2008) *EPSL*, 269, 529-538 [19] Morrison, D. A. (1998) *LPSC XXIX*, #1657 [20] Hiesinger, H. et al (2011) *GSA Spec. Pap. 477* [21] Heiken, G. H. et al (1991) *Lunar sourcebook: A user's guide to the Moon*, Cambridge Uni. Press, New York [22] Pike, R J. & Spudis, P. D. (1987) *Earth, Moon, Planets*, 39, 129-194 [23] Spudis, P. D. (1993) *The geology of multi-ring impact basins*, Cambridge University Press, Cambridge [24] Spudis, P. D. & Adkins, C. D. (1996) *LPSC XXVII*, #1627 [25] Croft, S. K. (1985) *Proc. 15th LPSC*, C828-C842

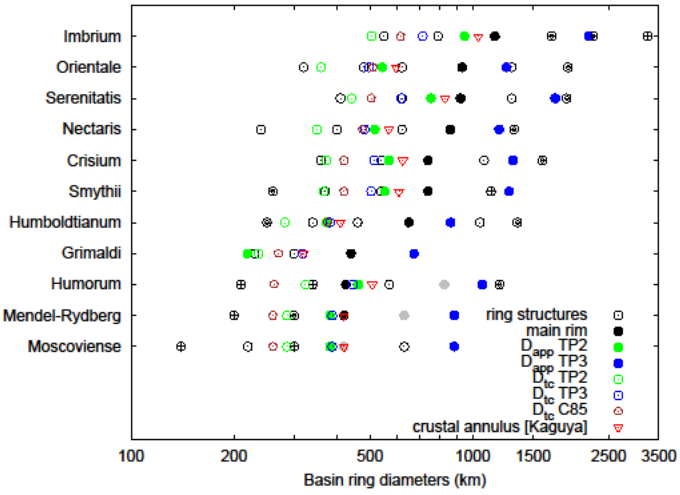

Figure 2. Structural features for a suite of 11 lunar basins. Data includes: ring diameters [22] (open black circles represent definite ring structures; partially filled circles represent uncertain ring structures), main rim diameter estimates [23] (black circles), alternative basin rim diameter estimates [24] (gray circles), transient crater diameter estimates from [25] (C85) and this study, and crustal annulus diameter estimates (Kaguya data). Data from this study for thermal profiles TP2 (green circles) and TP3 (blue circles) plot either side of scaling estimates and observations for a given basin feature. Dtc is the transient crater diameter; Dapp is the apparent basin rim diameter.

EXPLORING THE BOMBARDMENT HISTORY OF THE OUTER SOLAR SYSTEM VIA SATURNIAN SATELLITE CRATERING RECORDS. J. E. Richardson[1], D. A. Minton[1] and P. C. Thomas[2], [1]Purdue University, Department of Earth & Atmospheric Sciences, 550 Stadium Mall Drive, West Lafayette, IN 47907 (richardson@purdue.edu), [2]Cornell University, Center for Radiophysics & Space Research, Ithaca, NY 14850

Introduction: An apparent spike in the impact flux onto the Moon, including the formation of large lunar basins such as Imbrium and Orientale, after ~ 4 Gy ago has been attributed to an event called the Late Heavy Bombardment (LHB) [1–4]. The Late Heavy Bombardment (LHB) has long remained a puzzling and controversial topic in solar system chronology [1–5]. Recently, it has been suggested that the LHB was not limited to the Moon, but was a solar system-wide event caused by a dramatic rearrangement of the orbits of the giant planets [6–9].

It has been shown that the size frequency distribution of craters in the ancient terrains of the Moon, Mars, and Mercury are well matched by that of the main belt asteroids [8, 10–12]. However, all dynamical models for the LHB to date that are based on giant planet migration predict that the primordial Kuiper belt was very massive [13–17]. These models suggest that the mass flux of cometary population should have been comparable to or dominate over that of the asteroidal population in the inner solar system [7]. However, testing this requires a constraint on the small end of the Kuiper belt SFD that is relevant to crater counting, but which is currently poorly known [18]. Here, we use the cratering record of the small saturnian system satellites Hyperion, Phoebe, and Mimas to constrain the outer solar system impactor population, and show that the Kuiper belt is the most likely source region for these impactors. We also demonstrate that in order to reproduce the cratering record on these small sattellites, impactor flux levels ∼2-3 orders of magitude higher than current flux levels are necessary, indicating a period of heavy bombardment in these satellite's earlier histories.

Cratered Terrain Evolution Model (CTEM): Recent advances in computing technology and our understanding of the processes involved in crater production, ejecta production, and crater erasure have permitted us to develop a Cratered Terrain Evolution Model (CTEM) which simulates the appearance of a terrain after bombardment by an input projectile population over time [11]. Our previous study showed that the heavily-cratered regions of the lunar surface represent a crater population which is in crater density equilibrium ('saturation'), but which still retains a shape indicative of the impactor population which produced it [11]. Specifically, the SFD of the impactor population which best reproduces the crater density curve for heavily-cratered regions of the lunar surface is nearly identical to that of the current main asteroid belt (MAB), as suggested by Strom et al. [8], and points to the MAB as the primary source for impactors in the inner solar system. As we show below, we can apply the CTEM to recover the SFD of the impactor population of small saturnian satellites to obtain the outer solar system impactor SFD.

Small saturnian satellite craters: We investigate the impactor population for the outer solar system, beginning with the small saturnian satellites. These bodies share the unique characteristics of: (1) having been imaged at high-resolution by the Cassini ISS; (2) are small enough such that impact cratering is the dominant geologic process; and (3) have very low escape velocities (< 170 m s^{-1}) such that secondary cratering is negligible on these bodies – all circular (hyper-velocity) impact craters can be assumed to originate from objects either in heliocentric orbit or planetocentric orbit around Saturn. So far, adequate crater count statistics have been assembled for satellites Phoebe, Hyperion and Mimas. We use these crater counts as constraints in CTEM, by matching the observed crater SFDs with model runs crater counts.

Constraining the source region for saturnian satellite impactors: Fig. 1 shows the relative size-frequency distribution [19] for a common, heliocentric impactor population which is capable of reproducing the crater count data for Mimas, Phoebe, and Hyperion. This is compared to the relative size-frequency distribution for the main belt asteroids [20, 21] and outer solar system cometary impactors [22]. These derived impactor population curves display much better agreement with the outer solar system cometary population (originating in the Kuiper belt) derived by Zahnle [22] than with the observed size-frequency distribution of main belt asteroids, epsecially with regard to the shallow-sloped region between diamters of ~ 100 m and ~ 1000 m. Within crater count data and modeling errors, all attempts to utilize the MAB as the common impactor source for these three satellites have failed, for a variety of assumed impact speed or target material propeties. This points strongly to a unique outer solar system impactor source for the saturnian satellite system.

In addition, Fig. 2 shows the cumulative size-frequency distribution [19] for a common, heliocentric impactor population which is capable of reproducing the crater count data for Mimas, Phoebe, and Hyperion, as compared to the cumulative size-frequency distribution for the main belt asteroids [20, 21] and cometary outer solar system impactors [22]. Within our CTEM, the impactor flux levels required to reproduce the crater count statistics for each of the small saturnian satellites within a 5 Gyr time-span requires impactor flux levels that are 2-3 orders of magnitude higher than Zahnle's estimates for the current impactor flux level in the outer solar system [22]. This points strongly toward earlier periods of much higher impactor flux levels within the bombard-

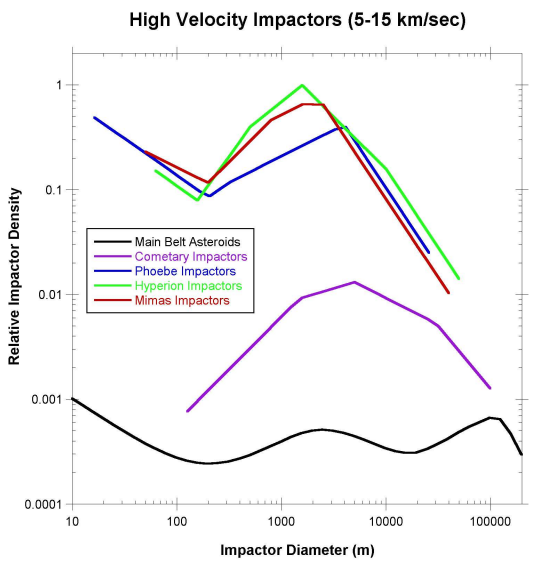

Figure 1: Saturnian system impactor population relative size-frequency distribution plots, emphasizing the differences in population shapes as a function of size. The saturnian system impactors are most similar to the derived shape of the OSS cometary (Kuiper belt) population.

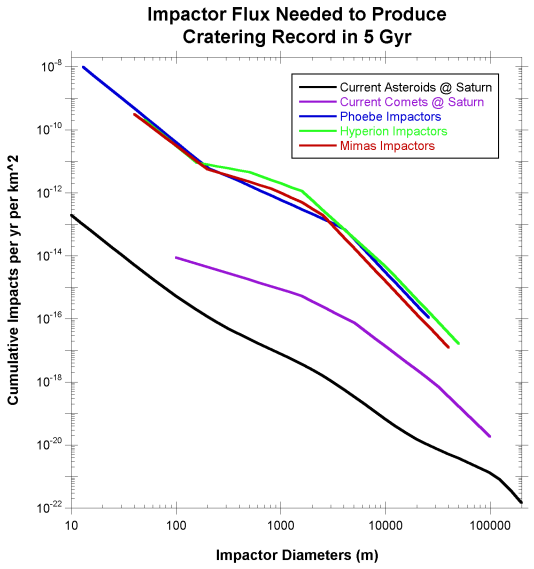

Figure 2: Saturnian system impactor population cumulative size-frequency distribution plots, emphasizing the differences in absolute flux levels for each population. The cratering records of the small saturnian sattellites require a bombarding population 2-3 orders of magnitude higher than estimates of the current impactor flux level in that region of the solar system.

ment histories of each of these satellites. That is, each has experienced earlier periods of heavy bombardment, the scars of which remain evident in their current cratering records.

In addition, we have performed an N-body study of the dynamical erosion of the asteroid belt over the age of the solar system [23]. One result of this study is an estimate of the relative impact flux of objects originating in the MAB onto major planets. On a per unit area basis, we find that that the total asteroidal impactor flux in the Saturn system is $\sim 2 \times 10^{-3}$ that of the inner solar system.

Summary and conclusions: We used a cratered terrain evolution model to constrain the outer solar system small body impactor population using small icy satellites of Saturn. We showed in Fig. 1 that this population is distinct from the main asteroid belt, and numerical simulations show that the contribution of main belt asteroids to the outer solar system is negligible. We conclude that main belt asteroids are an implausible source of impactors in the outer solar system, and that the SFD obtained here may be used to constrain the small end of the Kuiper belt population that is too faint to observe directly. Additionally, as shown in Fig. 2, model reproduction of the current cratering record of the small saturnian satellites requires earlier periods of much heavier bombardment when compard to current estimates of the impactor flux in the outer solar system.

References

[1] Turner G. et al. (1973) *LPSCIV*, 4, 1889. [2] Tera F. et al. (1973) *Abstracts of the Lunar and Planetary Science Conference*, 4, 723. [3] Tera F. et al. (1974) *Earth and Planetary Science Letters*, 22, 1. [4] Ryder G. (1990) *EOS*, 71, 313. [5] Chapman C.R. et al. (2007) *Icarus*, 189, 233–245. [6] Levison H.F. et al. (2001) *Icarus*, 151, 286–306. [7] Gomes R. et al. (2005) *Nature*, 435, 466–469. [8] Strom R.G. et al. (2005) *Science*, 309, 1847–1850. [9] Minton D.A. and Malhotra R. (2009) *Nature*, 457, 1109–1111. [10] Strom R.G. et al. (2008) *Science*, 321, 79. [11] Richardson J.E. (2009) *Icarus*, 204, 697–715. [12] Head J.W. et al. (2010) *Science*, 329, 1504–1507. [13] Hahn J.M. and Malhotra R. (1999) *AJ*, 117, 3041–3053. [14] Thommes E.W. et al. (2002) *AJ*, 123, 2862. [15] Hahn J.M. and Malhotra R. (2005) *AJ*, 130, 2392–2414. [16] Tsiganis K. et al. (2005) *Nature*, 435, 459–461. [17] Levison H.F. et al. (2008) *Icarus*, 196, 258. [18] Minton D.A. et al. (2008) *Workshop on the Early Solar System Impact Bombardment*, 1439, 43. [19] Group C.A.T.W. et al. (1979) *Icarus*, 37, 467. [20] Bottke W.F. et al. (2005) *Icarus*, 175, 111–140. [21] O'Brien D.P. and Greenberg R. (2005) *Icarus*, 178, 179. [22] Zahnle K. et al. (2003) *Icarus*, 163, 263. [23] Minton D.A. and Malhotra R. (2010) *Icarus*, 207, 744–757.

Martian mantle HSE abundances do not require late chondritic addition. K. Righter[1], [1]Mailcode KT, NASA Johnson Space Center, Houston, TX 77058; kevin.righter-1@nasa.gov

Introduction: The highly siderophile elements (Au, Re and the platinum group elements, PGE) can provide constraints on the processes of core formation and accretion for differentiated bodies [1]. For example, the near chondritic relative ratios of the HSE in the terrestrial upper mantle have been used to argue for the addition of chondritic material to the Earth's upper mantle following core formation [2]. More recently, analyses of martian meteorites have revealed an overall similarity to HSE contents in terrestrial basalts and mantle-derived melts [3] (Figure 1). This evidence has been used by some to argue that Mars also experienced late chondritic addition much the same as Earth [4]. The HSE database for martian meteorites will be reviewed and an assessment made of primitive mantle abundances of the HSE. It will be shown that the martian meteorite HSE abundances can be explained by derivation from a primitive mantle with a non-chondritic HSE pattern, thus obviating the need for late chondritic accretion to Mars.

Background: The abundances of 8 siderophile elements (Ni, Co, Mo, W, Ga, P, V and Cr) in the martian mantle can be explained by metal-silicate equilibrium during core formation at conditions of 14 GPa and 2000 ºC [5]. Any modeling of HSE partitioning between core, mantle and crust, must take this 1st stage of differentiation into account. Subsequent second stage evolution of the martian mantle has resulted in the formation of depleted and enriched reservoirs. Combining siderophile element modeling of the first stage, with mantle melting modeling of the second stage allows the HSE content of possible primitive mantle, lower mantle, and enriched and depleted mantle to be calculated.

Core formation modelling: Metal-silicate partitioning of Re, Au, Pd, Pt, and Ir can be predicted using simple expressions that quantify the dependency on temperature, pressure, oygen fugacity, and metallic and silicate liquid compositons [6,7]. For Mars, if core formation occurred at pressures near 14 GPa and 2000 ºC, and between peridotite liquid and FeNiS metallic liquid (Xs = 0.17), D(Au), D(Pt), D(Pd) and D(Ir) metal/silicate can be predicted. Using a core mass of 21%, and a melt fraction of 0.65 [5], the mantle abundances are: Au = 0.17 ppb, Pd = 5.1 ppb, Pt = 5.8 ppb, and Ir = 3.2 ppb. Similar exercise for Re and Os, where D(Re) = 100 and D(Os) = 1000, results in mantle abundances of Re = 1.2 ppb and Os = 2.4 ppb. The results for Pd are shown in Figure 1, where the martian upper mantle contains 5.1 ppb Pd compared to 7.1 ppb for the Earth.

The results are model dependent and critical information includes knowledge of D(metal/silicate) as a function of pressure and temperature, the percentage of mantle unmelted during the magma ocean stage, and the partitioning of elements between the deep solid and shallow molten mantle. Depleted mantle HSE concentrations can be estimated by inverting the HSE content of primitive depleted basalts.

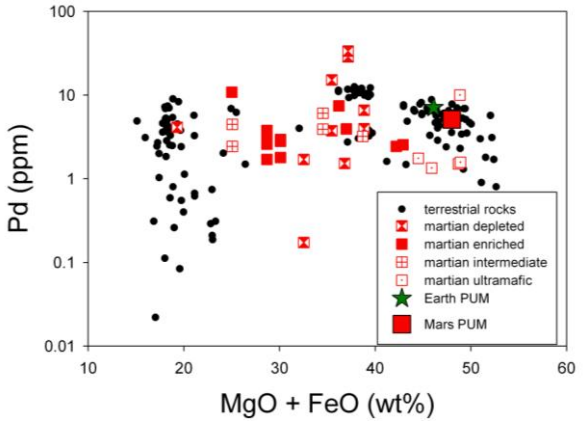

Figure 1: Pd (ppm) vs. MgO+FeO (wt%) for a variety of terrestrial igneous rocks (komatiites, basalts, peridotites), martian meteorites ([3] and references therein), and estimate of [8] for Earth's PUM composition. Also shown is the martian primitive upper mantle from this study and using MgO+FeO from [9].

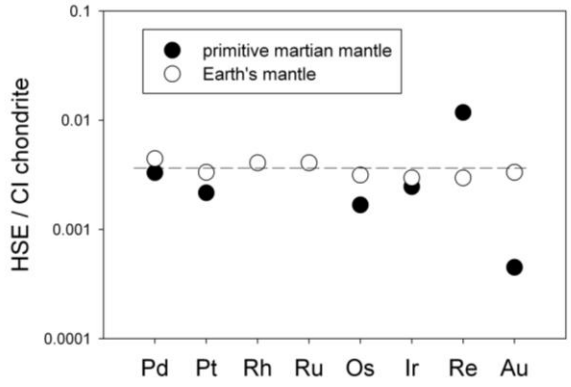

Figure 2: Calculated HSE contents of the primitive upper mantle of Mars from this study, as well as the Earth's PUM [8], both normalized to CI values [10].

Conclusions: The martian basalt array of HSE contents can be explained by melting of a mantle with non-chondritic relative HSE contents. This approach predicts a mantle with supra-chondritic Re/Os and sub-

chondritic Au/Ir and Pt/Ir ratios. Therefore a late chondritic veneer is not required to explain HSE content of martian basalts.

References: [1] Shirey, S.B., and Walker, R.J. Annual Review of Earth and Planetary Sciences 26, 423-500; [2] Chou, C.-L. (1978) In: Proc. 9th Lunar Planet.Sci. Conf., 219-230; [3] Brandon, A.D. et al. (2011) Geochim. Cosmochim. Acta, in press; [4] Bottke, W.F. et al. (2010) Science 330, 1527-1530; [5] Righter, K. and Chabot, N.L. (2011) Met. Planet. Sci. 46, 157-176; [6] Righter, K. (2011a) Earth Planet. Sci. Lett. 304, 158-167; [7] Righter, K., et al. (2011b) 42nd Lunar and Planetary Science Conference, #2373; [8] Becker, H. et al. (2006) Geochim. Cosmochim. Acta 70, 4528-4550; [9] Longhi, J. et al. (1992) The bulk composition, mineralogy and internal structure of Mars, in Mars, edited by H. H. Kieffer et al., 184 pp., Univ. of Arizona Press, Tucson, AZ; [10] Newsom, H.E. (1995) Global Earth Physics: A Handbook of Physical Constants, AGU Ref. Shelf, Vol. 1, AGU, 159-189.

REVISING THE EARLIEST RECORDED IMPACT HISTORY OF MARS AND IMPLICATIONS FOR THE LATE HEAVY BOMBARDMENT. S.J. Robbins[1] and B.M. Hynek[1,2], [1]LASP, UCB 392, University of Colorado, Boulder, CO 80309, [2]Geological Sciences Department, UCB 399, University of Colorado, Boulder, CO 80309.

Introduction: A topic debated in the solar system's impact history is the concept of the Late Heavy Bombardment – a hypothetical era of enhanced impacts some time around 3.8 Ga. In addition to questions about whether or not it actually occurred, issues about its origin, the length of time it spanned, and when it began and ended in the inner solar system are unknown. In theory, the largest craters should trace the early impact flux on a planet and show any increase during the Late Heavy Bombardment period. We have attempted to constrain this for Mars by age-dating four large basins and all craters with diameters $D \geq 150$ km via smaller superposed craters.

Crater Database: We have used the largest, most complete crater database of the planet Mars, containing 637,074 craters; 384,363 of these have diameters $D \geq 1$ km [1]. This database was created by identifying craters manually in THEMIS Day IR, Viking, and MOLA mosaics. Among other data, this database contains the center latitude, longitude, and diameter for each crater within it that were used in this work.

Geologic Mapping of Crater Rim Areas: Geomorphologic mapping was completed of the most pristine and intact regions of crater rims for all craters $D \geq 150$ km within the database. Besides the four basins that were mapped (Table 1), the database contains 101 craters $D \geq 150$ km (see Fig. **1** for locations). Of these, 73 could be mapped; the remaining 28 were too heavily modified for this purpose.

Age Determinations: The craters from Robbins & Hynek [1] that were within the mapping regions of each large crater/basin rim were extracted and the rim areas calculated in local projected coordinates. Cumulative size-frequency distributions (CSFDs) after Arvidson *et al*. [2] were created for each large crater's overlapping rim craters.

From these, we determined ages in two main ways, though all relied upon the chronology of Neukum *et al*. [3, 4]. The first method used the cumulative crater density at D = 10, 25, and 50 km, also known as $N(10, 25, 50)$ ages. We selected a broad range that was bound on the small end to eliminate as much erosion and secondary crater effects as possible, and we bound the large end to be as inclusive of craters as possible. Including basins, only 37 craters had discernable $N(50)$ ages, and 63 had $N(25)$ ages. All had $N(10)$ ages.

The second method used was to fit isochrons to the CSFDs. This was done "blindly" without looking at crater diameters, trying to match an $N(\#)$ age, nor trying to match an age determined by previous researchers [*e.g.* 5, 6, 7]. We chose locations on the CSFDs that best paralleled the isochron functions [3] and fit it in that range. We did this for all 77 mapable craters and basins. These are the ages quoted in Table 1.

Results: All four ages from Table 1 are illustrated in Fig. **2** in two ways. The first is a histogram binned in 0.1-Ga intervals with the different ages slightly offset within each bin for readability. The second method is a smoothed probability distribution. This was created by taking the determined age and associated uncertainties and creating a normalized, piece-wise Gaussian (because the uncertainties were often asymmetric). These were then summed for every crater with an age calculation. This procedure has three desirable effects. First, it helps to smooth the data for better visibility. Second, it will give lesser weight to an age with a large associated uncertainty and more weight to one that has a well defined age. Third, we can scale each normalized Gaussian by the crater diameter-cubed – a rough approximation of the mass of the impactor – to derive a mass flux distribution (Fig. **3** – large basins have been left out of this calculation).

To first order, the data show a clear spike in cratering approximately 4.0 Ga and a decline since that time. The youngest of these craters that was dated has an isochron age of 3.61 Ga and an $N(25)$ age of 3.46 Ga. The oldest dates to 4.23 Ga and 4.28 Ga via those methods. For ages before ~4 Ga, we find a sharp decrease in craters. However, we interpret this as obliteration of these large craters by subsequent crater formation, the formation of the large basins after these, and the vast Tharsis region that has resurfaced ~25% of the planet. An additional possibility is that the crust of Mars was not solid enough to support a large crater cavity before this time [8]. It is likely that the cratering rate continues to climb further back in time from our observed peak at ~4 Ga.

An artifact that requires note is that ages between the three $N(\#)$ differ and, on average, give progressively older ages as the # increases. The isochron ages are generally between $N(25)$ and $N(10)$ ages because the majority of that region in the CSFDs best paralleled the isochron function. This illustrates well the problem with using $N(\#)$ ages as well as uncertainties associated with isochrons. However, regardless of any chronology used, the results clearly show there was no significant spike at ~3.8 Ga at Mars in the cratering rate, inconsistent with a Late Heavy Bombardment.

Erosional History: To explore possible implications for the resurfacing history of Mars, we examined each CSFD to determine where the isochron "turn-off diameter" was located. This was where the CSFD slope shallowed at smaller diameters relative to the isochron function; this shallowing is most easily attributable to crater erasure through resurfacing processes. The results are shown in Fig. **4**. It is difficult to draw extended conclusions at this time, but we can state that prior to ~4.15 Ga, craters D > 10 km were easily removed from the surface, consistent with >1 km of material based on the complex crater depth/Diameter relationship [1]. After ~3.95 Ga, barring one outlier (Argyre), craters D > 5 km were and are preserved, consistent with <1 km of erosion based on the simple crater depth/Diameter relationship [1].

Implications for the Late Heavy Bombardment and Erosion: From this work, we can conclude several things: (1) Unless the Martian cratering chronology is significantly revised, we see no evidence for a Late Heavy Bombardment spike in the cratering rate around 3.8 Ga; there is either a continuous decay in the cratering rate past ~4.1 Ga, or the spike occurred during or prior to 4.1 Ga on Mars. (2) Age dating within the same chronology is fraught with uncertainty based upon the diameters chosen to age-date, and larger diameters result in progressively older ages. (3) Erosion decreased dramatically after ~4.0 Ga.

References: [1] Robbins & Hynek, 2011. [2] Arvidson et al. 1979. [3] Neukum et al. 2001. [4] Ivanov et al. 2001. [5] Nimmo & Tanaka 2005. [6] Werner 2008. [7] Fassett *et al.* 2011. [8] Hauck & Phillips, 2002. [9] Smith *et al.* 2001.

Table 1: Ages in Ga of four large basins dated in this work compared with previous results. Ages here are based upon fitting Neukum isochrons [3, 4].

	This Work	[5]	[6]	[7]
Hellas	4.15±0.02	4.08	3.99±0.01	4.04
Argyre	$3.94^{+0.02}_{-0.03}$	4.04	3.83±0.01	3.92
Isidis	$4.00^{+0.02}_{-0.03}$	3.93	3.96±0.01	3.96
Prometheus	$4.07^{+0.03}_{-0.04}$	*Not Dated Elsewhere*		

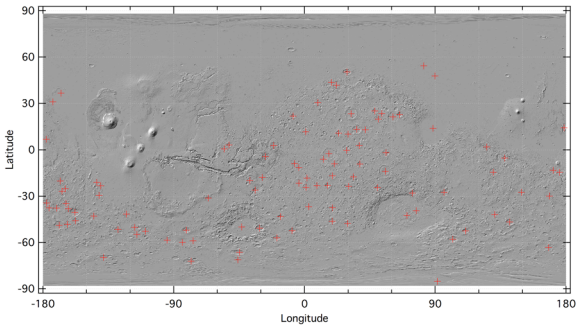

Figure 1: Red + mark the location of all craters $D \geq 150$ km. Background is MOLA shaded relief [9].

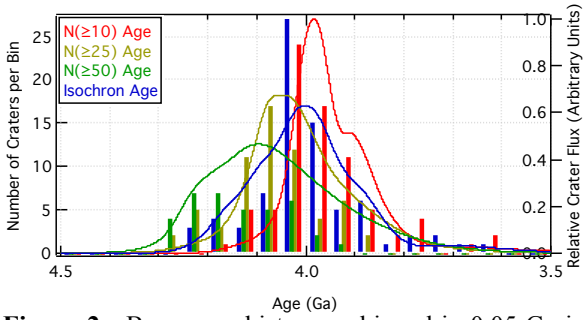

Figure 2: Bars are a histogram binned in 0.05 Ga intervals with the four different dating methods slightly offset for readability. The smoothed lines are a sum of Gaussian distributions based upon the ages and uncertainties calculated for each crater from method.

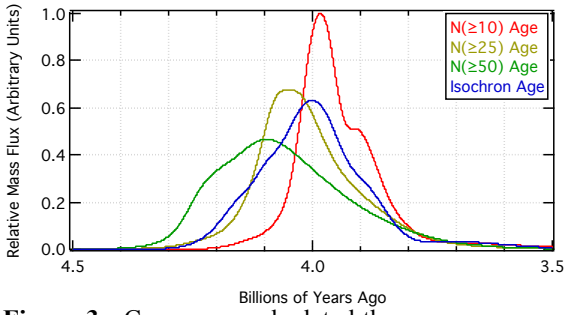

Figure 3: Curves are calculated the same way as ages from Fig. **2** except that each Gaussian for each crater has been scaled by D^3_{crater} to approximate the mass of the impactor. The large basins have been excluded.

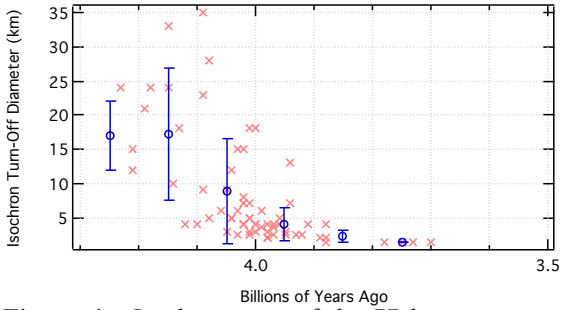

Figure 4: Isochron ages of the 77 large craters and basins plotted against the diameter at which CSFDs deviated from the isochron function. Blue points indicate mean and standard deviation of 0.1-Ga-wide bins.

The effect of the Caloris impact on the mantle dynamics and volcanism of Mercury

James H. Roberts and Oliver S. Barnouin, Johns Hopkins University Applied Physics Laboratory, 11100 Johns Hopkins Rd., Laurel, MD 20723-6099, United States, (James.Roberts@jhuapl.edu)

Introduction

MESSENGER has now imaged over 95% of the surface of Mercury, including the entirety of Caloris, the largest impact basin on Mercury [1]. These images reveal evidence for volcanic plains within and exterior to the basin that appear to be younger than the basin rim [2-4], and might be associated with the long-term aftermath of Caloris' formation. The broad influence of Caloris on the surface indicates that it might also affect heating of the deep mantle and thereby, the core. Here we investigate possible links between the Caloris impact on Mercury and volcanism within and surrounding the basin.

While the apparent age difference between the rim and plains [3-4] indicates that the plains materials cannot be impact melts, the thermal impulse from such an impact can alter the underlying mantle dynamics, producing volcanism late on. We use standard methods of impact scalings [5-8] and a finite element model of thermochemical convection in a spherical shell [9-11] to explore the melt production, and geodynamic evolution in the Mercurian mantle as a result of the Caloris impact.

Thermochemical Evolution

Figure 1 shows snapshots of the temperature, composition, and instantaneous melt fraction in the mantle within 30 ° of the impact site immediately before (a-c) and after the formation of Caloris by a projectile striking at 48 km/s (d-f), 24 km/s (g-i) and 12 km/s (j-l). Here, $Ra = 8.4 \times 10^6, B = 0.256$. Composition is shown in percent and varies between 0 for pristine mantle and 100 for the last remaining solid component (i.e. pure fortserite). The scale is saturated at a relatively low threshold (0.5%) to better show the boundary of incipient melting. Prior to the impact, only small amounts of melting occur in the convective upwellings. This melting occurs beneath the relatively thick stagnant lid where the temperature is the hottest. A significant fraction of the lower mantle of Mercury may be melted and mixed prior to any impact, simply due to the ambient mantle temperature and radioactive heating. The cooler stagnant lid is essentially unmelted prior to impact heating.

While the total energy delivered by the impactor is similar in all cases, the distribution of this energy depends on velocity. While all three projectiles produce a large amount of melt in the vicinity of the impact site,

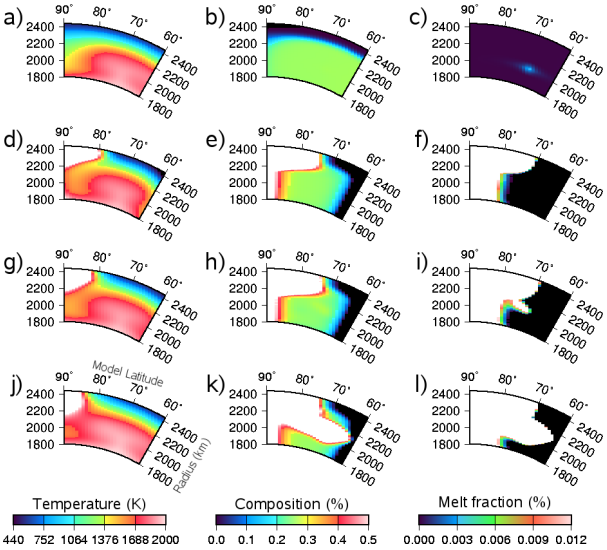

Figure 1: Temperature (left), composition (middle), and instantaneous melt production (right) in the Mercurian mantle within 30° of the impact site. immediately before (top row), and after a Caloris-forming impact at 48 km/s (second row), 24 km/s (third row) and 12 km/s (bottom row). All models are 2D axisymmetric and have $Ra = 8.4 \times 10^6$, $B = 0.255$, $E = 136$ kJ/mol, $V = 7.7$ cm^3/mol.

the broader distribution of heating in the slower impacts results in production of melt further away. In the case of the slowest projectile (12 km/s), significant melting occurs in the upwellings adjacent to the impact site.

The effect of the impact velocity on the distribution of melt can be illustrated by looking at the total melt fraction in a column, as shown in Figure 2. In each case the vast majority of melting occurs within 5° of the impact site. However, the 12 km/s projectile can also generate melting in the next upwelling over, thus producing a total column melt fraction of few percent at up to 20° from the impact site. The total amount of melting, however, is relatively insensitive to the velocity for a given impact energy, as shown in Figure 3. Prior to impact there is a significant amount of melting in convective upwellings where the plume temperature exceeds the solidus. The sharp rise in melt is due to the impact, the subsequent increase is due to upwelling material undergoing decompression melting. Similar total amounts of melt produc-

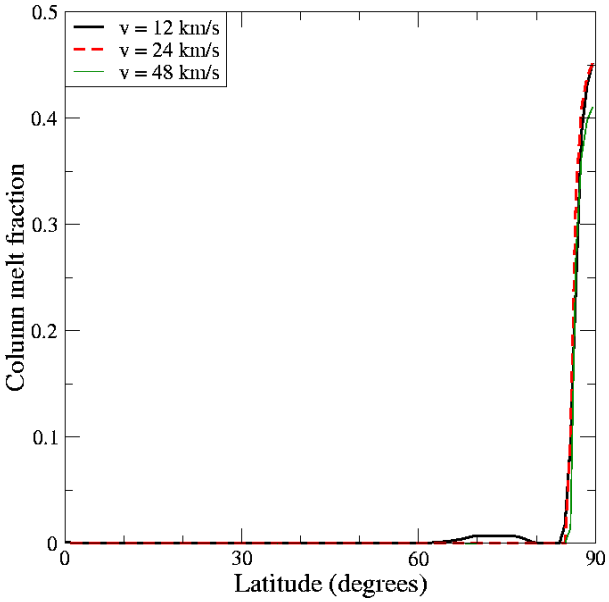

Figure 2: Total time-integrated column melt fraction vs. latitude immediately after formation of Caloris for the three impact velocities used for the models in Fig. 1.

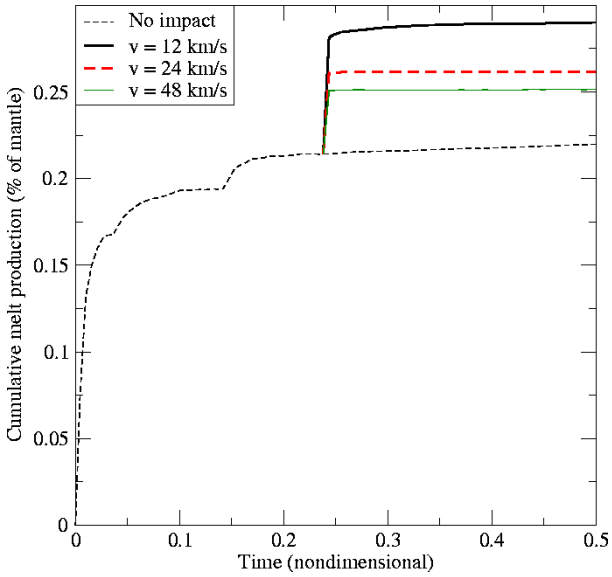

Figure 3: Evolution of the total melt production over time for the models in Fig. 1.

tion ($\sim 0.25\%$ of the mantle) are obtained in all cases.

Younger volcanism

These results suggest that a single impact may produce multiple episodes of volcanism. The shock heating distribution from larger projectiles penetrates into convective upwellings up to 800 km away; beyond the basin rim. This promotes melt production in these upwellings, beneath a relatively thick stagnant lid. The associated melt is thus produced at depth and may be erupted to the surface much later than the direct impact melts. This is consistent with the relatively young age of the exterior plains [2-4]. We also find that impacts may sample different regions of the mantle. Direct impact melts are primarily in the near surface, while exterior melting is located in deeper mantle plume heads. Volcanic plains may therefore reveal pre-existing compositional stratification of the crust and mantle [2,12]. An additional interesting implication is that Impact melting may actually suppress volcanism at later times by prematurely using up the more easily melted components.

Effect on the core

We note that an impact capable of forming Caloris cannot significantly heat the core and should not affect the dynamo. This is consistent with observations of a present-day global magnetic field at Mercury [13]. The shock heating decays relatively quickly away from the impact site, due to the high expected impact velocity at Mercury (42.5 km/s [14]), and thus the small size of the projectile. We note, however, that the heating from a slow vertical impact could be mimicked by a fast oblique impact. Furthermore, while the median impact velocity at Mercury is high [14], the distribution is broad and some slower impacts are expected.

References

[1] Murchie, S.L. et al. (2008) *Science* 321, 73-76. [2] Denevi, B.W. et al. (2009) *Science* 324, 613-618. [3] Strom, R.G. (2008) et al. *Science* 321, 79-81. [4] Fassett, C.I. et al. (2009) *EPSL* 285, 297-308. [5] Melosh, H.J. (1989) *Impact Cratering*, Oxford Univ. Press. [6] Holsapple, K.A. (1993) *AREPS* 21, 333-373. [7] Pierazzo, E. et al. (1997) *Icarus* 127, 408-423. [8] Watters, W. A. et al. (2009) *JGR* 114, E02001. [9] Roberts, J.H. and S. Zhong (2004) *JGR* 109, E03009. [10] McNamara, A.K. and S. Zhong (2004) *JGR* 109, B07402. [11] Roberts, J.H. and O.S. Barnouin (2011) *JGR*, in revision. [12] Ernst, C.M. et al. (2010) *Icarus* 209, 210-223. [13] Anderson, B.J. et al. (2008) *Science* 321, 82-85. [14] Le Feuvre, M. and M. A. Wieczorek. (2008) *Icarus* 197, 391-206.

How much Earth-like material could the Moon accrete?

Julien Salmon[1] and Robin M. Canup[1], [1]Southwest Research Institute, Department of Space Studies, Boulder, CO, USA (julien@boulder.swri.edu)

Introduction

The Earth's Moon is believed to have accreted from a circumterrestrial disk generated by the impact of a Mars-size object into the proto-Earth [1]. A key constraint is explaining the similar compositions of the Earth and the Moon (O-isotopes in particular [2]). Most impact simulations find that the majority of the disk material comes from the impactor [3, 4], which is thought to have had a composition significantly different from that of the Earth, given the observed compositional variations between the Earth and other inner Solar System objects [5].

Disk material within the Roche limit can be described as a two-phase, melt-vapor fluid that evolves under two competitive processes [6, 7]: (1) gravitational instabilities in the melt, resulting in high collision rates, rapid viscous spreading, and vaporization due to energy released in collisions, and (2) radiative cooling of the gravitationally stable vapor phase, leading to its condensation. The balance of these processes regulates how rapidly the inner disk can spread and deliver material to the region exterior to the Roche limit where the Moon accretes.

It has been proposed that diffusive mixing between the Earth's and the disk's atmospheres could chemically equilibrate the disk with the Earth in $\sim 10^2$ to 10^3 years [5]. Prior N-body simulations of Moon formation from a circumterrestrial disk found rapid accretion in less than a year [8, 9], although these were purely particulate models that did not account for a two phase, Roche-interior disk.

Model

In our model (an improved version of [10]), material within the Roche limit is represented by a fluid disk, while exterior moonlets are tracked with direct N-body simulation. We have modified SyMBA [11] to include the accretion criterion of [12] and a simple analytical model for the inner disk. We treat the inner disk as a uniform density slab of mass M_d initially extending from the Earth's surface to the Roche limit at $a_R \approx 2.9 R_\oplus$. The disk spreads viscously with either a radiation-limited viscosity [6] or an instability-driven viscosity [13], whichever is smaller at a given time. Disk material spreading onto the planet is lost, while mass spreading beyond a_R is removed from the disk and added to the N-body code as new moonlets.

Interactions between the disk and the orbiting bodies at 0-th order Lindblad resonances result in an additional "kick" to the orbiting bodies, which gain angular momentum from the disk and cause the disk's outer edge, r_d, to recoil inward. The disk would efficiently absorb scattered objects small enough to encounter a disk mass greater than their own during a single pass through the inner disk. We thus consider that any N-body particle with mass $< 0.1 M_d$ and within an orbital radius $r < \gamma r_d$ is absorbed by the inner disk, where we let γ = 0 (no capture, bodies pass freely through the inner disk), 0.9 and 0.95. A captured particle is removed from the N-body simulation and its mass added to that of the disk.

Results

We use initial configurations with a Roche-interior disk and an outer N-body disk, varying the total mass in the inner and outer disks (M_T) and the radial extent of the outer disk.

A typical simulation shows three accretion phases: (1) outer bodies rapidly accrete and confine the inner disk within the Roche limit; (2) remaining orbiting objects recede due to torques from the disk, allowing the inner disk to viscously spread outward; and (3) the inner disk spreads back out to the Roche limit and spawns new moonlets that are accreted by the outer object(s) (Figure 1). The start of phase (3) is regulated by the slow, radiation-limited viscous spreading of the disk, and increases the final accretion timescale to several hundreds of years, which could be compatible with required timescales for equilibration. An example evolution of the mass of the largest body and the fraction of its mass derived from the inner disk is plotted in Figure 2.

Figure 3 shows the fraction of the final Moon derived from the inner disk vs. the final Moon's mass at the end of simulations that considered M_T = 2 to 2.4$M_☾$. Colors correspond to different values of γ: 0 (black), 0.90 (green), and 0.95 (red). Allowing bodies that pass within the disk to be absorbed by the disk significantly increases the predicted fraction of inner disk material that ends up on the Moon. However, bodies with a mass $> 0.8\ M_☾$ have $< 55\%$ of their mass derived from the inner disk.

Discussion

Material initially orbiting exterior to the Roche limit accretes very rapidly (in months), but delivery of material from the Roche-interior disk proceeds slowly, resulting in a total lunar accretion timescale of $\sim 10^2$ years. Moon-disk resonant interactions limit the fraction of the inner disk that is ultimately incorporated into the final

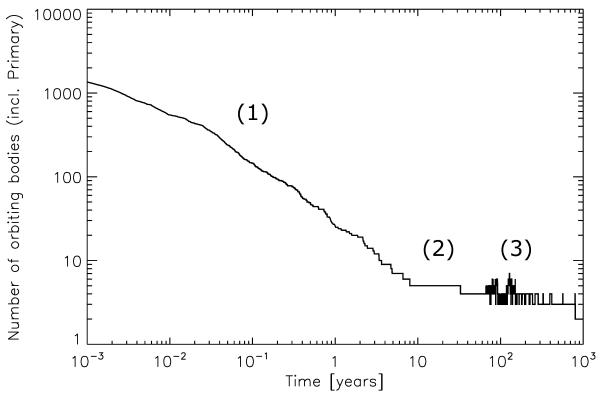

Figure 1: Evolution of the number of orbiting bodies. First orbiting objects collide and accrete, and they confine the inner disk below the Roche limit (1). Viscous spreading and outward migration of the moons allow the disk to reach the Roche limit (2), and new moonlets are produced and finally accrete on the moon (3). This simulation had $M_d = 1.50 M_{\leftmoon}$, and an initial outer disk with $0.50 M_{\leftmoon}$ and extending to $4 R_{\oplus}$.

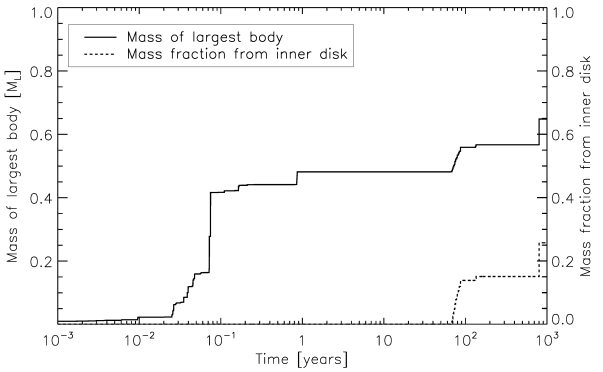

Figure 2: Mass of the largest body (solid line), and the fraction of its mass composed of material derived from the Roche-interior disk (dashed line) for the simulation shown in Figure 1. First the largest body grows through collisions and confines the ring below the Roche limit. As the body recedes away through resonant interactions, the inner disk can spread back out to the Roche limit. Then new moonlets are spawned, and growth of the Moon continues. After $\sim$ 200 years, the inner disk is depleted and the moon reaches its final mass of $0.65 M_{\leftmoon}$, 25% of which originated in the inner disk.

Moon. The 3-phase accretion process found in our simulations implies that only material accreted during the final stage is derived from the inner disk. Provided equilibration can occur, Earth-like material might then be concentrated in the outer portions of the Moon, depending on whether there is substantial cooling of the Moon between phases (1) and (3). For appropriately large moons, the fraction of the Moon comprised of equilibrated material remains fairly small, typically less than 0.5. Further improvements, in particular a full numerical simulation of the Roche-interior disk [14, 15] that accounts for the radial dependence of the disk viscosity, may result in an increased fraction of inner disk material in the final Moon. A compact, $M_T > 3 M_{\leftmoon}$ initial disk would also increase this fraction, although such disks have not been produced by impact simulations.

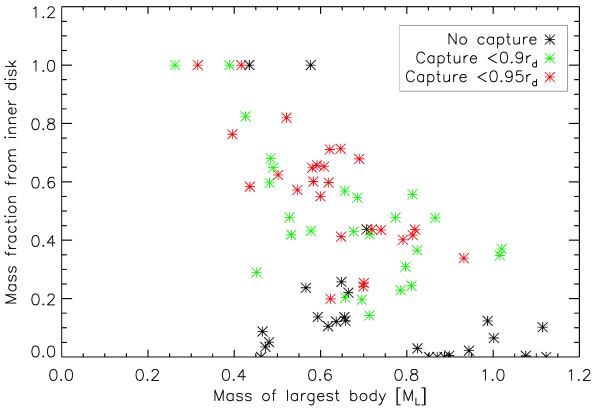

Figure 3: Mass fraction of the Moon composed of material accreted from the Roche-interior disk vs. the mass of the largest body, for different capture criteria. For cases where the 2nd largest body has a mass $> 30\%$ that of the largest, we plot the mass and mass fraction of the combined body. Black points are simulations where N-body objects pass freely through the inner disk, while green and red points correspond to cases where bodies are assumed to be absorbed by the inner disk if they pass within $0.9 r_d$ or $0.95 r_d$, respectively. Allowing capture of bodies in the inner disk significantly increases the mass fraction of inner disk material that ends up on the Moon.

Acknowledgements

This work has been funded by NASA's LASER program and the NASA Lunar Science Institute.

References

[1] Cameron, A. G. W. and Ward, W. R., LPSC VII, 120-121, 1976.
[2] Wiechert, U., Halliday, A. N., Lee, D.-C., Snyder, G. A., Taylor, L. A., and Rumble, D., Science, 294, 345-348, 2001.
[3] Canup., R. M., Icarus, 168, 433-456, 2004.
[4] Canup., R. M., Icarus, 196, 518-538, 2008.
[5] Pahlevan, K., Stevenson, D. J., Earth Planet. Sci. Let., 262, 438-449, 2007.
[6] Thompson, C., and Stevenson, D.J., ApJ, 333, 452-481, 1988.
[7] Ward, W. R., AJ, in press, 2011.
[8] Ida, S., Canup, R. M., and Stewart, G. R., Nature, 389, 353-357, 1997.
[9] Kokubo, E., Ida, S., and Makino, J., Icarus, 148, 419-436, 2000.
[10] Canup, R. M., and Ward, W. R., LPSC XXXI, 2000.
[11] Duncan, M. J., Levison, H. F., and Lee, M. H., AJ, 116, 2067-2077, 1998.
[12] Canup, R. M., and Esposito, L. W., Icarus, 113, 331-352, 1995.
[13] Ward, W. R. and Cameron, A. G. W., LPSC IX, 1205-1207, 1978.
[14] Charnoz, S., Salmon, J., and Crida, A., Nature, 465, 752-754, 2010.
[15] Salmon, J., Charnoz, S., Crida, A., and Brahic, A., Icarus, 209, 771-785, 2010.

Crater Size-Frequency Distributions and Chronologies of Asteroids. N. Schmedemann[1], T. Kneissl[1], G. Michael[1], R.Wagner[2], G. Neukum[1], A. Nathues[3], H. Sierks[3], [1]Institute of Geosciences, Freie Universität Berlin, Berlin, Germany, [2]German Aerospace Center, Institute of Planetary Research , Berlin, Germany, [3]Max-Planck-Institut für Sonnensystemforschung, Katlenburg-Lindau, Germany, (nico.schmedemann@fu-berlin.de)

Introduction: In recent years several space probes visited a number of small bodies. Right now the Dawn mission [1] is gathering imaging data from an orbit around the asteroid 4 Vesta. The asteroid Main Belt is believed to be the source region of impactors in the inner solar system [2]. For decades the lunar cratering record has been investigated and even probed by sample return missions. Thus, it is well suited for comparison with other planetary surfaces. In the case of Vesta it is even possible to test cratering chronologies against the radiometric ages of HED meteorites, since Vesta is probably the only source of HED meteorites in the solar system [7].

Crater Size-Frequency Distribution (CSFD): Scaling laws have been derived by several groups e.g. [3, 4] to predict the relation between projectile size and crater size with respect to numerous impact properties like impact speed, angle, target materials, etc. In this work we utilize the scaling laws by [4]. Because the CSFD of impact craters on the Moon is well known, we can use it together with scaling laws to predict the CSFD of other celestial bodies like asteroids and test it against observations we got from space probes. Fig. 1 shows the lunar CSFD in comparison with measurements derived from a number of small asteroids like Gaspra, Ida, Steins and Lutetia. It is obvious that low gravity targets like asteroids display a significantly flatter distribution of large craters. Despite slightly different material properties of the investigated bodies the scaling is dominated by the impact velocity and surface gravity. This results in highly similar CSFD throughout the mentioned asteroids. Vesta, however is much more massive and consequently has a CSFD lying in between the lunar CSFD and the shown small asteroid CSFD. Our measurements on Dawn imaging data are in very good agreement to our modeled CSFD for Vesta.

Asteroid Chronologies: As the lunar surface has accumulated a cratering record dating back to the early solar system history and sample return missions provided radiometrically datable material, we now have a ground truth calibrated lunar chronology available [5]. Scattering processes caused by collisions among asteroids, dynamical interaction with major bodies as well as non-gravitational forces scatter projectiles from the Main Belt all over the solar system [6]. This processes left behind a detailed cratering record on many planetary surfaces which are less affected by resurfacing processes. The travelling time of meteorites from the Main Belt to e.g. the lunar surface is short [6]. It is about an order of magnitude less than the half life time value derived for the exponential decay in the lunar cratering rate [2].

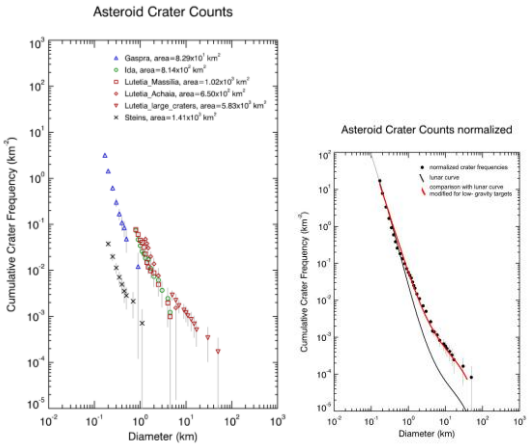

Fig.1: *Left: Crater measurements on asteroids Gaspra, Ida, Lutetia and Steins show a high intrinsic similarity to each other. Right: Normalized measurements from the left hand-side (dark points) display a flatter CSFD than the lunar curve (black curve). Scaling laws account for different impact properties and predict a well fitting model CSFD for small asteroids (red curve).*

Thus, it is very likely that any time dependent development of the impactor population in its source region, the asteroid Main Belt is directly projected into the cratering records of the planetary surfaces. Therefore, we use a lunar-like chronology for asteroids and scale it to the respective impact rates. This scaling is primarily based on an attempt by [6] but incorporates as much observational data as possible. In the case of Vesta we have radiometric Ar-Ar ages of HED meteorites [7] available, which seem to be in excellent agreement with our results from crater counting.

Acknowledgement: This work was supported by the German Space Agency (DLR) on behalf of the Federal Ministry of Economics and Technology, grant 50 OW 1101.

References

[1] Russell, C. T., Barucci M. A., et al.: "Exploring the asteroid belt with ion propulsion: Dawn mission history, status and plans." Advances in Space Research **40**(2): pp 193-201, 2007. [2] Neukum G. and Ivanov B. A.: "Crater size distributions and impact probabilities on Earth from Lu-

nar, terrestrialplanet, and asteroid cratering data". In: Gehrels T (ed) Hazards due to comets and asteroids". University of Arizona Press, Tucson, 359–416, 1994. [3] Housen, K. R. and K. A. Holsapple (2011). "Ejecta from impact craters." Icarus 211(1): 856-875. [4] Ivanov B. A.: "MARS/MOON CRATERING RATE RATIO ESTIMATES", Chronology and Evolution of Mars **96,** 87–104, 2001. [5] Neukum, G., B. A. Ivanov, et al. (2001). "Cratering records in the inner solar system in relation to the lunar reference system." Space Science Reviews 96(1-4): 55-86.[6] O'Brien, D. P. and R. Greenberg (2005). "The collisional and dynamical evolution of the main-belt and NEA size distributions." Icarus **178**(1): 179-212.[7] Bogard, D. D. and D. H. Garrison (2003). "39Ar-40Ar ages of eucrites and thermal history of asteroid 4 Vesta." Meteoritics & Planetary Science, vol. 38, no. 5: 669-710.

Questions About Lunar Origin. Fred S. Singer

In 1975 William K. Hartmann and Donald R. Davis suggested that, at the end of the planet formation period, several satellite-sized bodies had formed that could collide with the planets or be captured. They proposed that one of these objects may have collided with the Earth, ejecting refractory, volatile-poor dust that could coalesce to form the Moon. This collision could help explain the unique geological properties of the Moon.

The impact hypothesis was devised mainly to circumvent what was thought to be a low probability of lunar capture. (Yet, strangely, capture appears to be the preferred hypothesis for the origin of the outer moons of Jupiter and some other planetary satellites.) But the impact hypothesis has similar probability problems that are hardly ever mentioned -- in addition to more fundamental problems, all of which can be overcome only with various *ad hoc* assumptions.

The impact hypothesis (Hartmann; Benz, Cameron, Melosh; Canup, Asphaug) of lunar origin seems to have found general acceptance – in spite of the fact that its probability is low and the physics of the lunar formation is not readily transparent, being obscured by a complicated computer program. Nevertheless, one can raise certain questions that an impact process should answer:

1. For what range of impact parameters a is there an appreciable chance of forming the Moon? If a is close to the Earth radius R, then the impact is only glancing and the process becomes operationally indistinguishable from "capture"; if $a \ll R$, then the probability of forming a Moon from Earth material appears low (as evident from arguments of angular momentum conservation).

2. Therefore how many Mars-like bodies must impact in order to have a reasonable chance to produce the present Moon? And why is impact origin more probable than capture? Also: If there are so many bodies available, why didn't it happen on Venus or Mars?

3. At what stage of terrestrial accretion does the hypothetical impact occur? Early or late? Different papers give different answers.

4. What is the mass of the impactor? Twice lunar or more like that of Mars? Different papers give different answers.

5. In the calculation, what is the assumed pre-impact spin of the Earth? The initial papers on impact formation of the Moon did not consider a pre-impact rotation of the Earth. What restraints are there on the pre-impact angular momentum? E.g., could a retrograde impact produce the Moon? Or: How to be sure that the total angular momentum matches the present value of the Earth-Moon system? How does the Earth spin angular momentum vector change during and following the impact? What fraction of the total angular momentum is taken up by the debris emanating from the impact? What fraction is carried away by the escaping debris?

6. What happens to the splashed-out material from the impact; how many particles escape and how many return on ballistic orbits? Whence comes the angular momentum for a bound lunar orbit? How and where does "captured" material assemble and what exactly is the initial lunar orbit?

7. At what Earth distance does the Moon assemble? At Roche limit or at ~ 10 Earth radii? Different papers give different answers.

8. If assembly proceeds into an equatorial orbit, as one might expect, how does one account for the present lunar orbit without any *ad hoc* assumptions? [cf. Goldreich (1966) argument]

9. If the initial Moon orbit is retrograde, or within the synchronous orbit limit of the spinning Earth, will not the Moon spiral in and thus not survive?

10. Just what is the dynamics of assembly from a ring in the presence of tidal perturbations? Responding to the most massive agglomeration of material, the Earth's tidal bulge would drive it outward and at the same time despin the Earth – thereby increasing the synchronous orbit radius; this would drive smaller agglomerations (now within the synchronous limit) into inward-spiraling orbits -- thus preventing a complete assembly. Has this feature been taken into account?

11. Similarly, if subsequent to the formation of the Moon, the Earth's spin is changed by another large impact that puts the lunar orbit within the synchronous limit, what happens then to the probability of lunar survival? How do later impacts affect the total angular momentum.

[One cannot discern answers to these questions from existing publications. For example, the Canup papers do not indicate how the spin period of the Earth changes over time; nor do they show the tidal distortion. There is also the Roche limit problem and others that I have not mentioned.]

12. In addition to the dynamical problems just discussed, how does the impact hypothesis deal with chemical (Saal 2007) and geological (Borg 2011) findings? Initially, the impact hypothesis was supported by the similarity of lunar chemistry with that of the Earth's mantle. Recent publications show also the existence of water and other volatiles in lunar rocks and raise questions of their survival at the high temperatures generated by the impact.

References:

Goldreich, P. 1966. *Rev. Geophys*. **4**, 411

Canup, R. M. and E. Asphaug 2001. *Nature*, **412**, 708-712

Canup, R. M. 2004. *Icarus* **168** (2): 433

Borg, L. et al. 2011. *Nature* **477,** 70–72

Saal, A. E. et al 2008. *Nature* **454**, 192-195

Benz, W, AGW Cameron, HJ Melosh 1989. *Icarus* **81**, 113-131

****

The formation of Jupiter and the Jovian Early Bombardment. D. Turrini[1], A. Coradini[1], C. Federico[2], M. Formisano[1,3], G. Magni[4], [1] Institute for Physics of Interplanetary Space INAF-IFSI, via Fosso del Cavaliere 100, 00133 Rome, Italy (e-mail: diego.turrini@ifsi-roma.inaf.it); [2] Department of Earth Science, University of Perugia, Perugia, Italy; [3] Department of Physics, University of Rome "La Sapienza", Rome, Italy; [4] Institute for Space Astrophysics and Cosmic Physics INAF-IASF, Rome, Italy.

Introduction: The first phase in the lifetime of the Solar System is that of the Solar Nebula, when the Solar System was constituted by a circumsolar disk of gas and dust particles where planetesimals and planetary embryos were forming. This phase is assumed to start 4568.2 Ma ago [1] with the condensation of the Ca-Al-rich inclusions and to end in less than 10 Ma [2] with the dispersal of the nebular gas.

Across this $\Delta T < 10$ Ma timespan planetary accretion was acting in the Solar Nebula to form the planetesimals, the planetary embryos and the giant planets. According to meteoritic evidences, some of the accreting planetesimals differentiated extremely early in the history of the Solar System, i.e. about 1-2 Ma after the formation of CAIs (see [3] and references therein). Such primordial differentiation was due to the presence of short-lived radionuclides, mainly ^{26}Al and ^{60}Fe (ibid) in bodies larger than 20 - 30 km in radius (ibid). In particular, the spectral connection between Vesta and the Howardite-Eucrite-Diogenite (HED) suite of achondritic meteorites suggests that Vesta formed and differentiated very early in the history of the Solar System, likely only a few Ma later than CAIs (see e.g. [3,4] and references therein).

In the following we report the results of our crossed investigation of the thermal history of Vesta and of the primordial bombardment triggered by the formation of Jupiter. The goal of this project is to assess if the Dawn mission could allow us to probe a previously unexplored phase in the life of the Solar System.

The Model: We simulated the dynamical evolution over 2 Ma of a template of the forming Solar System composed of the Sun, the accreting Jupiter, a swarm of planetesimals, Vesta, Ceres [5,6] and a set of other target bodies [7]. The aim of our simulations was to estimate the effects of the formation of Jupiter on the collisional evolution of Vesta and of other primordial bodies existing in the asteroid belt.

Across the first half of this 2 Ma-long temporal window, Jupiter's core is assumed to accrete from a Mars-sized embryo of 0.1 $M_\oplus$ to the critical size of 15 $M_\oplus$ [5]. Across the second half of the temporal interval spanned by our simulations, Jupiter is assumed to rapidly accrete its gaseous envelope [5], increasing its mass with an e-folding time of 5000 years [8]. While accreting its gaseous envelope, Jupiter could have migrated inward due to exchange of angular momentum with the circumsolar disk (see [9] and references therein). To evaluate the effects of Jupiter's migration, we considered five different scenarios [5]: Jupiter forming at its present position, Jupiter migrating inward by 0.25, 0.5 and 1 AU with an e-folding time of 5000 years and Jupiter migrating inward by 1 AU with an e-folding time of 25000 years.

The planetesimals spans between 2-10 AU, are initially located on low-eccentricity and low-inclination orbits and, in the dynamical model, are represented by 80000 massless particles [5,6]. To evaluate their effects on the collisional history of Vesta, Ceres and the other target bodies we associated to each planetesimal mass and density values and a normalization factor derived by their formation region and the assumed formation scenario [5]. The size-frequency distributions of the planetesimals we considered are those due to their formation in a quiescent [10] or in a turbulent nebula [11] and that due to to the primordial collisional evolution of the asteroid belt [12]. During the dynamical evolution of our template of the Solar System we evaluated the probabilities of planetesimals impacting Vesta and Ceres [5] or other bodies [7] through a statistical approach similar to the method devised by Opik [13]. The effects of the impacts on the target bodies were estimated using the scaling-laws from [14] and [15], the latter in the angle-averaged form supplied by [16].

The Jovian Early Bombardment: Our results indicates that the formation of Jupiter causes a phase of

	Collisionally evolved planetesimals (Morbidelli et al. 2009)			
Migration Scenario	N_{coll}	Crustal Erosion (km)	$Q_D/Q^*_D \geq 0.01$	$Q_D/Q^*_D \geq 1$
No Migration	15158.5	0.17	0.00	0.00
0.25 AU	20976.3	0.21	0.00	0.00
0.50 AU	36132.1	1.61	0.66	0.00
1.00 AU	66419.1	11.57	5.09	0.01

Table 1: the Jovian Early Bombardment in a disk populated by collisionally evolved planetesimals [6] following the size-frequency distribution of the best-fit case from [12].

primordial bombardment we labeled the Jovian Early Bombardment (JEB in the following, [5]). While the migration of Jupiter enhances the intensity of the JEB due to the sweeping of the resonances across the asteroid belt, the formation of the giant planet is necessary and sufficient condition for triggering the JEB [5]. Planetesimals from both the inner and the outer Solar System participate to the JEB, but the leading role in determining the effects of the JEB is played by the planetesimals affected by the 3:1 and the 2:1 resonances with Jupiter [5].The survival of the considered target bodies to the JEB depends on the size distribution of the planetesimals populating the Solar Nebula, the abundance of large planetesimals (i.e. D > 100 km) in the disk being a critical factor to this regard [5,7]. Another critical factor is the location of the target bodies respect to the two previously mentioned resonances [5,7]. If the disk of planetesimals was dominated by large bodies, like in the case of planetesimals formed in turbulent circumstellar disks, the JEB would cause the ablation of bodies of 500 km or smaller [7]. Conversely, disks dominated by small planetesimals (i.e. D < 20 km), like those formed in quiescent circumstellar disks or produced by collisional evolution, represent more favorable environments for the survival of bodies of 200 km or bigger [7]. Planetesimals of 200 km, however, would survive only in the scenario where Jupiter does not migrate [7]. In all other scenarios, they are generally disrupted if Jupiter migrated by 05 AU or more [7].

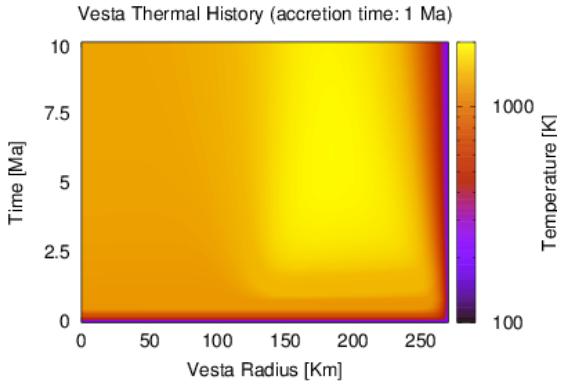

Figure 1: temporal evolution of the thermal profile of Vesta over 10 Ma under the effects of the decay of short-lived radionuclides assuming an accretion time of Vesta of 1 Ma [17].

Vesta and Ceres [5,6] would undergo an intense cratering that would saturate their surfaces with craters as big as 150 km, with a tail of few bigger craters (200-300 km). Under the simplifying assumption of a uniform distribution of the craters, on Vesta the JEB could excavate up to a depth of about 10 km (see Table 1 and [6]). Assuming a depth-to-diameter ratio of 1:7, however, the JEB could excavate the crust of Vesta either locally or regionally (see Fig. 1 and [6]).

The role of Vesta: The geophysical history of Vesta. as inferred by HED meteorites, suggests that its differentiation could have ended in a few Ma: as such, Vesta could be the only body we know of whose solid crust was already formed at the time of the formation of Jupiter. This hypothesis is supported also by the results of theoretical studies of the thermal history of Vesta (see Fig. 1 and [17]). The local or regional excavation of the primordial crust of Vesta would have caused large-scale effusive phenomena similar to the Lunar maria [5,6,18]. Therefore, the data that Dawn mission is collecting on Vesta could allow us to test the Jovian Early Bombardment hypothesis and to investigate the early evolution of the Solar System [19].

References: [1] Bouvier A., Wadhwa M. (2010). Nature Geoscience, 3, 637; [2] Meyer M. R.(2008). Proc. of Intern. Astron. Union, 4, 111; [3] Scott E. R. D. (2007), An. Rev. of Earth and Planet. Sci., 35, 577; [4] Keil K. (2002), in Asteroids III, Eds. W. F. Bottke Jr., A. Cellino, P. Paolicchi, and R. P. Binzel, University of Arizona Press; [5] Turrini D., Magni G., Coradini A. (2011), MNRAS, 413, 2439; [6] Turrini D., Coradini A., Magni G., Formisano M., Federico C. (2011), abstract presented at the EPSC-DPS 2011; [8] Turrini D., Coradini A., Magni G. (2011). ApJ, under revision. [8] Coradini A., Magni G., Turrini D. (2010). SSR, 153, 411; [9] Papaloizou J. C. B., Nelson R. P., Kley W., Masset F. S., Artymowicz P. (2007) in Protostars and Planets V, Eds. B. Reipurth, D. Jewitt, and K. Keil, University of Arizona Press; [10] Coradini A., Federico C., Magni G. (1981), A&A, 98, 173; [11] Chambers J. E. (2010), Icarus, 208, 505; [12] Morbidelli A., Bottke W. F., Nesvorny D., Levison H. F. (2009), Icarus, 204, 558; [13] Opik E. J. (1976), in Interplanetary Encounters, Eds. Kopal Z., Cameron A. G. W., Elsevier; [14] Benz W., Asphaug E. (1999). Icarus, 142, 5; [15] Holsapple K. A., Housen K. R. (2007). Icarus, 187, 345 [16] Svetsov V. (2011). Icarus, 214, 316; [17] Federico C., Coradini A., Pauselli C., Formisano M., Turrini D., in preparation; [18] Formisano M., Federico C., Coradini A., Turrini D. (2011), abstract presented at the EPSC-DPS 2011; [19] Coradini A., Turrini D., Federico C., Magni G. (2011). SSR, DOI 10.1007/s11214-011-9792-x.

Additional Information: The authors wish to dedicate this work to their friend and colleague A.C., who passed away after a long illness on September 5th, 2011. This research has been supported by the Italian Space Agency (ASI) through the ASI-INAF contract I/015/07/0. The computational resources used in this research have been supplied by IFSI-Rome through the project “HPP - High Performance Planetology”.

APPLICATION OF THE ^{182}Hf-^{182}W ISOTOPE SYSTEM TO CONSTRAINING THE TIMING OF LATE ACCRETION TO THE EARTH AND MOON. R. J. Walker[1], M. Touboul[1] and I. S. Puchtel[1], [1]Department of Geology, University of Maryland, College Park, MD 20742 USA (rjwalker@umd.edu).

Introduction: Over the past two decades, the short-lived ^{182}Hf-^{182}W isotopic system (^{182}Hf → ^{182}W + β^- where $t_{½}$ = 8.9 Myr) has been widely used for dating early solar system processes, due to the unique geochemical properties of the system [1-2]. As a moderately siderophile element (MSE), W is largely, but not completely, extracted from the silicate mantles of planetary bodies during segregation of metallic cores [e.g., 3]. Hafnium, in contrast, is lithophile and is essentially wholly retained in the silicate portions of planetary bodies. Therefore, determination of the abundance of the daughter nuclide ^{182}W, relative to other stable, non-radiogenic isotopes (e.g., ^{184}W), is of special interest for constraining the timing of planetary core formation. For example, the higher than chondritic ^{182}W/^{184}W ratio of the terrestrial mantle has been interpreted to reflect core segregation and generation of supra-chondritic Hf/W in the mantle during the first ~30 Myr of solar system history, while ^{182}Hf was extant [4-5].

Following the cessation of significant core segregation, the Hf/W ratio of the Earth's mantle would likely have been further modified by post-core-formation events, such as the crystallization of transient magma oceans, partial melting of the mantle, or subsequent crystal-liquid fractionation processes [3]. If such events occurred before ^{182}Hf became extinct, additional ^{182}W isotopic variations would have been generated in the mantle. It is even likely that ^{182}W isotopic heterogeneities were created in the mantle after ^{182}Hf was no longer extant. The term "late accretion" is used to describe the process of mass addition to the Earth by continued accretion subsequent to cessation of core formation. It is a process that has been commonly invoked to account for the relatively high abundances of the highly siderophile elements (HSE: including Os, Ir, Pt and Re) present in the mantle [6,7]. Late accretion equivalent to 0.3 to 0.8% of the total mass of the mantle, the amount necessary to account for the observed mantle abundances of HSE [8], would have lowered the ^{182}W/^{184}W of the mantle by 10 to 30 ppm, as materials with comparatively ^{182}W-depleted compositions, such as planetesimals with bulk chondritic compositions, were accreted to Earth.

Willbold et al. [9] recently reported ~13 ± 4 ppm ^{182}W enrichments, relative to younger terrestrial rocks and standards, in 3.8 Ga rocks from the Isua greenstone belt, Greenland. This study provided the first evidence for W isotopic heterogeneity in terrestrial materials. Willbold et al. [9] concluded that the ^{182}W rich isotopic composition of the Isua suite preserves the composition of the mantle prior to a final stage of late accretion to the Earth and Moon, termed the terminal bombardment, that has been previouslyhypothesized, based on common 3.8 to 3.9 Gyr ages for lunar impact melt rocks associated with the major impact basins [10-11]. Willbold et al. [9] argued that the addition of materials of chondritic bulk composition (μ^{182}W = -200) that were rich in W, as well as HSE, would have lowered the W isotopic composition of the bulk mantle from an older, more radiogenic composition. They posited that the Isua rocks are remnants of the prior, primordial mantle. This hypothesis is consistent with that of Maier et al. [12] in which it was concluded that a gradual increase in the abundances of HSE is recorded in mantle sources of Archean komatiites formed between ~3.5 and 2.9 Ga rocks, and that this reflects a downward mixing of the HSE into the deep mantle sources of the komatiites.

As a test of the late stage, late accretion hypotheses to affect both W isotopes and HSE abundances, we report W isotope composition data for 3.47 Ga komatiites from the Komati Formation of the Barberton greenstone belt, South Africa [13], and 2.82 Ga komatiites from the Kostomuksha greenstone belt, Baltic Shield, Russia [14]. Puchtel and Walker [15] estimated that the Komati and Kostomushka komatiite sources contained ~45 and ~75 %, respectively, of the late accretionary component now present in the modern mantle.

Analytical Methods: We recently developed a new technique to measure ^{182}W/^{184}W to a 2σ precision of ±4.6 ppm using negative thermal ionization mass spectrometry [16]. After chemical purification of W through a four-step ion exchange chromatographic separation, the W isotopic composition is measured as WO_3^- by negative thermal ionization mass spectrometry using a *Thermo-Fisher Triton* instrument. Data are initially corrected for oxide interferences, assuming a predefined O isotope composition, and for mass fractionation, by normalization to ^{186}W/^{184}W or ^{186}W/^{183}W, using an exponential law. A small second-order effect, likely reflecting a mass dependent change of O isotope composition in the measured W oxides, is corrected by normalization to ^{183}W/^{184}W using a linear law. Repeated analysis of both standard solutions and rocks demonstrate external reproducibility of ^{182}W/^{184}W within ±4.5 ppm (2σ SD).

Results: The μ^{182}W values (where μ^{182}W values are the deviation in ppm from the terrestrial reference standard) for four Komati samples average +2.6 ± 4.1

(2σ SD), and are indistinguishable from terrestrial standards and the modern La Palma basalt (Canary Islands) we repeatedly analyzed ($\mu^{182}W$ = +0.1 ± 2.4) (**Fig. 1**). In contrast, the eighteen Kostomuksha komatiite samples analyzed (including replicate digestions) have $\mu^{182}W$ values that average +14.8 ± 4.8 (2σ SD), which is well-resolved from the terrestrial standard (**Fig. 1**).

Discussion: Although the 13 ppm enrichment in ^{182}W in rocks from Isua is similar in magnitude to that of the Kostomuksha komatiites, the interpretation that Willbold et al. [9] applied to the Isua rocks is problematic for the Kostomuksha rocks. To test a similar model for the Komati and Kostomuksha sources, we modeled mixing between a primordial, ^{182}W-enriched, yet HSE depleted reservoir, and a bulk chondritic composition (**Fig. 2**). Total HSE content is expressed as the percent deviation of content in the mantle source, relative to the concentration in the primordial mantle. The effects of contributions of late accreted materials ranging from 0.3 to 0.8% of the total mass of the mantle are calculated, assuming that the HSE present in the silicate Earth today were entirely derived from late accretion. Given the estimates that the Komati and Kostomushka komatiite sources contained ~45 and ~75 %, respectively, of the late accretionary component now present in the modern mantle, the older Komati komatiites should show more radiogenic $\mu^{182}W$ (~9 ppm) than the Kostomushka komatiites (~4 ppm). This is not observed and suggests that the Kostomuksha source cannot simply be primordial mantle that had been largely stripped of HSE by core formation. We also note that there is minimal overlap between uncertainties in the W isotopic composition of the Komati komatiites and the mantle mixing model of **Fig. 2**, suggesting that the downward mixing model of Maier et al. [12] is not viable for at least the Komati komatiites. We instead attribute the enrichment in the Kostomuksha komatiites to reflect preservation of an early Earth (within ~30 Myr of solar system formation) differentiation product.

Conclusions: If late accretion was responsible for establishing HSE abundances in the mantle following core formation, this process likely dominantly occurred prior to the postulated late heavy bombardment. Thus, W isotopes can be used to limit the proportion of mass added to the Earth and Moon during this event.

References: [1] Lee D-C. and Halliday A.N. (1995) Nature **378**, 771. [2] Harper C.L. and Jacobsen S.B. (1996) *GCA* **60**, 1131. [3] Righter K. and Shearer C.K. (2003) *GCA* **67**, 2497. [4] Kleine et al. (2002) *Nature* **418**, 952. [5] Yin et al. (2002) *Nature* **418**, 949. [6] Chou C-L. (1978) *Proc. Lunar Planet. Sci. Conf. 9th*, 219. [7] Morgan J.W. et al. (2001) *Meteor. & Planet. Sci.* **36**, 1257. [8] Walker R.J. (2009) *Chem. der Erde* **69**, 101 [9] Willbold M. et al. (2011) *Nature* **477**, 195. [10] Terra F. et al. (1974) *EPSL* **22**, 1. [11] Dalrymple G.B. and Ryder G. (1996) *J. Geophys. Res.* **101**, 26069. [12] Maier W.D. et al. (2009) *Nature* **460**, 620. [13] Kröner A. et al. (1996) *Precam. Res.* **78**, 105. [14] Puchtel I.S. et al. (1998) *EPSL* **155**, 57. [15] Puchtel I.S. and Walker R.J. (2011) 2011 *Goldschmidt Conf. abstr.* [16] Touboul M. & Walker R.J. (in press) *Intl. J. Mass Spectrom.*

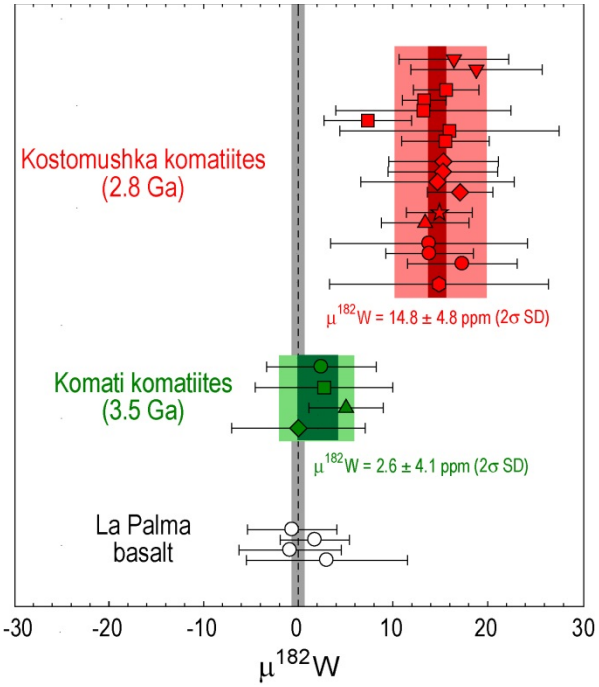

Figure 1. $\mu^{182}W$ values for Komati and Kostomuksha komatiites. Error bars represent 2σ SD.

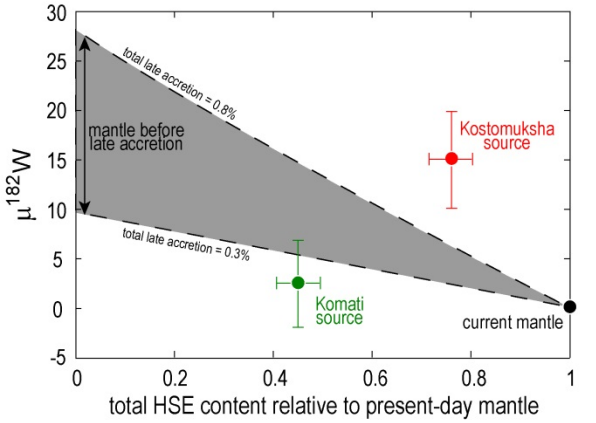

Figure 2. Plot of $\mu^{182}W$ versus total HSE content relative to present-day mantle (in %).

Geochemical Signatures and Magmatic Stability of Impact Produced Zircon. M. M. Wielicki[1], T. M. Harrison[1] and A. K. Schmitt[1] [1]Department of Earth and Space Sciences, University of California, Los Angeles, 595 Charles E. Young Drive East, Los Angeles, CA 90095 (mwielicki@ucla.edu).

Introduction: The impact history of the early solar system, including Earth and the Moon, remains a contreversial issue within planetary science. Since the Apollo program, the concept of a late heavy bombardment (LHB) or lunar catalclysm has been hypothesized. The LHB is a spike in the flux of bolides within the inner solar system from 3.8-4.0 Ga that would have resurfaced the Moon and ~30% of Earth. Evidence for such an event exists in widespread isotopic resetting of Apollo samples at ~3.9 Ga [1] as well as K-Ar ages of lunar meteorites [2].

Recent studies have suggested that the mineral zircon ($ZrSiO_4$) has the potential to record large scale impact events. Overgrowth rims with ages of ~3.9 Ga on Hadean Jack Hills zircons from Western Australia have been suggested as the only terrestrial signal of the LHB event [3]. Lunar zircons have also been used as evidence for large scale impacts on the Moon as early as 4.18 Ga [4]. However the geochemical signatures of zircons produced within impact events are poorly understood and caution must be used when assigning an impact as opposed to igneous origin. Although much data exists on igneous zircon little work has been done on impact produced zircon. We present ion microprobe U-Pb ages, Ti-in-zircon thermometry and trace element geochemistry for impact produced zircons from five large preserved terrestrial craters to compare with the Hadean zircon population in order to determine if they have an impact origin. Results from this study can be used to help distinguish zircons crystallized within an impact event from igneous grains on terrestrial or lunar samples. Zircon saturation modeling of hypothetical crustal rock compositions undergoing thermal excursions associated with the LHB are also developed to predict the expected Ti-in-zircon temperature spectra.

Results:

*U-Pb Geochronolgy***.** U-Pb geochronology of zircons from the Sudbury and Manicouagan impact melts agree well with published ages, however those for Vredefort and Morokweng do not (no impact produced zircon was observed within the Popigai samples). An impact age of ~1980 Ma for Vredefort is younger than the previously published age of ~2020 Ma [5], but previous ID-TIMS results may contain relic zircon. Morokweng U-Pb zircon ages (~150 Ma) are slightly older than previously published TIMS U-Pb age of ~145 Ma [6]. No relic zircons were discovered associated with the target rocks ruling out the possibility of inheritance and leaving open the possibility that the published ages reflect post-impact effects.

Inherited zircon, from the target rock, was present in impactites from Vredefort and will be depth profiled to determine if overgrowth rims dating to the impact event are present on these grains.

Ti-in-zircon thermometry. Applying the Ti-in-zircon thermometer to impact proiduced zircons from known terrestrial impact sites and comparing results to the remarkably low temperatures [~680°C; 7] associated with Hadean zircons could provide evidence in assessing a possible impact origin for these ancient grains. Crystallization temperatures from Ti-in-zircon thermometry of 111 zircons separated from Sudbury, Vredefort, Morokweng, and Manicouagan impact sheets indicate an average crystallization temperature of 773±87°C. When impact temperatures are compared to that of the Hadean zircons, a Kolmogorov-Smirnov test shows that these are two distinct populations ($p \approx .002$), and that impact formed zircons are not a dominant source of Hadean zircons. As expected, impact produced zircon crystallization temperature (T_{zir}^{xtln}) values are consistent with that calculated from bulk rock zircon saturation systematic for the two presumably undifferentiated melts (Manicouagan, Vredefort). Zircon T_{zir}^{xtln} values for Sudbury and Morokweng, both differentiated bodies, are 50-100°C higher than that predicted from bulk saturation (T_{zir}^{sat}), consistent with previous observations [8].

Trace Element Geochemistry. Trace element analyses of impact produced zircons yield results consistent with crustal formation in an igneous environment, similar to Hadean zircons. They are characterized by a HREE enrichment and display positive Ce-anomalies and negative Eu-anomalies. The positive Ce-anomaly could be explained by an oxidized magma source where more Ce^{4+} is present than Ce^{3+}, thus less Ce will be compatible within the zircon crystal lattice. However this cannot explain the presence of a negative Eu-anomaly, unless we assume crystallization of plagioclase before zircon saturation as Eu can easily substitute for Ca within plagioclase and reduce the amount of Eu within the residual melt. Plagioclase tends to be a dominant mineral within most of the impact rocks studied which supports the above assumption. REE patterns can be used to help determine whether or not the zircons are neo-crystalline or inherited by comparing the REE patterns of zircons within the impact melt

sheet and those from the presumed target rocks. Due to the slow diffusion of REE within zircon [9] and the relatively short residence times of impact melts, different REE patterns would be a direct result of crystallization from variable sources and not due to resetting of the geochemical information. Although impact-produced zircon is indistinguishable from that of igneous or Hadean grains in REE, plots of U vs. Yb and U/Yb vs. Hf or Y [10] suggest that some inference can be made to the target rock composition (continental vs. oceanic crust).

Zircon Saturation Modeling. To potentially translate zircon growth features into constraints on impact events, such as the Late Heavy Bombardment (LHB), we developed a zircon saturation model that estimates the zircon crystallization temperature spectrum associated with thermal excursions predicted from an LHB-type event. Such modeling results can then be compared to the crystallization temperatures for detrital Hadean zircons of Western Australia, to estimate the amount that are impact produced. Zircon production from an impact event is controlled by ambient temperature, Zr content and composition of the target material, as well as the impact energy. Impacts need to be sufficiently large to permit decompression melting of uplifted middle to upper crust (i.e., low energy bolides will not produce melt sheets and thus impact zircon). We modeled the LHB using the thermal model and hypothesized bolide flux of [11]. Target compositions for modern and Archean crust are estimated from large geochemical databases and selected through a Monte Carlo process allowing the spectrum of compositions to be randomly accessed. Model results for impact produced zircon with a target of Archean composition yield a zircon crystallization temperature distribution significantly higher than that observed for Hadean zircons from Western Australia, evidence that impact produced zircons are not a significant source for this population. The model developed in this study can also be applied to lunar compositions to predict the crystallization spectrum associated with an LHB event on the lunar surface and compared to results from lunar zircons.

Discussion: Understanding the geochemical signatures in zircons associated with impact events is essential if such grains are to be used as impact indicators. Results from this study can provide a basis for comparison of impact produced zircon to grains from other crystallization environments. Such constraints could determine the impact origin of ancient terrestrial and lunar zircon and provide a better understanding of the early solar system impact history.

References:

[1] Tera F. et al. (1974) *EPSL, 22*, 1-21. [2] Cohen B.A. et al. (2000) *Science, 290*, 1754-1756. [3] Trail D. et al. (2007) *GCA, 71*, 4044-4065. [4] Pidgeon R.T. et al. (2007) *GCA, 71*, 1370-1381. [5] Kamo S.L. et al. (1996) *EPSL*, 144, 369-387. [6] Hart R.J. et al. (1997) *EPSL*, 147, 25-35. [7] Harrison T.M. et al. (2008) *EPSL, 147*, 476-486. [8] Harrison T.M. et al. (2007) *Geology, 35*, 635-638. [9] Cherniak D.J. et al. (1997) *Geology, 134*, 289-301. [10] Grimes C.B. et al. (2010) *Geology,35*, 643-646. [11] Abramov O. and Mojzsis S.J. (2009) *Nature, 459*, 419-422.

UNDERSTANDING THE SIGNIFICANCE OF LUNAR SAMPLE DATA FOR INTERPRETING LUNAR IMPACT HISTORY N.E.B. Zellner[1], T. Swindle[2], J.W. Delano[3], [1]Department of Physics, Albion College, Albion, MI 49224 (nzellner@albion.edu), [2]University of Arizona, Lunar and Planetary Laboratory, Tucson, AZ 85721, [3]New York Center for Studies on the Origin of Life, Department of Earth and Atmospheric Sciences, University at Albany (SUNY), Albany, NY 12222.

Introduction: The lunar impact flux is not well-undestood but is driving models of solar system and planetary formation. It is also being used to support observational and experimental data that could be interpreted as supporting ideas about the cometary delivery of terrestrial water (i.e., Comet Hartley) and the origin of life (i.e., hot origin of life). A variety of lunar samples are being investigated to study the timing of lunar impacts, including lunar impact glasses [e.g., 1, 2, 3], lunar melt rocks [e.g., 4, 5, 6, 7], lunar meteorites [e.g., 8], and lunar zircons [e.g., 9]. In particular, these samples are being used to address whether or not the Moon experienced a late heavy bombardment (LHB) or terminal lunar cataclysm between 3.8 and 3.9 billion years ago (Ga) [e.g., 10], but they can also give us insight into the nature and timing of impact events throughout the age of the Solar System [e.g., 1, 3, 11]. It is important, though, to place the magnitude of the impact events, whether cataclysmic or not, into the overall context of impact rate over time and to interpret the data so that the impact flux is neither overinflated nor underreported.

Lunar Sample Studies: We have looked at the ages of lunar samples from various investigators in order to try to reconcile the impact glass, meteorite, and breccia data records. These data include impact glass data from the Apollo 12, 14, 16, and 17 landing sites [1, 2, 3, 12, 15], lunar meteorite data [8], asteroid meteorite data [13], and impact melt data [4, 5, 6, 7]. Reconciling the data sets is important because if impacts were occurring in the inner solar system during specific epochs, all of these samples should be formed in these events.

*Old Ages:*As early as 1973, lunar sample ages indicated that several of the large basins on the Moon were formed in ~200 Ma between 3.8 and 4.0 Ga [20]. Since then, other investigators have found support for the LHB in Ar/Ar ages of impact melts from the Apollo 15 and 17 landing sites [5, 6] and in U/Pb or Rb/Sr ages of lunar highland samples [10], for example. This supposed LHB has been interpreted as being responsible for impact sterilization of the Earth [16] and for the hyperthermophilic last universal common ancestor of life [e.g., 17]. More recent investigations into lunar zircon shock ages [9] and ages of melt rocks from the Apollo 16 and 17 landing sites [7, 21], though, indicate that old impacts did occur, and recent orbital data is influencing our reinterpretation of the number of large impact basins [18] and the sources of Apollo samples [19].

Young Ages: Several authors [3, 14, 15] have reported that a large number of impacts have occurred in the last 500 Ma and that this is consistent with an increase in the meteoroid bombardment of the inner Solar System. While these data are consistent with an increase in the recent impact flux, they do not require that explanation [3, 15]. Published ages of 25 glass samples from the Apollo 14, 16 and 17 landing sites [1, 2, 12], as well as unpublished data from the same authors, do not show this recent rise in impact flux, though young ages with large uncertainties in those ages are represented.

Data Analyses: To attempt to reconcile the age data from the different sample sets, ideograms reflecting the probable age distributions of these sample were created (Figure 1), with 2σ uncertainty in the ages across all data sets. When possible, multiple samples formed in the same event (i.e., impact glasses [2] or melt rocks [7]) were removed from the data set so that the impact flux was not overinflated. Additionally, ages with uncertainties $\geq$50% of the age were removed from the data sets because those ages are not especially useful. Finally, in the case of the Apollo 14 glasses [14], all ages $\geq$ 3000 Ma were removed since we do not know if these are volcanic glass ages or impact glass ages.

A background continuum for impacting objects was defined so that signficant impact

events above that background flux would become more apparent (Figure 2). The average of the "overall" curve is 0.07005 and the standard deviation of the points is 0.042451.

Discussion: With a more consistent treatment of the data, Figure 1 shows that the ideograms of ages from multiple lunar samples do follow similar patterns, but differences also exist. For example, the lunar impact glasses show an impact event about 2800 Ma while the meteorites do not. Additionally, only the Apollo 12 impact glasses show an increase in the recent lunar impact flux, strengthening the argument that these glasses were produced in local cratering events.

Figure 2 shows the same data as in Figure 1, but with the background continuum, defined as the average probability (over all data sets) that a sample would have a particular age, removed. Anything above one standard deviation above the average could be considered "significant". The LHB barely breaches the 1-StDev mark, while the recent impact flux really does seem to be significant, if the Apollo 12 data can be believed to represent a global flux. Removing the Apollo 12 data greatly affects this curve, however.

Conclusion: Lunar samples can address the complex question of what the lunar impact flux has looked like over time. Taking into account the 'everyday' background impact flux that the Moon has experienced over time is important so that the significance of prominenat peaks in ideograms and histograms of impact sample ages is appropriately interpreted.

References: [1] Zellner, N.E.B. *et al.* (2009) *GCA*, **73**, 4590-4597. [2] Delano, J.W. *et al.* (2007) *MAPS*, **42**, 6, 993-1004. [3] Levine, J. *et al.* (2005) *GRL*, **32**, L15201. [4] Barra, F. *et al.* (2006) *GCA*, **70**, 6016-6031. [5] Dalrymple,G. and Ryder, G. (1993) *JGR*, **98**, 13085-13095. [6] Dalrymple, G. and Ryder, G. (1996) *JGR 101*, 26069-26084. [7] Norman et al. (2006) *GCA*, **70**, 6032-6049. [8] Cohen, B. *et al.* (2000) *Science*, **290**, 1754-1756. [9] Nemchin, A. and Pidgeon, R. (2008) 39th LPSC, 1558.pdf. [10] Tera F. *et al.* (1974) *EPSL*, **22**, 1-21 [11] Delano, J.W. (2010) LEAG 2010, 3035.pdf. [12] Zellner N.E.B. *et al*. (2009) *MAPS*, **44**, 839-852. [13] Bogard (1995) *MAPS*, **30**, 244-268. [14] Culler T. *et al.* (2000) *Science*, **287**, 1785-1788. [15] Hui *et al*. (2010) *Proc. 9th ASSC*, 43-54. [16] Maher and Stevenson (1988) *Nature*, **331**, 612-614. [17] Bada J. (2004) *EPSL*, **226**, 1-15. [18] Frey and Romine (2011) *42nd LPSC*, 1190.pdf. [19] Spudis (2011) *42nd LPSC*, 1365.pdf. [20] Turner *et al.* (1973) *Proc. 4th LSC*, 1889-1914. [21] Fernandes V. *et al.* (2008), *Bombardment 2008*, 3028.pdf.

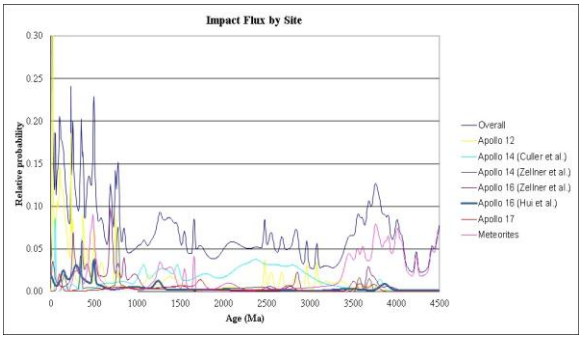

Figure 1. Ideogram of ages of lunar impact glasses and asteroidal meteorites. Note that the averaged flux (i.e., the "Overall" curve) is dominated by the Apollo 12 impact glass ages.

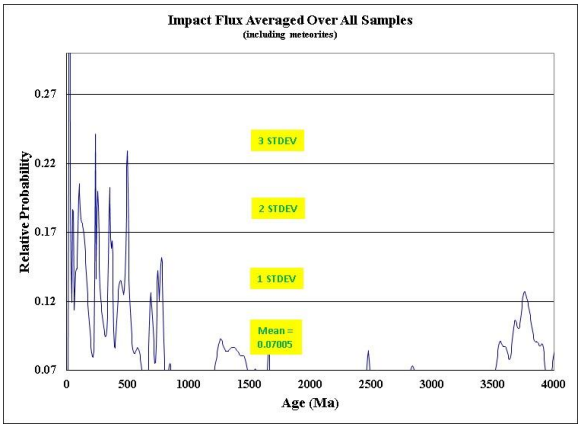

Figure 2. Ideogram of the averaged impact flux, with the continuum flux substracted out. Any event above 1 StDev can be considered "significant". Again, the recent flux is dominated by the Apollo 12 data.

NOTES

NOTES